University of South-Eastern Norway
Faculty of Technology, Natural Sciences and Maritime Studies

Doctoral dissertation no. 6
2018

Christian Ahoba-Sam

Low temperature methanol synthesis catalysed by a copper nanoparticle-alkoxide system

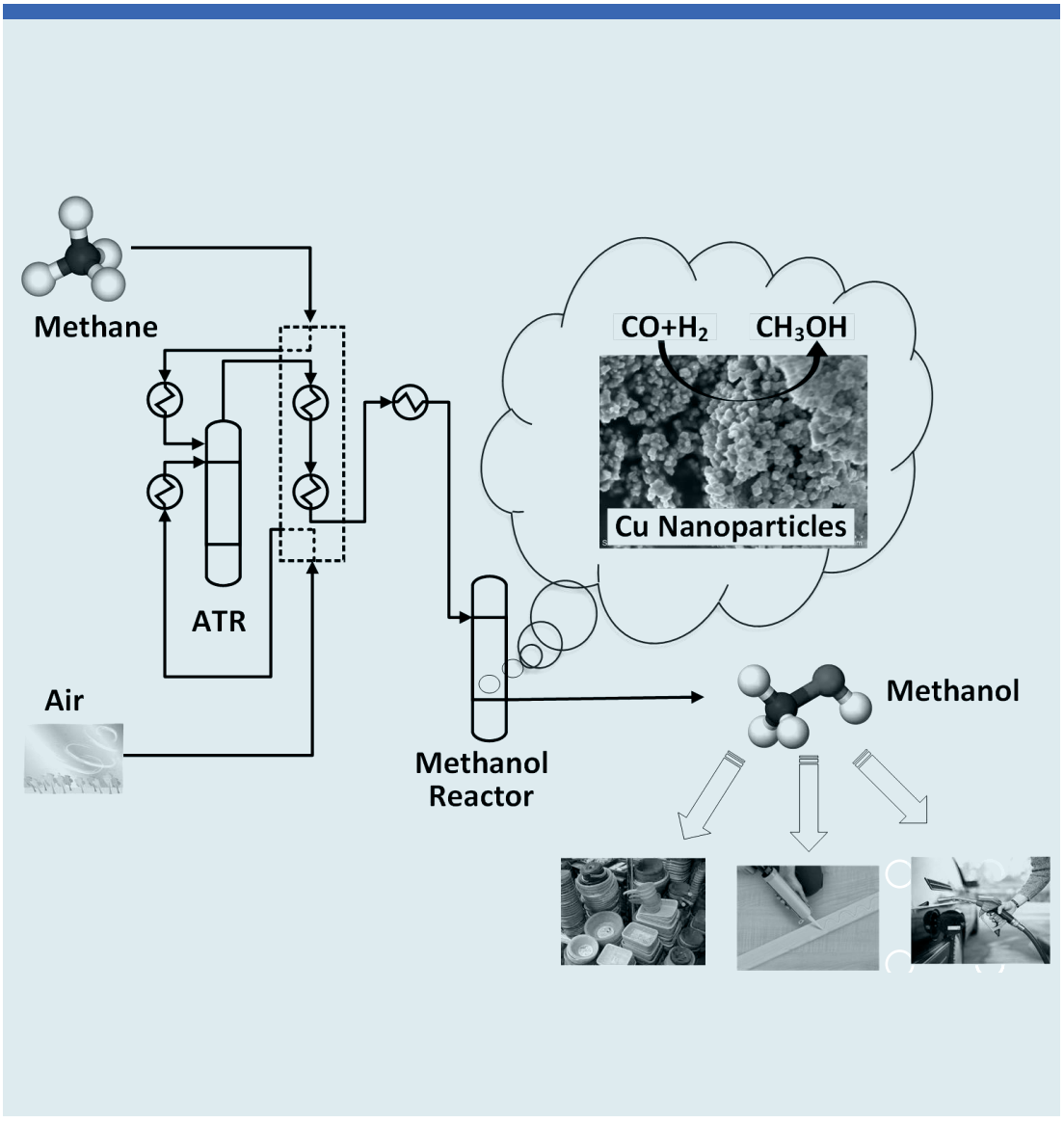

Christian Ahoba-Sam

Low temperature methanol synthesis catalysed by a copper nanoparticle-alkoxide system

A PhD dissertation in
Process, Energy and Automation Engineering

Faculty of Technology, Natural Sciences and Maritime Studies
University of South-Eastern Norway
Porsgrunn, 2018

Doctoral dissertations at the University of South-Eastern Norway no. 6

ISSN: 2535-5244 (print)
ISSN: 2535-5252 (online)

ISBN: 978-82-7206-479-1 (print)
ISBN: 978-82-7206-480-7(online)

Print: University of South-Eastern Norway

Now all glory to God, who is able, through his mighty power at work within us, to accomplish infinitely more than we might ask or think. (Ephesians 3:20 NLT)

Preface

The work presented in this thesis has been carried out between January 2015 and March 2018 in partial fulfilment of the requirement for the degree of Doctor of Philosophy (Ph.D) at the University of South-Eastern Norway (USN). This work was funded by the Research Council of Norway, under the 'CO_2 as Future Feed' project as part of NANO2021, project number 228157/O70. I am grateful to the Research Council for funding the project.

The study was under the main supervision of Prof. Klaus-Joachim Jens and Prof. Unni Olsbye as the co-supervisor. My profound gratitude goes to Prof. Jens for offering me the opportunity to perform this work. I thank both supervisors for their encouragement and supervision during the course of the study. Special appreciation goes to Prof. Olsbye who introduced me to the field of catalysis during my MSc studies at the University of Oslo, and thus paving the way for this PhD study.

Aside the major work carried out at USN, a significant portion of the analytical studies was performed at the Centre for Material Science and Nanotechnology (SMN), University of Oslo. I am grateful to the Catalysis group, REXC (Norwegian national resource centre for X-ray diffraction and scattering) and NorTEM (the Norwegian Centre for Transmission Electron Microscopy) for allowing me to use their facilities. I also thank Dr. David Wragg, Dr. Phuong Dan Nguyen and Domas Birenis for their assistance with the usage of the XRD and TEM instruments.

As part of the PhD fellowship, a four-month period was spent at the Newcastle University, UK, in collaboration with Dr. Kamelia Boodhoo. I thank Dr. Boodhoo for allowing me to work in her lab as well as all the fruitful discussion we had during my stay at Newcastle. I also appreciate Dr. Fernando Russo Abegao, Rob Dixon, Maggie White, Megan Beard, Sahr Sana, Tolu Kolawole and the entire Process Intensification group at the School of Engineering for making my stay at Newcastle worthwhile.

My gratitude also goes to all the technical personnel at USN, particularly Øyvind Johansen, Fredrik Hansen, Eivind Fjelddalen, Nora Furuvik, Mathias Henriksen, Arve Lorentzen, Dr. Joachim Lundberg and Hildegunn Haugen for their support. I thank Prof. Lars Erik Øi for assisting me with the simulation work. I am grateful to all my colleagues including, Dr. Zulkifli Idris, Dr. Li Lu, Li Bo, Per Morten Hansen, Michal Sposob and Cornelius Emeka Agu for their support. I am also thankful for the opportunity given me to co-supervise Hilda Hilde Amundsen towards her MSc during the period of my PhD.

I am forever grateful to my family and friends for their support and encouragement. Special appreciation goes to Patrick Ebo Ahoba-Sam, Abeku Gyan-Quansah and my Parents, who have been supportive throughout my education. I am indebted to my beloved Rhoda for her immense support, understanding and love shown me during the period. My love to Nyansa and Enyimpa for bearing with the long hours I spent away from home in the course of my studies. You all made me experience 'life' after all those stressful moments in the lab.

Christian Ahoba-Sam

Porsgrunn, April 2018

Abstract

Methanol (MeOH) synthesis at low temperature in a liquid medium presents the possibility of achieving full syngas conversion per pass. The Low temperature MeOH synthesis (LTMS) process is advantageous over the current technology for MeOH production since the former is thermodynamically favourable and gives a high yield per pass. The LTMS involves two main steps, (i) MeOH carbonylation to form methyl formate and (ii) hydrogenolysis of methyl formate to form MeOH. The initial aim of the present work was to develop, characterize and evaluate the catalyst system involved in the LTMS process. A once-through catalyst system involving copper (II) acetate and methoxide was used to obtain up to 92 % conversion (> 94 % selectivity to MeOH) per batch at 20 bar syngas pressure and 100 ^{o}C temperature within 2 h. XRD and TEM characterization of the slurry catalyst system revealed that about 10 ± 5 nm Cu_2O/Cu^0 nanoparticles were involved in the catalytic process. Decreasing Cu nanoparticles sizes led to increased MeOH production due to an increase in active Cu surface area, which enhanced methyl formate hydrogenolysis. Agglomeration of the Cu nanoparticles in the course of MeOH production was identified as a major cause for the deactivation of the Cu nanoparticle component of the LTMS catalyst system.

Furthermore, with the aim of investigating the role of solvents polarity on the LTMS, MeOH production maximized for solvents with dielectric constant (ε) around 7.2, similar to the polarity of diglyme. A probe of possible side reactions of the main intermediate revealed that, in the presence of methoxide, low polar solvents enhanced decarbonylation of methyl formate while high polar solvents enhanced a nucleophilic substitution to form dimethyl ether and sodium formate. Relatively moderate polar solvents such as diglyme appeared to give a good balance in minimizing possible side reactions of methyl formate and therefore enhanced MeOH production.

In addition, the spinning disk reactor (SDR) was used to synthesize on-purpose Cu nanoparticles with predefined particle sizes for catalysing the LTMS reaction. By maintaining the same chemical recipe, Cu nanoparticle sizes were tuned down to 3 nm

when physical conditions were varied to shorten for example micromixing time, mean residence time and relative residence time distribution. This subsequently led to uniform nucleation and ultimately formation of smaller Cu nanoparticle sizes with narrow particle size distribution. At the end, a model was proposed for a complete LTMS process with the help of Aspen HYSYS simulation tool, using an air-blown autothermal reformer, for a full conversion per pass at 60 bar syngas (0.31 CO: 0.62 H_2: 0.07 N_2) and 100 ^oC MeOH synthesis temperature.

List of papers

Article 1

Ahoba-Sam C., Olsbye U., Jens K-J., Low temperature methanol synthesis catalysed by copper nanoparticles; Catalysis Today, 2018, 299, 112, doi.org/10.1016/j.cattod.2017.06.038

Article 2

Ahoba-Sam C., Olsbye U., Jens K-J., The Role of Solvent Polarity on low temperature methanol synthesis catalysed by copper nanoparticles, Frontiers in Energy Research, 2017, 5, 15, doi.org/10.3389/fenrg.2017.00015

Article 3

Ahoba-Sam C, Boodhoo K.V.K, Olsbye U., Jens K-J., Tailoring Cu nanoparticles catalyst for methanol synthesis using the spinning disk reactor, Materials, 2018, 11, 154, DOI: 10.3390/ma11010154

Article 4

Ahoba-Sam C., Øi L.E., Jens K-J., Process Design of a Novel Low Temperature Methanol Synthesis Process Using an Air-blown Autothermal Reformer, (Submitted manuscript to Linköping Electronic Conference Proceedings)

List of Conference Contributions

LOW TEMPERATURE METHANOL SYNTHESIS BY A Cu ALKOXIDE SYSTEM

Oral presentation delivered at Norwegian Catalysis Symposium, Bergen, November 2015

LOW TEMPERATURE METHANOL SYNTHESIS CATALYSED BY COPPER NANOPARTICLES

Poster presentation delivered at Natural Gas Conversion Symposium 11, Trømso, June 2016

LOW TEMPERATURE METHANOL SYNTHESIS; SOLVENT EFFECT

Oral presentation delivered at CO_2 utilization conference XIV, Sheffield, September 2016.

TAILORED Cu NANOPARTICLES USING SPINNING DISK REACTOR FOR METHANOL SYNTHESIS

Oral presentation delivered at Applied Nanotechnology and Nanoscience International Conference, Rome, October 2017.

PROCESS SIMULATION AS A TOOL FOR DESIGN OF A NOVEL LOW TEMPERATURE METHANOL SYNTHESIS PROCESS USING AIR-BLOWN AUTOTHERMAL REFORMER

Presentation to be delivered at International Conference of Scandinavian Simulation Society, Oslo, September 2018.

Abbreviations

AC	Activated Carbon
ATR	Autothermal Reformer
access ATR*	Attenuated total reflection accessory
BASF	Baden Aniline and Soda Factory
BET	Brunauer–Emmett–Teller
Btu	British thermal unit
DEE	Diethyl ether
DLS	Dynamic light scattering
DMC	Dimethyl carbonate
DME	Dimethyl ether
DMSO	Dimethyl sulfoxide
DMT	Dimethyl terephthalate
FT	Fischer Tropsch
FT-IR	Fourier-transform infra-red
GC	Gas chromatography
ICI	Imperial Chemical Company
IHS	Information Handling Services
IL	Ionic liquid
IR	Infra-red
LTMS	Low temperature methanol synthesis
MeCN	Acetonitril
MeF	Methyl formate
MeOH	Methanol
MMA	Methyl methacrylate
MMT	Million metric tons
MS	Mass spectrometry
MSD	Mass spectrometry detector
MTBE	Methyl tert-butyl ether

MTO	Methanol to olefin
MW	Micro-wave
NP	Nanoparticle
OECD	Organization for Economic Co-operation and Development
PC	Personal computer
ppm	Parts per million
PSA	Pressure swing absorber
ROH	Alcohol
SDR	Spinning disk reactor
SEM	Scanning electron microscopy
STR	Stirred tank reactor
TCD	Thermal conductivity detector
TEM	Transmission electron microscopy
THF	Tetrahydrofuran
TOPAS	Total pattern analysis solution
XANES	X-ray absorption near edge structure
XPS	X-ray photoelectron spectroscopy
XRD	X-ray diffraction

Table of contents

1 Introduction

Rapid population and economic growth implies increasing consumption of energy on a daily basis [1]. The world's consumption of energy is estimated to rise by 28 % between 2015 and 2040 as illustrated in **Figure 1.1**. While humankind has depended on fossil fuels (natural gas, oil and coal) over the last three centuries for energy and material technology development [2], the current global economic growth and environmental concerns requires the need for a more sustainable, efficient and cleaner source of energy. Even though non-fossil based sources provide some options, only a small fraction of energy is currently supplied from such source leaving a major dependence on fossil. It is projected for example that, fossil fuel will provide about 85 % of the commercially consumed energy worldwide for the next few decades [3]. However, the exhausting nature of fossil coupled with the alarming CO_2 emission requires better CO_2 utilization to curb this concern. Therefore, one realistic approach is to improve the efficiencies and recycling of existing carbon-based energy and material sources to minimize the carbon footprint [4, 5].

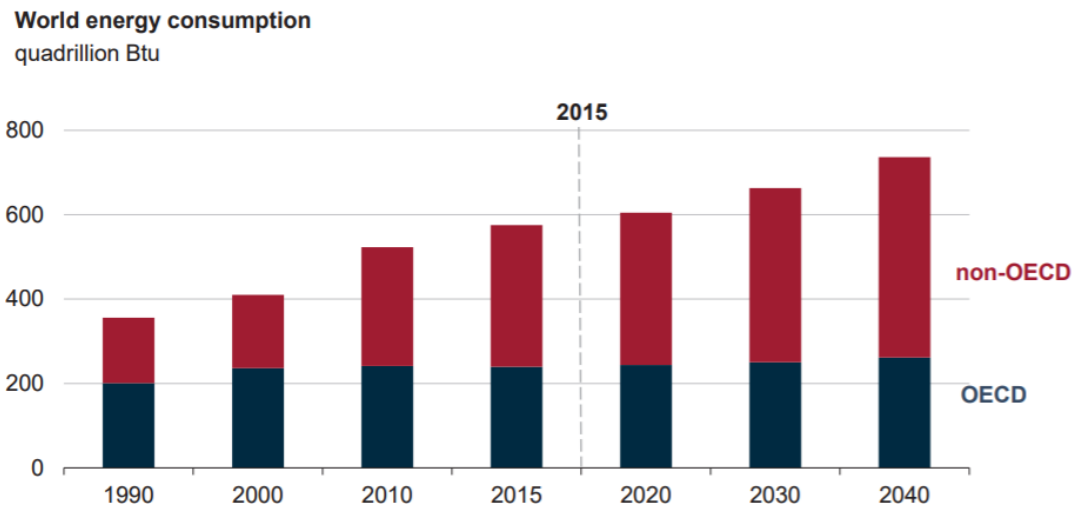

Figure 1.1: World energy consumption between 1990 to 2050, adopted from [1]

A pragmatic approach to improve on existing carbon-base technologies, is to transform syngas (composed of H_2 and CO) from non-conventional energy sources into standard fuels and chemical feedstock. Syngas can be produced from several feedstock such as

natural gas, heavy oil and biomass [6]. Biomass presents a greener and renewable alternative, however this has the potential of competing with crops for food production on arable land. Increasing advocates and policies for cleaner technologies makes coal and petroleum less attractive for syngas production. In addition, increasing difficulty in accessibility of oil coupled with high fluctuation of its price makes it less dependable [7]. Natural gas on the other hand is relatively abundant, cleaner (compared to oil and coal) and cheaper providing a viable option for syngas production [8, 9].

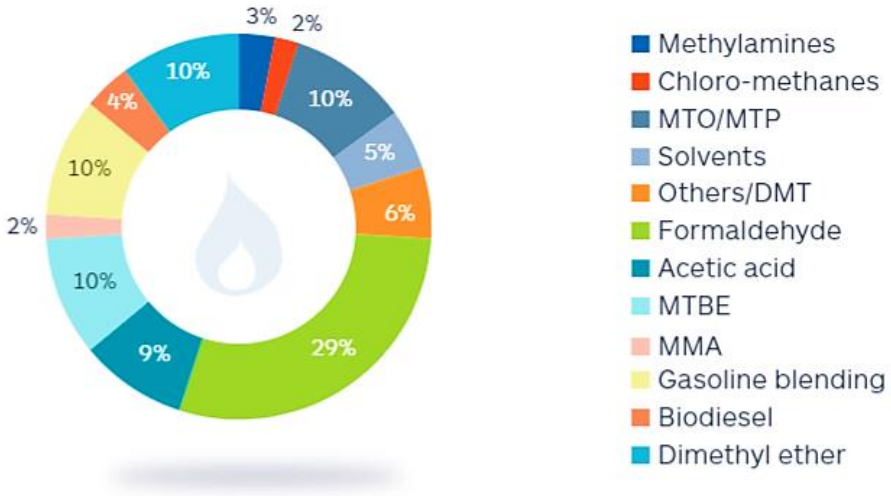

Figure 1.2: World MeOH demand in 2015 by end use adopted from [10]

One important chemical bridging syngas towards energy and material applications is methanol (MeOH). MeOH has been identified as a potential multipurpose molecule for energy and CO_2 storage [11]. According to the IHS (Information Handling Services) Markit, worldwide demand for MeOH reached about 70 MMT (million metric tons) in 2015 and is expected to surpass 95 MMT by 2021 with emerging applications in energy, especially in Northeast Asia [10, 12]. **Figure 1.2** shows some of the worldwide applications of MeOH by end use. For example, MeOH can be used as solvent or as an intermediate for producing a wide variety of chemicals including formaldehyde (which is the building block of several low-cost resins and adhesives), methyl tert-butyl ether (MTBE), acetic acid, methyl methacrylate (MMA) and other fine chemicals. MeOH stores both carbon and hydrogen in the liquid form at ambient temperature, that is readily

transportable [13] and it serves as a base chemical for direct conversion into light olefins, gasoline and hydrocarbons over acidic zeolites in the MTO and MTH processes [14], thereby providing an alternative to today's fossil energy sources and petrochemical feedstocks.

The current MeOH synthesis technology dates back to the 1960s, when Imperial Chemical Industries (ICI, now Johnson Matthey Catalysts) succeeded in commercializing a Cu-based catalyzed technology [15, 16]. The ICI process was based on Cu/ZnO catalyst with highly desulphurized syngas, which operated at about 200 - 300 ^{o}C temperature and 50-100 bar syngas pressure. This has been the main technology for MeOH production until date. However, with upgraded versions of the Cu-based catalyst and plant designs, the licensed ICI Cu-based technology shares the market for MeOH plants construction with other major competitors such as Lurgi, Mitsubishi Gas Chemicals and Haldor Topsoe [17].

The MeOH synthesis technology continuous to be improved on catalyst development and energy efficiency in the various parts of the plants. One major motivation has been to operate at lower temperature and pressure conditions in order to reduce the operation and capital cost involved in MeOH production [17]. Although ICI technology is highly optimized, thermodynamic limitations restrict syngas conversion per pass to about 20 % at the current operating conditions. For example, hydrogenation of CO is an exothermic reaction (Equation (1.1)), and typically requires a relatively lower temperature to maximize conversion per pass [18]. As a result, the ICI process involves several rounds of recycling to optimize production [19].

$$\mathrm{CO} + 2\mathrm{H_2} \rightleftharpoons \mathrm{CH_3OH} \qquad \Delta\mathrm{H} = -90.6\,\mathrm{kJ/mol} \qquad (1.1)$$

Furthermore, the low conversion per pass of the ICI process requires the use of 'pure' syngas other than nitrogen-diluted syngas for the MeOH synthesis. That is to say, the presence of N_2 diluent reduces the partial pressure of syngas and thereby lowers syngas conversion the more. It is important to note that in the overall ICI MeOH synthesis process, syngas production accounts for more than half of the total capital cost due to

the need for a cryogenic oxygen-blown autothermal reformer [20, 21]. The lowest cost of syngas production is by the use of air-blown rather than pure cryogenic O_2-blown autothermal reformer [22]. Full conversion per pass will allow the use of N_2 diluted syngas for methanol production since recycling will not be necessary. Therefore, there is a need to develop an alternative low-temperature MeOH synthesis process.

About a century ago, Christiansen identified and patented a low temperature methanol synthesis (LTMS) process in 1919 [23]. This process was based on a transition metal and alkoxide co-catalyst system carried out in a liquid solvent at about 120 ^oC temperature. The LTMS reaction is a stepwise process, firstly involving carbonylation of methanol to form methyl formate (MeF) and secondly, MeF hydrogenolysis to form MeOH as indicated in Equations (1.2) and (1.3), leading to (1.1) as the overall reaction. It is suggested that alkali metal promotes the carbonylation by forming metal alkoxide which has an increased electron density on their oxygen compared to the oxygen on alcohols[24]. The hydrogenolysis of the MeF is suggested to occur via a formaldehyde intermediate [25] and subsequent reduction to form MeOH.

$$CO + CH_3OH \rightleftharpoons HCOOCH_3 \qquad (1.2)$$

$$HCOOCH_3 + 2H_2 \rightleftharpoons 2CH_3OH \qquad (1.3)$$

One potential drawback in the alkoxide system is its sensitivity to the presence of water and carbon dioxide [26, 27] . That is, the metal alkoxide component of the catalyst forms a stable hydroxide or carboxylates when in contact with water or carbon dioxide respectively, and therefore brings the reaction to a halt. This led to less attention paid on the LTMS process compared to the ICI process. However, with adequate optimization of syngas production, water and carbon dioxide produced in the Authormal reformers can be highly minimized. Moreover, an additional syngas pre-treatment cleaning step to absorb the remaining ppm of H_2O and CO_2 from syngas produced before feeding into MeOH reactor will drastically reduce their presence.

Among the transition metals tested for the LTMS reaction, copper and nickel-based catalysts have shown good activity for the MeOH yield. Various Ni-based compounds

including $Ni(CO)_4$ (nickel tetracarbonyl) and $Ni(OCOCH_3)_2$ (nickel II acetate) in combination with alkali-metal alkoxide co-catalysts have been shown to be very active for syngas conversion between 80 to 120 ^oC and 10 to 50 bars syngas pressure [28, 29]. However, in the Ni-based system, there is an inevitable formation of $Ni(CO)_4$ [29] complex which is volatile and highly toxic [30]. This poses a potential handling risk on an industrial scale. Therefore, Cu-based catalysts have received much attention than the Ni for the LTMS process. Raney copper, copper on silica support, copper chromate as well as copper salts are among the identified Cu-based materials, though these were not as efficient as Ni [27, 31, 32]. The CuO/Cr_2O_3 catalyst seems to be most widely used, where milling of CuO and Cr_2O_3 physical mixture seems to create lattice defects leading to an increased surface area and catalyst activity [32, 33].

The LTMS reaction presents the possibility of achieving a full conversion of syngas to MeOH per pass at relatively low temperature (<120 ^oC) and pressure (<100 bars) conditions. Considering the relatively milder operating conditions, the LTMS process presents some flexibility in the choice of siting a MeOH plant in addition to the possible remote areas. An upstream production of MeOH will decrease transportation difficulties associated with compression and transportation of gas feedstock from remote areas, which otherwise indirectly contributes to greenhouse gas emissions [34]. Our group has revisited this century old LTMS process using copper alkoxide catalyst system [31, 35]. We present a simple means of developing Cu catalyst through a one-pot approach to further advance the LTMS concept with a proposed process design to go with it.

1.1 Aim of Thesis

Generally, the aim of the present study was to develop, characterize and evaluate the Cu alkoxide catalyst system involved in the LTMS process. Since in the alkoxide assisted MeOH synthesis, hydrogenolysis of MeF is the rate-determining step [27], particular emphasis was placed on developing a more active Cu catalyst. Issues regarding the role of Cu particle sizes, deactivation pathways and the role of solvent were considered. We

further investigated the synergistic relationship between the two catalysts, Cu and alkoxide and to which extent such highly active catalysts can hydrogenate CO_2 indirectly, via a carboxylate intermediate. Lastly, we aimed to propose a process design for the LTMS process with an air-blown autothermal reformer using simulation tools to optimize conditions. Specific objectives set to meet the above aims are as follows:

- to characterize the Cu particles in the slurry involved in the LTMS reaction
    - to investigate the role of Cu nanoparticle sizes in the LTMS reaction
    - to identify the role of particle size in deactivation
- to investigate the role of solvent (polarity) in the LTMS reaction and to identify the role of solvent in deactivation of the process.
- to investigate how the spinning disk reactor (SDR) could be used to develop on-purpose Cu particles with defined sizes and to scale-up Cu-nanoparticles production for LTMS reaction using the SDR.
- to investigate the synergistic relationship between Cu catalysts and alkoxide involved in the LTMS reaction by focusing on hydrogenolysis of formate and carbonate.
- to design a complete process for LTMS from methane using an air-blown autothermal reformer and to optimize conditions using thermodynamic simulation tools.

1.2 Scope of the Thesis

This work was put together as an article based thesis, with common reference, appendix and notations. A major portion of the work is published in peer reviewed articles (see page VII). Outline of the various chapters are as follows:

Chapter 2 consists of the literature review, as an overview of the state of the art in low temperature MeOH synthesis. Particular emphasis will be based on alkoxide assisted

MeOH synthesis and compared to other suggested approaches. The chapter ends with a summary of methods of producing Cu nanoparticles involved in nano-catalysis.

Chapter 3 consists of the experimental approach adapted in this work.

Chapters 4-8 will provide insight into the results and discussions of the thesis.

Chapter 9 gives an overview of the work by way of conclusion and directions to further work.

2 Literature Overview Relevant for Low Temperature MeOH Synthesis

The origin of MeOH synthesis dates as old as Adam and Eve, as MeOH was produced as a by-product of burning wood, and hence named as *wood alcohol* [36]. However, in modern times, synthetic MeOH production from synthesis gas and solid catalysts was first developed and implemented by BASF in 1923. This was based on zinc oxide and chromia (ZnO/Cr_2O_3) catalyst operating at 250-350 bar and up to 450 ^oC. Despite the rather harsh operating conditions, the process yielded low activity and therefore suggested a high investment cost for the MeOH production. Just around the same period in 1925, other metallic catalysts, including Cu-based catalysts were also reported to give relatively good activity for the MeOH synthesis, but had a shorter catalyst lifetime [37]. Decades later, with further catalyst development and enhanced availability of syngas from partial oxidation of natural gas, coupled with improved desulphurization, Imperial Chemical Industries (ICI, now Johnson Matthey Catalysts) succeeded in commercializing a Cu-based lower pressure MeOH synthesis technology in the 1960s [15, 16]. The ICI process was based on Cu/ZnO catalyst and operated at about 200-300 ^oC temperature, 50-100 bar pressure. This represented a significant energy savings compared to the previous technologies and has been the main approach for MeOH production until date.

After the 1960's, research and development on the ICI process has been enormous such that the process, feedstock and catalyst systems are highly optimized [22, 38], nevertheless, the process has not been without some major drawbacks. For example, hydrogenation of CO is an exothermic reaction (Equation (1.1)), and typically requires a relatively lower temperature to maximize conversion per pass [18]. Since the ICI process involves relatively higher temperature, syngas conversion is thermodynamically limited as conversion per pass is barely limited to 20 %. As a result, the ICI process requires several recycling to optimize MeOH production [19]. In addition, it is important to note that syngas production accounts for more than half of the total capital cost in the ICI MeOH process due to the use of cryogenic oxygen-blown autothermal reformer [20, 21]. The lowest cost of syngas production however is by the use of air rather than pure

cryogenic O_2-blown autothermal reformer [22]. The presence of N_2 diluent reduces the partial pressure of CO and H_2 such that it leads to further reduction in syngas conversion per pass. A full conversion per pass technology at relatively lower pressure conditions will allow the use of N_2 diluted syngas for methanol production since recycling will not be essential.

2.1 The Low Temperature MeOH Synthesis (LTMS)

The low temperature MeOH synthesis (LTMS) in broader terms is used to describe the MeOH synthesis process carried out below the 200-300 ^oC conventional CO/CO_2 hydrogenation temperatures. The traditional LTMS as developed by Christiansen in 1919 [23] was carried out between 80 to 120 ^oC in liquid medium with the added advantage to absorb heat generated during the exothermic MeOH reaction (Equation (1.1)). Further, the traditional LTMS process was an alkoxide-assisted approach, which occurred via a MeF intermediate. In the following sections, we will review the alkoxide-assisted MeOH synthesis catalysed by a transition metal alkoxide system. The role of the individual catalyst will be discussed stepwise, that is the carbonylation and hydrogenolysis steps and then together as a concurrent system. Furthermore, other non-alkoxide low temperature approach will be briefly discussed, in comparison with the traditional approach.

2.1.1 Carbonylation

Carbonylation involves the addition of a carbonyl onto another molecule. In relation to LTMS, this will involve the addition of CO onto an alcohol (ROH) to form an alkyl formate as illustrated in Equation (2.1) using MeOH as an example. Carbonylation of MeOH is very rapid in the presence of alkoxide catalyst [23, 24, 39]. The alkali alkoxide are excellent in carbonylation of MeOH even at room temperature [29]. However

Christiansen's [39] equilibrium considerations revealed that the carbonylation reaction is highly reversible. Although carbonylation is rapid at initial times when temperature is increased, however overall conversion decreases with increasing temperature [40, 41].

$$CO + CH_3OH \rightleftharpoons HCOOCH_3 \qquad (2.1)$$

The type of alkali metal attached to the alkoxide plays a role in the overall performance of the alkoxide. Kinetic studies [24, 27, 41] have shown that CO carbonylation is first order with respect to both CO and MeOH in the presence either CH_3OK or CH_3ONa with similar apparent activation energy of about 68 kJ/mol. Rate expression deduced for carbonylation reaction is given by Equation (2.2). When the type of alkali metal was varied, the rate was in the order CH_3CH_2OK > CH_3CH_2ONa> CH_3CH_2OLi, [24]. This was attributed to the differences in the ionization potentials of the alkali metal in the carbonylation step. That is the lower the ionization potential of the alkali metal, the higher the catalytic activity.

$$r = 2.88 \times 10^9 e^{(-\frac{10126}{T})} C_{Catal} C_{MeOH} P_{CO} \qquad (2.2)$$

The type of alcohol used as the alkoxide source also plays a role in the carbonylation reaction. The kinetic study by Tonner et. al. [24, 42] showed that the rate of carbonylation increases in the order CH_3ONa < CH_3CH_2ONa < $CH_3CH_2CH_2ONa$ < $CH_3CH_2CH_2CH_2ONa$ < $(CH_3)_2CHCH_2ONa$ < $(CH_3)_2CHONa$ < $(CH_3)_3CONa$ < $CH_3CH_2CH(ONa)CH_3$. Their results indicated that as chain length of the alcohol increased and the substitution close to the OH increased, carbonylation rate also increased, except when there was a severe steric hindrance. This suggested that electron-directing effect was an important factor for carbonylation as for example, benzyl alcohol with strong electron withdrawing showed slow rate. They concluded that the mechanism involves alkoholate donation of electrons to the 2p orbital in C of CO and picks proton (H^+) from ROH (R is an alkyl group) to regenerate the alkoxide as illustrated in Equations (2.3) and (2.4). That is, any substitution that increases the electron density will increase the rate of carbonylation reaction.

$$RO^{-}Na^{+} + CO \rightleftharpoons ROOC^{-}Na^{+} \qquad (2.3)$$

$$ROOC^{-}Na^{+} + ROH \rightleftharpoons ROOCH + RO^{-}Na^{+} \qquad (2.4)$$

The initial amount of alcohol added plays a role in the induction during MeOH synthesis. During MeOH synthesis, an induction period is usually observed as a result of inadequate amount of alcohol for carbonylation. Variation of the initial amount of alcohol showed that increasing the amount of alcohol decreases induction period during testing [28]. Addition of excess alcohol did not significantly increase MeOH yield but eliminated the induction period. Since alkyl alkoxide is effective in catalysing carbonylation, enough amount of alcohol will help initiate the reaction at rapid rate and hence no induction. That is, the induction period occurs when the MeOH formed is not enough and it takes the induction period to accumulate enough alcohol (or MeOH) for appreciable amount of protons (H^{+}) available to restore the consumed alkoxide.

There are a few suggestions on how to make the alkoxide catalyst system. Caubere et. al. [43-45] has shown that an alkoxide system can be made from alcohols and NaH, which is a relatively inexpensive and simple reducing agent, (Equation (2.5)). They reported that NaH's 'super' basicity could pose some challenges as unselective reduction especially when in the presence of other functional groups could occur. A possible inclusion of some transition metals such as Co or Ni can help to control its basicity for carbonylation as well as hydrogenation reactions. Further discussion on the hydrogenation process will be highlighted in subsequent sections. Nevertheless, the alkoxide system made from only NaH and alcohol is relatively straightforward by simple addition. There are more stringent precautions to take however when handling the very reactive and flammable NaH [46].

$$CH_3OH + NaH \rightarrow CH_3ONa + H_2 \qquad (2.5)$$

An alternative route for making the alkali metal alkoxide system is via a hydroxide (e.g. NaOH) and MeOH reaction [40, 47, 48]. This route, as illustrated in Equation (2.6) is rather a fast equilibrium reaction and highly reversible. The H_2O produced in the process needs to be constantly removed to push the reaction towards the alkoxide product,

which therefore makes this option more involving compared to the NaH route. One approach is by evaporation of the water [48], where both hydroxide and alkoxide were considered non-volatile and only H_2O and alcohol boiled off. Alternatively, other authors reported that H_2O can be removed by using an excess amount of activated drying agent such as molecular sieve [40]. Overall, the hydroxide approach is safer than the NaH, but will be cost and energy intensive.

$$CH_3OH + NaOH \rightleftharpoons CH_3ONa + H_2O \qquad (2.6)$$

2.1.2 Hydrogenolysis of Methyl Formate

Hydrogenolysis can be defined as a process where there is carbon-carbon or carbon-hetero atom (O,N,S e.t.c) sigma bond cleavage accomplished by hydrogen (H_2) [49], as illustrated in Equation (2.7). This is a well-known process used in large-scale industrial production of fatty alcohols from natural fatty acid esters [25]. Furthermore, hydrogenolysis of short-length formate and monoesters are widely used for the production of MeOH and EtOH. Hydrogenation, which simply means the addition of H_2 to an unsaturated bond, is often indiscriminately used instead of hydrogenolysis. However, in this thesis, the two terms are different and will be used as defined above. In the LTMS process, the MeF produced from carbonylation undergoes hydrogenolysis to produce MeOH. Hydrogenolysis of MeF therefore will involve the cleavage of a C-O bond as illustrated in Equation (2.8).

$$C - X + H_2 \rightleftharpoons C - H + X - H \qquad (2.7)$$

Sørem's [50] thermodynamic calculations revealed marginal differences in conditions can lead to a significant effect on hydrogenolysis of MeF in liquid medium. Theoretically, pressure above 60 bars, temperatures below 180 ^oC, more than $1/5^{th}$ of reactor volume filled with liquid reagents and about MeF initial concentration greater than 5 mol % can lead to 98 % conversion. Several transition metals have shown some activity for hydrogenation and hydrogenolysis reactions [28, 33, 51], however not all have been

attractive as factors such as the cost, availability (or abundance) and safety issues play important role. Among the transition metals, Ni and Cu-based catalysts have gained more attention for MeF hydrogenlysis.

$$ROOCH + 2H_2 \rightleftharpoons ROH + CH_3OH \qquad (2.8)$$

2.1.2.1 Ni-based catalyst

The use of Ni as a hydrogenolysis catalyst was earlier patented in 1986 by the Brookhaven National Laboratory [52, 53]. Ni among other Mo, W, Co, Pd and Cr was shown to be very active in the LTMS as a hydrogenolysis catalyst [28, 53]. Typically, at 100 ^{o}C temperature, and 50 syngas (composed of $2H_2$/CO) bar pressure, Ohyama S. [28, 29, 54] reported that up to 92 % syngas conversion and 97 % selectivity to MeOH could be attained per batch in 2 h when $Ni(CO)_4$/CH_3OK were used as catalyst system. When the syngas was charged, formation of MeF initially increased to a maximum and then decreased. Meanwhile formation of MeOH remained constant until the MeF reached its maxima and then rapidly increased when the MeF formation declined. This variation of the products during the reaction indicated that MeF was an intermediate product, which is consumed with time. Furthermore, the product variation also suggested that the LTMS process involves two-steps; carbonylation for MeF formation discussed earlier, followed then by the hydrogenolysis step.

When the Ni source was varied, the activity was in the order $Ni(CH_3COO)_2$ > $NiCl_2$ >$NiSO_4$ and almost no activity with $Ni(NO_3)_2$ and Ni metal [54]. To identify the active component of Ni involved, an XAFS study showed that $Ni(CH_3COO)_2$ transforms into $Ni(CO)_4$ during reaction conditions. Further spectroscopic study showed that a hydridocarbonylnickel in the form of either $\{HNi(CO)_3\}^-$ or $\{HNi_2(CO)_6\}^-$ or both derived from $Ni(CO)_4$ was the active component [29, 55]. The formation of the active Ni ions corresponded with the rapid formation of MeOH, an indication that the $\{HNi(CO)3\}^-$ or/and$\{HNi_2(CO)_6\}^-$ was involved in the hydrogenolysis step. Whether the starting Ni was $Ni(CO)_4$ or $Ni(OCOCH_3)$, the peak for $Ni(CO)_4$ was observed which rapidly converted to the hydridocarbonylnickel

anion. This in summary implied that the $Ni(CO)_4$ is an important component of the Ni-alkoxide system which could not be avoided.

The necessary formation of $Ni(CO)_4$ in the Ni-alkoxide catalytic system is of a great concern. This is because $Ni(CO)_4$ is highly volatile and toxic [30, 56]. This poses a danger in their usage on industrial scale and even laboratory scale since a more stringent safety measure needs to be adhered to. This could be the reason why the Ni-alkoxide system, despite its high activity has not been industrialized. There is therefore a need to seek for active non-toxic alternative hydrogenation catalysts. In the next section, we examine the use of Cu-based catalyst as the hydrogenation catalyst.

2.1.2.2 $CuCr_2O_3$-based catalyst

Among the transition metals tested for hydrogenolysis of esters, Cu-based systems have received enormous interest [57]. Since the discovery of the MeOH synthesis via MeF described by Christiansen[23], Cu-based catalysts, in particular copper chromite (CuO/Cr_2O_3) oxide, have been much studied [25, 32, 50, 58]. CuO/Cr_2O_3 oxides were initially developed by Adkins et. al. [59] for hydrogenation and hydrogenolysis of a wide range of carbonyls. Consequently, several authors have used the CuO/Cr_2O_3 among other Cu-based catalysts for MeF hydrogenolysis.

2.1.2.2.1 Method of Catalyst development

Adkins et. al. [59, 60] first prepared copper chromite using a mixture of dichromate salt and cupric salt solution. The dried solution was exposed to flames of a Bunsen burner, which spontaneously decomposed to form fine powder of CuO/Cr_2O_3. The CuO/Cr_2O_3 made was active for hydrogenolysis of different esters at about 150-175 ^oC. By varying the composition, the catalyst, with excess CuO over cupric chromite ($CuCr_2O_4$) showed enhanced activity and therefore they stated that CuO was an active component with $CuCr_2O_4$ acting as a stabilizer.

Ohyama et. al. [32, 33, 57] introduced another CuO/Cr_2O_3 catalyst preparation route by using a physically milled mixture of CuO and Cr_2O_3 which was also active for MeF hydrogenolysis. When either CuO or Cr_2O_3 were milled and used separately as catalysts, very low activity was observed as compared to the mixture. Long milling time of the CuO and Cr_2O_3 mixture showed smaller particle size with high surface area. They reported that the long-term milling did not only lead to decrease in the catalyst size but also led to an increase in the intimate contact between fine CuO and Cr_2O_3 interfaces/grains with enhanced disorder in CuO crystallites. The particles with increased CuO and Cr_2O_3 interface and high surface area showed the highest activity for MeOH productivity. This further suggested that the smaller particle size increased the interface and ultimately promoted MeF hydrogenolysis.

Aside the above mentioned 'top-down' approaches, there are other 'bottom-up' approaches for fabricating copper chromite with diverse morphology for catalytic activities. For example, sol-gel [61, 62], hydrothermal [63] co-precipitation and ceramic method [64] have been reported to be used for synthesizing copper chromite. Most of these processes involve multiple steps using copper salt and dichromate salt mixture homogenised in appropriate solvent, accompanied by longer duration for the copper chromate formation.

2.1.2.2.2 Active site

In determining the nature of the active phase of Cu for the hydrogenolysis, Yureva and Plyasova [65] revealed that the nature of the Cu in a CuO/Cr_2O_3 depended on the method of hydrogen interaction during reduction. They reported that when a parent spinel CuO/Cr_2O_3 is treated with H_2 gas at 200-350 ^oC, a unique metallic Cu nanoparticle segregation occurs but reverts to the parent-like spinel structures when H_2 was replaced with He. They suggested that the spinel bulk absorbs protons from H_2, which helps in reducing Cu ions to metallic Cu nanoparticles epitaxially bonded to the oxide surface. The reduced state of the Cu in the oxide has been observed to exhibit high activity in

hydrogenolysis reaction [66, 67]. That is, the active Cu component appeared to be a reduced Cu or metallic Cu.

Additionally, Liu et. al. [68] used H_2 or N_2 at different temperature (230-270 ^oC) for the reduction of LaCuMn oxides and CuZn/AC (AC = activated carbon) to produce different Cu^+/Cu^0 compositions. When the different Cu^+/Cu^0 were tested for MeOH synthesis, separate Cu^+ and Cu^0 gave relatively lower conversions, compared to a 3 Cu^+:1Cu^0 mixture which gave the highest MeOH yield. They suggested that the active state of Cu for the MeOH synthesis is a mixture of Cu^+ and Cu^0 with some synergistic effect between the two states.

Furthermore, Prudnikova et. al. [69] used Cu containing $ZnAl_2O_4$, $CrFeO_4$ and $ZnCr_2O_4$ in different compositions to determine the active state of Cu in the methanol synthesis. They reported that the activity of the catalyst depended on the coordination environment of the Cu, such that gradual reduction of Cu ions to metallic Cu formation led to a decrease in activity. This was however in contrast to the proposed active component in the CuO/Cr_2O_3 catalyst. Nevertheless, it is important to note that the active sites can vary depending on the specific chemical environment and reaction conditions. Overall, the presence of Cu was necessary for the MeOH formation.

2.1.2.3 Other Cu sources

Ohyama's [58] study showed that when SiO_2 was impregnated with Cu, Co, Ni, Rh, Pd, Pt, only Cu, Pd, Co and Rh were catalytically active. Co/SiO_2 and Rh/SiO_2 showed highest conversion of CO but produced mainly higher hydrocarbons, and some MeOH and CO_2. This is not surprising as Co and Rh are known Fischer–Tropsch (FT) synthesis catalysts [70], and exhibited such in the liquid phase at 200 ^oC. Pd showed the highest MeOH selectivity even though it showed quite low conversion. They further tested Cu-Zn-Cr, which exhibited the higher activity for MeOH synthesis at 180 ^oC compared with the impregnated SiO_2.

Monti et. al. [71, 72] showed that Cu ion exchanged on SiO_2 was active for MeF hydrogenolysis. Their spectroscopic data indicated that the rate of MeF's carbonyl adsorption on Cu corresponded to the rate of hydrogenolysis of the MeF. In the presence of CO, hydrogenolysis rate decreased, however when the supply of CO is stopped, the activity was restored, suggesting a reversible inhibition of hydrogenolysis by CO. Nonetheless, the relative peak of MeF absorption did not change with or without CO, depicting a possible non-competition with CO and H_2 coverage on the catalyst surface.

Tonner et.al. [73] in an attempt to understand the LTMS, studied dehydrogenation of MeOH to MeF over different Cu based catalyst in gas-solid phase at 220 ^oC, and 1 bar. This is the reverse reaction of MeF hydrogenolysis. Cu on chromite, magnesia, chromia and silica together with Raney Cu and Cu oxide powder were all active for the dehydrogenation. The relative surface area of the Cu and Cu interaction (dispersion) with the oxide support seemed to play a role in the specific rate of MeF formation. Overall, Cu chromite catalyst emerged to be significantly more active with fewer side reactions such as decarbonylation than the others. Addition of either CO or H_2O did not affect the dehydrogenation reaction. On the other hand, Raney Cu deactivated rapidly among the other active catalysts but could be restored with either He or H_2 flow at 220 ^oC for 3 h. Addition of CO as well as increasing H_2O content and its consequent increase in CO_2 levels did not retard the deactivation profile, an indication that neither CO, CO_2 nor H_2O were responsible for the deactivation. They suggested that the deactivation was due to the adsorption of formaldehyde traces over the surface of the catalysts.

In summary, Cu appears to be active for the hydrogenation/hydrogenolysis reactions. Even though oxide support may play some role in reducing sintering or as a promoter. The exact state of Cu remains controversial, as reports on both metallic Cu and Cu oxides have been reported to be active.

2.1.2.4 Kinetics and mechanism

Liu et. al.'s [27, 74] kinetic study showed that the rate of hydrogenolysis over CuO/Cr_2O_3 catalyst increased with increasing temperature. Typically, between 140-180 ^oC temperature was an optimum range, above which rate declined and by-products such as methane formation increased. Based on fitting their experimental data to kinetic models using a non-linear regression method, they came up with a Langmuir-Hinshelwood type rate expression, shown in Equation (2.9). The expression suggested a dissociation of MeF after adsorption on the catalyst and a rather small H_2 adsorption that can easily be inhibited by the CO adsorption as suggested earlier.

$$r = \frac{1871.5e^{(-\frac{8347}{T})}C_{MeF}P_{H_2}C_{Catal}}{1 + (0.039C_{MeF})^{\frac{1}{2}} + 0.096P_{CO}} \qquad (2.9)$$

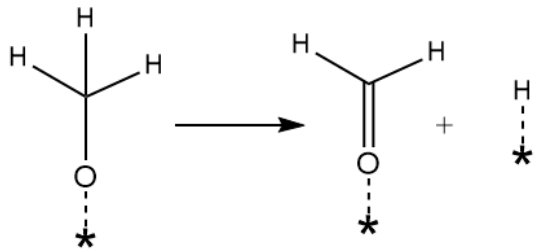

Scheme 2.1: C-H (D) bond breaking from methyl group

The reverse reaction of hydrogenolysis was studied using deuterium labelled MeOH for dehydrogenation to MeF over CuO/Cr_2O_3. It was observed that the rates of dehydrogenation (or dedeuteriation) between 180 to 200 ^oC for CH_3OH, CH_3OD, CD_3OH and CD_3OD were relatively 8.5, 4.4, 2.1, 1 respectively [75]. This was an indication of a large primary isotopic effect, which occurs at the methyl group involving a C-H (D) bond breaking as a slow step illustrated in **Scheme 2.1**. This is an indication that MeF hydrogenolysis may involve a hemiacetal formation and confirmed a possible formaldehyde adsorbed on the catalysts as an intermediate which is hydrogenated.

Furthermore, Monti et. al.'s [71, 72] spectroscopic study of MeF hydrogenolysis over Cu ion exchanged on SiO_2 indicated that the rate of MeF carbonyl adsorption on Cu

corresponded to the rate of hydrogenolysis of the MeF. When MeF was labelled with different numbers of deuterium, the rate of hydrogenolysis remained the same, suggesting no kinetic isotope effect. However, during the hydrogenolysis, transesterification rapidly occurred with low retention of the initial MeF's identity. Moreover, when only SiO_2 was used, there was neither change in the identity of the initial MeF nor any hydrogenolysis occurred. This was an indication that the hydrogenolysis involved transesterification of the MeF and were both catalysed by the Cu. When non-labelled MeF (CH_3OOCH) was reacted with D_2 (deuterium), no CD_3OH was observed ruling out any exchange at the aldehyde position. They suggested a possible hemiacetal species intermediate formed by either (i) a single addition to the carbon atom of associatively adsorbed MeF or (ii) addition of deuterium to the oxygen and then the carbon of the carbonyl group. Their proposed mechanism shown in **Scheme 2.2**.

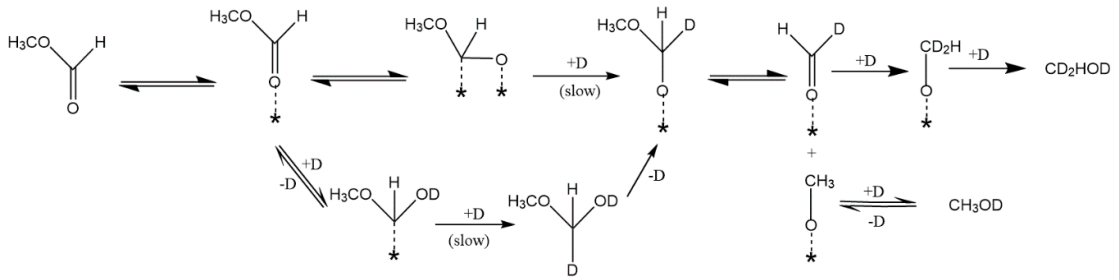

Scheme 2.2: Proposed hydrogenolysis mechanism [72]

2.1.3 Concurrent Reaction

The route to MeOH from syngas so far, has been discussed as a step-wise reaction, (i) carbonylation catalysed by alkali metal alkoxide and then (ii) hydrogenolysis catalysed by Cu-based system. While, this helps in understanding the mechanism as well as optimizes reaction conditions at each step; we will consider a third option, a concurrent system in a Cu alkoxide catalyst system. It is worthwhile knowing whether there is any synergistic relationship between the two steps and the catalysts involved.

Concurrent approach to MeOH synthesis based on a CuO_2/Cr_2O_3 and CH_3OK at 100-180 ^oC has shown to give high activity per batch [76]. For example, kinetic studies have shown that the rate of the reversible carbonylation reaction is about 5 orders of magnitude faster than the rate of hydrogenolysis [27, 74] . This implies that the hydrogenolysis reaction will be rate limiting during a concurrent process. In addition, carbonylation is favoured by low temperature while hydrogenolysis is favoured by relatively higher temperatures. It is expected that operating a concurrent system will not be adequately optimized for each step. However, when the two are run concurrently, the rate of syngas conversion is better than when hydrogenolysis is run separately. This suggested that the concurrent reaction is not a mere summation of the two steps but a possible synergy between the alkoxide and Cu catalyst system. Furthermore, the adsorption experiment of excess CH_3OK on CuO/Cr_2O_3 catalysts showed that at room temperature, some CH_3OK were adsorbed on the CuO/Cr_2O_3 catalyst. The adsorbed CH_3OK has been suggested to promote the synergistic relationship during the concurrent experiment.

Ohyama [26] reported that a combination of CuO/Cr_2O_3 and CH_3OK at 100 ^oC and 5 MPa showed high activity for MeOH production compared to CuO/ZnO conventional MeOH catalyst. When solvent was varied for the concurrent reaction, MeOH productivity was in the order glyme > diglyme > THF > triglyme >> ethylene glycol. This indicated that the aprotic polar solvents were more active than the protic polar solvent, an indication of possible stabilization of the CH_3O^- by protonation. When the type of alkoxide was varied, MeOH was only produced with CH_3OK or CH_3ONa but not for $(CH_3)_3OK$. They suggested that the role of the alkoxide system is to weakly interact (secondary bond) with the MeF for hydrogenolysis such that the bulky alkoxide was sterically hindered from such interaction.

Furthermore, Bo & Jens' [31, 35] study has also shown a possible synergistic effect in a 'once through' Cu-alkoxide system. They observed that, increasing the amount of either CH_3OK or Cu (Raney Cu or $Cu(CH_3COO)_2$) or both led to an increase in MeOH formation. When CO and H_2 were fed together, the amount of MeOH formed were more than three

times the amount of MeOH made when the CO and H_2 were fed step-wise at different times in the same catalyst system. Clearly, it appears there is a synergy between the two steps, however the mechanism for this effect is not well established.

2.1.4 Catalyst Deactivation

When the activity of the catalyst decreases with time, it is termed deactivation of the catalyst [77]. A catalyst with longer life time or easily regenerated is usually preferred as it has an effect on the economics of the process. It has been observed that syngas conversion decreases linearly with time (or number of batches) during a typical concurrent MeOH synthesis [35]. The source of deactivation in the concurrent system could be from either of the catalyst or both.

Ohyama [26] reported that during a concurrent process, the reduction of activity could appreciably be restored when fresh CH_3OK was added. This indicated that consumption of the alkoxide was the main source of deactivation. They suspected that CH_3OK could be consumed by trace amounts of H_2O and CO_2 from the starting syngas reactants or by-products from water gas shift reaction (see Equation (2.10) [78, 79]). The H_2O and CO_2 react with alkoxide to produce formate and carboxylates respectively as illustrated in Equations (2.11)-(2.13). In a carbonylation study, Lui et. al. [27] observed formate, CO_2, and dimethyl ether as products. When excess CO_2 was added to alkoxide, no CO carbonylation was observed due to a reaction between CO_2 and alkoxide as illustrated in Equation (2.13). This was an indication of an irreversible poisoning of the alkoxide by CO_2.

$$CO + H_2O \rightleftharpoons CO_2 + H_2 \qquad (2.10)$$

$$H_2O + CH_3OK \rightleftharpoons CH_3OH + KOH \qquad (2.11)$$

$$CO + KOH \rightleftharpoons KOOCH \qquad (2.12)$$

$$CO_2 + CH_3OK \rightleftharpoons KOCOOCH_3 \qquad (2.13)$$

In a hydrogenolysis study, Sørum [50] reported that CO, H_2O and CO_2 can all retard MeOH formation such that minimizing their presence led to increase in activity. They observed that CO adsorbs strongly than H_2 and therefore competes with H_2 for adsorption on the CuO/Cr_2O_3 catalyst surface. They suggested that H_2O on the other hand reacts with MeF to give CO_2 (Equation (2.14)), which subsequently reacts with surface OH to form bicarbonate (Equation (2.15)). Therefore leading to the reduction in the hydrogenolysis process over time.

$$HCOOCH_3 + H_2O \rightleftharpoons CH_3OH + CO_2 + H_2 \quad (2.14)$$

$$* - OH + CO_2 \rightleftharpoons * - HCO_3 \quad (2.15)$$

On the other hand, other authors have attributed the deactivation during hydrogenolysis to a blocking of the active sites with a polymer. Monti et. al. [71] reported that in the presence of a high amount of CO, a residue material suspected to be a polymerization of formaldehyde is formed which leads to a continuous deactivation of the $Cu\text{-}SiO_2$ catalyst. They suggested that formaldehyde formed during the LTMS forms part of a polymer. Although the polymer does not adsorb on the active Cu site, it eventually accumulates over both the support and the catalyst surface making the active site inaccessible. Furthermore, Tonner et.al.'s [73] study of dehydrogenation of MeOH to MeF over CuO/Cr_2O_3, revealed that addition of either CO or H_2O content and it consequent increase in CO_2 levels did not retard the deactivation profile. This indicated that neither CO, H_2O nor CO_2 were responsible for the deactivation of CuO/Cr_2O_3 for the reverse reaction of hydrogenolysis. They also attributed the deactivation to adsorption of formaldehyde polymer traces over the active Cu surface.

Overall, while there is some consensus on the adverse effect of H_2O and CO_2 on the alkoxide system, the deactivation pathway of the Cu-based catalyst remains unclear. Nevertheless feed cleaning by absorbing H_2O and CO_2 from syngas before MeOH synthesis reactor will reduce their contribution to deactivation. Further, if a very active hydrogenolysis catalyst is developed, hydrogenation of formaldehyde will be rapid such that polymer formation will be suppressed. Moreover, such active catalyst could present the possibility of hydrogenating carboxylates formed from CO_2 formation.

2.1.5 Alternative Low Temperature MeOH synthesis

2.1.5.1 Alcohol-Assisted Approach

Alcohol assisted MeOH synthesis advanced by Tsubaki et. al. [80-87] is yet another approach to making MeOH at lower temperatures than the current conventional technique. This approach also uses Cu-based catalysts and syngas ($CO/CO_2/H_2$) reactants for MeOH synthesis at about 180 ^oC temperature using ethanol as solvent. Over a Cu/ZnO catalyst, MeOH yield increased with increasing ethanol whilst no MeOH was produced at temperatures below 180 ^oC. They observed that the rate of the reaction increased with increasing CO_2 content as opposed to the rate retarding when the reaction was carried out in only CO and H_2. Here the presence of CO_2 was activating and necessary for the synthesis process. Fan et. al. [88, 89] also reported that when CO_2 and H_2 were the reactants, an initial increase in ethyl formate was observed and then decreased at the expense of MeOH with time and temperature. The alcohol assisted approach is suggested to involve 3 major steps as illustrated in Equations (2.16)-(2.19) as; (i) hydrogenation of CO_2 (or CO) to formic acid, (ii) formic reaction with ethanol to form ethyl formate, and (iii) hydrogenolysis of ethyl formate into ethanol and MeOH . Therefore, ethanol played a dual role as a solvent as well as a catalyst.

$$CO + H_2O \rightleftharpoons CO_2 + H_2 \qquad (2.16)$$

$$CO_2 + H_2 \rightleftharpoons HCOOH \qquad (2.17)$$

$$HCOOH + C_2H_5OH \rightleftharpoons HCOOC_2H_5 + H_2O \qquad (2.18)$$

$$HCOOC_2H_5 + 2H_2 \rightleftharpoons CH_3OH + C_2H_5OH \qquad (2.19)$$

Cu-based catalyst with various oxide supports is believed to be the active component for the alcohol-assisted route. When different ratios of Cu/Zn mole ratios prepared by co-precipitation were tested, the highest syngas conversion was observed for Cu/Zn=1, which also exhibited the highest Cu BET surface area [84, 90]. Jeong et. al.'s [91] investigation indicated that the size of the Cu in Cu/ZnO influences the catalyst activity in the MeOH synthesis. When the pH of the conventional co-precipitation was varied,

the particles prepared at pH = 8 gave the smallest and most acidic Cu crystallites and consequently the highest MeOH yield. This revealed that Cu crystallite size as well as its acidity have the tendency to influence MeOH synthesis.

Cu on other supports aside ZnO has also been shown to be active for the alcohol assisted MeOH synthesis between 150 ^{o}C to 180 ^{o}C. For example, Cu on either MnO or MgO support was observed to be very active for syngas conversion with high MeOH selectivity [87, 92]. Hu et. al. reported on alkali metal promoting behaviour of a Cu/MgO catalyst for the MeOH synthesis [93-96]. When Cu/MgO was doped with different alkali metal in the presence of HCOOM (where M was alkali metal) activity decreased in the order Na > K > Rb > L. They suggested that moderate basicity was more favourable for the MeOH synthesis over Cu/MgO as Na and K showed the highest activity. When the alkali metal was varied for the HCOOM, HCOONa was most active and more stable. In the absence of HCOOM, Cu/MgO was active but activity rapidly decayed with time. The total moles of Na in the HCOONa and Cu/MgO-Na showed a linear dependence on activity and they suggested a synergistic effect for the MeOH synthesis. This approach also supports Tsubaki's suggested mechanism with formate intermediate formation since the presence of HCOONa enhanced activity.

The alcohol-assisted mechanism discussed so far presents a very interesting pathway for making MeOH. The alcohol-assisted approach has the advantage of CO_2 and H_2O tolerance, which is deactivating in the low temperature MeOH synthesis assisted by alkoxide. Nevertheless, the operational temperature in the alcohol-assisted mechanism is still higher than thermodynamically allowed for full syngas conversion per pass at comparable pressure. The alcohol-assisted MeOH synthesis operates at almost twice the temperature at which that of the alkoxide-assisted operates. Therefore, the alcohol-assisted mechanism have lesser conversion (or specific activity) per batch compared to the alkoxide-assisted MeOH process. Furthermore, operating the alcohol-assisted mechanism will require pure syngas without N_2 in order to maximize conversion per pass. It is also interesting to note that both the alcohol assisted and the alkoxide-assisted mechanisms involve an ester, alkyl formate intermediate formation. In addition, both

systems require a Cu-based catalyst, the activity of which is enhanced by the addition of a base or a basic environment. It will be interesting to determine whether both processes approach similar mechanisms but at different temperature regime.

2.1.5.2 Nano-catalysis Involved in Low MeOH Synthesis

Other groups have also considered the use of nanoparticles in MeOH synthesis at lower temperature conditions than the conventional ICI MeOH synthesis. Vukojevic et. al. [97] reported on the use of aluminium-stabilized Cu colloids of about 5 nm for MeOH synthesis in a quasi-homogeneous system. The 5 nm metallic Cu colloid particles which were produced by trialkylaluminium reduction of copper acetylacetonate, was observed to be active for MeOH synthesis in THF solvent. The activity of Cu colloidal system, using 74 H_2: 20 CO: 6 CO_2 syngas was found to be comparable with the commercial ICI $CuO/ZnO/Al_2O_3$ catalyst (around 5 $mol_{MeOH}/kg_{Cu}h$) at 150 ^oC coupled with MeF intermediate. They suggested that the presence of ZnO was not an absolute necessary component for the heterogeneous MeOH synthesis catalyst based on Cu.

Ceria supported Cu nanoparticles is also reported to be active for MeOH synthesis [98, 99]. Shen et. al.'s [98] work using co-precipitated 10 wt % 14 nm Cu in 4 nm CeO_2 particles showed a higher $2H_2$:1CO syngas conversion to MeOH relative to a commercial $Cu\text{-}ZnO\text{-}Al_2O_3$ catalyst at 195 ^oC. During the MeOH synthesis, initial metallic Cu particles oxidized to Cu_2O while their mean particles halved accompanying an increase in activity. Further oxidation of Cu_2O to CuO and growth of CeO_2 particles led to a gradual deactivation. They suggested that the Cu^+ was the activate Cu species which is stabilized by the CeO_2.

Aside the direct syngas conversion, CO_2 can be converted to MeOH indirectly via carbonates. Tamura et. al.[99] for example reported that dimethyl carbonates can be converted to MeOH over Cu/CeO_2 at 160 ^oC and about 80 bar H_2 pressure in THF. They observed almost 100 % dimethyl carbonate conversion with more than 90 % selectivity to MeOH after 24 h. XANES, XRD and TEM data indicated that sub-nanoparticle (< 1nm)

metallic Cu 1 nm formed from Cu(I)/CeO2 exhibited high hydrogenolysis activity. Similarly, Lian et. al [100] also showed that the CO_2 via ethylene carbonates can undergo hydrogenolysis using CuO/Cr_2O_3 nano-catalysts at 180 ^oC and 50 bar H_2. They observed up to 60 % and 93 % selectivity to MeOH and ethylene glycol respectively, with CH_4, CO and CO_2 as side products. Activity severely dropped when metallic Cu was washed with aqueous $FeCl_3$, and suggested that metallic Cu in the Cu/Cr_2O_3 was the catalytic active species made during H_2 reduction pre-treatment.

Overall, Cu particles appear to be effective in MeOH synthesis. Even though the state of the Cu can be controversial, it is imperative that the chemical and operating environment can have an effect on the active state. Nevertheless, most of the reported work support a reduced Cu than a fully oxidized Cu (Cu^{2+}). Employing oxide support can also be valuable in getting the right environment for the active state of the Cu, and these supports can be variance. The mechanism involved in MeOH synthesis, appears to have some common intermediates and the possibility of some slight deviation at different temperatures need to be investigated. Irrespective of the mechanism, whether direct or indirect synthesis approach, the role of the Cu nanoparticles needs to be addressed, whether some intrinsic properties are involved or the mere exposed surface. Study of Cu nanoparticles without any support or any strongly binding ligands can help to unearth the role of the nanoparticles, as there will be no oxide-support property to account for. Furthermore, it is important to device a faster, cheaper and environmentally friendly way of making such active Cu nanoparticle catalyst to facilitate the reaction.

2.2 Cu nanoparticles for Catalysis

A catalyst is a material that speeds up the rate of chemical reaction without taking part in the stoichiometry of the reaction. Catalysts provide alternative pathway for a reaction by lowering the activation energy of the reaction. **Figure 2.1** shows the difference in the energy barriers and reaction pathways of catalysed (lower) and non-catalysed (upper) reaction. Typically, reactants bond with the catalyst, thereby

weakening the reactant's interatomic bonds. Thus increasing the probability of a favourable orientation of the reactant molecules as well as increasing the number of collisions between the reactant molecules. Nevertheless, both catalysed and non-catalysed reactions have the same initial and final potential energies. Therefore, a catalyst only affects the kinetics and does not change the thermodynamics of the reaction. [101]

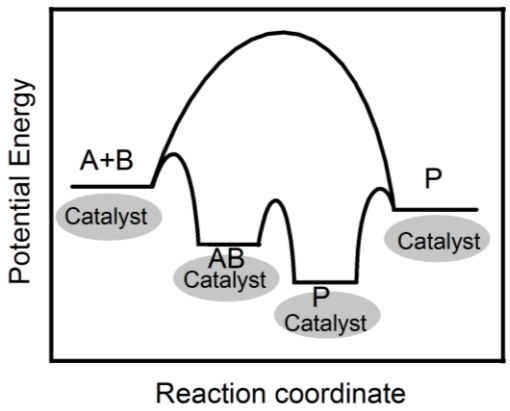

Figure 2.1: Potential energy diagram versus progress of reaction for a non-catalysed reaction (upper path) and a catalysed reaction (lower path). Adapted from[101]

A catalyst can be in the form of atom, smaller or larger molecules or even solid surfaces. Catalytic processes can simply be distinguished based on the phase of the reactants and the catalyst involved. When both catalyst and reactants are in the same phase, for example, when both are in liquid phase, it is classified as homogeneous catalysis. When the catalyst and the reactant phases differ, for example solid catalyst and gas reactants, it is classified as heterogeneous catalysis. It is important to note that both homogeneous and heterogeneous catalysis are complimentary in applications as the advantages and drawbacks of one is usually the opposite of the other. For example, homogeneous systems which arise from the molecule type of catalysts, have better mass transport efficiency, are more active and selective but are difficult to recycle or recover the catalyst after the process. Heterogeneous catalysis on the other hand deals with solid surface catalysts, which are easy to recover but require more drastic reaction conditions and are less mass transport efficient. [102]

One domain that bridges a traditional solid catalyst and molecular catalyst is the use of nanomaterials as catalyst [103]. Nanomaterials are materials in the nano meter (10^{-9} m) dimension. The surface energy and morphology of nanoparticles are highly size dependent, which coupled with larger surface area translates into an enhanced reactivity of nanocatalysts [104, 105]. Nanocatalysts exhibit high reactivity compared to the bulk due to the different sizes and shapes, which gives rise to distinct quantum properties [103, 106]. As shown in **Figure 2.2**, the functional sites of nanomaterials can be ordered to specific reactivity compared to non-nanomaterials. This therefore gives nanomaterials both homogenous and heterogeneous catalysts-like properties such as mass transfer efficiency, selectivity and ease in recovery.

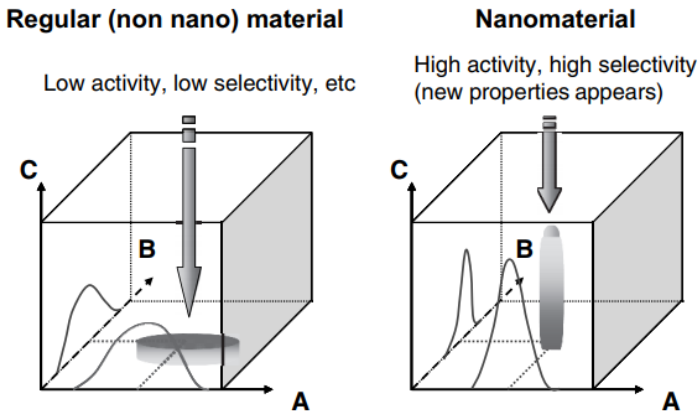

Figure 2.2: Nanoarchitecture: an avenue to superior precision. Axes are: A: composition of functional sites; B: ordering level of sites; C: functional properties of material, adopted from [103]

2.2.1 Cu Nanoparticles Synthesis

The earth's abundance and inexpensive source of copper compared to other noble metals makes them attractive for several applications including catalysis [107]. The process of fabricating nanomaterials is very important in obtaining the right size and morphology for catalytic applications [108, 109]. Synthesis of Cu nanoparticles (NP) has therefore attracted much attention over some time now due to its unique applications. The procedure for making Cu NP can either be by a 'bottom-up' or 'top-down' approach. Even though both approaches present their own advantages and disadvantages, the

'bottom-up' approach is commonly used since it provides more flexibility in controlling particle size and morphology. Some of the reported method of synthesis include chemical treatment, electrochemical synthesis, photochemical techniques, sonochemical method and thermal treatment. Chemical reactions involved for Cu NP synthesizes can be (a) reduction, (b) oxidation, (c) hydrolysis or (d) condensation, depending on the desired product. If metallic Cu for example is the desired product, reduction of either Cu(I) or Cu(II) is employed. On the other hand, when CuO is desired, hydrolysis of the Cu precursor followed by dehydration is used. [110].

Some of the important procedures in the chemical treatment is sub-classified as (i) wet chemical, (ii) reverse micelle, (iii) microwave (MW)-assisted (iv) biosynthesis and (v) ionic liquid (IL)-assisted method. The wet chemical technique is mostly used to produce metallic Cu NP, which involves a reducing agent that provides electrons to reduced Cu salts. Such processes could involve capping agents to stabilize and control particle growth [111]. The reverse micelle involves water in oil microemulsions, where polar head of surfactants molecules are attracted to aqueous core whilst the apolar part is directed outside. This forms a nanoreactor (nanometer scaled) droplet to uniformly control the size and shape of the Cu NP during precipitation [112]. MW-assisted technique has also been reported to give a high rate and high yield Cu NP when the synthesis reaction is exposed to microwave irradiation [113, 114]. Some plant extracts have also been used as both reducing and capping agents in what is termed as biosynthesis of Cu NP [115]. The IL-assisted synthesis is a straightforward top-down technique using ionic liquid to solvate Cu microparticles to dissociate into nanoparticles [116]. In a review by Gawande et. al., [110] a summary of the above mentioned chemical treatment techniques with specific examples and their approximate Cu particles sizes have been sufficiently discussed. Overall, different protocols with multi-steps were required to fabricate particularly Cu NP size and shape.

A straightforward recipe for making on-purpose Cu NP, with the flexibility of physically fine-tuning particle sizes for example by mere variation of physical parameters will be a valuable contribution to nanoparticle synthesis. The use of the spinning disk reactor

(SDR) present one of such straightforward approach for nanoparticle synthesis. The SDR is a continuous-flow process intensification reactor with an enhanced production efficiency, safety, minimal cost and minimal waste technology [117, 118]. When a liquid is introduced unto the centre of a rotating disk, the centre of rotating surface generates an outwardly flowing film on the rotating surface. Initial shear stress generated at the disk accelerates the film tangentially. Subsequently, as the liquid nears the local angular velocity, it moves as a thin film under the prevailing centrifugal acceleration. Once the surface is fully wetted, thin films (about 50 μm) is generated. This thin film has short diffusion and conduction path length for excellent heat, mass and momentum transfer.

Based on the Nusselt theory, the residence time, t_{res} of liquid reagents traveling with Q flow rate, from r_{in} to r_{out} on the disk can be expressed by Equation (2.20), where μ is dynamic viscosity and ω is angular velocity. (Nusselt's theory assumes there is no shear at gas-liquid surface, film is ripple-free and no tangential slip at disc-liquid surface). Hence, increasing the flow rate and rotation speed for example will lead to a shorter residence time and consequently affect the crystallization process [119]. Notably, the key characteristics of the thin film flow include rapid mixing, heat and mass transfer, plug flow and short residence times of the order of seconds [120]. This makes the SDR very useful for performing exothermic reactions with a water-like medium. The SDR can therefore be employed in a sol-gel process for the synthesis of nanoparticle where micromixing and macromixing time is essential in controlling nucleation and crystal growth.

$$t_{res} = \frac{3}{4}\left(\frac{12\pi^2\mu}{Q^2\omega^2}\right)^{\frac{1}{3}}\left(r_o^{\frac{4}{3}} - r_i^{\frac{4}{3}}\right) \qquad (2.20)$$

3 Experimental

This chapter consists of the experimental procedure for MeOH synthesis. In particular, the reactor set-up for the MeOH synthesis as well as the synthesis techniques used for Cu-based nanoparticles are reported and discussed. The analytical instruments used for analysing products from the syngas conversion as well as characterization of the catalyst system is also discussed.

3.1 The Reactor Set-up

The schematic diagram of the set-up used in this work is shown in **Figure 3.1**. A high-pressure (100 bar) batch reactor was used for the major part of this work. This consisted of a 200 ml volume and 60 mm diameter wide stainless steel hpm-020 type autoclave (Premex Reactor AG). The interior part of the batch reactor was lined with a replaceable 316-alloy stainless steel liner to preserve the reactor from corrosion. A 52.62 x 3.53 mm Teflon (FKM-80 BS233) O-ring was placed in between the reactor and the lid to seal the reactor completely from leakage. The reactor was equipped with pressure sensors and a thermocouple inserted into it to monitor internal pressure and temperature respectively. The thermocouple was inserted into the liquid to monitor the liquid temperature, while the pressure sensor was placed above the liquid to monitor gas pressure. The internal temperature and pressure in the reactor was independently logged onto a PC.

Furthermore, a dip-tube was inserted into the reactor for liquid sampling, together with other valves to control inlet and outlet of gas. A spring-operated Nupro security relief valve was set at 100 bars for safety. The reactor was stirred using a magnetic stirrer head attached to a stirrer with oblique impeller blades (approximately 30^{o} angle). The impeller extended to near the bottom of the reactor to ensure adequate mixing. The magnetic stirrer head was externally attached to an electric BCH Servo Motor. The Motor was coupled with a lexium 23 drive to give a high rotation precision for rotations

ranging between 1000 to 3000 rpm. The autoclave reactor was inserted into a metal block heated by silicon oil controlled by a Huber Ministat 230 thermostat with adjustable operating temperatures between -33 to 200 ^{o}C. The reactor set-up was placed in a fume cupboard for safety and the laboratory was equipped with H_2 and CO detectors to monitor possible gas leakage.

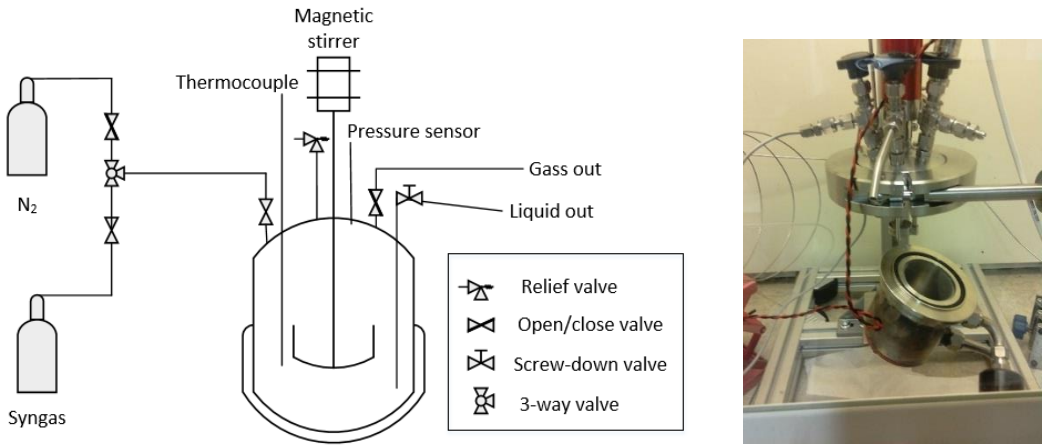

Figure 3.1: Experimental set-up for the methanol synthesis

3.2 Low Temperature MeOH Synthesis

3.2.1 Once Through Experiment; Synthesis of Cu Nanoparticles

In the one-pot experiments, a known amount of solvent was added to a weighed amount of copper acetate ($Cu(OAc)_2$, 98 %) and dry sodium hydride (NaH, 95 %) in the batch reactor (all liquid and solid reagents were purchased from Sigma-Aldrich). Under about 1 bar N_2 blanket, the mixture was stirred and heated to a predetermined temperature for a set period of time. The internal temperature was typically set to about 80 to 150 ^{o}C. Thereafter the reactor was cooled to ambient temperature (< 30 ^{o}C) followed by addition of known amount of MeOH (99.8 %). The resulting mixture was stirred at ambient temperature for about 30 min to ensure that all NaH had reacted to give the sodium methoxide co-catalyst. An approximately 1 ml slurry sample was taken

for analysis using the dip tube in-between the reaction steps. The resulting slurry was directly tested for MeOH synthesis as described in the following section.

3.2.2 Catalytic Testing

Generally, the MeOH synthesis was performed by placing known amounts of catalyst and solvent in the reactor. The reactor was purged with the reactant gas to ensure no air was present and then charged with the same to the set pressure for the experiment at ambient temperature. Mostly syngas made up of $2H_2$/CO (± 2%, premixed) pressurized to 20 bar was used for the concurrent experiments, while different gas compositions such as CO, CO_2, H_2 and N_2 were used for the step-wise studies. After the reactant gas pressure was set in the reactor, the mixture was heated to the set temperature for the experiment coupled with stirring at a set rotation speed. The standard rotation speed and reaction temperature were respectively 3000 rpm and 100 ^oC with variations in some of the experiments. After a set reaction time, the reactor was cooled to ambient temperature. Reactant conversion was determined either by the difference in pressure drop or by gas chromatography (GC) or both depending on the focus of the particular study. However, by combination of the two, mass balance from gas pressure drop and syngas GC analysis for concurrent experiments was determined to be about 85 ± 5 %.

3.2.3 CuO/SiO_2 Catalyst Synthesis

CuO/SiO_2 catalyst was prepared mainly for performance comparison with Cu catalyst prepared from the once through system. Similar protocols were followed as reported in [121] and [122] albeit with some modifications. About 100 ml of 0.5 M $Cu(NO_3)_2{\cdot}3H_2O$ was prepared in a three necked round bottomed flask. Then a 100 ml 1 M L-ascorbic acid was added dropwise while stirring. 49 g of 40 wt % SiO_2 dispersed in water was added to the mixture, and then aged for 3 hr at 100 ^oC. The resulting slurry mixture was

cooled, centrifuged and washed with distilled water 3 times. The wet sample was oven dried at 70 ^{o}C overnight. The dried particles were calcined at 550 ^{o}C for 3 h. The calcined CuO/SiO_2 catalyst was then characterized and tested for LTMS reaction without further pre-treatment.

3.2.4 Cu Nanoparticle Synthesis using Spinning Disk Reactor

The spinning disk reactor (SDR) was used for tuning the particle size of copper nanoparticles. Schematic diagram of the SDR set-up used in this work is shown in **Figure 3.2** similar to the one described elsewhere [117, 118]. A 10 cm diameter smooth surfaced stainless steel disk, driven by a 125 W electric motor, coupled with a digitally controlled rotating disk was used. The temperature of the disk surface was controlled with a regulated water-bath, which circulated beneath the disk to ensure constant disk temperature. Aqueous solution of the copper precursor was placed in one line and that of the reducing agent placed in the second line, and both fed directly onto the centre of the spinning disk. The solutions were pumped unto the disk using a Watson Marlow 323 peristaltic pump coupled with a dampener at the discharge end to ensure a smooth flow of reagents. The feeding tubes were made of Viton, with 3.2 mm hole ends, set at 6 mm distance perpendicular to the centre of the spinning disk. The reaction was carried out under a N_2 blanket to minimize direct contact of the reaction with air.

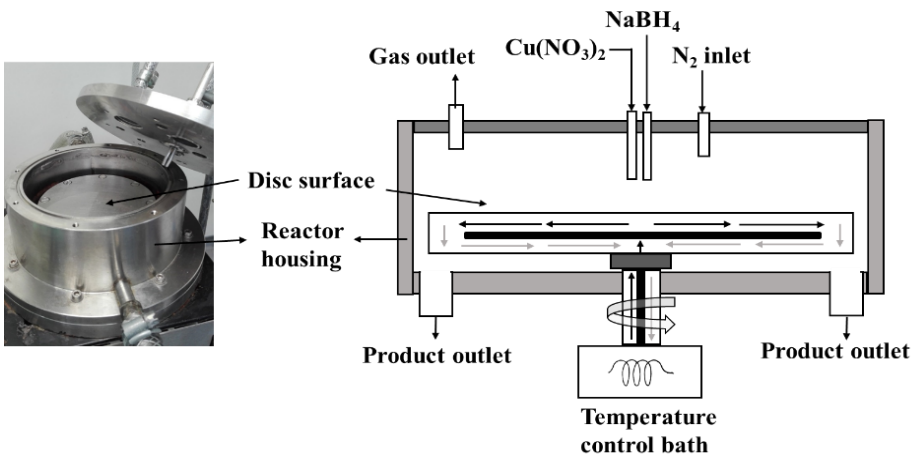

Figure 3.2: Scheme of SDR set-up used in making Cu nanoparticles

3.3 Analysis Methods

3.3.1 Gas Chromatography, MSD & TCD

One major analytical tool used in this work is the gas chromatography (GC) coupled with a mass spectrometry detector (MSD) and thermal conductivity detector (TCD). The chromatographic method is used to separate a solute sample between a mobile and a stationary phase. In GC, the *mobile phase* is an inert *carrier* gas while the *stationary phase* is either a column consisting of a wide-bore *packed* tube filled with particulate material (2-4 mm diameter and 2-6 m long) or a *capillary* coated open tubular column. Capillary columns (about 150-300 µm internal diameter and 30-100 m long) are more efficient in separation since they have a long column, which increases resolution. On the other hand, packed columns are cheaper, and efficient in light gas analysis. Samples injected into the GC, are carried through the column by the carrier gas while the different compounds are separated when they interact with the stationary phase and elute at different *retention times* depending on the degree of interaction with the stationary phase. [123]

The eluent from the GC can be identified and quantified using various detectors including thermal conductivity detector (TCD) and mass spectrometry detector (MSD). The TCD operates based on the thermal conductivity of the mobile phase as it passes over tungsten-rhenium wire filament. The changes in thermal conductivity of the mobile phase due to the presence of solute compensated by a reference gas is detected and measured as a signal proportional to the solute's concentration. The TCD can detect all solutes with different thermal conductivity as a universal detector but is limited in sensitivity compared to other popular detectors [123]. The MSD on the other hand is extremely sensitive and has diverse applications. A sample introduced into the MSD is ionized and is accompanied by some molecular fragmentations. Consequently, the ion fragments are accelerated and separated according to their mass-to-charge ratio and detected in proportion to their abundance. The MSD functions under high vacuum to

allow ion fragments to reach the detector without colliding with other gaseous molecules. [124].

An Agilent 7890A GC was used for analysing liquid and gas samples in this work. The schematic of the GC flow design used is shown in **Figure 3.3**. The GC was equipped with both capillary and packed columns, which directly eluted into the MSD and TCD respectively. CARBOWAX 007 series 20 M capillary column with dimensions 60 m x 320 µm x 1.2 µm was used for the liquid analysis. This was programmed as follows; temperature was ramped by 15 ^{o}C/min from 40 ^{o}C initial temperature to 200 ^{o}C in most cases and held at 200 ^{o}C for 3 min, at 0.47 bar (6.8 psi) constant pressure. The liquid sample was injected using an Agilent 7683B autosampler and analytes identified and quantified by an Agilent 5975 MSD. 0.54 mg Heptane was added to each sample vial as an internal standard. The gas injection valve was connected to 2.7 m Porapak Q and 1.8 m Molecular Sieve 5 Å packed columns in series and elute into the TCD for analysis of permanent gases and up to C_2 hydrocarbons. The gas stream flow direction was controlled using 10 and 6-port valves, which also allows for backflashing heavier analytes via a 0.9 m Hayesep Q pack column.

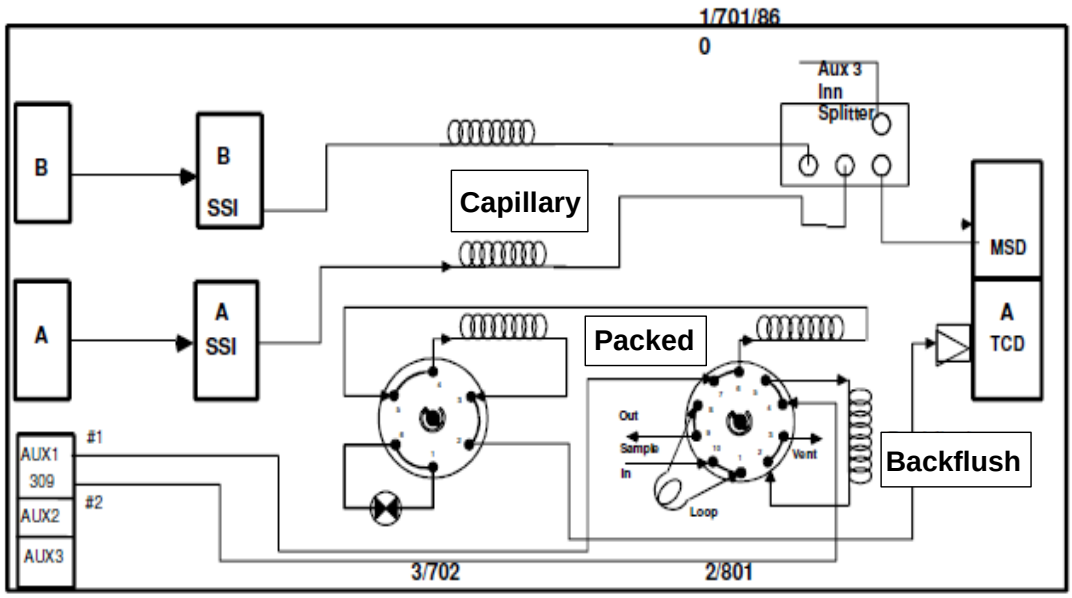

Figure 3.3: Schematic showing the GC-MS flow set-up design

3.3.2 X-ray Diffraction (XRD)

X-ray diffraction (XRD) helped to identify the crystalline phases and the crystallite sizes of the Cu-based catalysts used in this work. The X-ray beam interacts with crystalline surfaces to give a characteristic diffraction pattern of the sample. The diffraction occurs by elastic scattering of the X-ray photons by the atoms in a periodic lattice of the crystalline material. When the photon path length is equal to the integer multiple of the wavelength of the X-ray beams, it implies that the diffractive beams are in phase and produces a constructive interference. This interference allows the use of Bragg's law to relate the wavelength of the beam (λ), the diffraction angle Θ, and the lattice spacing, d (distance between two lattice planes) as shown in **Figure 3.4** and expressed by Equation (3.1). The lattice spacing is a characteristic of the crystalline material. The relative intensity and positions of peaks in the powder diffraction pattern can be compared to known phases, which make it easy to identify a known framework. The unit cell dimensions can be determined using the peak position while the peak width helps to determine the crystal size. [125]

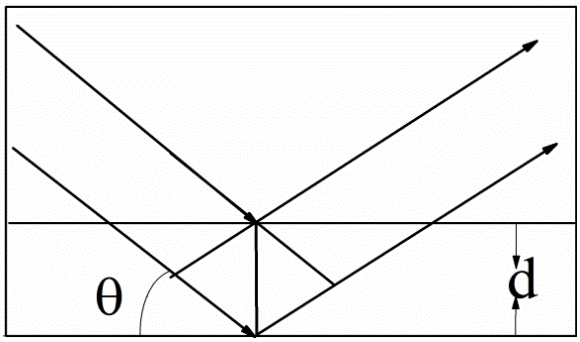

Figure 3.4: Simple schematic representation of photons reflecting from atomic planes

$$n\lambda = 2dsin\theta \qquad (3.1)$$

The XRD measurement in this work was based on powder techniques. A routine Bruker D8 Discover diffractometer was used for analysing dry samples while a multi-purpose Bruker D8 A25 diffractometer was used for analysing slurry samples. The routine

powder instrument uses Cu K-alpha radiation with wavelength, λ= 1.5406 Å and a Lynxeye detector. The dry samples were prepared by mixing with isopropanol on a glass plate and the liquid portion allowed to evaporate in order to attain flat surface. The plate was mounted on a standard stage and the X-ray diffractogram was measured at 0.021° step/s for an interval of 5-90 ° 2 theta.

The multi-purpose instrument uses Mo K-alpha radiation with wavelength, λ= 0.71076 Å and Lynxeye detector with "hardened" chip for Mo radiation. The stage of multi-purpose instrument was adjustable providing the flexibility to use a spinning capillary sample holder for analysing the slurry samples. The slurry samples were prepared by pipetting about 10-15 µL of the sample into a capillary tube with 0.5 mm internal diameter, and then centrifuged at 2000 rmp for 10 min to settle the solid portion at the bottom. The tube was then mounted and adjusted on the capillary spinner such that the X-ray beam measures around the capillary bottom where the particles were concentrated. The X-ray diffractogram was measured at 0.023 ° step/s for an interval of 15-35° 2 theta. Total Pattern Analysis Solution (TOPAS) software was used for quantitative Rietveld analysis of the diffractogram. This software fits theoretical diffraction pattern to a measured diffraction pattern using non-linear least square algorithms [126]. This method was used to quantitatively determine the phase composition and crystallite sizes of the catalysts used in the current work.

3.3.3 Transmission Electron Microscopy (TEM)

Transmission electron microscopy (TEM) is a microscopic technique used to study in detail properties of solid materials including, size, morphology, composition and crystallographic information of the sample. The use of electrons with its characteristic small wavelength (< 1 Å) makes the TEM very versatile for probing details of materials to nanometre and sub-nanometre scale. A ray path diagram showing two basic operation mode of the TEM is shown in **Figure 3.5**. A high accelerated electron beam (usually around 120-400 KeV) passes through series of condenser lens to produce

parallel rays that impinge on the sample. The transmitted electrons (attenuated based on density and thickness of the sample) forms a 2-dimensional projection of the sample, which is magnified by a series of optical lenses to give an image (bright field) on a screen. The TEM can easily be switched into a diffraction mode, adjusting the image-system lenses such that the back focal plane of the objective lens acts as the object plane for the intermediate lens. [127, 128]

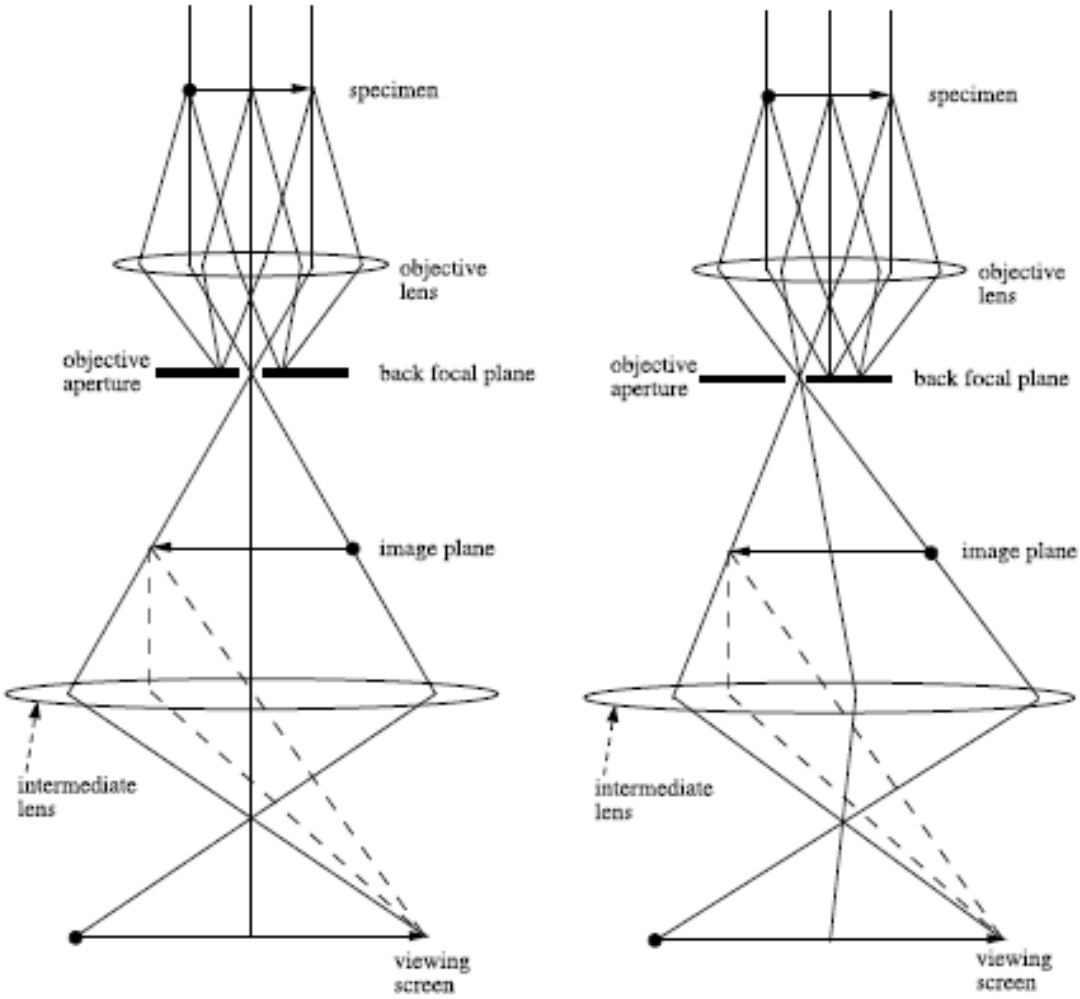

Figure 3.5: Ray diagram of the TEM operating in bright-field mode (left) for imaging and dark field mode (right) for diffraction, adopted from [127]

A Joel 2100F TEM was used to characterize the Cu-based nanoparticles used in this work. Samples were prepared by adding methanol and placed in ultrasound bath for about 30 min to separate agglomerated particles, since thicker agglomerates will limit electron

beam transmission. The solution was then dropped onto a carbon film supported by either a nickel or copper grid. The grid was then allowed to dry overnight and placed carefully on an appropriate sample holder. The sample is then mounted in the goniometer of the TEM with all necessary precautions in order not to introduce other foreign materials aside the sample since the TEM operates under vacuum (~10^{-9} bar).

3.3.4 Dynamic Light Scattering (DLS)

The dynamic light scattering (DLS) method can be used to determine the size of particles usually in the sub-micron scale. DLS measures the speed of particles undergoing Brownian motion, also known as the translational diffusion coefficient (D) and relates it to the size of the particles. The smaller the particles, the more rapid it moves in a liquid medium with a known viscosity (η), at a constant temperature (T). The particle size, (as diameter assuming the particle is a sphere) can be estimated using the Stokes-Einstein equation expressed in Equation (3.2), where k is Boltzmann's constant. Therefore, DLS operates by illuminating the particles with a laser and analysing the fluctuation of the scattered light intensity to determine the particle sizes. [129]

$$d_h = \frac{kT}{3\pi\eta D} \qquad (3.2)$$

The mean particle size and particle size distribution were determined using a DLS (Malvern instrument, Model HPPS) with a He-Ne laser light source of λ= 633 nm. The instrument allows for measuring a wide range of particles diameter, ranging from 0.6 to 6000 nm. Sample preparation was rather straightforward by placing about 1.5 ml diluted sample in a cuvette and inserting into the Malvern instrument. All measurements were carried out at 25 ^{o}C.

3.3.5 Infra-red Spectroscopy

Infra-red (IR) spectroscopy is a spectroscopic technique based on vibration of atoms in a molecule when infrared radiation pass through them. The IR signal can only be seen for the molecular vibration that causes changes in dipole moments. IR radiation is absorbed when in resonance with the frequency of the vibration of the atomic oscillator. This is described using a simple harmonic oscillator for a diatomic molecule as expressed in Equation (3.3), where v is the frequency of vibration, k is the force constant and μ is the reduced mass. This implies that molecules with stronger interatomic bond and lighter mass have higher vibration frequencies. A simple schematic diagram of how the IR operates is shown in **Figure 3.6**. When the IR light is emitted, it splits and reflects back in the beamsplitter. The movement of one of the mirrors varies total path length to create constructive and destructive interference called interferogram. As the interferogram passes through the sample, different characteristic wavelengths are absorbed and detected as energy versus time variable. Fourier transform mathematical expression is used to convert this relation into intensity versus frequency spectrum. [130, 131]

$$v = \frac{1}{2\pi}\sqrt{\frac{k}{\mu}} \qquad (3.3)$$

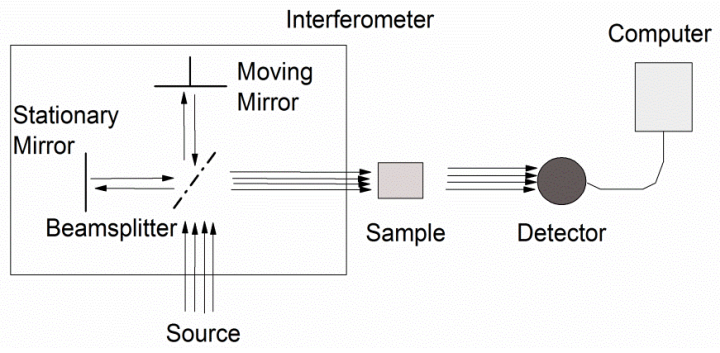

Figure 3.6: Simple schematic representation of FTIR operation adapted from [131]

Some of the chemical component in the slurry after the catalytic study was identified using the FTIR. Perkin Elmer Spectrum One FTIR was used with Harrick Access attenuated total reflectance (ATR) accessory. Typically, three drops of sample were

dropped on the ATR accessory prism (made of ZnSe crystal) and inserted into the FTIR for measurement.

Results and Discussion

4 The Role of Cu Nanoparticles in the LTMS Process

The previous study of the LTMS reaction by Bo & Jens [35], involved a once through approach to MeOH synthesis. Their approach consisted of a straight forward mixing of copper acetate ($Cu(CH_3COO)_2$) and sodium hydride (NaH) and further addition of syngas to produce MeOH at relatively low temperature conditions in one pot. As a continuation of their work, the initial objective was to characterize the 'Cu' involved in the LTMS. Cu nanoparticles were identified to be made in the process which led to the main objective of this section, to investigate the role of the Cu nanoparticle size on the LTMS reaction.

4.1 Characterization of a Typical Once-Through LTMS Reaction System

The once-through process involved the preparation of the catalyst system and then the MeOH synthesis step in one pot. **Figure 4.1** shows a typical once through MeOH synthesis procedure. Here, both the Cu catalyst and the MeOH synthesis were carried out at 100 ^oC. After the addition of NaH to the $Cu(CH_3COO)_2$, 0.35 bar pressure rise was observed and was attributed to H_2 formation (Equation (4.1)) from GC analysis. Thereafter, addition of excess MeOH to consume the remaining NaH and to form sodium methoxide ($NaOCH_3$) co-catalyst further yielded 1.38 bar H_2 pressure, as expressed in Equation (4.2). The MeOH synthesis was then performed by the addition of 20 bar syngas at 100 ^oC. This lead to 89 % conversion based on the syngas pressure drop. The intention of the addition of the NaH to the Cu-precursor was to make a reduced Cu-based catalyst as illustrated in Equation 4.1. The evolution of the H_2 gas depicted that a Cu-based catalyst was produced by the hydride reduction. However, either Cu^+ or Cu^0 or a mixture of the two could have been made in the process. In case Cu^+ is formed, a further reaction with H^- could lead to the formation of CuH, although CuH is highly unstable at the working conditions [132].

$$Cu^{2+}_{(\text{diglyme})} + 2H^- \rightarrow Cu + H_2 \quad (4.1)$$

$$NaH_{(s)} + CH_3OH_{(l)} \rightarrow CH_3ONa_{(\text{diglyme})} + H_{2(g)} \quad (4.2)$$

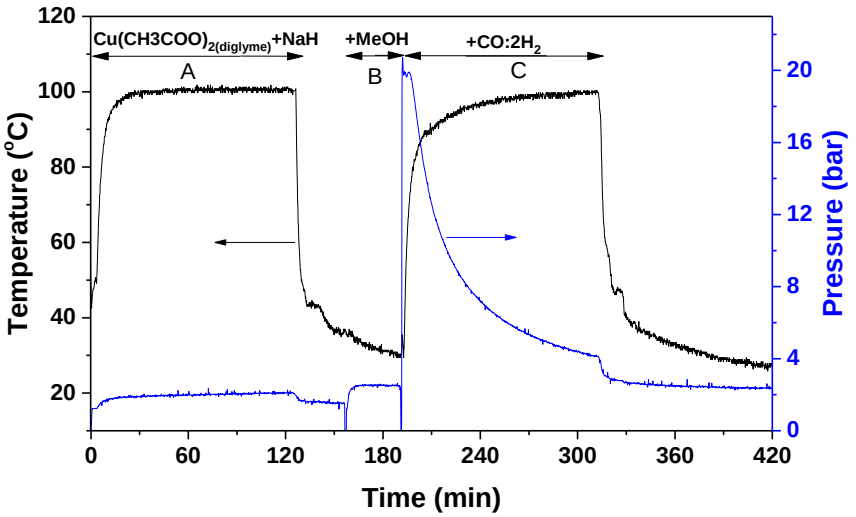

Figure 4.1: Typical LTMS procedure, A= 3.6 mmol $Cu(CH_3COO)_2$ + 18 mmol NaH in 50 ml diglyme, B= addition of 49 mmol MeOH, C=20 bar $2H_2$:1CO charged, stirring =3000 rpm

The slurry system was characterized to determine the composition, oxidation state and crystallite sizes of the solid crystallites present. The XRD of the slurry after each step was measured in capillaries without drying off the liquid portions. **Figure 4.2(a)** shows the X-ray diffractogram of the catalyst system, after each step as shown in Figure 4.1. The diffractogram right after the Cu^{2+}-H^- reaction, designated as A showed a mixture of Cu, Cu_2O and NaH crystals present. The main diffractogram phases present after the addition of MeOH designated as B showed a mixture of Cu_2O and Cu. It is important to note that the NaH surplus shown in diffractogram A disappeared in the diffractogram B, indicating total dissolution of all the NaH, and hence the rise in H_2 pressure in Figure 4.1, as expressed in Equation (4.2). The phase after the MeOH synthesis, designated as C, showed predominantly Cu^0 present. The Cu phase composition and the average crystallite sizes were quantified from the XRD line broadening using the Rietveld analysis. **Figure 4.2(b)** shows for example the Rietveld analysis of the diffractogram B in **Figure 4.2(a)**. The diffractogram B consisted of 20 % Cu^0 and 80 % Cu_2O phases. The mean crystallite size for the Cu_2O in the diffractogram B was estimated to be 7.6 ± 0.8 nm. The diffractogram C was predominantly Cu^0 with a mean crystallite size of 10 ± 1 nm. This implied that the Cu particles size slightly increased during the MeOH synthesis.

(a)

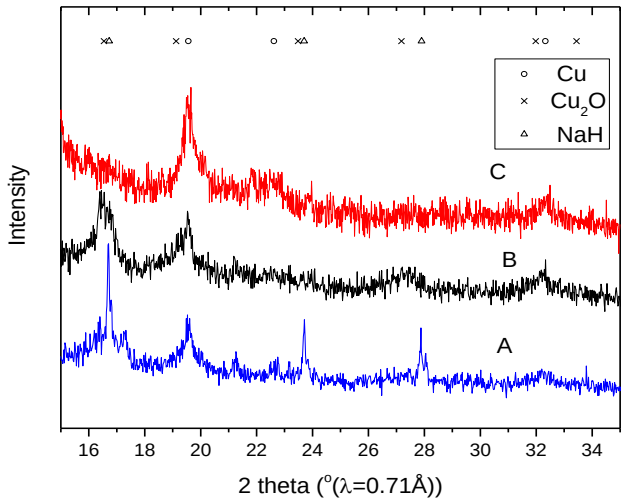

(b)

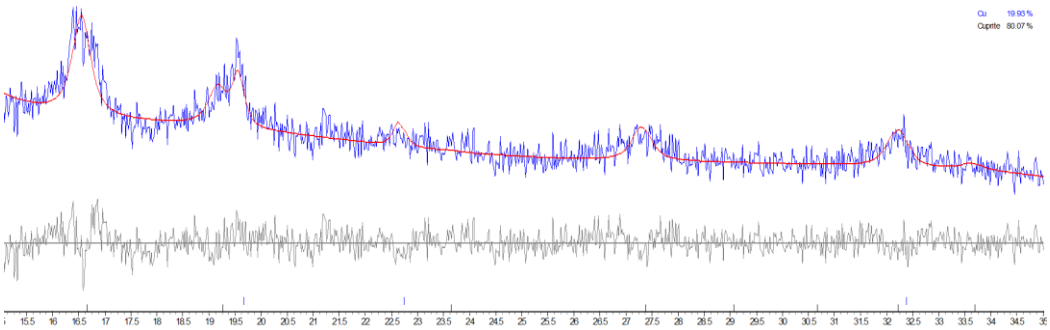

Figure 4.2: (a) X-ray diffractogram of the slurry after each step in Figure 4.1, (b) Rietveld analysis of diffractogram B

The diffractogram B predominately showed Cu_2O rather than Cu^0 during the hydride reaction. Although the reactor was purged with N_2 and the reaction performed under N_2, an oxide was observed. Glavee et. al's [133] study of borohydride reduction of Cu^{2+} in water or diglyme under vacuum produced mainly Cu^0 crystallites accompanied by stoichiometric release of H_2. However, when the isolation of the Cu^0 was done under ambient conditions, Cu_2O was observed. Aside this, oxygen can dissolve in the solvent used, as oxygen solubility in organic solvents increases with increasing hydrocarbon chain length [134]. It is important to note that the hydride reduction was also carried out under N_2 pressure, which could also contain some ppm of oxygen. Overall, the presence of oxygen can be from several sources since the reaction was not done under vacuum. Further, the diffraction C predominately showed metallic Cu^0 phase after the MeOH synthesis. This was possible considering the highly reducing environment

consisting of 20 bar H_2 and CO mixture at 100 ^oC for 2 hr. A study of the chemical state of Cu using an XPS has shown that 2 bar syngas either reduces Cu^{2+} to Cu^0 at 250 ^oC in 1 hr or Cu^{2+} to Cu^+ at 100 ^oC at the same duration [135]. As a result, it was not surprising that the Cu_2O reduces to Cu^0 after the MeOH synthesis.

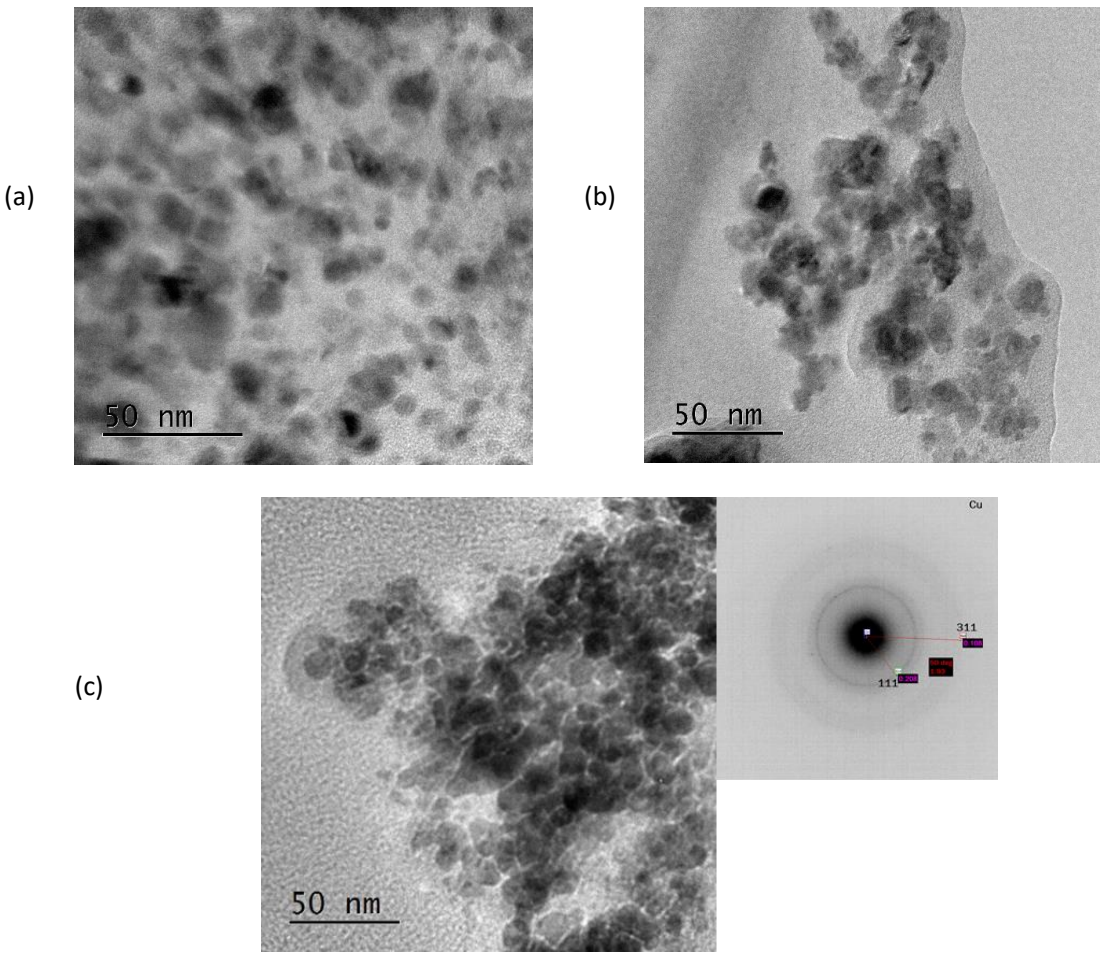

Figure 4.3: TEM images of the solid portion of the catalyst system for a typical 100 °C LTMS reaction shown in Figure 4.1. (a) after step A showing 10 ± 5 nm particle sizes. (b) after step B showing 10 ± 5 nm particle sizes. (c) after step C showing 10 ± 3 nm particle sizes

The solid portion of the catalyst was further characterized with TEM and is shown in **Figure 4.3**. Unlike the XRD measurement with the entire slurry, the samples for the TEM were diluted in MeOH, sonicated and dried overnight. Since MeOH was used as solvent for separating agglomerated particles as well as dissolving the soluble component of the slurry, Cu particles were essentially expected. This was further ascertained with EDS and

electron diffraction. The **Figure 4.3(a)** and **(b)** show the catalyst after steps A and B respectively. In both cases, about 10 ± 5 nm spherical particles with some agglomerates were observed. **Figure 4.3(c)** shows TEM image and the electron diffraction of the catalyst after MeOH synthesis (step C). Again, about 10 ± 3 nm spherical Cu particles were observed for the sample after the LTMS reaction.

The particles after step C however appeared to be of a narrower size distribution compared to that of the steps A and B. The similarity in the particles after the steps A and B was not surprising since the addition of MeOH in the TEM preparation made both samples similar. The electron diffraction measured for the sample after step C showed that the particles were polycrystalline and the indexing confirmed a metallic Cu phase to be present just as observed from the XRD. Overall, the mean crystallite sizes estimated from the XRD were within the range of the observed particle sizes from the TEM images.

4.2 Effect of Multiple Syngas Charging on the Activity of the Catalyst System

To investigate the recycling stability of the Cu catalyst, the catalyst system was charged multiple times with syngas. The catalyst system was prepared in a similar sequence as was done in **Figure 4.1**. **Figure 4.4(a)** shows the temperature and pressure profile sequence of the multiple charging experiment. After charging with 20 bar syngas, and allowed to react at 100 ^{o}C for 2 h, the reactor was cooled to about 25 ^{o}C and then degassed. This was repeated for 6 times. **Figure 4.4(b)** shows the catalyst activity for 7 consecutive batches. Syngas conversion decreased linearly after each consecutive batch from 92 % to 61 % for the 1st and 6th batches. To avoid excessive reduction of the amount of catalyst present, about 1 ml of the slurry was sampled before the 1st and after the 6th batches. The product analysis after the 6th batch showed 94 % and 6 % selectivity to MeOH and MeF respectively.

(a)

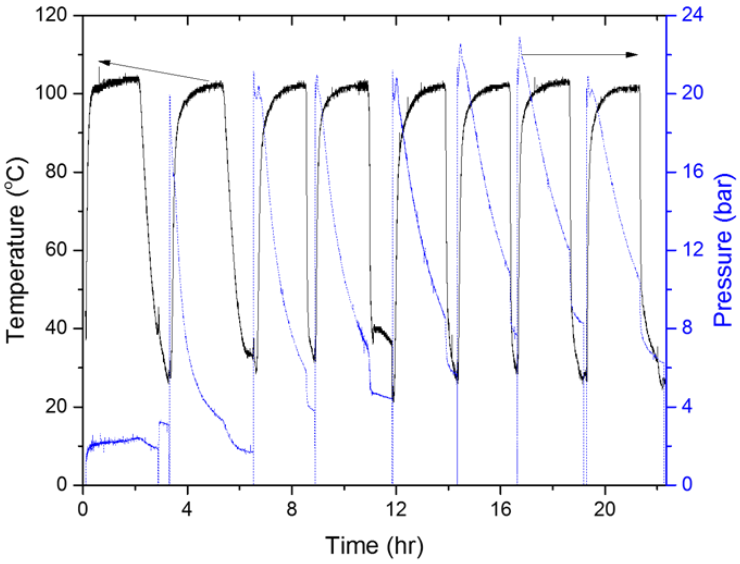

(b)

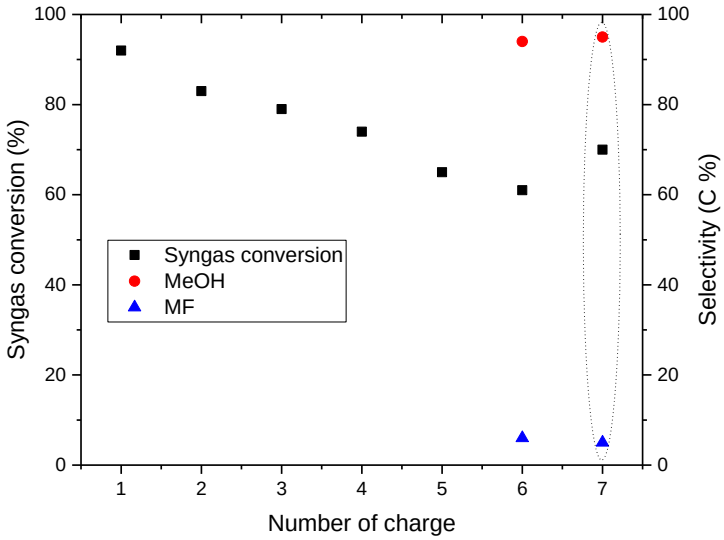

Figure 4.4: Multiple charging of syngas experiment (a) Temperature and pressure profile (b) Syngas conversion and selectivity of the multiple charging of syngas reaction, $Cu(CH_3COO)_2$ = 5.0 mmol, NaH = 25 mmol, in 50 ml diglyme, MeOH = 73.0 mmol and $2H_2$:CO = 20 bar

The decrease in conversion between the 1st and the 6th batches represented a 31 % drop in activity. Since the catalyst system consisted of two parts, the Cu and the methoxide, an addition of the component mainly responsible for the decrease should restore activity. In view of that, 8 mmol of NaH (in 49 mmol MeOH), representing 31 % of the starting methoxide was injected into the 7th batch of the reactor and charged with syngas. This led to a slight increase of syngas conversion to 70 %, with 95 % and 5 %

selectivity to MeOH and MeF respectively shown in **Figure 4.4(b)**. It is important to note that the percentage purity of the anhydrous MeOH used for making the methoxide was 99.8 % containing about 0.002 % water according to the product specification sheet. However, the contribution from such ppm of water to deactivation of the methoxide is just about 0.02 %, very insignificant to the conversion estimated. Therefore, the methoxide component of the catalyst may not be entirely responsible for the deactivation observed.

The slurry system before the 1st and after the 6th batches was characterized using the XRD and TEM and is shown in **Figure 4.5**. The X-ray diffractogram shown in **Figure 4.5(a)** indicated that the sample after the 6th batch (i.e. spent catalyst) was predominantly Cu^0 with sharper peaks while that before the 1st batch (i.e. fresh catalyst) was predominantly Cu_2O phase with broader peaks. Rietveld quantification of the diffractogram estimated the mean crystallite sizes to be 8 ± 1 and 16 ± 1 nm for the fresh and spent Cu catalysts respectively. **Figure 4.5(b)** shows the TEM image of the spent catalyst. Here, particle sizes ranged between 6 to 25 nm, with the larger particles dominating. The increase in both crystallite and particle sizes with repeated batches suggested agglomeration of the Cu particles with time.

(a)

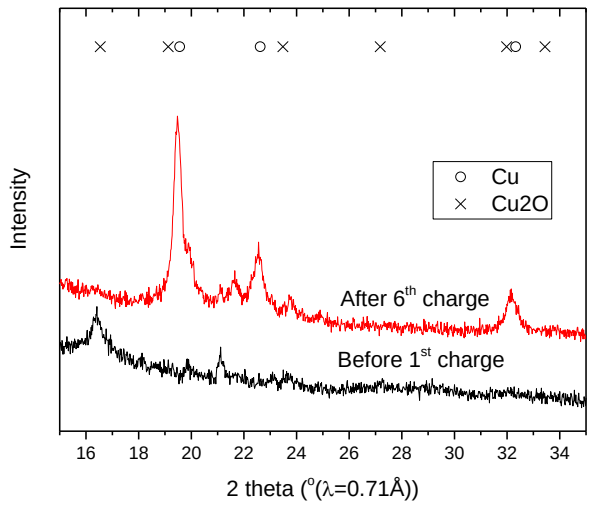

(b)

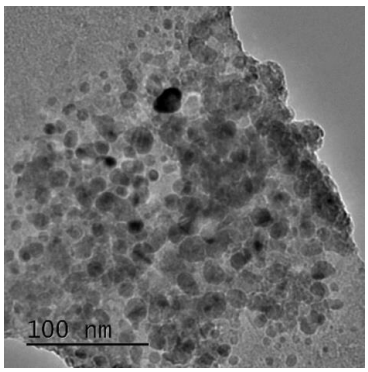

Figure 4.5: X-ray diffraction (a) and TEM image (b) of spent Cu catalyst slurry (after 6th charge) (+ XRD of fresh catalyst before 1st charge)

The oxidation state of the Cu nanoparticles during the LTMS reaction deserves some comments. From **Figure 4.2(a)** and **4.5(a)**, Cu^0 was observed after the 1st and 6th charges respectively. This was in contrast to the Cu_2O phase observed for a typical fresh system before charging with syngas. As discussed earlier, XPS study has revealed that oxidized Cu easily reduces in the presence of syngas at 100 °C [135]. Recently, Liu et. al.'s [68] Cu oxidation state study has also suggested that a blend of Cu^0/Cu^+ on oxide support are the active sites for LTMS reaction. However, even when Cu^0 was predominantly present in our case after the 1st batch, high activity (>80 %) was still observed. This therefore suggested that metallic Cu surface was the preferred active phase in the LTMS reaction studied.

Furthermore, the increase in particle size of the Cu implies a decrease in the available surface for activity. The traditional approach for determining Cu surface area using N_2O [136] was challenging in our system since it is associated with higher temperature than our operating conditions, and would not give a representative measurement. Nevertheless, the effect of the agglomeration can be estimated if all the particles are assumed to be spherical and total volume of Cu remain the same in the fresh and spent catalyst as expressed in Equation (4.3). Using the mean Cu crystallite sizes determined from the XRD and Equation (4.4), the surface area ratio between the fresh and spent Cu catalyst was estimated to be about 2.

$$\frac{\text{Number}_{\text{fresh}}}{\text{Number}_{\text{spent}}} \cong \left(\frac{\text{Volume}_{\text{fresh}}}{\text{Volume}_{\text{spent}}}\right)^{-1} \tag{4.3}$$

$$\frac{\text{Cu Surface area}_{\text{fresh}}}{\text{Cu Surface area}_{\text{spent}}} = \left(\frac{\text{Area}_{\text{fresh}}}{\text{Area}_{\text{spent}}}\right) \times \left(\frac{\text{Volume}_{\text{fresh}}}{\text{Volume}_{\text{spent}}}\right)^{-1} = \frac{\text{Diameter}_{\text{spent}}}{\text{Diameter}_{\text{fresh}}} \tag{4.4}$$

To put the surface area ratios into perspective, it will be important to consider the mean particle size after the 1st batch from **Figure 4.2(a)**. The mean Cu^0 crystallite size after the 1st batch was estimated to be 10 nm while that after the 6th batch in **Figure 4.5(a)** was estimated to be 16 nm. This represents a Cu^0 surface area (fresh/spent) ratio of 1.6. The activity observed after the 1st batch was 92 %, whilst that after the 6th batch was 61 %. This represents an activity ratio of 1.5 after 1st/6th charges. Therefore there was a strong

correlation between the particle size growth in regards to surface available and the reduction in MeOH synthesis activity. The cause of deactivation in the LTMS reaction has been suggested in literature [28] to be due to the reaction of the sensitive alkoxide co-catalyst with trace amount of CO_2 and H_2O from either the syngas feed or as a by-product during MeOH synthesis. As stated earlier, although some ppm of water might be in the anhydrous MeOH used for making the methoxide, the one-time addition of the small quantity cannot be responsible for the successive decline in catalytic activity. Hence the successive decline in the catalytic activity was mainly due to the reduction of the available active sites of the Cu nanoparticles as the particle size became larger.

So far, the successive decline of the catalytic activity has been attributed to reduction of available active Cu surfaces. Even though, detailed mechanism of the deactivation was not studied, some inference can be made to predict the route to the decline of the active sites over time. In the LTMS reaction, Cu is suggested to be mainly responsible for the hydrogenolysis of MeF which is the rate limiting step [27]. There is a potential of CO competing with H_2 for available sites to retard activity. However, after each batch, the reactor was degassed and hence CO poison from previous batches was minimized. Meanwhile, since the hydrogenation process is highly exothermic [39], temperature of the reaction on the nanoparticles would rise each time MeOH was produced. Such hot spots on the Cu nanoparticles increases the chances of particle agglomeration over time. It is important to note that Cu crystallite sintering is a very common deactivating path for Cu catalysts [137]. Considering the high surface energy associated with nanoparticles, the 10 nm Cu particles without any oxide support will easily react with each other to form larger particles to minimize its surface energy [138]. Therefore, we predict that the starting soft Cu catalyst agglomerated over time, which led to a decline in available active sites for the MeOH synthesis.

4.3 Effect of Cu Particle Sizes on the LTMS

To vary the Cu nanoparticle size, temperature for the preparation of the catalyst was varied. Subsequently, the varied particle size would be tested to determine their role in

the LTMS reaction. **Figure 4.6** shows the X-ray diffractogram of the slurry prepared at different temperatures in a similar way as discussed in **Figure 4.1** just before charging with syngas. The diffractogram showed increase in relative peak sharpness and intensity with increasing temperature, ranging between 80 to 149 ^{o}C. This suggested that temperature increased the crystallization of the Cu particles such that the Cu densification increased with temperature.

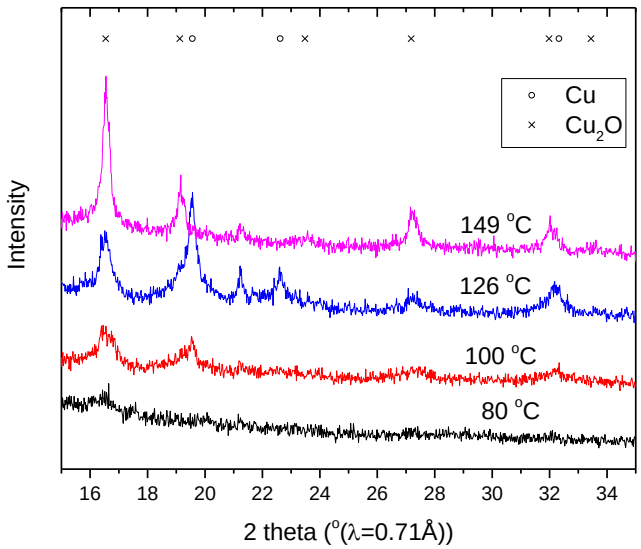

Figure 4.6: X-ray diffractogram of the slurry of the catalyst system at different preparation temperatures

Figure 4.7 shows the Rietveld quantification of the diffractogram shown in **Figure 4.6** for the freshly prepared slurry catalyst system. **Figure 4.7(a)** shows the % composition of the Cu phases at the different preparation temperatures. Cu_2O % composition dominated with lesser % composition of Cu^0 at all temperatures, except at 126 ^{o}C, where 50/50 % of the two was observed**. Figure 4.7(b)** shows the mean crystallite sizes at the different preparation temperatures. The crystallite sizes of the Cu_2O were 5±2, 7.6±0.8, 15±2 and 21±1 nm for the 80, 100, 126 and 149 ^{o}C preparation temperatures respectively. This represented an exponential increase of particle size with temperature. The theory associated with crystallization depicts that the rate of nucleation and particle

growth exponentially depends on temperature [139]. Hence, the observed exponential increase in the crystallite sizes with temperature was in order.

(a)

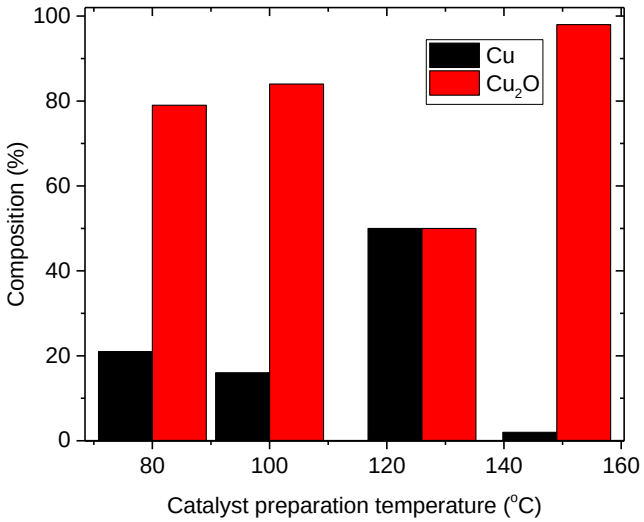

(b)

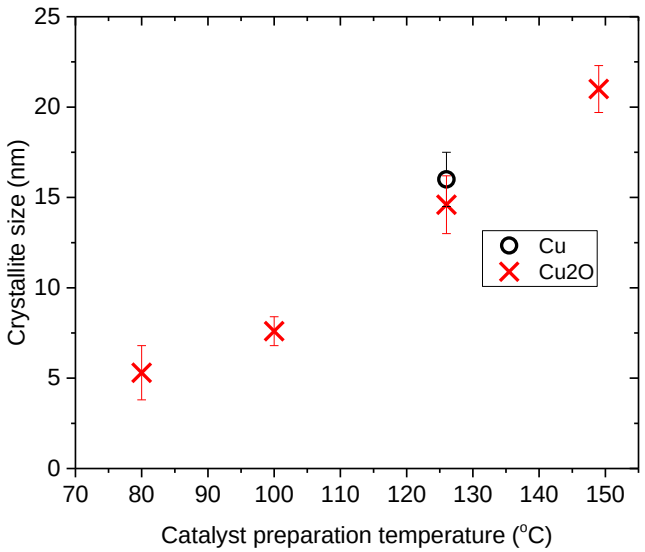

Figure 4.7: Rietveld analysis of the Cu crystallites from the X-ray diffractogram before LTMS reaction in Figure 4.6 (a) Cu crystallites composition, (b) Cu crystallite sizes

The varied Cu nanoparticle sizes were tested to determine their influence on the LTMS reaction at 100 °C. **Figure 4.8** shows the conversion and selectivity versus Cu_2O crystallite sizes. Each test was done thrice and the average and standard deviations plotted. Syngas conversion was 84 ± 3, 87 ± 3, 83 ± 2, and 70 ± 2 % for the particles made

at 80, 100, 126, and 149 °C Cu catalyst systems, corresponding to 5±2, 7.6±0.8, 15±2 and 21±1 nm Cu_2O crystallite sizes respectively. Selectivity to MeOH was a 96 ± 1, 96 ± 1, 88 ± 1 and 80 ± 1 while selectivity to MeF was 4 ± 1, 4 ± 1, 13 ± 1 and 20 ± 1 for the 5±2, 7.6±0.8, 15±2, 21±1 nm Cu_2O crystallite sizes respectively. While syngas conversion and selectivity to MeOH increased with decreasing crystallite sizes, selectivity to MeF decreased with decreasing crystallite sizes. Even though the selectivity was similar for the crystallites made at 80 and 100 °C, the conversion was slightly lower in the 80 °C catalyst with the least Cu_2O crystallite size. From the **Figure 4.6**, the diffractogram for 80 °C catalyst system showed the lowest intensity, which implies that a lower amount of Cu probably crystallized out of solution within the time period for the catalyst preparation. This could contribute to the slightly lower activity compared to the catalyst made at 100 °C. Nevertheless, when both conversion and selectivity to MeOH are considered, the overall yield of MeOH decreased with increasing Cu_2O crystallite size.

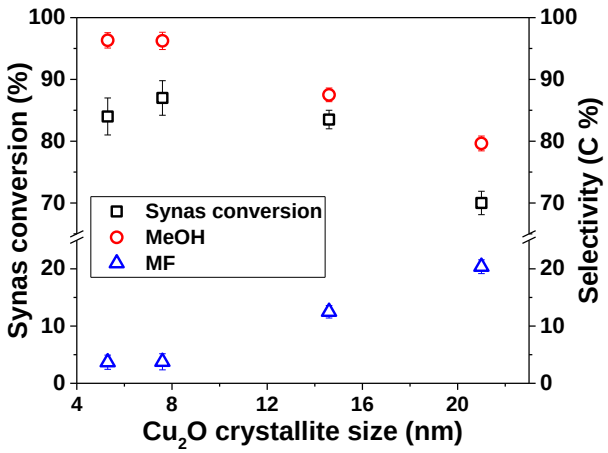

Figure 4.8: Syngas conversion and selectivity verses Cu_2O crystallite sizes prepared at different temperature, ($Cu(CH_3COO)_2$ = 3.6 mmol, NaH=18 mmol in 50 ml diglyme, MeOH = 49 mmol, 2H2:1CO=20 bar, at 100 °C.

(a)

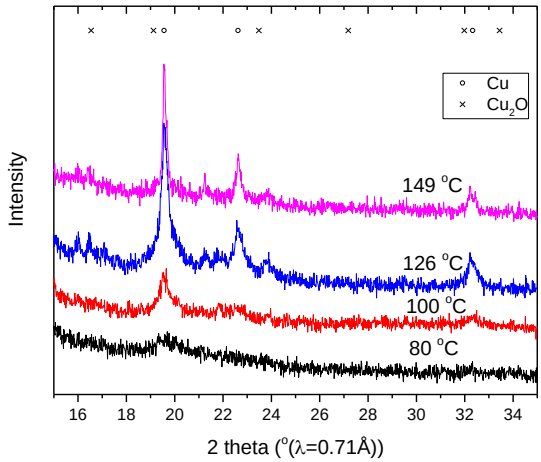

(b)

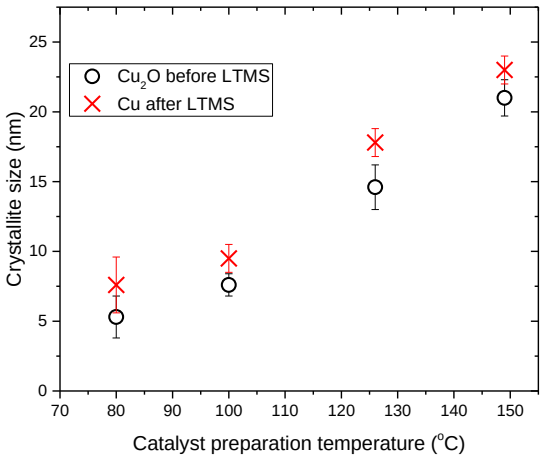

Figure 4.9: (a) X-ray diffractogram and (b) Rietveld analysis of Cu crystallite sizes of the slurry catalyst system after LTMS reaction

The spent catalyst system was characterized by XRD and TEM. **Figure 4.9(a)** shows the X-ray diffractogram of the spent catalyst. Cu^0 was the main phase observed for all the different catalyst preparation temperatures. **Figure 4.9(b)** shows the Rietveld analysis of the crystallite sizes based on the diffractogram shown in **Figure 4.9(a)** and compared with the freshly prepared catalyst. The Cu^0 crystallite sizes were 8 ± 2, 10 ± 1, 18 ± 1 and 23±1 nm for the particles made at 80, 100, 126, and 149 °C preparation temperatures respectively. This represented about 2 to 3 nm general increase in crystallite sizes after the LTMS reaction.

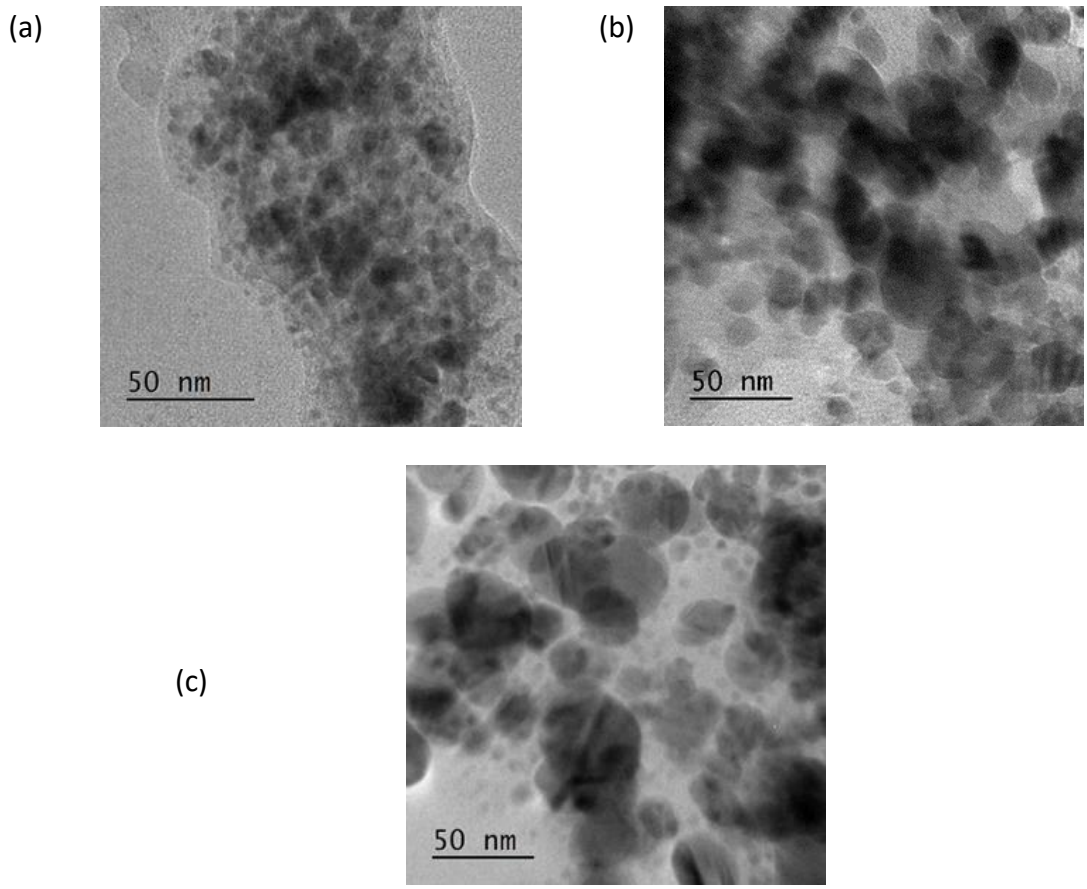

Figure 4.10: TEM image of Cu catalyst after LTMS reaction, Catalyst system prepared at (a) 80 ^{o}C showing 7±4 nm particle sizes, (b) at 126 ^{o}C showing 18±6 nm particle sizes, (c) 149 ^{o}C showing 25±6 nm particle sizes

Figure 4.10 shows the TEM image of the spent Cu catalyst at the different preparation temperatures. The mean Cu particle sizes observed for the 80 ^{o}C catalyst system was about 7 ± 4 nm. At 126 and 149 ^{o}C, the mean particls sizes were 18 ± 6 and 25 ± 6 nm respectively. Furthermore, larger agglomerates up to 40 and 50 nm were observed at the 126 and 149 ^{o}C preparation temperatures respectively. As already shown in **Figure 4.3(c)**, the mean particle size of the catalyst prepared at 100 ^{o}C was 10 ± 3 nm. Overall, the catalyst prepared at 100 ^{o}C showed a tighter particle size distribution compared to the catalyst prepared at other temperatures. This can be attributed to the catalyst system's exposure to the same temperatures during catalyst preparation and the MeOH synthesis. The 100 ^{o}C catalyst system had the least temperature fluctuation over a longer period, which promoted a more uniform particle growth compared to the other catalysts prepared and tested at different temperatures.

So far, the temperature variation for the Cu catalyst preparation resulted in an exponential crystallite and particle size dependence on temperature. These Cu catalysts used for the LTMS reaction showed an increase in MeOH yield with decreasing particles size. On the other hand, the selectivity to MeF increased with increasing particles size. It is reported that there is a strong correlation between Cu surface area and MeOH production [32, 140]. In Ohyama and Kishida's [32] report, physical milling of CuO/CrO_3 led to an increase in Cu surface area which enhanced MeOH production. As already expressed in Equation (4.4), smaller particle sizes have more surface area per gram available for the catalysis. Even though a direct surface area measurement was not performed in our system, we can predict the trend in the relative surface area based on the particle sizes of the Cu catalysts. Since the Cu particles are active catalysts for hydrolysis of MeF, increasing the relative surface area as a result of decreasing mean particles size led to increase in MeOH production. In a similar vein, the amount of MeF was more when particle sizes increased as there were fewer active Cu surface area available for the hydrogenolysis step.

4.4 Summary

The once-through LTMS reaction at 100 ^oC catalyzed by Cu-alkoxide system has been characterized. The Cu catalyst was produced by hydride reduction of the Cu^{2+} precursor ($Cu(CH_3OO)_2$) in diglyme at varied temperatures. Cu_2O and Cu nano-crystallites were identified as the Cu phases present in the freshly prepared catalyst before the MeOH production. The Cu nanoparticle and crystallite sizes increased exponentially with temperature i.e. between 5 to 21 nm crystallite sizes at 80 to 149 ^oC respectively. When the nanoparticles were tested for MeOH synthesis at 100 ^oC, MeOH production increased with decreasing particles size. Upon MeOH production, Cu^0 nano-crystals were solely observed with 8 to 23 nm crystallite sizes depicting about 2 nm average growth in crystallites. Furthermore, with 100 ^oC as the standard temperature for both Cu catalyst preparation and MeOH synthesis temperature, up to 92 % conversion and

94 % selectivity to methanol was achieved. However, repeated charging of the same catalyst system led to a successive decline of syngas conversion. Among the two main catalyst components, the relative increase in Cu particle sizes correlated well with the decline in activity. Thus the densification of softer Cu nanoparticles over time during the MeOH production was suggested as the major deactivation route for the Cu catalyst. Overall, decreasing Cu nanoparticle size, which correlates with increasing active specific Cu surface area, was attributed to increase in MeF hydrogenolysis and thus increased MeOH production.

5 The Role of Solvent Polarity in the LTMS Process

LTMS reaction is typically performed in a liquid medium. Since the MeOH synthesis reaction is exothermic, the presence of solvent in the LTMS reaction helps to dissipate excess heat released during the reaction. However, aside heat dissipation, how can the selected solvent influence the chemical environment for both catalyst formation (in the one-pot system) and the actual MeOH synthesis reaction. To the best of our knowledge, very little has been reported on the choice of solvent for the LTMS process. Xing-Quan et. al. [141] for example reported that in a $CuCl_2$ and CuO/Cr_2O_3 catalysed LTMS reaction, MeOH production decreased with increasing solvent polarity. However, adequate explanation with regards to how the polarity affect the chemical reaction was not given. In this section, the role of solvent polarity on the entire LTMS process was studied. In particular, the role of solvent polarity on the nature of Cu-based catalyst formed, MeF intermediate and the overall LTMS reaction was studied.

5.1 The Role of Solvent Polarity in the Once-Through LTMS Process

To investigate the role of solvent polarity on the LTMS reaction, different aprotic solvents with varied polarity were used. Only aprotic solvents were used because NaH and methoxide ($NaOCH_3$) can easily react with any loosely bound protons. **Table 5.1** shows list of the solvents used and together with some of their properties. The % purity of the solvent used were more than 99 %, and were used as purchased without any pre-treated. Five of the selected solvents were ethers with varied hydrocarbon chain length coupled with different boiling points (pt.) and heat capacity. The dielectric constants (ε) of the selected solvents which is usually used as a measure of the solvent polarity [142] ranged between 2.33 and 41.13 (adopted from [143, 144]).

The experimental procedure and characterization for the once-through LTMS reaction has been extensively discussed in Chapter 4, using diglyme as the solvent. Similar experimental procedure was followed just as was described in Section 4.1 (see **Figure**

4.1), but with different solvents. **Figure 5.1** shows the syngas conversion and product selectivity versus ε of the solvents in a once-through LTMS reaction at 100 ^{o}C. The syngas conversions were 51, 87, 85, 80, 74, 30 and 14 % in diethyl ether (DEE), diglyme, THF, glyme, tetraglyme, acetonitrile (MeCN) and DMSO respectively. This implies that the conversion initially increased with ε from 4.19 for DEE, to a maximum at ε = 7.23 for diglyme, and then successively declined with increasing ε for THF, glyme, tetraglyme, MeCN and DMSO with ε = 7.36, 7.55, 7.79, 35.87 and 47.13 respectively. The product selectivity to MeOH and MeF however remain roughly the same at >90 % and <10 % respectively in all the solvents.

Table 5.1 : List of Solvents used and their properties adopted from [143-145], (ε = dielectric constant)

Solvent	*Formula*	*% Purity*	*ε*	*Boiling pt. / °C*	*Heat capacity / J/mol.K*
Toluene (Methylbenzene)	C_7H_8	≥99.5	2.33	111	157
DEE (Diethyl ether)	$C_4H_{10}O$	≥99.9	4.19	35	176
Diglyme (1-Methoxy-2-(2-methoxyethoxy) ethane)	$C_6H_{14}O_3$	≥99.5	7.23	162	274
THF (Tetrahydrofuran)	C_4H_8O	≥99.9	7.36	66	124
Glyme (1,2-Dimethoxyethane)	$C_4H_{10}O_2$	99.5	7.55	85	193
Tetraglyme (2,5,8,11,14-Pentaoxapentadecane)	$C_{10}H_{22}O_5$	>99	7.79	275	457
MeCN (Acetonitrile)	C_2H_3N	99.8	35.9	82	92
DMSO (Dimethyl sulfoxide)	C_2H_6OS	≥99	47.1	189	153

The selected solvents for the LTMS differed in polarity represented by ε, boiling point, heat capacity and hydrocarbon chain length which is directly related to their molar masses as illustrated in the **Table 5.1**. Considering solvents with similar functional group, the ε of the ethers followed the order DEE < diglyme < THF < glyme < tetraglyme. The syngas conversion appears to decrease with the ε with the exception of the DEE. The molecular mass or the chain length of the ethers was in the order THF < DEE < glyme < diglyme < tetraglyme. The heat capacity of the ether solvents followed the same order

as the molecular mass of the solvents, while the boiling points differed slightly in order as DEE < THF < glyme < diglyme < tetraglyme. Overall, with the exception of the ε, neither the molar mass, heat capacity nor the boiling points followed the trend of syngas conversions observed.

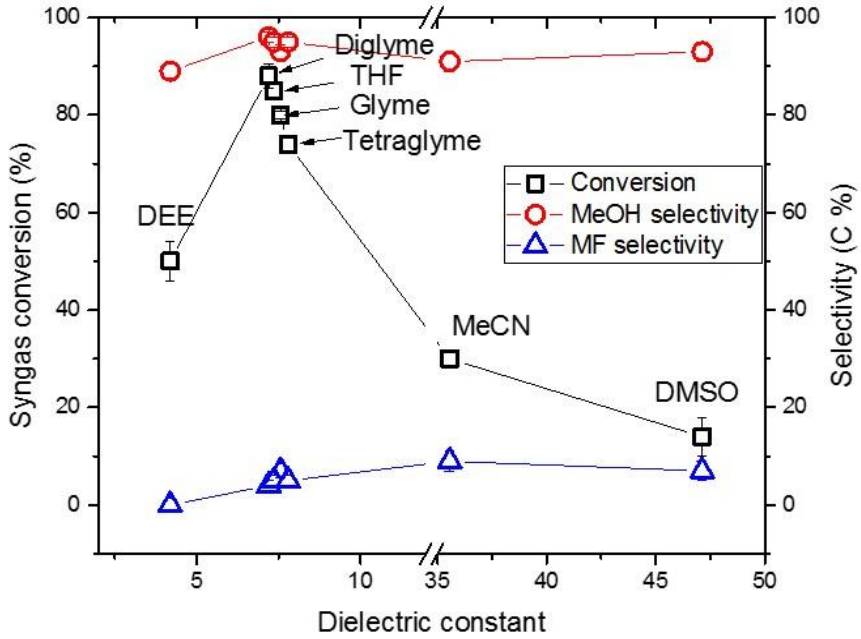

Figure 5.1: Syngas conversion and selectivity versus dielectric constant of solvent in the 'once through' Cu nanoparticles catalysed reaction

Furthermore, the solvents were extended to include non-ether based solvents such as MeCN and DMSO for the once-through experiments. The MeCN and DMSO with respective ε = 35.87 and 47.13, showed even less syngas conversion compared to the ethers. Even though, the boiling points and the heat capacity of the MeCN and DMSO were in the same range as some of the ether solvents, the conversions varied significantly. Considering that the solvent helped to dissipate excess heat released during the MeOH synthesis reaction, the conversions were supposed to follow a similar trend as the heat capacity. However, this was not the case, as for example 14 % conversion was observed when DMSO with 153 J/mol.K heat capacity was used as solvent compared to the 85 % conversion when THF with 124 J/mol.K heat capacity was used. Comparably, the ether solvents, which had narrower ε values, showed a narrower

decline in the syngas conversion whilst a wider decline of conversion was observed for the MeCN and DMSO. This suggested that, the solvent polarity played an important role in the LTMS reaction as solvents with similar polarity as diglyme showed an enhanced MeOH production.

5.2 The Role of Solvent Polarity on Cu Nanoparticle Size in the Once-Through LTMS Process

In the previous Section (5.1), the use of diglyme appeared to favour MeOH production, however the exact role is yet to be established. It was interesting to determine whether this solvent had an effect on the Cu nanoparticles formed in the once-through process. As discussed in Chapter 4, MeOH production increased with decreasing the Cu nanoparticle sizes. Our focus in this sub-section is therefore to determine the role of solvent polarity in the Cu-nanoparticle sizes.

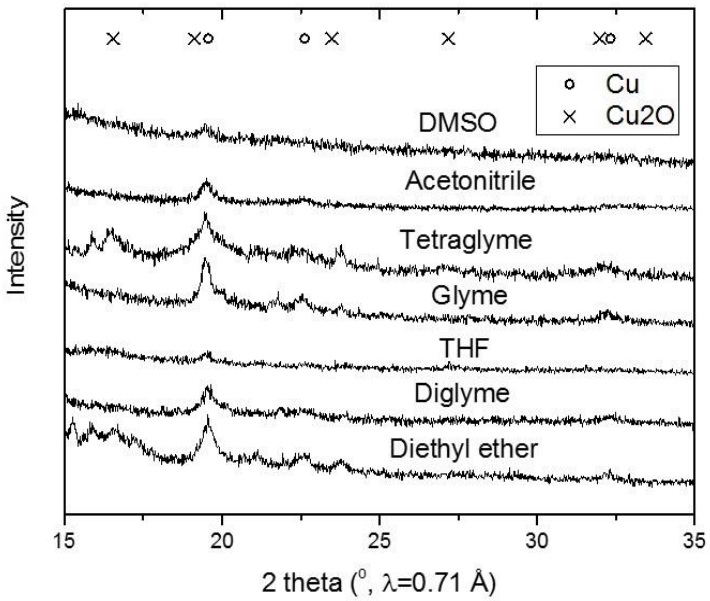

Figure 5.2: X-ray diffractogram of the slurry after LTMS reaction for the different polar solvents

The slurry collected after the LTMS was characterized using XRD and TEM. **Figure 5.2** shows the X-ray diffraction of the catalyst system after the LTMS reaction. The

diffractogram showed predominantly Cu^0 phases with varying intensities and peak broadness in the different solvents. Furthermore, TEM images of the catalyst particles made in the different solvents are shown in **Figure 5.3**. The TEM image of the Cu particle made in diglyme has earlier been shown **Figure 4.3**. A summary of the mean particle size from the TEM images and the Rietveld quantification of the diffractogram in relation to the solvents and their ε is shown in **Figure 5.4**. Overall, the Cu particles crystallite sizes and mean particle sizes were similar in most solvents. The mean sizes of Cu particles made in the ether solvents were about 9 to 10 nm, which was slightly larger than the particles made in the MeCN and DMSO with about 7 nm mean size.

In the ether solvent, similar Cu particle sizes were made. The ether solvent as discussed earlier differ in some physical properties aside their polarity difference. One of which is the difference in hydrocarbon chain length, with different number of oxygen within their structure. The presence of electron rich oxygen presents a possibility of the different ethers forming chelates around the starting Cu^{2+} ion, to direct the Cu particle structure and size. However, with the observed similarities in the spherical Cu nanoparticle sizes in all the ether solvent, the chain length of the solvent did not significantly distinguish between the particles formed. Nonetheless, it is possible that the excess amount of solvents used could provide enough oxygen for dative bonding if chelating was important in determining the shape and size of the Cu particles.

The nanoparticles made in the non-ether solvents were slightly smaller than those made in the ether solvents. Whilst the mean particle size in the MeCN (ε = 36) and DMSO (ε = 47) was around 7 nm, the mean particle size of the ethers (ε = 4.2–7.8) was about 9 to 10 nm. It has been observed in other wet chemical methods that, the rate of nucleation increases with decreasing solvent polarity as ion saturation is increased [146, 147]. Faster rate of nucleation implies larger number of nuclei and subsequently smaller particles with narrow size distribution. The opposite is expected with increasing solvent polarity if longer growth time (~24 h) is allowed. In contrast, we observed slightly smaller crystallite and particle sizes in the more polar solvent, which could probably be due to shorter growth time (2 h) applied in our case.

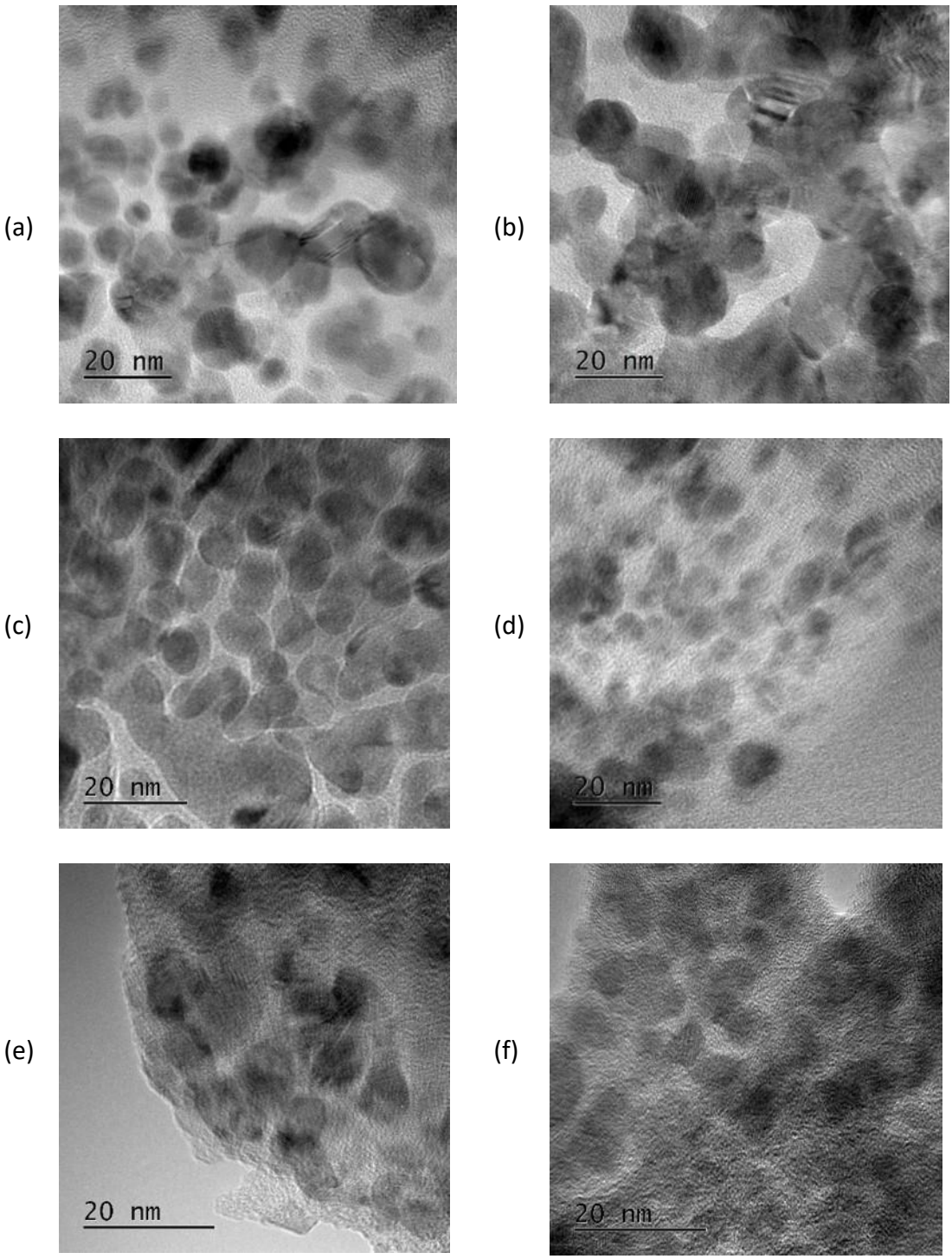

Figure 5.3: TEM images of Cu nanoparticles after LTMS reaction in the different solvents, (a)= Diethyl ether (DEE), (b)= Glyme, (c)= Tetraglyme, (d)= THF, (e)= MeCN, (f)= DMSO

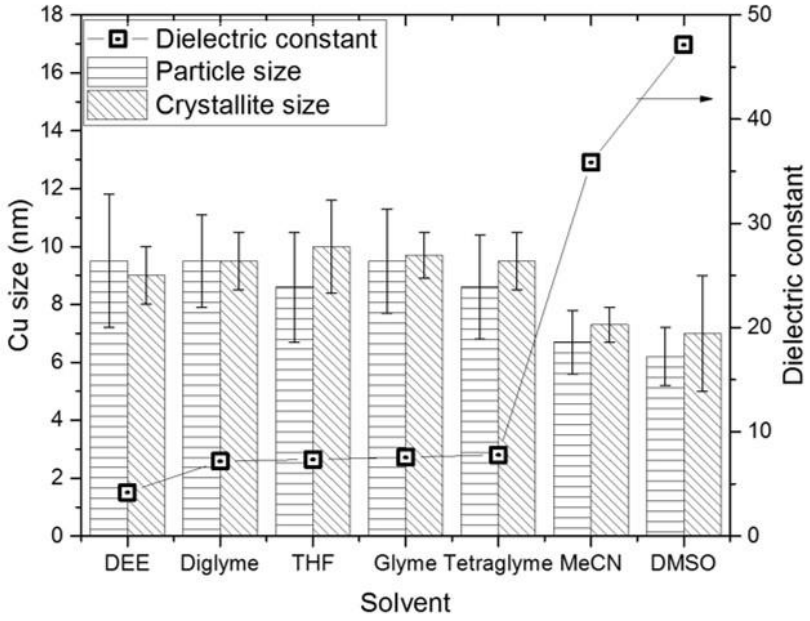

Figure 5.4: Comparison of the Cu particles sizes and dielectric constants in the different solvents after LTMS reaction

Despite the smaller Cu particle sizes made in the more polar solvent, the least amount of MeOH were observed in those solvents. From the Chapter 4, MeOH production was enhanced with decreasing Cu nanoparticle size as a result of increase in MeF hydrogenolysis. Since hydrogenolysis is the rate determining step in the LTMS reaction, it was expected that the smaller Cu particles will enhance MeOH production rather than the very low conversion observed. Hence, other component in the slurry system other than sizes of the Cu nanoparticles dictated the trend of MeOH production with the different solvents.

5.3 The Role of Solvent Polarity on the LTMS Process using CuO/SiO_2 Catalyst

So far, the influence of the solvent polarity has been studied in only the once-through system, such that both Cu catalyst and MeOH synthesis were done in one pot. Unexpectedly, lower MeOH production was observed in the catalyst systems with smaller Cu nanoparticles sizes. In all the solvents used, the Cu nanoparticle size

produced were quite tight ranging from 7 to 10 nm. It will be interesting to study a different source of Cu-based catalyst, which formation was not influenced by any of the solvents used. Moreover, a little larger size of Cu nanoparticles will help to discriminate between the influence of the Cu catalyst and the solvent used.

A CuO/SiO_2 catalyst was prepared via a sol-gel approach using $Cu(NO_3)_2$, L-ascorbic acid and SiO_2 dispersed in water, detail of which is reported in Section 3.2.3. To eliminate the influence of the solvent polarity on the formation process of the Cu, the slurry was dried and calcined before the dry powder was used for the LTMS reaction. **Figure 5.5(a)** shows the X-ray diffractogram of the calcined CuO/SiO_2. Mainly, crystalline CuO [148] with amorphous SiO_2 [149] phases were observed. Rietveld analysis of the diffractogram estimated 30 ± 5 nm CuO crystallite size. Furthermore, TEM imaging and electronic diffraction of the calcined CuO/SiO_2 was obtained and shown in **Figure 5.5(b)**. The electron diffraction was indexed to contain (110), (002), (11-2) and (112) for CuO planes.

(a)

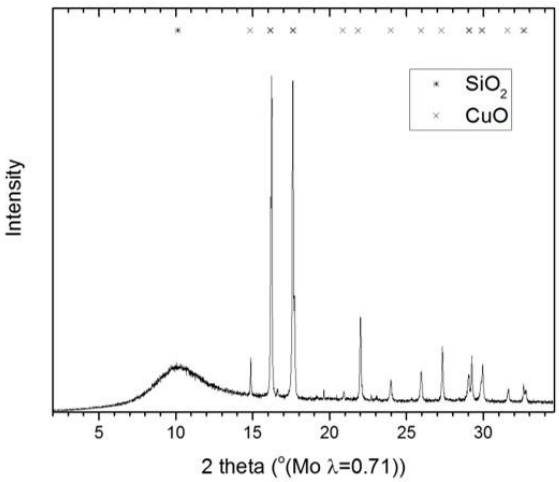

(b)

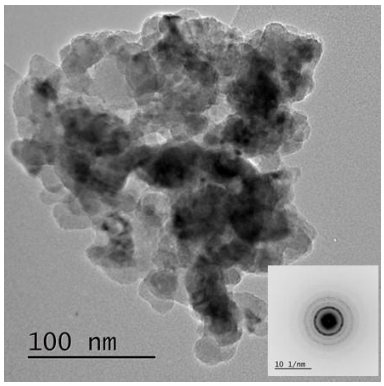

Figure 5.5: X-ray diffractogram (a) and TEM image with an inserted electron diffraction (b) of calcined CuO/SiO_2 catalyst

The calcined CuO/SiO_2 was then used for the LTMS reaction. Since the Cu-based catalyst was already made, solvent and the methoxide co-catalyst were added to the CuO/SiO_2, followed by charging the reactor with syngas to 20 bars. **Figure 5.6** shows the syngas conversion and product selectivity versus ε of the different solvents used. The syngas

conversions were 28, 39, 76, 74, 20 and 12 % in toluene, DEE, diglyme, THF, MeCN and DMSO respectively. Here, conversion initially increased with ε, for toluene with ε= 2.33 from 28 % to a maximum of 76 % for diglyme with ε = 7.23 and then successively declined with increasing ε to 12 % for DMSO. Once again, despite the differences in the conversions with ε, the selectivity to MeOH and MeF remained fairly the same in all the solvents at >90 % and <10 % respectively.

The syngas conversion in the once-through catalyst system was higher than the conversion observed in the CuO/SiO_2 system. Since the source of the Cu catalyst were different in the two systems, it is not surprising that there are differences in the activity. However, it is important to point out that the Cu particle size was different in the two cases. While the once through system used < 10 nm Cu nanoparticles, about 30 nm Cu nanoparticles were involved in the CuO/SiO_2 system. Having established in the Chapter 4, coupled with other reports [32, 33] on the effective role of Cu nanoparticle sizes in the LTMS reaction, it is expected that the activity was lower in the CuO/SiO_2 system with larger particle size than the once through system with smaller Cu nanoparticle sizes.

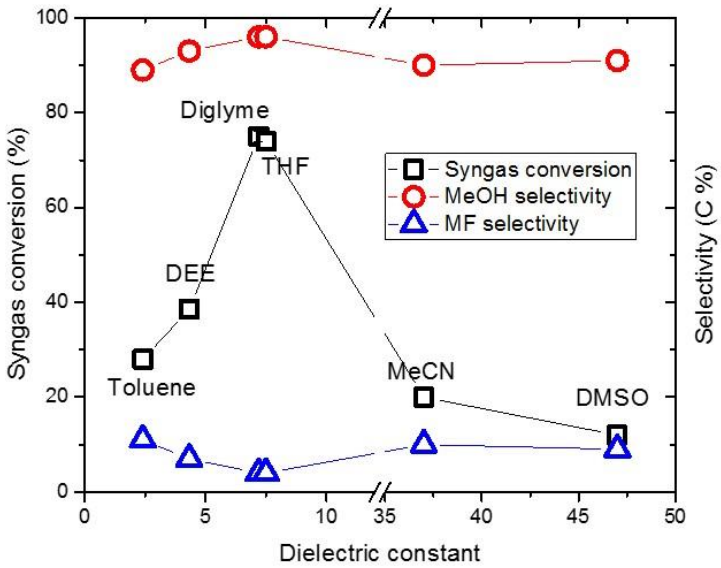

Figure 5.6: Syngas conversion and selectivity versus dielectric constant of solvent in the CuO/SiO_2 catalysed reaction

Despite the difference in the conversions in the two Cu catalyst systems, the conversion and selectivity in the CuO/SiO_2 followed the same trend as was observed in the once

through system. The similarities in the trend of activity in the two systems therefore eliminates the Cu catalyst source or sizes as the main source of the activity variation with solvent polarity. It is important to find out what exactly the role of solvent's polarity in the LTMS reaction is. We can consider the solubility of the syngas in the solvent for example. Since the composition of syngas is relatively non-polar, it is expected to be less soluble in polar solvent [150]. That is, the strong polar interaction between polar molecules should make it difficult for non-polar molecules to penetrate. Nevertheless, the trend of activity which increased in the order toluene < DEE < diglyme, is rather opposite to approaching non-polarity based on their ε values. To this end, it will be useful to consider the influence of the solvent's polarity on side reactions, in the LTMS process since the Cu nanoparticles were not the bottle neck for the observed trend.

5.4 The Role of Solvent Polarity on the Side Reaction of the LTMS Process

Up to now, the focus of the solvent's polarity has been on the overall LTMS reaction. Even though the trends in activity as a result of the variation of solvent's polarity has been consistent, the actual chemical effect is yet to be uncovered. The trend in activity with the different solvent was observed to be independent of the source and size of the Cu catalyst. The LTMS reaction involves two major steps, carbonylation to form MeF and hydrogenolysis of the MeF. Since traditionally, the Cu particles play a major role in the second step, it will be valuable to consider the effect of the solvent's polarity on the MeF intermediate. MeF is known to undergo two major reactions in the presence of $NaOCH_3$; (i) decarbonylation, which is a highly reversible reaction [39], illustrated in Equation (5.1), and (ii) nucleophilic substitution reaction [39, 151], illustrated in Equation (5.2). Therefore, if the hydrogenolysis step is not fast enough, MeF can undergo multiple reactions in the presence of $NaOCH_3$.

$$CH_3OOCH \rightleftharpoons CO + CH_3OH \quad (5.1)$$

$$CH_3OOCH + NaOCH_3 \rightleftharpoons CH_3OCH_3 + NaOOCH \quad (5.2)$$

To examine the role of the solvent's polarity on possible side reactions, the MeF in the presence of $NaOCH_3$ was heated to 100 ^oC for 1 h under 1 bar N_2 gas in the different polar solvents. The pressure rise, equivalent CO released, amount of MeOH and MeF realised after cooling the mixture is shown in **Table 5.2**. In the GC gas phase analysis, MeOH, dimethyl ether (DME), MeF, N_2 and CO were observed. However, it was difficult to distinguish between MeOH and dimethyl ether (DME) on the Porapak Q GC column, as their peaks overlapped. Hence the N_2 and CO which was well separated on the Molecular Sieve GC column was quantified and reported in **Table 5.2**. The relative amount of CO with respect to N_2 was reported as CO equivalent. The liquid portion showed that the amount of MeF drastically reduced from 33 mmol to below 4 mmol in all the solvent. Moreover, some traces of DME was observed in all the liquid analysis, however due to its high volatility, quantified amount will not be accurately represented. In all, the pressure rise and CO equivalent released increased with decreasing solvent's polarity as well as the amount of MeF and MeOH decreased with increasing solvent polarity.

Table 5.2: Solvent effect on MeF and $NaOCH_3$ reaction, 20 ml solvent, MeF = 33 mmol. $NaOCH_3$ = 18.75 mmol, MeOH = 49 mmol, in 20 ml solvent, N_2 = 1 bar, CO equivalent=CO/(CO+N_2) × pressure rise, CO and N_2 was determined from gas analysis while the MeF was determined from liquid analysis.

Solvent	*Pressure rise / bar*	*CO equivalent / bar*	*MeF / mmol*	*MeOH /mmol*
Toluene	3.0	1.9	3.43	80
DEE	2.9	1.7	2.12	63
Diglyme	2.5	1.2	1.77	46
MeCN	1.2	0.6	1.00	30
DMSO	0.8	0.3	0.41	21

The total amount of products analysed in the GC showed that the total C counts were getting lower with increasing solvent polarity. This implied that not all the products were accounted for in the GC. Hence, the resulting mixture after the MeF reaction was further analysed using an FTIR instrument equipped with an ATR (attenuated total reflection)

accessory cell to identify hidden molecules, which were IR active. **Figure 5.7** shows the IR spectra of the resulting mixtures after the MeF and methoxide reaction in the various solvents. The grey lines represented the pure solvents' spectra, while the black lines represent the resulting mixture spectra for the B-G spectra. For easy comparison, the spectra in A were pure MeOH, MeF and sodium formate (NaOOCH) spectra. In the spectra B-G, the bands 2830, 2700, 1650, 1570, 1360 and 770 cm^{-1} which is attributed to NaOOCH [152] were observed in all the mixtures. This indicated that NaOOCH was made in all the solvents.

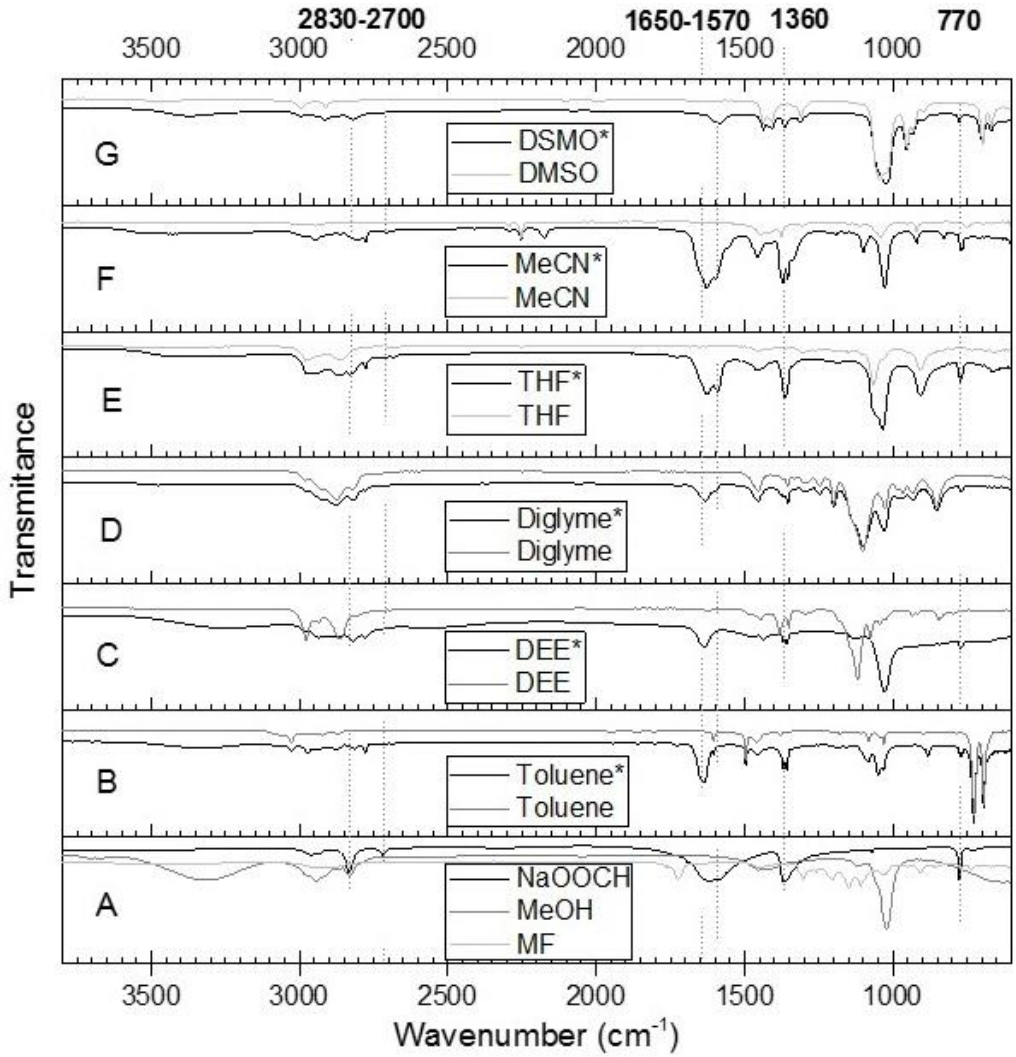

Figure 5.7: ATR-IR spectra of solvent (B-G in grey), and reaction mixture (B-G, black with *). The spectra A is for MeOH, MeF and NaOOCH. The NaOOCH (in black) was adopted from NIST data base [152]

The MeF reaction in the different polar solvents undertook two main reaction paths. All the products shown in Equations (5.1) and (5.2) were observed from the analysis of the resulting mixture in all the solvents. This indicated that the MeF was involved in the carbonylation reaction and the nucleophilic substitution reactions, resulting in the formation of CO + MeOH, and DME + NaOOCH respectively. However, only the CO + MeOH were quantified, while the DME + NaOOCH were qualitatively determined to be present. Assuming that the MeF undertook only the two reaction paths, then from the starting amount of MeF, the remaining C counts for a mass balance can be attributed to the nucleophilic reaction. In that case, the nucleophilic substitution reaction increased with solvent polarity.

The decarbonylation reaction was favoured in the less polar solvents. The relative higher amount of CO released, coupled with higher amount of MeOH in the less polar solvents suggested that carbonylation-decarbonylation which is a fast equilibrium step in the LTMS reaction exhibited preference for a less polar environment. This was not surprising as CO is relatively non-polar and will solubilize better in a less polar than more polar solvents [150]. Therefore, lowering solvent polarity increases the mass transfer of CO in the solvent, thereby enhancing MeOH production. The nucleophilic reaction on the other hand, was favoured in the more polar solvents. It is generally known that bimolecular reactions involving ionic intermediates are better stabilized in polar environment [153]. Hence, considering the fact that the formation of ionic salts was involved, it is not surprising that the nucleophilic pathway was favoured in the more polar solvents. However, this indicated that increasing solvent's polarity will increasingly destabilize the MeF intermediate which can lead to side products outside the expected products in the LTMS reaction. Since the DME and the NaOOCH formed are not involved in the main LTMS steps, their formation could adversely reduce the overall MeOH production especially if the hydrogenolysis step is slower.

In the overall LTMS reaction studied for the different aprotic polar solvents in the previous Sections (5.1 & 5.3), the highest MeOH production was observed in diglyme with $\varepsilon = 7.2$. So far, while the decarbonylation-carbonylation step was favoured in less

polar solvents, highly polar solvent reduces the MeF stability for nucleophilic reactions. It therefore appears that the hydrogenolysis, decarbonylation and nucleophilic reactions have a comparable activation barrier, such that slight changes in polarity can favour one over the other reactions. As a result, irrespective of the solvent's polarity, the amount of MeF in the LTMS remained relatively low. Hence, it appears that good compromise in the chemical environment is required to encourage both the carbonylation step and hydrogenolysis. Some level of polarity was required to achieve maximum conversion. This was because, since the hydrogenolysis is the rate determining step, any environment to destabilize the MeF will enhance the LTMS reaction. Nonetheless, this destabilization should be moderate otherwise it will lead to side reactions which will drastically reduce the MeOH production when the nucleophilic pathway is enhanced.

The formation of NaOOCH from the nucleophilic reaction poses an important catalyst deactivation pathway. So far, most of the deactivation in the LTMS reaction in relation to the methoxide catalyst has been attributed to the presence of H_2O and CO_2. However, it appears that irrespective of the solvents used, NaOOCH was formed. Even though, in the overall LTMS reaction, relatively low amount of this side reaction is expected to occur in a moderately polar solvent, the continuous formation can eventually consume all the starting methoxide present. Therefore aside Cu agglomeration as one path to catalyst deactivation in the LTMS reaction, NaOOCH formation is also another path to the methoxide deactivation, the importance of which increases with increasing solvent's polarity.

5.5 Summary

The importance of solvent's polarity in the LTMS reaction was studied using 8 different aprotic polar solvents. In the overall LTMS reaction, polar solvent with similar polarity as diglyme with ε= 7.2 produced maximum amount of MeOH production. This trend was independent of the Cu nanoparticle sizes. Furthermore, the differences in ether-solvent

polarity and chain length did not have any major effect on the size of Cu nanoparticles formed in the once through system. Overall, the solvent polarity seemed to dictate the side reaction of the main intermediate in the LTMS reaction. MeF in the presence of $NaOCH_3$ undergoes two main reactions (i) decarbonylation to form CO and MeOH and (ii) nucleophilic substitution reaction to form DME and NaOOCH. Decreasing solvent's polarity increased the decarbonylation as non-polar CO solubilized better in less polar solvents, while nucleophilic substitution reaction was enhanced with increasing polarity since it involves polar ionic salt formation. The pathway of the nucleophilic substitution reaction presents a deactivation pathway for the methoxide catalyst in the LTMS reaction, the importance of which increased with increasing polarity of solvent. Overall, moderately polar solvents such as diglyme present a good compromise with carbonylation and a moderate polar environment for hydrogenolysis of MeF.

6 Hydrogenolysis Reaction in the LTMS Reaction; a Synergistic Perspective

The LTMS reaction has been discussed so far based on a concurrent approach, where both carbonylation and hydrogenolysis occurred in one pot. However, previous reports have shown that, when the reactions are carried out in a step-wise approach, the rate of MeF hydrogenolysis is much slower compared to when both steps are combined [27, 74]. This implied that, the concurrent approach is not a simple summation of the main two reaction steps. Hence, in this section, our aim was to investigate the relationship between the Cu-based and the alkoxide catalysts involved in the LTMS, with particular focus on the hydrogenolysis step. Furthermore, we investigated to which extent the determined synergy can be applied to CO_2 hydrogenation directly or indirectly via a carbonate intermediate.

6.1 Hydrogenolysis of Methyl formate using CuO/SiO_2 Catalyst

The MeF hydrogenolysis reaction was done using the CuO/SiO_2 catalyst characterized in Section (4.2.3). **Figure 6.1** shows the effect of pressure on the hydrogenolysis reaction at 100 ^oC in diglyme solvent. The main product was MeOH with less than 1 % selectivity to CO and CO_2 within the 9 to 18 bar H_2 partial pressure tested. The highest conversion observed was below 10 % even at 18 bar of H_2 pressure within 2 h. This was much less, compared to over 75 % syngas conversion observed in the concurrent reaction system discussed in Chapters 4 and 5. Generally, the H_2 conversion increased with increasing H_2 pressure. Since the total number of reactants were more than the total number of products formed from the stoichiometry in Equation (6.1), MeOH formation was expected to increase with pressure.

$$CH_3OOCH + 2H_2 \rightleftharpoons 2CH_3OH \quad \Delta H = -47.5\ \mathrm{kJ/mol} \quad (6.1)$$

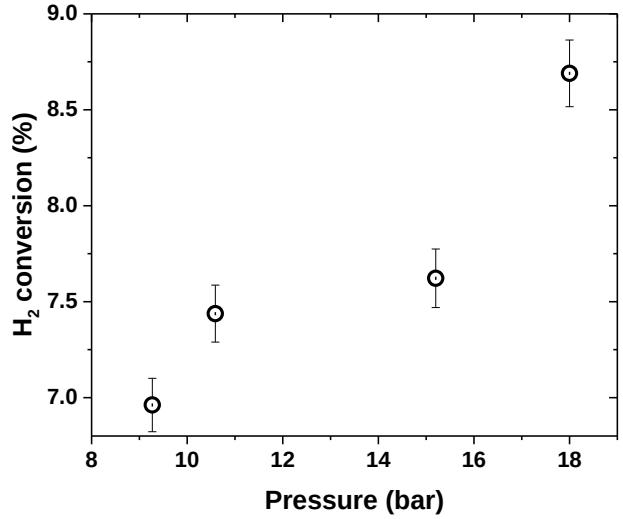

Figure 6.1: Effect of pressure on MeF hydrogenolysis; $CuSiO_2$=0.45 g, 2 h, 40 ml diglyme, MeF = 81 mmol, 100 ^oC

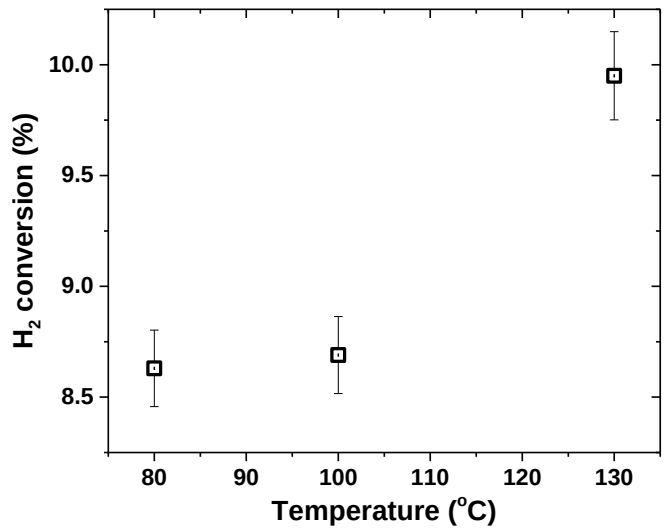

Figure 6.2: Effect of temperature on MeF hydrogenolysis; $CuSiO_2$=0.45 g, 2 h, 40 ml diglyme, MeF = 81 mmol, H_2 pressure = 18 bar

The effect of the reaction temperature was also studied on the hydrogenolysis reaction and is shown in **Figure 6.2**. Here, hydrogenolysis increased with increasing the reaction temperature from about 8 to 10 % H_2 conversion. Selectivity to MeOH was observed to be around 99 % within 80 to 130 ^oC temperatures. The remaining products were CO and CO_2. The CO and CO_2 could originate from parallel decarbonylation and decarboxylation of the MeF. Even though the hydrogenolysis is an exothermic reaction, conversion

increased from 80 to 130 ^{o}C. Sørum's detailed study of the MeF hydrogenolysis suggested that, to obtain more than 50 % conversion, more than 160 ^{o}C temperature and H_2 partial pressure above 60 bar is required [50]. Considering, the maximum of 130 ^{o}C and 18 bar H_2 partial pressure conditions applied in this study, the lower conversion was not surprising since our operating conditions were far below Sørum's operating conditions for MeF hydrogenolysis. However, it was clear that the conversions achieved for the hydrogenolysis step alone was much less, than the conversions observed in the concurrent study at similar operating temperature and H_2 partial pressure.

6.2 Hydrogenolysis of Methyl Formate Catalysed by Cu-Alkoxide System

The Cu-based catalyst appears to give relatively lower conversion when comparable operating conditions for a standard LTMS reactions were applied. As a result we investigated a possible active component formed during the concurrent LTMS reaction. **Table 6.1** shows different catalyst components for MeOH production at 100 ^{o}C. 1 bar N_2 was added to the reacting gas as an inert to aid in determining conversion and selectivity of the gas phase. No syngas conversion was observed when only CuO/SiO_2 nanoparticles were used as catalyst within 1 h reaction time. This was in contrast to the situation when Cu-alkoxide catalyst system was present, where 60 % syngas conversion was observed. Even though some others [97] have observed syngas conversion over Cu nanoparticles, without the presence of alkoxide, these were carried out at about 140 to 170 ^{o}C for more than 3 h reaction time. Thus, lower reaction temperature was used in our study and hence no activity observed within 1 h reaction time.

To check whether ionic copper methoxide was responsible for the LTMS reaction, $Cu(OCH_3)_2$ was tested for syngas activity. When $Cu(OCH_3)_2$ was used alone as catalyst, no syngas conversion was observed, except in combination with CuO/SiO_2 catalyst when 12 % syngas conversion was observed. This indicated that ionic copper methoxide had very little or no influence on the LTMS reaction. Furthermore, with the observed formation of NaOOCH during the solvent effect study in Chapter 5, NaOOCH was tested

to see whether their formation was essential for the LTMS reaction. When the NaOOCH was added to the CuO/SiO_2 catalyst, 10 % syngas conversion was observed. Similar to the $Cu(OCH_3)_2$, the NaOOCH hardly played a role in the LTMS reaction at our operating conditions. That is, even though some activity was observed using the $Cu(OCH)_3$ and NaOOCH in combination with CuO/SiO_2, their contribution to the overall syngas conversion was rather marginal compared to the activity in the presence of $NaOCH_3$.

Table 6.1: Variable catalyst composition for MeOH production, $CuSiO_2$= 0.45 g, $NaOCH_3$= 19 mmol, NaOOCH = 19 mmol, MeF = 81 mmol, $Cu(OCH_3)_2$=10 mmol, 100 ^oC, N_2 = 1 bar, total pressure = 20 bar, 1 h

Reactants	***Catalyst system***				***Conv***	***Selectivity (%)***		
	$CuSiO_2$	***$NaOCH_3$***	***NaOOCH***	***$Cu(OCH_3)_2$***	***(%)***	***MeOH***	***MeF***	***CO***
$CO+H_2$	*	*			60	98	2	-
$CO+H_2$	*				0	-	-	-
$CO+H_2$				*	0	-	-	-
$CO+H_2$	*			*	12.2	100	0	-
$CO+H_2$	*		*		10	100		
MeF + $CO+H_2$	*				4	100	-	-
MeF+H_2	*				8.7	99	-	<1
MeF+H_2	*	*			26.5	59		41

Since inclusion of the $Cu(OCH)_3$ and NaOOCH in the syngas reaction did not show substantial activity, they were not included as catalyst for testing the MeF hydrogenolysis. When syngas, with 16 H_2: 3CO: $1N_2$ composition was used as the reactant gas, only 4 % H_2 conversion was observed. The hydrogenolysis over the CuO/SiO_2 showed almost twice the activity when only H_2 was used without the CO. It is known that CO and H_2 compete for active sites on the Cu-based catalyst [27], and therefore the observed reduction in activity in the presence of CO was not surprising. When $NaOCH_3$ was added to the Cu nanoparticles, 26.5 % H_2 conversion was observed. Even though a significant decarbonylation reaction occurred, the conversion due to hydrogenolysis tripled as compared to the case without $NaOCH_3$.

The observed enhancement of the hydrogenolysis in the presence of $NaOCH_3$ suggested a possible synergistic relationship between the Cu nanoparticles and the $NaOCH_3$

catalyst. To probe this further, the amount of $NaOCH_3$ added to the Cu nanoparticles were varied for MeF hydrogenolysis and shown in **Figure 6.3**. The H_2 conversion increased sharply with increasing the amount of $NaOCH_3$ up to about 3 mmol, where H_2 conversion levelled off with increasing $NaOCH_3$. At the same time with the sharp increase in hydrogenolysis, marginal amount of CO was released. However, at the point of levelling off of the hydrogenolysis, an exponential increase in the CO was observed. This indicated that, the $NaOCH_3$ played two main roles, assisting in hydrogenolysis reaction as well as the decarbonylation side reaction.

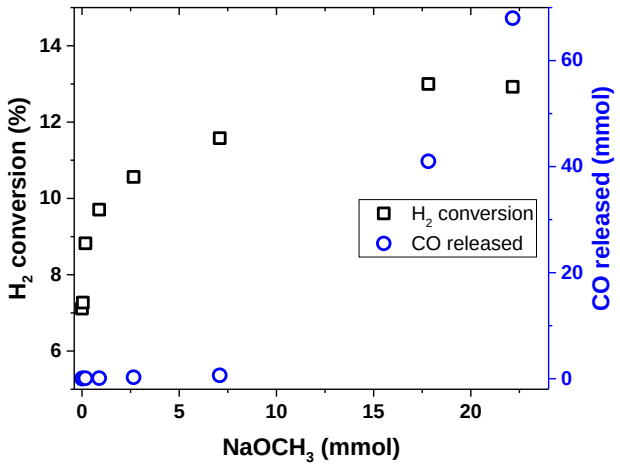

Figure 6.3: $NaOCH_3$ variation on hydrogenolysis of MeF, H_2 pressure = 10 bar, CuO/SiO_2 = 0.50 g (6.3 mmol), MeF = 81 mmol 100 °C, dig = 40 ml, 1 h

The increase in the hydrogenolysis of MeF in the presence of $NaOCH_3$ suggests some relationship between the two catalysts. Considering the fact that hydrogenolysis increased when there was little CO released, both catalysts seem to play an important role in the catalysis. After 7 mmol $NaOCH_3$, further increase in the amount of $NaOCH_3$ only went into increasing the decarbonylation reaction. This implies that, the $NaOCH_3$ probably occupied the surface of the Cu catalyst to promote the hydrogenolysis of the MeF. When the amount of $NaOCH_3$ exceeded a certain maximum for the hydrogenolysis promotion, further increase only went into enhancing the side decarbonylation reaction. Furthermore, the hydrogenolysis activity could also have been reduced by the increase in the amount of CO. As has already been reported, CO appears to compete with H_2 for available active Cu sites, and hence continuous increase in CO production

could further reduce the hydrogenolysis reaction [50]. Nevertheless, $NaOCH_3$ clearly shows a promoting effect on the Cu-nanoparticles for the hydrogenolysis reaction.

6.3 Direct and Indirect CO_2 hydrogenation using the Hydrogenolysis Catalyst System

The identified role of the Cu-alkoxide system investigated in the LTMS reaction can be extended to include CO_2 hydrogenation. CO_2 is known to poison the LTMS reaction catalyst system particularly the alkoxide co-catalyst [26, 27]. That is, the CO_2 reacts with methoxide to form a methyl carbonate salt as illustrated in Equation (6.2). However, a very active hydrogenation catalyst will be able to hydrogenate the carbonate salt formed. Without such an active catalyst, the inclusion of CO_2 for the LTMS reaction might continue to have an adverse effect on the methoxide system. However, to what extent will the CO_2 affect the LTMS reaction if for example CO is replaced by CO_2? One alternative is to study CO_2 hydrogenation via a carbonate intermediate, and then compare with a direct CO_2 hydrogenation using the catalyst system used for the LTMS catalyst in this work.

$$CO_2 + NaOCH_3 \rightleftharpoons NaOOCOCH_3 \qquad (6.2)$$

To investigate the role of the Cu nanoparticles and its associated hydrogenolysis co-catalyst, a dimethyl carbonate (DMC) was used, and compared with MeF, as shown in **Table 6.2**. When $CuSiO_2$ alone was used as catalyst, 24 % and 25 % H_2 conversion was observed for the MeF and the DMC hydrogenolysis reactions respectively over a 12 h reaction time. Here, 99 % selectivity to MeOH was observed with minor amount of CO and CO_2 selectivity. In both cases, the selectivity to CO_2 was about 4 times more than the selectivity to CO. When the hydrogenolysis was carried out with the $CuSiO_2$ and $NaOCH_3$ catalysts, the conversion in DMC was 12 %, just about a third of the conversion in the MeF hydrogenolysis, which was 36 % after 6 h reaction time. MeOH was once again the main product, comprising of 93 and 91 % for the MeF and the DMC hydrogenolysis reactions respectively. Based on the results in the **Figure 6.3**, the

amount of $NaOCH_3$ was limited to 2.7 mmol, where CO release was minimal. The selectivity to CO and CO_2 were 5.8 and 1 % respectively for the MeF reaction. No CO was however observed in the dimethyl carbonate reaction, with about 9 % selectivity to CO_2.

Table 6.2: Hydrogenolysis of MeF and DMC over $CuSiO_2$ catalysts; $CuSiO_2$ = 0.45 g, Dig=40 ml, 100 ^oC, H_2 = 19 bar, $NaOCH_3$ = 2.7 mmol, DMC = 55 mmol, MeF = 83 mmol

Reaction	*Time (h)*	*H_2 conversion (%)*	*Selectivity (%)*		
			MeOH	*CO*	*CO_2*
MeF + H_2	12	24	98.9	0.2	0.8
DMC + H_2	12	25	99.4	0.1	0.5
MeF+$NaOCH_3$+H_2	6	36	93.2	5.8	1.0
DMC+$NaOCH_3$+H_2	6	12	91.4	0.0	8.6

Table 6.3: Once through catalyst system for hydrogenolysis; ($Cu(CH_3COO)_2$ = 3.6 mmol, $NaOCH_3$ = 19 mmol, MeOH = in 50 ml diglyme, total 20 bar, at 100 ^oC, DMC = 55 mmol, MeF = 83 mmol

Reaction	*Time (h)*	*H_2 Conversion (%)*	*Selectivity (C %)*			
			MeOH	***MeF***	**CO**	**CO_2**
MeF + H_2	2	42	66.9	-	32.5	0.6
DMC+H_2	2	12	69.8	20.9	2.3	7.0
1CO+2H_2	2	73	95.4	4.6	-	0
1CO_2+3H_2	24	38	80.1	19.8	0.1	-

The once through catalyst preparation system was also tested for the CO_2 hydrogenation reactions. **Table 6.3** shows the once through LTMS reaction for hydrogenolysis using Cu-alkoxide catalyst system. The Cu-alkoxide catalyst was prepared in a similar way as in Section 4.1 at 100 ^oC. H_2 conversion was 42 % in MeF reaction while 12 % conversion was observed in the dimethyl carbonate reaction. In the MeF reaction, about 67 % selectivity to MeOH was observed, with 32 and 1 % selectivity to CO and CO_2 respectively. In the DMC reaction, aside 70, 2 and 7 % selectivity to MeOH, CO and CO_2 respectively, 21 % selectivity to MeF was observed. Apart from these products, there were traces of dimethyl ether. To put the hydrogenolysis into perspective, CO and CO_2 hydrogenation was carried out using similar Cu-alkoxide catalyst system just as was carried out in the hydrogenolysis reaction. Whilst 73 % H_2 conversion was observed in the CO hydrogenation reaction after 2 h, 38 % H_2 conversion

was observed in the CO_2 hydrogenation reaction after 24 h. Here, 80 and 20 % selectivity to MeOH and MeF respectively were observed for the CO_2 hydrogenation reactions. Comparably, in the CO hydrogenation, about 95 and 5 % selectivity to MeOH and MeF was observed.

Cu nanoparticles were effective for DMC hydrogenolysis without any alkoxide promotion. Considering the increment of activity when methoxide was added in the MeF hydrogenolysis, no such enhancement was observed in the dimethyl reaction. Moreover, even though it appeared that there was a certain threshold amount of $NaOCH_3$ required after which the excess influences CO formation during the MeF hydrogenolysis, this was not the case in the dimethyl carbonate reaction. Rather, moderate amount of CO_2 was released, which was much less than the CO released in the MeF reaction when $NaOCH_3$ was included in the once through catalyst system. Lian et. al. [100] have reported that various Cu-based nano-catalysts were sufficient for ethylene carbonates hydrogenolysis at 180 ^oC and 50 bar H_2 pressure. Even though, lower operation temperature and pressures were used in this work, appreciable amount of hydrogenolysis of DMC was realized. Therefore, the promotion effect of methoxide on the Cu-based catalyst for the MeF hydrogenolysis was not necessary for the DMC hydrogenolysis. Hence, Cu nanoparticles was mainly responsible for the hydrogenolysis of the DMC.

Furthermore, Cu nanoparticle size influenced the hydrogenolysis of the formate and the carbonate. The hydrogenolysis of the DMC within 2 h for the once through catalyst system was at similar conversions as was observed for the 12 h reaction with the CuO/SiO_2 catalyst. With the promotion effect of the methoxide, the MeF hydrogenolysis reaction showed higher conversion within 2 h in the once through Cu catalyst system compared to the over 6 h CuO/SiO_2 system. As previously characterized, the CuO/SiO_2 catalyst consisted of about 30 ± 5 nm CuO (Section 5.3) while the Cu particles in the once through system was 10 ± 5 nm Cu_2O particles (Section 4.1). Moreover, the size of Cu nanoparticles has been shown in Chapter 4 to influence LTMS reaction particularly with

respect to the hydrogenolysis reaction. Hence the observed results in the two Cu-based catalysts confirm the role of Cu nanoparticle size in the hydrogenolysis reaction.

It appears there is a relationship between the hydrogenolysis of MeF and the DMC. In both reactions, CO and CO_2 products were observed as products and followed similar trend to selectivity in the absence of methoxide over the 12 h reaction time. When methoxide was added, although the trend to selectivity differed, the selectivity to the CO and CO_2 products increased in both reactions. That is, decarbonylation and decarboxylation in the MeF and DMC reactions respectively, increased. Considering the fact that, in the MeF and DMC contained carbonyl and carboxyl functional groups respectively, the presence of methoxide influenced the release of these groups. Methoxide is well known to catalyse both carbonylation [24] and carboxylation [154] reactions, and hence the observed decarbonylation and decarboxylation in the presence of methoxide is not surprising.

Furthermore, in the presence of the methoxide in the once through reaction, significant selectivity to MeF was observed for the hydrogenolysis of the DMC within 2 h. Even though, this was not observed in the 6 h CuO/SiO_2-alkoxide catalysed reaction, it appears that, the hydrogenolysis of the DMC was initially preceded by hydrogenation and subsequently split into MeOH and MeF, after which the reaction assumed the usual hydrogenolysis mechanism. It has been suggested that MeO-C cleavage to form MeOH and MeF occurs first before subsequent hydrogenlysis of the MeF using a ruthenium-based homogeneous catalyst [155-157]. It is possible that a similar trend in the homogeneous system occurred in our catalyst system. In addition, the presence of methoxide promoted only hydrogenolysis of MeF but not that of DMC. Our preliminary explanation is that, if MeO-C cleavage occurred as an initial step, then there would be adequate amount of methoxy group on the Cu-catalyst surface (either adsorbed by or near the reaction sites). Any extra methoxide added might not have direct effect on the hydrogenolysis of the DMC, just as was observed for the hydrogenolysis of MeF, where excess methoxide rather engaged in promoting side reaction. This notwithstanding, a

more detailed kinetics and mechanistic study will throw more light on the mechanism to either confirm or disprove this assertion.

Overall, the LTMS synthesis appears to have a window for CO_2 utilization, but will require further attention on designing a more active Cu catalyst. The Cu-alkoxide appears to be a good starting point, as about 36 % H_2 conversion could be achieved after 24 h. However it is important to note that, recycling the methoxide catalyst will still be an issue to deal with as no significant activity was observed when the CO_2+H_2 charging was repeated. Nevertheless, the ability of the Cu-based catalyst to indirectly hydrogenate the CO_2, serves as a window of opportunity for further exploration. For example, if a form of methoxide is used as reactant rather than a catalyst, then the CO_2 hydrogenolysis reaction can be performed under the LTMS reaction conditions as expressed in Equations (6.2) and (6.3). Alternatively, a direct conversion of CO_2 to organic carbonate [154, 158], and then subsequently as an intermediate can be used for the hydrogenolysis as expressed in Equation (6.4). Hence CO_2 utilization in the LTMS reaction conditions is highly possible but will require a closer attention especially in designing a co-catalyst to optimize the entire catalyst system.

$$\mathrm{NaOOCOCH_3} + 3\mathrm{H_2} \rightleftharpoons 2\mathrm{CH_3OH} + \mathrm{NaOH} \qquad (6.3)$$

$$\mathrm{H_3COOCOCH_3} + 3\mathrm{H_2} \rightleftharpoons 3\mathrm{CH_3OH} \qquad (6.4)$$

6.4 Summary

The study of hydrogenolysis of MeF over Cu-based catalyst has been shown to be slower than when LTMS reaction is carried out concurrently. Although reaction conditions such as temperature and pressure increase hydrogenolysis, the relative conversion simply do not match up to a typical one pot LTMS in a Cu-alkoxide catalyst system at 100 ^{o}C reaction temperature. Among the possible active component that could be responsible for the enhanced activity in syngas conversion, only $NaOCH_3$ showed an increase in MeF activity. Thus $NaOCH_3$ showed a promoted MeF hydrogenolysis reaction such that increasing $NaOCH_3$ led to a sharp increase in hydrogenolysis. However, after a certain

threshold, further increase in $NaOCH_3$ only led to decarbonylation rather than a further promotion of hydrogenolysis. This suggested that there is a certain synergistic relationship between the Cu-based catalyst and the methoxide for hydrogenolysis. When the catalyst system was extended to DMC hydrogenolysis, relative conversions were comparable to the MeF hydrogenolysis conversions. It appeared that hydrogenolysis of MeF and DMC followed similar mechanisms but will require further study to confirm that. Moreover, direct hydrogenation of CO_2 in a similar reaction condition as the LTMS reactions were feasible, but will require methoxide to be a reactant rather than a co-catalyst.

7 Tailoring Cu Nanoparticles using Spinning Disk Reactor

The size of Cu nanoparticles has been shown to influence MeOH production. Previously, we have observed that increasing active Cu surface area due to decreasing Cu particle size increases MeOH productivity. This implies that a relatively easy approach for producing on-purpose Cu nanoparticle sizes is important in the LTMS process. Most of the reported methods for making defined Cu nanoparticle sizes involve entirely different experimental protocols and chemical recipes for making different particle sizes [110]. To the best of our knowledge, a straight-forward method for fine tuning Cu nanoparticle sizes with narrow particle distribution for catalysing MeOH synthesis by mere changing of physical operating parameters while maintaining the same chemical recipe is lacking. One promising continuous-flow process technique with an enhanced uniform micro-mixing ability to control the nucleation and growth in precipitation reaction during nanoparticle fabrication is by using the spinning disk reactor (SDR) [117]. The focus of this section is to use the spinning disk reactor (SDR), to finely tune Cu nanoparticle size for the LTMS process.

7.1 Preliminary Study of Cu Borohydride Reduction Reaction

The SDR is a continuous-flow process with short residence time for fine-tuning nanoparticles fabrication and is therefore more beneficial for processing fast reactions, which occur within the short time of residence on the disk surface. Cu borohydride reduction reaction, expressed in Equation (7.1) is one example of such fast reaction [133]. The preliminary study in a stirred tank reactor (STR) showed that drop-wise addition of 0.021 M aqueous $NaBH_4$ unto aqueous 0.011 M $Cu(NO_3)_2$ reacts instantaneously to produce a black precipitate. The resulting slurry was oven dried at 70 ^oC after stirring for 60 min. **Figure 7.1** shows the X-ray diffractogram and SEM images of the oven dried samples. Cu_2O was observed as the predominant phase, with 25 ± 1 nm crystallite size. Even though Cu^0 was the expected phase per Equation (7.1), it is possible

the particles easily oxidised on the surface such that Cu_2O was the main product considering the fact that, the slurry sample was oven dried in static air.

$$Cu^{2+} + 2BH_4^- + 6H_2O \rightarrow Cu \downarrow + 7H_2 + 2B(OH)_3 \qquad (7.1)$$

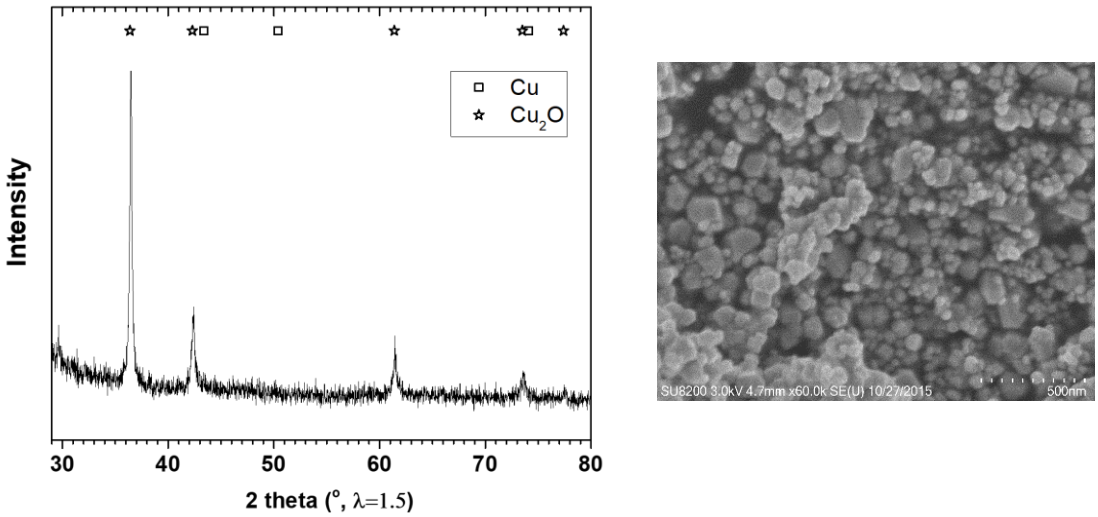

Figure 7.1: XRD (left) and SEM (right) of Cu NP made in a stirred tank; 0.011 M $Cu(CH_3COO)_2$ and 0.021 M $NaBH_4$ in water, stirred at 700 rpm

Similar experiment was carried out using diglyme rather than water as solvent, and the XRD and SEM characterization shown in **Figure 7.2**. Here, the resulting slurry sample after 60 min of stirring was put in a capillary for the XRD measurement without drying. Contrary to the experiment in aqueous medium, Cu^0 was the predominant phase with about 10.8 ± 0.4 nm crystallite size. Since diglyme samples were not subjected to drying, relative exposure to air was low and therefore the resulting crystals predominantly remained in the reduced oxidation state. Furthermore, it appears the crystallites in the diglyme solvent were smaller than was observed for the water samples. It is possible the presence of the diglyme solvent with its lone pairs of electrons provided some sort of chelates around the Cu ions [159] which controlled the particle growth and also minimized agglomeration.

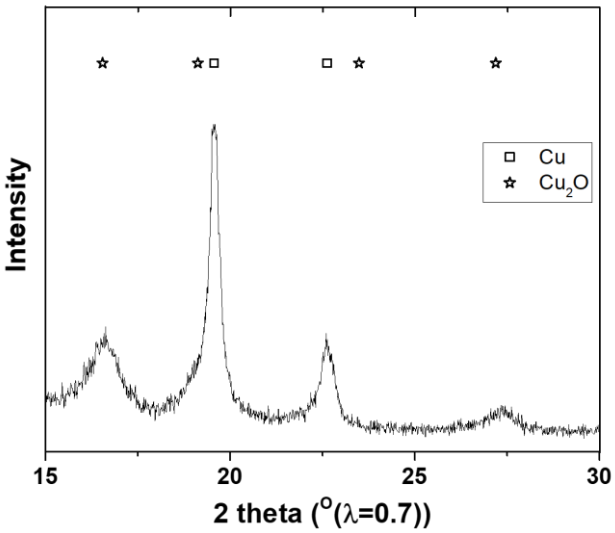

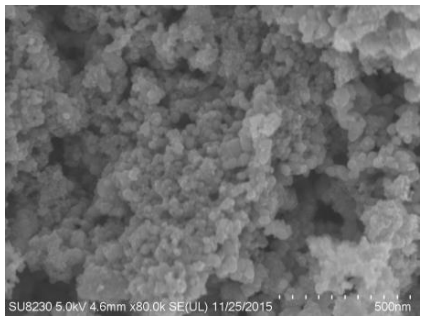

Figure 7.2: XRD (left) and SEM (right) of Cu NP made in a stirred tank; 2.2 mmol $Cu(CH_3COO)_2$ and 2.5 mmol $NaBH_4$ in 15 ml diglyme

The STR was used as a preliminary study to set the stage for the use of the SDR for Cu nanoparticles synthesis. In the following sections, we will investigate whether the Cu nanoparticle size and size distribution can be controlled by varying physical and chemical parameters in the SDR process. To avoid agglomeration of the particles that exited from the SDR, the slurry samples were collected in starch as has been used elsewhere [160]. The influence of starch on the particle size distribution is shown in **Figure 7.3**. Wider particle size distribution with larger mean particle sizes ranging from 10 to 15 nm were observed in the samples without starch. However when the particles were collected in starch gelatine, a narrower particle size distribution with about 6 ± 1 nm mean particle size was observed. Furthermore, no significant differences was observed in the particle size distribution as well as the mean particle sizes for the 1 to 33.3 1 g/L starch concentrations. The starch therefore served as a capping agent to stabilize and prevent further agglomeration of the Cu nanoparticles made. Hence, 1 wt % or 10 g/L starch gelatine concentration was selected for collecting the slurry samples that exited from the SDR.

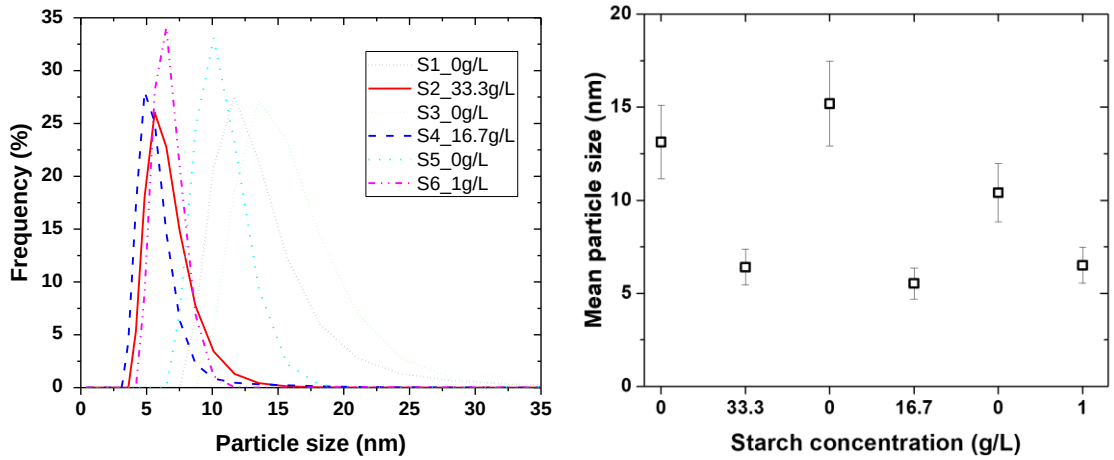

Figure 7.3: Effect of starch concentration on particle size distribution (left) and mean particles size (right) after 1 day, 0.01 M $Cu(NO_3)_2$/0.02 M $NaBH_4$, flow ratio=2, flow rate=5.5 ml/s disk speed= 2400 rpm

7.2 Effect of Rotation of Disk Speed and Flow Rate on Particle Size

The effect of the rotation speed of the SDR on the nanoparticle size and particle size distribution were studied using aqueous $Cu(NO_3)_2$ and aqueous $NaBH_4$ streams at 5 ml/s total flow. The resulting effluent was collected in starch to minimize further agglomeration and particle growth after sample collection. **Figure 7.4** shows the effect of the rotation speed on the particle size distribution and mean particle size. The faster the disk rotation speed the tighter the particle size distribution. The mean particle size using 0.01 M $Cu(NO_3)_2$ and 0.02 M $NaBH_4$ streams decreased with increasing disk rotation speed from 35 to 8 nm for the 400 to 2400 rpm speed respectively. When the concentration of the reagents were increased to 0.05 M and 0.10 M for the $Cu(NO_3)_2$ and $NaBH_4$ respectively, the trend in the particle size distribution and mean sizes were similar. The mean particle size decreased from 55 nm at 400 to 10 nm at 2400 rpm disk rotation speed at the 0.05 M $Cu(NO_3)_2$ concentration.

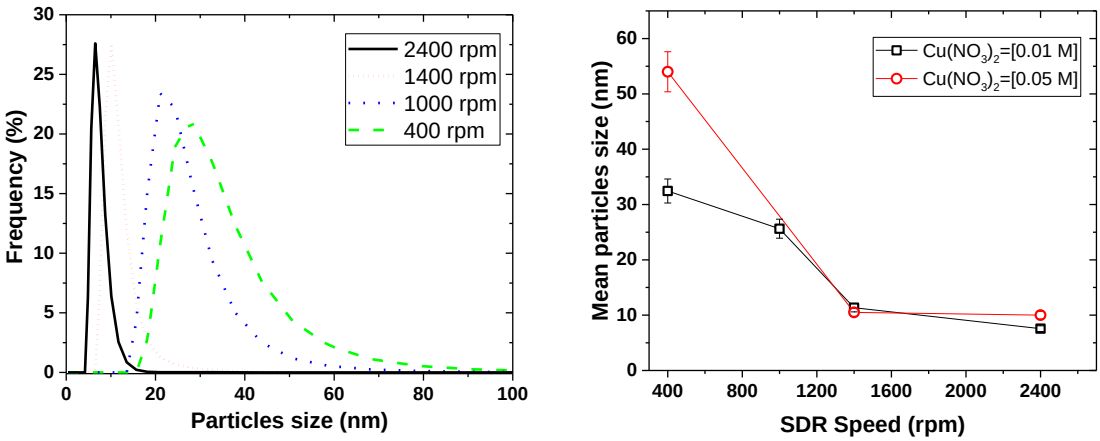

Figure 7.4: Effect of SDR spinning on particle size distribution (left) and mean particle size (right) at 0.01 M $Cu(NO_3)_2$/0.02 M $NaBH_4$ and 0.05 M $Cu(NO_3)_2$/0.10 M $NaBH_4$, total flow rate=5.5 ml/s, disk speed= 2400 rpm

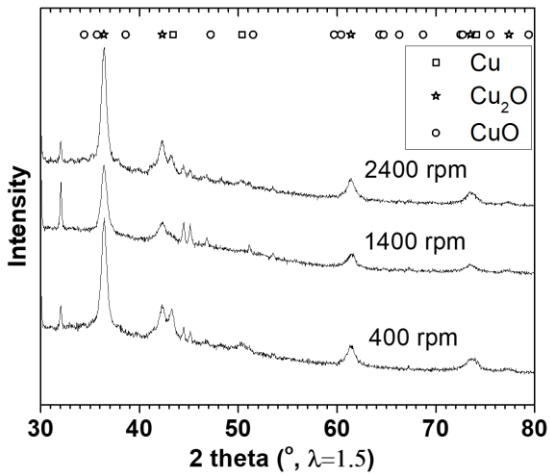

Figure 7.5: XRD of the dried sample from the 0.05 M Cu precursor experiment in Figure 7.4

The resulting mixture was oven dried at 70 °C and characterized using XRD to ascertain the formation and phase of Cu crystallite produced. **Figure 7.5** shows the XRD of Cu nanoparticles produced from the 0.05 M $Cu(NO_3)_2$ starting concentration experiment. The X-ray diffractogram showed Cu_2O as the predominant crystallite phase followed by some Cu^0 peaks. Since the entire mixture was dried without washing off the salt formed, some sharp reflections from $NaNO_3$ was also observed. Rietveld analysis of the mean crystallite sizes of the dried Cu_2O phase was estimated to be 10 ± 1, 9.5 ± 0.7, and 9.5 ± 0.5 nm for 400, 1400, and 2400 rpm respectively. That is, the crystallite sizes of the dried

Cu_2O particles were similar for all the 3 disk rotation speed samples but varied in the mean particle sizes and size distribution.

The total flow rate of the reagent stream was varied at constant flow ratio and 2400 rpm rotation speed. **Figure 7.6** shows the effect of the total flow rate on particle size distribution and the mean particle size. This was done using 0.02 M $NaBH_4$ flow to 0.01 M $Cu(NO_3)_2$ flow ratio of 2 and 2400 rpm disk rotation speed at 25 ^oC. The faster the total flow, the narrower the particles' distribution. The mean particle size decreased from 14 ± 1 to 3.2 ± 0.2 nm with increasing total flow rate from 3 to 9 ml/s respectively. In addition, the resulting sample from the 9 ml/s total flow experiment was oven dried at 70 ^oC and characterized with XRD and TEM. **Figure 7.7** shows the XRD and TEM image of the 9 ml/s sample. Rietveld analysis of the diffractogram showed Cu_2O as the main phase with about 4 ± 1 nm crystallite size. The TEM imaging revealed approximately 3–5 nm spherical shaped crystals, which were surrounded by large amorphous materials suspected to be the starch used for keeping the particles from agglomerating. Overall, the XRD and TEM results confirmed that Cu_2O nanocrystals were produced after drying with representative particle sizes as reported using the dynamic light scattering measurement.

Generally, the particle size distribution narrowed with increasing disk rotation speed and total flow rate. This can be explained based on the degree of micromixing achieved in the course of the synthesis. During the synthesis process, the thin film formed on the disk surface when the liquid reagents are introduced experiences an increase in shear effect and surface wave intensity as rotation speed and total flow increases [117, 118]. Mohammadi's [117] results showed that increasing rotation speed and flow rate leads to shorter micromixing time during TiO_2 nanoparticle synthesis. Shorter micromixing time implies a more rapid homogeneous mixing at the molecular level, which enhances a more uniform supersaturation within a shorter time. Shorter micromixing time leads to faster and uniform nuclei formation compared to crystal growth [161]. Hence, increasing the disk rotation speed and flow rate led to uniformly-sized nuclei, which eventually led to a tighter particle size distribution.

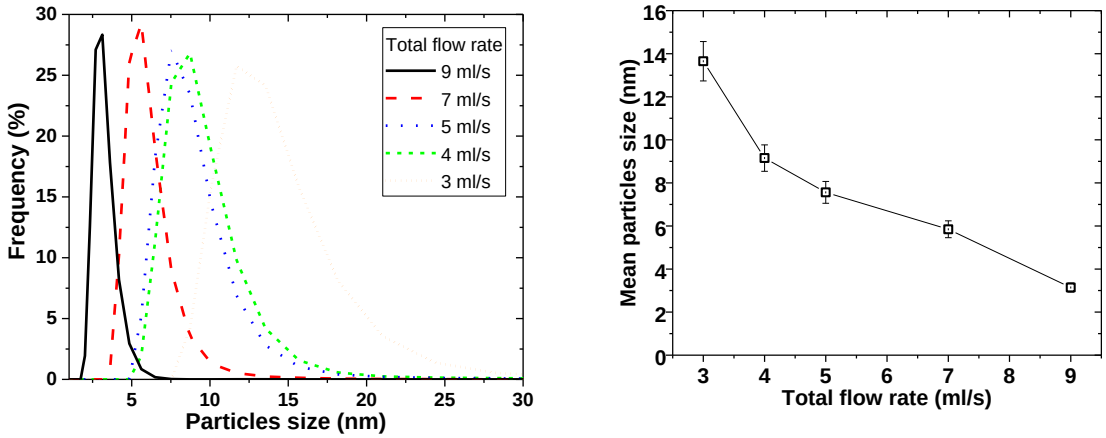

Figure 7.6: Effect of flow rate on particle size distribution (left) and mean particle size (right), 0.02 M $NaBH_4$ (in 0.004 M NaOH)/0.01 M $Cu(NO_3)_2$ flow ratio = 2, disk speed = 2400 rpm.

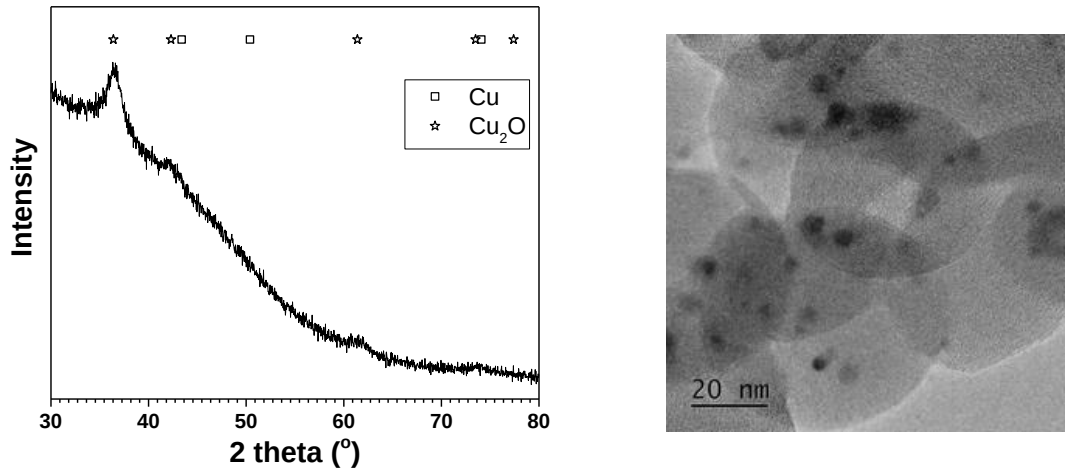

Figure 7.7: XRD (left) and TEM image (right) of the 9 ml/s sample from Figure 7.6

Furthermore, increasing the disk rotation speed and total flow rate led to smaller mean particle size. Mean residence time and residence time distribution is known to influence final particle size and size distribution respectively [117, 162-164]. Increasing the disk rotation speed and total flow rate led to a shorter residence time for the nuclei formed upon initial contact of the reactants on the disk surface. This slowed down rapid agglomeration of the nuclei, thereby limiting particle growth on the disk surface. Moreover, it is well established that the residence time distribution of the film formed on the disk surface approaches plug flow regime under high disk rotation speed and flow rate [163]. A plug flow regime implies that virtually all the particles will be subjected to the same mean residence time and processing conditions due to minimal radial

dispersion. Thus, a uniform particle size exits from the disk which results in a narrow particle size distribution. Overall, the disk rotation speed and flow rate has a considerable impact on the hydrodynamics of the film during the nanoparticles synthesis. The smallest particle size with tightest size distribution was therefore achieved at 2400 rpm rotation and 9 ml/s flow rate.

7.3 Effect of Rotation Speed on Particle Size Using Different Cu Precursors

Figure 7.8 shows the effect of the disk rotation speed on the particle size distribution and mean size distribution for 3 different starting Cu (II) salts. The trend in particle size distribution and mean particle size at the different rotation speeds were the same for all the Cu precursors. Thus, the faster the disk rotation speed, the narrower the particle size distribution, coupled with deceasing mean particle size. At 1440 rpm, the $Cu(CH_3COO)_2$ precursor showed the smallest particle of 8.1±0.5 nm, while the $CuCl_2$ and $Cu(NO_3)_2$ followed with 10.6 ± 0.7 and 11.7 ± 0.9 nm particle sizes respectively. However, considering the relative uncertainties, the mean particle sizes for different precursors were similar at the same rotation speed, especially at 400 and 2400 rpm, with mean particle size of 24 ± 3 and 7 ± 1 nm respectively. The observed trend in the rotation speed follows the same pattern as discussed for the $Cu(NO_3)_2$ precursor earlier, and hence the particle size and particle size distribution was dictated by the relative effect of micromixing time, mean residence time and residence time distribution discussed earlier.

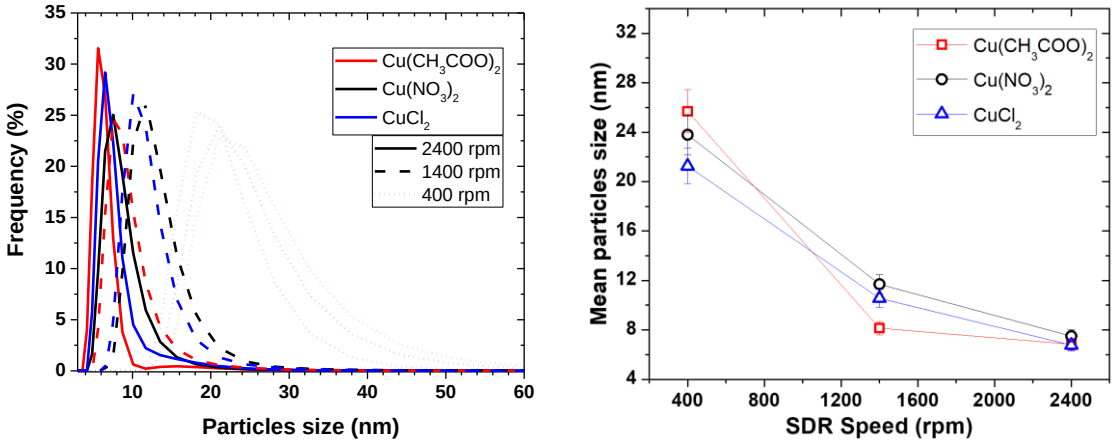

Figure 7.8: Effect of SDR disk speed on particle size distribution (left) and mean particle size (right) for different Cu precursors, 3 ml/s of 0.01 M Cu^{2+} and 3 ml/s of 0.04 M $NaBH_4$ (in 0.004 M NaOH).

7.4 Effect Reducing Agent Concentration and pH on Particle Size

Figure 7.9 shows the effect of $NaBH_4$ concentration on the particle size distribution and mean particle size at constant $Cu(NO_3)_2$ concentration. The particle size distribution narrowed from 0.02 M to 0.04 M $NaBH_4$ concentration, and then remained relatively the same distribution to 0.10 M. Meanwhile, the mean particle size in a similar trend decreased initially from 7.6 ± 0.5 to 4.3 ± 0.3, and then remained about the same size with increasing $NaBH_4$ concentration. **Figure 7.10** shows the effect of flow ratio on the particle size distribution and mean particle size at 5 ml/s total flow rate. The mean particle size increased from 7.6 ± 0.5 to 17 ± 1 nm for 0.5 to 1.5 $Cu(NO_3)_2/NaBH_4$ flow ratios respectively. The mean particle size remained the same for the $Cu(NO_3)_2/NaBH_4$ flow ratios below 0.5 however. Since the $NaBH_4$ was dissolved in NaOH solution, the effect of the amount of OH^- on the particle size was also studied. This was done at a constant $Cu(NO_3)_2/NaBH_4$ concentration but varied the amount of NaOH in the $NaBH_4$ stream. **Figure 7.11** shows the effect of pH on the particle size distribution and mean particle size. The particle size distribution became broader with increasing pH or OH^- concentration. The mean particle size as well increased linearly with increasing pH.

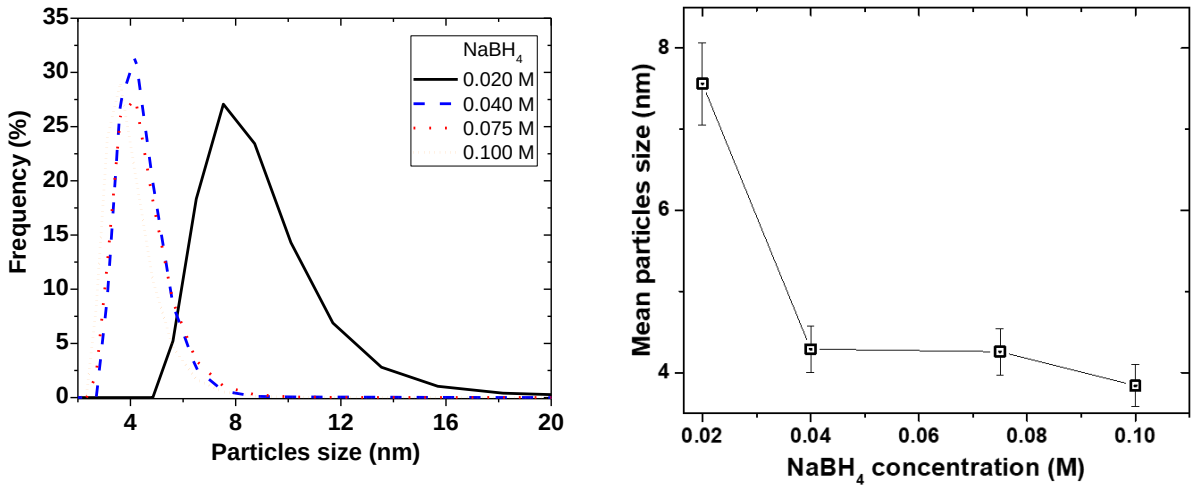

Figure 7.9: Effect $NaBH_4$ concentration on particle size distribution (left) and mean particle size (right) at 0.01 M $Cu(NO_3)_2$, disk speed= 2400 rpm, 5 ml/s total flow rate.

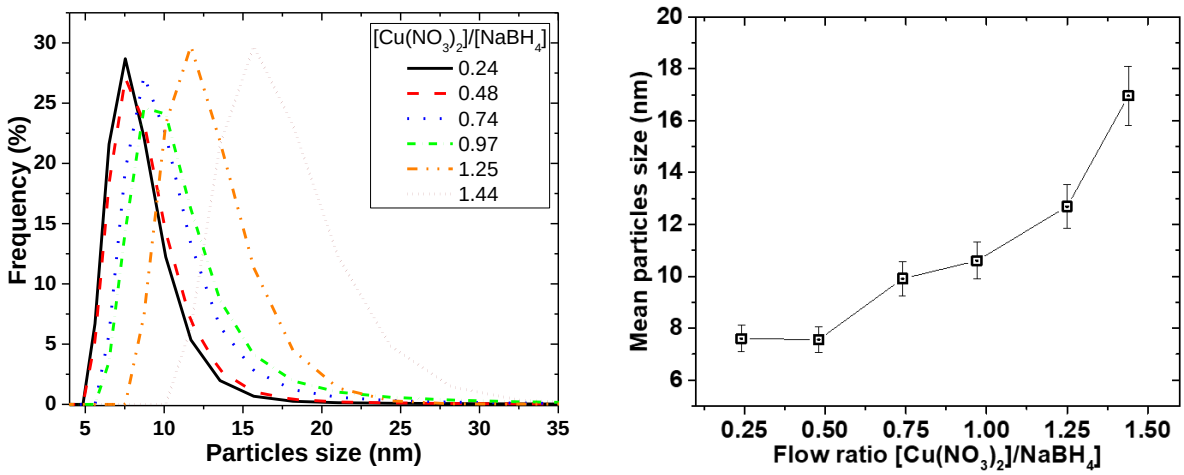

Figure 7.10: Effect of flow ratio on particle size distribution (left) and mean particle size (right), at 0.01 M $Cu(NO_3)_2$, 0.02 M $NaBH_4$ (in 0.004 M NaOH), disk speed=2400 rpm, 5 ml/s total flow rate.

The stoichiometry of the Cu nanoparticle synthesis as illustrated in Equation (7.1), shows that the amount of BH_4^- required is more (twice) than the amount of Cu^{2+} for the reduction reaction. This implies that, for adequate reduction reaction, Cu^{2+} must be the limiting reagent between the two reactants. When the BH_4^- becomes the limiting reagent, the reduction process is delayed and as a result a delay in micromixing and an increase in the relative time for homogeneous nuclei formation. This leads to patchy particle growth and bigger particle size formation. On the contrary, when Cu^{2+} becomes limiting, the reaction becomes faster and all the Cu^{2+} reacts in a shorter time period such

that the excess amount of $NaBH_4$ will have no further effect on the particle size and size distribution.

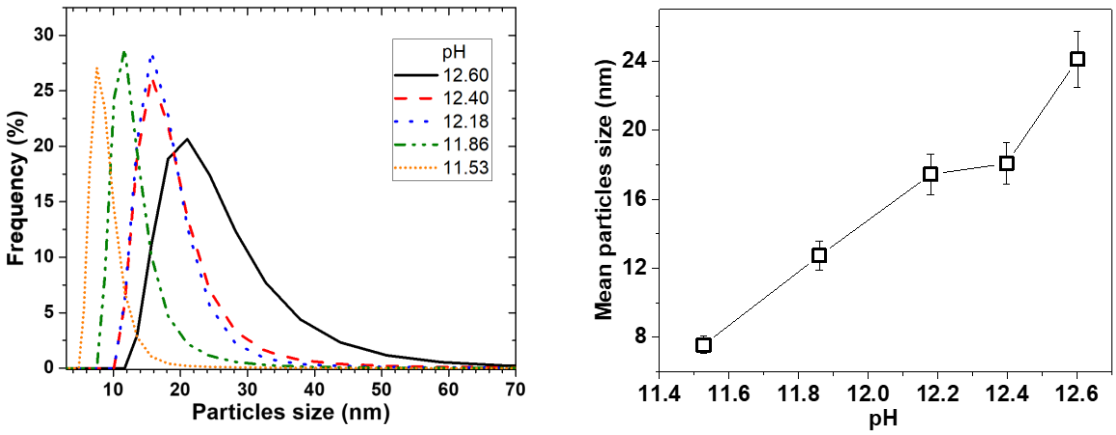

Figure 7.11: Effect of pH (by varying only NaOH concentrations) on particle size distribution (left) and mean particle size (right), at 0.01 M $Cu(NO_3)_2$, 0.02 M $NaBH_4$, disk speed = 2400 rpm, 5 ml/s total flow rate.

Furthermore, the Equation (7.1) also showed that the reduction reaction involves hydrolysis of $NaBH_4$. Considering that $NaBH_4$ dissolves in water as well as reacts with water, an addition of NaOH was necessary to keep adequate amount of BH_4^- in solution. Hydrolysis of $NaBH_4$ for example is known to decrease with increasing pH [165, 166]. The relative availability of the BH_4^- will have a direct influence on the precipitation reaction as the reaction occurs within the short residence time of the film on the disk. As the amount of OH^- increased, the BH_4^- hydrolysis necessary for the reduction reaction was suppressed leading to the observed linear increase of the particle size with pH.

7.5 Scaling-up Cu Nanoparticle Production

To scale-up the production, a longer continuous processing time was allowed for production of a larger quantity of the Cu nanoparticles. The starting concentration of $Cu(NO_3)_2$ and corresponding $NaBH_4$ concentration were varied in larger volumes (about 1-2 L) while maintaining all other flow conditions constant. **Figure 7.12** shows the effect

of the $Cu(NO_3)_2$ concentration on the particle size distribution and the mean particle size at 2400 rpm and 9 ml/s total flow rate. The mean particle size increased from 7.6 to 22 nm with 0.01 to 0.05 M concentrations respectively as the particle size gently but successively widens. Overall, particle size increased with concentration. Chang et. al [167] made similar observations where particle sizes increased from 48.3 to 93.0 nm when starting $Cu(SO_4)_2$ concentration was increased from 0.01 to 0.40 M. Increase in concentration, increases the probability of nuclei colliding with each other for particle growth, leading to the observed increase in particle size and particle size distribution with concentration.

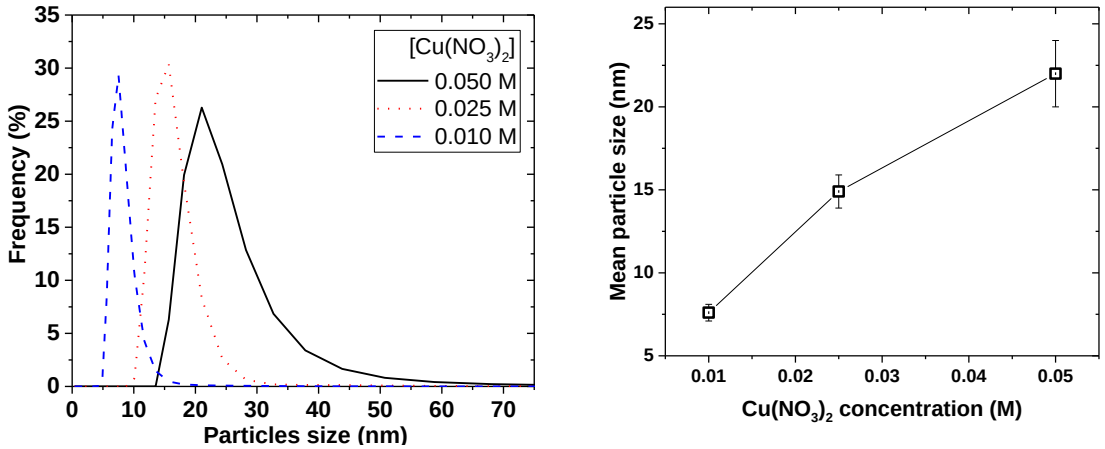

Figure 7.12: Effect of reagent's concentration on particle size distribution (left) and mean particle size (right), at $1Cu^{2+}$:$4BH_4^-$ concentration, disk speed= 2400 rpm, 9 ml/s flow for a 3 L total volume stream

The particles were oven dried at 90 °C for further characterization without washing. **Figure 7.13** shows the X-ray diffractogram for the samples made from the different concentrations as well as the TEM image of the dried sample made from the 0.01 M $Cu(NO_3)_2$ starting concentration. Cu_2O and Cu^0 were the main phases observed, aside the presence of $NaNO_3$ phase. The crystallite sizes of the Cu_2O phase slightly increased from 8.6±0.2 to 10.8±0.3 nm with increasing concentration. Indexing of the electron diffraction of the TEM confirmed the presence of predominantly Cu_2O polycrystalline particle with (111) and (220) planes. The approximately 10 nm spherical shaped Cu_2O particles, with fairly even particle size distribution observed in the TEM image, indicated

that the process could be scaled-up. The challenge however, is the isolation of the particles, as the resulting slurry was colloidal in nature and centrifuging proved futile.

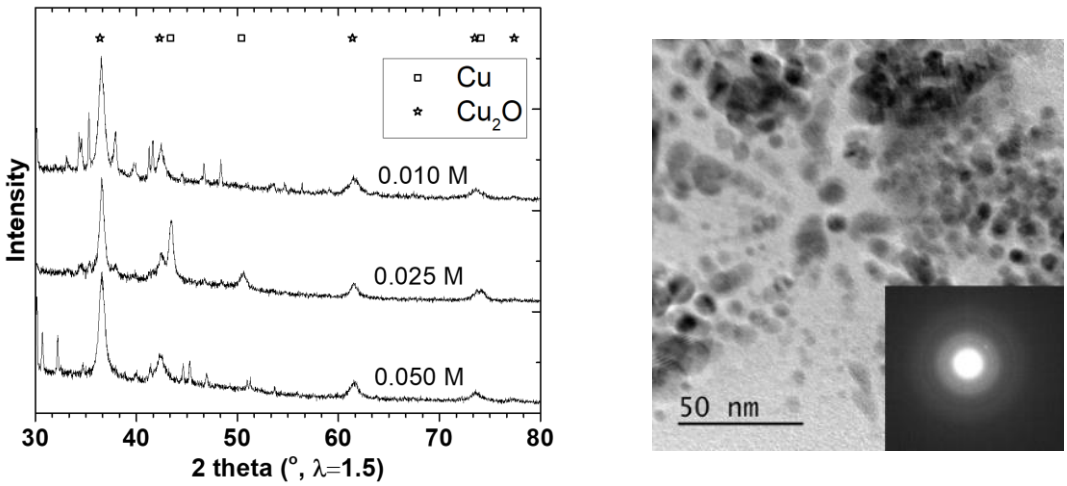

Figure 7.13: XRD (left) characterization and TEM image of the 0.01 M $Cu(NO_3)_2$ concentration (right) of the scaled-up sample from Figure 7.12

7.6 Testing the Cu Nanoparticles for LTMS Reaction

The different operation conditions were varied to tailor different Cu nanoparticle sizes to test for LTMS reaction. **Figure 7.14** shows the XRD and MeOH activity of four tailored Cu nanoparticles. The samples B1 S, B4 S and B5 S were collected in starch, while the sample B1 NS was a repeat of B1 without starch. The samples collected in starch were predominantly Cu_2O and Cu^0 phases, while CuO was the main phase observed in the sample without starch. The Cu_2O crystallite sizes were estimated from the XRD Rietveld analysis to be 8.6 ± 0.5, 9.0 ± 0.6, and 9.5 ± 0.7 nm for B1 S, B 4 S, and B 5 S respectively and 9.4 ± 0.7 nm for the CuO crystallite of the B1 NS sample. The mean particle size of the B1 S, B4 S, B5 S and B1 NS corresponded to 21 ± 1, 26 ± 2, 29 ± 2 and 38 ± 2 nm mean particle sizes respectively. The particle size of the B1 sample collected in starch was smaller with a more reduced oxidation state than the sample without starch. This suggested that in addition to reducing the rate of particle agglomeration, the starch also decreased the relative exposure of the particles to oxidation.

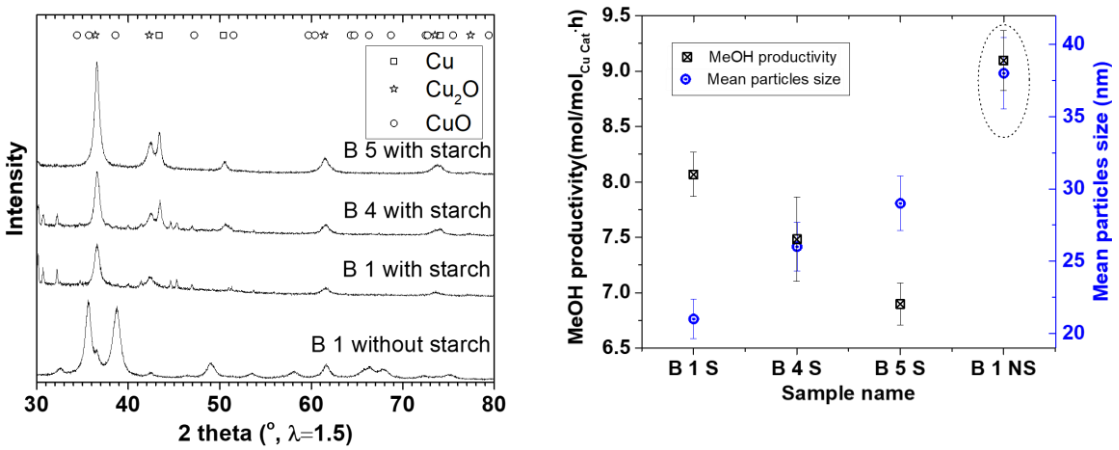

Figure 7.14: XRD (left) and MeOH productivity (right) for scale-up Cu nanoparticles; Conditions for the MeOH synthesis; $2H_2/CO$ = 20 bar, $NaOCH_3$= 9 mmol, THF solvent = 30 ml, 100 °C.

The tailored samples were used for MeOH synthesis, as the source of Cu in combination with methoxide co-catalyst as was done in the previous LTMS reactions. For ease in comparison, the amount of MeOH produced per the amount of Cu present and the reaction time was presented as MeOH productivity. The MeOH productivity increased with decreasing mean particle size for the catalysts with starch. As has already been discussed, decreasing particle size implies an increase in active surface area which enhances activity. On the other hand, the sample B1 (NS) without starch showed a higher productivity compared to the B1 (S) with starch. Since smaller nanoparticle size and reduced oxidation state of Cu usually promote the MeOH synthesis reaction [68], the absence of starch could play a role in the observed difference in activity. That is, the presence of starch in the B1 S sample presented a mass transfer limitation which lowered activity compared to the B1 NS sample with starch absent. Nevertheless, the Cu nanoparticles produced with the SDR was active for the LTMS reaction but would need further process optimization for nanoparticles production with less particle isolation difficulty.

7.7 Summary

The use of the SDR presents one fast approach for making targeted Cu nanoparticles for MeOH synthesis. The Cu nanoparticles were synthesized by borohydride reduction. By increasing disk rotation speed and total flow rate, with its consequent effect on short micromixing time, the final Cu nanoparticle sizes can be tuned up to 3 nm with narrow particle size distribution. Moreover, factors that enhance the reduction reaction, such as lower pH and the right stoichiometric ratio between the reagents influence smaller particle size and narrower particle size distribution. XRD and TEM characterization of the oven dried synthesized particles showed a predominantly Cu_2O and some Cu spherical polycrystalline nanoparticles formed. The process was scaled-up for catalysis, and was observed to be active for MeOH synthesis at 100 ^oC. Overall, the use of the SDR presented a promising and straightforward approach for tuning on-purpose Cu nanoparticles as catalyst for MeOH synthesis by varying physical operating conditions while using the same chemical recipe.

8 Simulation of an Air-Blown ATR LTMS Process Design

The LTMS process has been discussed in this work to be very promising in achieving close to full syngas conversion per pass due to the relatively lower operating temperatures compared to the original ICI MeOH synthesis process. The current work has shown that up to about 92 % syngas conversions can be achieved at 100 ^{o}C and 20 bar syngas pressure. One advantage of such high to full conversion per pass is the inclusion of N_2 diluent in syngas for the LTMS process if there is no need for recycling unreacted reactants. Since the inclusion of N_2 can be tolerated in the LTMS process, normal or O_2 enriched air can be used as a cheaper alternative for producing syngas in an autothermal reformer (ATR). In this section, our focus is to model a complete LTMS process concept, using the Aspen HYSYS simulation tool. A model process using an air-blown ATR will be proposed based on the simulation for a complete LTMS process.

8.1 Process description and Model Used for the Design

The syngas production and MeOH synthesis units were separately simulated to select reasonable conditions for the complete LTMS process. **Figure 8.1** shows the syngas production process, involving an air-blown ATR. The syngas production was based on partial oxidation of hydrocarbon from natural gas and O_2. For simplicity, pure CH_4 (methane) was used as the hydrocarbon feed and was assumed to be without any sulphur or heavier hydrocarbons while the source of O_2 was air consisting of $21O_2$:79 N_2. The air was compressed to satisfy the stoichiometry of CH_4 to O_2 according to the Equation (8.1). Both CH_4 and the compressed air were pre-heated before feeding into the reactor (ATR).

$$\mathrm{CH_4} + \frac{1}{2}\mathrm{O_2} \rightarrow \mathrm{CO} + 2\mathrm{H_2} \qquad \Delta H = -36\,\frac{kJ}{mol} \quad (8.1)$$

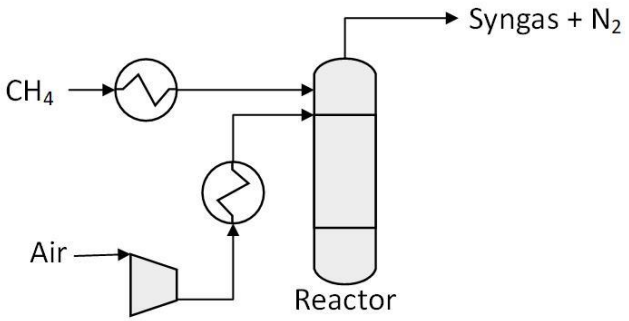

Figure 8.1: Syngas production process, involving an air-blown ATR

The MeOH production was based on a hydrogenation of CO in the presence of N_2 diluent. In effect, the syngas mixture produced from the ATR can be fed directly into the MeOH reactor as shown in **Figure 8.2**. However, molecules such as H_2O, CO_2, CH_4 and some other hydrocarbons could be present in the syngas produced. In addition, the highly exothermic reaction of the partial oxidation [168] implies that the syngas produced will require some further treatment such as cooling before it can be used in the MeOH reactor. Hence, for the optimization of the process in the MeOH reactor, only $CO/H_2/N_2$ in different specified compositions were used as reactants. The syngas plus N_2 was mixed with a liquid solvent and then sent to the MeOH reactor. The mixing unit was necessary since the LTMS reactions were carried out in a liquid medium. To simplify the model, MeOH was selected as the liquid medium.

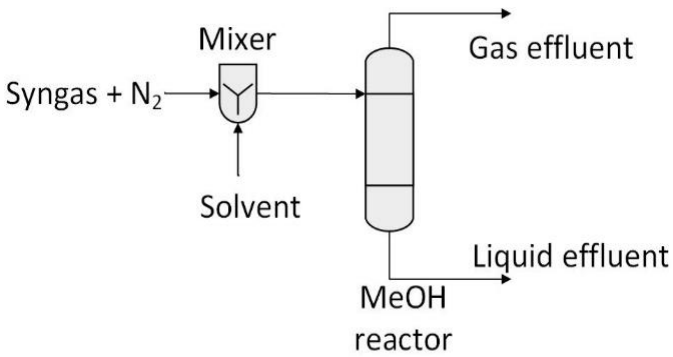

Figure 8.2: LTMS process for N_2 diluted syngas

The simulations were performed using Aspen HYSIS version 8.6 program. Based on the Aspen program, three systems were considered, namely, syngas production in the ATR reactor, MeOH synthesis in the MeOH reactor and the combination of the two processes. Gibbs reactors were used for simulating the ATR and MeOH reactors. The Gibbs reactor uses the theoretical free energy minimum to calculate the equilibrium composition in the process. Peng-Robinson equation of state [169] fluid package was used for all the simulations. The optimized conditions for the individual process was put together to design an overall LTMS process.

In the overall process, extra treatments were required for the air feed as well as the syngas produced before the MeOH synthesis in the MeOH reactor. Firstly, a pressure swing absorber (PSA) was included to regulate the O_2/N_2 ratio in the air. The PSA operates by adsorption and desorption of certain gas components based on their affinity to solid adsorbents (usually microporous and mesoporous materials such as zeolites) when pressure is increased or decreased [170]. Secondly, an absorber was included to minimize H_2O and CO_2 content in the syngas produced before the MeOH reactor process. CH_4 was assumed to be inert in the MeOH reactor, to eliminate the effect of methanation in the calculations.

8.2 Process simulation and Optimization

8.2.1 Process Simulation and Optimization for Syngas Production

To optimize the temperature required for the partial oxidation in the ATR reactor, the temperature of the ATR gas inlet was varied. This was calculated based on $0.30CH_4$: $0.15O_2$: $0.55N_2$ feed composition set to 20 bars. The composition indicated that the $2CH_4$:$1O_2$ stoichiometry was maintained, coupled with $21O_2$: $79N_2$ air composition. **Figure 8.3** shows the effect of temperature on the syngas produced. Generally, CH_4 conversion increased with temperature, mainly from 600 to 1200 ^oC, after which the

increase was insignificant. CO and H_2 production increased while H_2O and CO_2 side products decreased with increasing temperature. Considering the significance of temperature on the reactor material, 1200 ^oC was selected as a reasonable temperature for the syngas production.

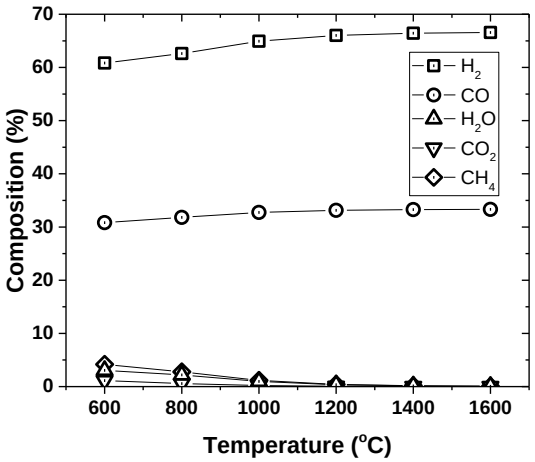

Figure 8.3: Effect of temperature on the syngas production, 20 bar

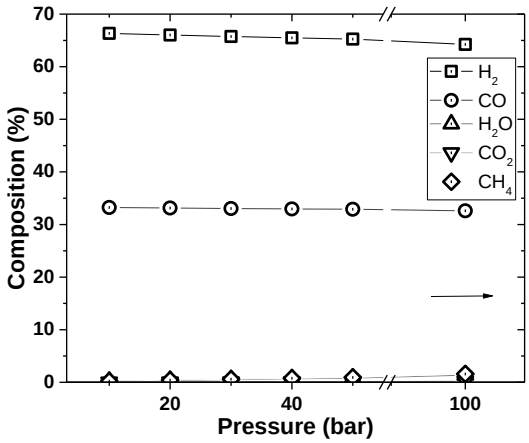

Figure 8.4: Effect of pressure on the syngas production, 1200 ^oC

The pressure of the feed was also varied to optimize the inlet pressure for the syngas production. Similar feed composition just as was used in the temperature variation calculations was used in the feed pressure estimation. **Figure 8.4** shows the effect of pressure on the syngas produced. CH_4 conversion increased while side products decreased with decreasing pressure, mainly from 100 to 10 bar. The H_2/CO ratio remained around 2 below 30 bar inlet pressure. Overall, the influence of pressure was less severe compared to that of temperature on the syngas production. 20 bar feed pressure was therefore chosen as a reasonable pressure for the feed inlet into the ATR reactor assuming similar pressures are released from natural gas pipelines.

8.2.2 Process Simulation and Optimization for MeOH Synthesis

The temperature and pressure for MeOH synthesis reaction was varied to optimize reaction conditions for the LTMS process. **Figure 8.5** shows the effect of temperature

on syngas conversion at 20 and 100 bar. The syngas was composed of 0.21H_2: 0.41CO: 0.39N_2. Conversion exponentially increased with decreasing temperature from 300 to 120 ^oC, and then began to level off. The conversion was however higher in the 100 bar calculation than in the 20 bar calculations until below 60 ^oC, where the level of conversion became the same at both pressures. At 100 ^oC for instance, about 99 % conversion in the 100 bar reaction was calculated, while at the 20 bar, 94 % conversion was estimated. Nonetheless, considering the fact that, experimentally, lower activity is observed below 100 ^oC [26, 35], 100 ^oC was selected as a reasonable operating temperature for the MeOH synthesis process.

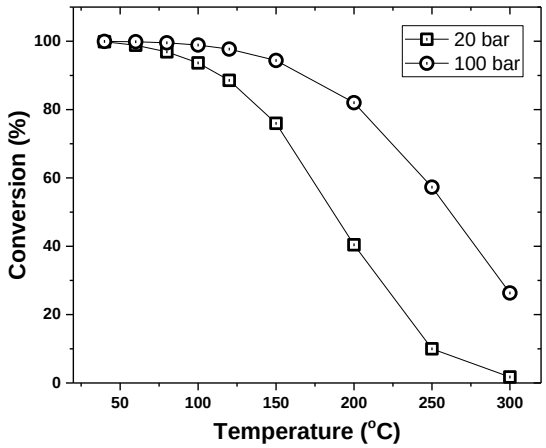

Figure 8.5: Effect of temperature on the LTMS process

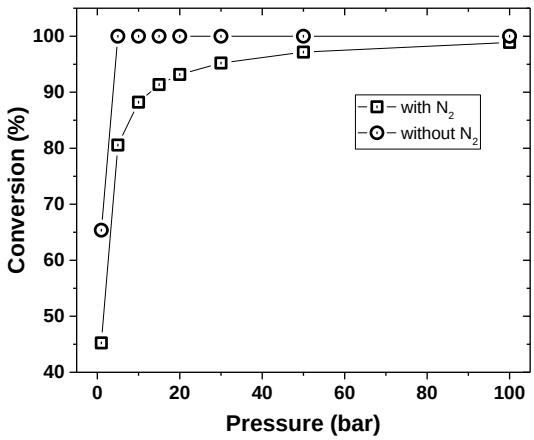

Figure 8.6: Effect of pressure on the LTMS process at 100 ^oC

Figure 8.6 shows the effect of pressure on syngas conversion with and without N_2 diluent within 1 to 100 bar. The syngas with N_2 diluent consisted of 0.21 H_2 : 0.41 CO : 0.39 N_2 while the syngas without N_2 consisted of 0.67 H_2 : 0.33 CO composition. The conversion for the syngas with N_2 rapidly increased from 45 to 95 % within 1 to 30 bar, and then gradually to 99 at 100 bar. The conversion for the syngas without N_2 however was 100 % within the pressure range studied, except below 5 bar where 65 % conversion was observed at 1 bar. This indicated that the presence of N_2 plays an important role in conversion by lowering syngas partial pressure. Nonetheless, for a normal air-blown ATR

system, 100 bar syngas pressure was a reasonable pressure for the MeOH synthesis at 100 ^{o}C.

Realising the importance of N_2 diluent in the syngas conversion, the N_2 content in the syngas was varied to determine an optimal N_2 content in syngas for an enriched air system in the MeOH synthesis process. **Figure 8.7** shows the effect of N_2 diluent concentration on LTMS process at 100 ^{o}C. This was done by maintaining the H_2/CO ratio of 2 but different amount of N_2 composition. At each specific N_2 composition, syngas conversion increased with pressure. This indicated that increasing the CO and H_2 partial pressures in the feed composition enhances MeOH production.

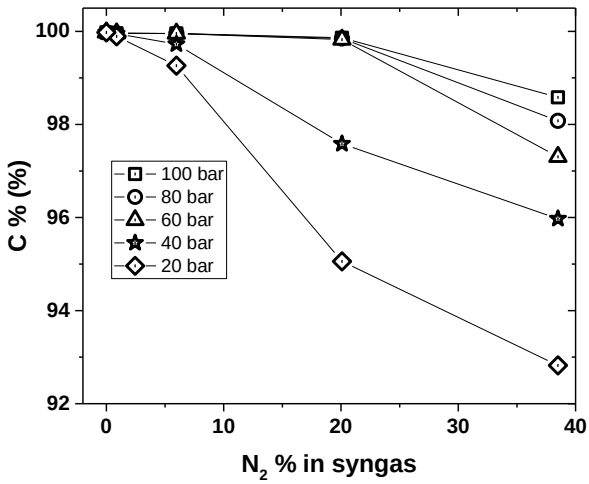

Figure 8.7: Effect of N_2 diluent concentration on LTMS process at 100 ^{o}C

Generally, syngas conversion increased with decreasing N_2 diluent concentration. When the N_2 % composition was decreased from 39 to 7 %, a full conversion was observed within 60 to 100 bar. Further reduction of N_2 composition to 1 % led to full conversion with 20 to 100 bar. However, such reduction of N_2 requires an expensive air purification process. One way out is the use of PSA for example, which can be used to enrich air up to 90 % O_2 content in air at a relatively cheaper cost [171]. Hence 0.31CO: 0.62H_2: 0.07N_2 composition was selected as a reasonable composition for the enriched air-blown ATR system for the LTMS process. This implies that, aside maintaining the 2CH_4: O_2 ratio, the O_2: N_2 for the enriched air-blown system will be 0.70:0.30 for the ATR process. In that

case, 60 bar syngas pressure was chosen as a reasonable pressure for the MeOH synthesis at 100 ^{o}C for the enriched air-blown system.

8.2.3 Process Simulation and Optimization for Overall LTMS Process

The individual optimized processes were put together to simulate an overall LTMS process. **Figure 8.8** shows the raw Aspen HYSYS flow-sheet of the overall LTMS process in an enriched air-blown system. The flow-sheet differs from that of normal air-blown system by the inclusion of the PSA which is the unit involved in enriching air. **Table 8.1** shows the selected operating conditions and resulting calculated composition in the normal air-blown ATR system. The air-blown system consisted of CH_4 and $0.21O_2$: $0.79N_2$ feed. The partial oxidation was carried out at 20 bar and 1200 ^{o}C. The exiting syngas from the ATR with 1356 ^{o}C temperature was successively cooled to 30 ^{o}C. This was then compressed to 100 bar after removal of H_2O and CO_2 by the H_2O/CO_2 absorption unit. The compressor's adiabatic efficiency was specified to 75 %. The starting 3990 kmol/h CH_4 yielded 3842 kmol/h MeOH at the 100 ^{o}C MeOH synthesis temperature.

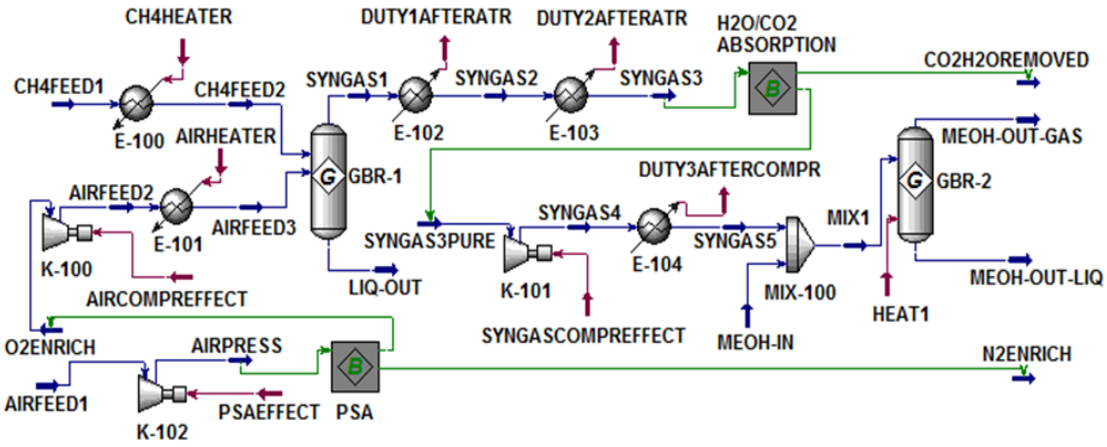

Figure 8.8: Aspen HYSYS flow-sheet for the overall standard LTMS process

Table 8.1: Specifications of Operation Conditions for the Overall LTMS Process for normal air-blown ATR system.

Parameter	*Molar flow (kmol/h)*	*Pressure (bar)*	*Temperature (°C)*	*Main composition*
CH_4Feed	3990	20	20	1 CH_4
CH_4Feed2	″	″	1200	″
AirFeed	9500	1.01	20	0.21 O_2 : 0.79 N_2
AirFeed2	9500	20	515	0.21 O_2 : 0.79 N_2
AirFeed3	″	″	1200	″
Syngas1	19375	″	1356	0.20 CO : 0.40 H_2 : 0.39 N_2
Syngas2	″	″	652	″
Syngas3	″	″	30	″
Syngas4	19375	100	265	″
Syngas5	″	″	30	″
Mix1	″	″	″	″
MeOH out	11642	″	100	0.33 CH_3OH: 0.64 N_2

Table 8.2: Specifications of Operation Conditions for the Overall LTMS Process for enriched air-blown ATR system.

Parameter	*Molar flow (kmol/h)*	*Pressure (bar)*	*Temperature (°C)*	*Main Composition*
CH_4Feed	3990	20	20	1 CH_4
CH_4Feed2	″	″	1200	″
AirFeed	14250	1.01	20	0.21 O_2:0.79 N_2
AirPress	″	1.50	66.5	″
O_2Enrich	2850	1.10	67	0.70 O_2:0.30 N_2
AirFeed2	″	20	595	″
AirFeed3	″	″	1200	″
Syngas1	12727	″	1439	0.31 CO: 0.62 H_2: 0.07 N_2
Syngas2	″	″	687	″
Syngas3	″	″	30	″
Syngas3pure	12678	20	33.5	″
Syngas4	″	60	186	″
Syngas5	″	60	100	″
Mix1	″	″	″	″
MeOH out	4839	″	″	0.81CH_3OH: 0.18 N_2

The selected operating conditions and resulting calculated composition in the enriched air-blown ATR system is shown in **Table 8.2**. The starting 0.21 O_2: 79 N_2 air was filtered in the PSA to produce 0.70 O_2: 0.30 N_2 enriched air feed. The enriched air and CH_4 were partially oxidized at 20 bar and 1200 °C, with a resulting 1439 °C exiting syngas

temperature. After successive cooling of the hot syngas to 30 ^{o}C and H_2O/CO_2 absorption, the syngas was compressed to 60 bar at the same adiabatic efficiency as was specified for the normal air-blown system. The starting 3990 kmol/h CH_4 yielded 3919 kmol/h MeOH at 60 bar and 100 ^{o}C MeOH synthesis temperature.

A summary of the energy flow during the overall LTMS process is displayed in **Table 8.3**. The negative connotation in the heating segment represented the heat demanding process while the positive represented the heat releasing process. The difference in the heat demanding and heat releasing process was estimated to be 7.68 x 10^8 kJ/h for the normal-air blown system while that of the enriched air-blown system was 6.10 x 10^8 kJ/h. This indicated that the surplus heat would cover the heat demand in the overall LTMS process after recovery in both normal and enriched air-blown systems. The energy demand with regards to compression will be 2.80 x 10^8 kJ/h and 1.23 x 10^8 kJ/h for the normal and enriched air-blown process respectively. By comparing to the amount of MeOH production, the energy demand in the process due to compression can be estimated to be 2270 MJ/ton and 983 MJ/ton MeOH product for the normal and enriched air-blown process respectively.

Table 8.3: Heat/Energy flow for the overall LTMS process

Heating	***Air-blown (10^6kJ/h)***	***Enriched-air (10^6kJ/h)***
CH4HEATER (-)	306	306
AIRHEATER (-)	219	60.2
DUTY1AFTERATR (+)	451	315
DUTY2AFTERATR (+)	366	252
DUTY3AFTERCOMPR (+)	141	32.2
HEAT1 (+)	335	377
Compression		
PSAEFFECT	-	19.4
AIRCOMPREFFECT	144	47.6
SYNGASCOMPREFFECT	135	56.4

8.3 Process Discussion

The main difference in the process described so far and the conventional ICI MeOH synthesis process is the inclusion of N_2 due to the thermodynamically allowed full conversion per pass at low temperature conditions. As mentioned earlier, cryogenic production of O_2 from air is capital intensive and the possibility to operate a MeOH plant with an air-blown ATR process is cost effective [20, 22]. Even though, some level of air purification is needed in the enriched air-blown system, the use of a PSA unit will be cheaper than the use of cryogenic air separation [171] considering the 70 % O_2 (in air) purity estimated for the partial oxidation in this work. Furthermore, the exothermic partial oxidation in the ATR which resulted in 1356 and 1439 ^oC outlet temperature raises material suitability concerns. However, a typical ATR reactor burner operates above 2000 ^oC [168], therefore we expect that a gas outlet stream with a good heat transfer will not pose more challenges than present in existing ATR reactor technologies.

When the heat component of the process was considered, the excess energy produced was sufficient to cover the energy demand for heating in the overall process. Besides covering the energy demand, a surplus of 7.68 x 10^8 and 6.10 x 10^8 kJ/h in the normal and enriched air-blown systems respectively were realized. This implies that, if the surplus energy is not recovered, the energy lost in normal air-blown system will be higher than that of the enriched air-blown system. The surplus energy can be recovered for power generation in steam turbines [172] for example, which can be used subsequently to power the compressing units. In terms of compression, 2.80 x 10^8 kJ/h and 1.23 x 10^8 kJ/h energies were required for the normal and enriched air-blown process respectively. This implies that the enriched air-blown system also requires lower energy to power the compressing unit compared to the normal air-blown system.

The calculations revealed that temperature and partial pressure of the syngas are important for full conversion per pass. Below 120 ^oC, with the right syngas partial pressure, full conversion per pass could be achieved. However, the relative amount of N_2 in the reactant gas affected the pressure required for full conversion. In a normal air-

blown system for example, 100 bar pressure was required while similar conversion could be attained at 60 bar in the enriched air-blown system. The relatively high amount of N_2 present in the syngas requires larger reactor volume size with it consequent capital cost for the MeOH synthesis. Hence, the use of the enriched air-blown system, which reduces the 36 % N_2 composition in syngas (from normal air) to 7 % (from enriched air) minimizes such added capital cost on the larger reactor size. Furthermore, with the same starting amount of CH_4 the energy demand due to compression, relative to MeOH production was estimated to be 2270 and 983 MJ/ton MeOH product for the normal air-blown and the enriched air-blown systems respectively. This implies that a relatively high energy is required to compress the normal air-blown system mainly due to compressing excess unreactive N_2. Overall, the enriched air-blown system has considerable advantages over the normal air-blown system.

Figure 8.9 shows a simplified flow design of the overall air-blown LTMS process. The proposed process, involves a possible pre-heating of the ATR feed by heat exchanges from the exiting syngas from the ATR. Even though full conversion is possible at 60 bar and 100 ^oC in the enriched air-blown system, one potential drawback is the presence of H_2O and CO_2 in the syngas feed. Experimentally, H_2O and CO_2 levels are required to be less than 10 ppm [26, 27], otherwise they would react with the methoxide catalyst component to render it inactive. Even though in the process simulation, conditions to minimize H_2O and CO_2 production were adopted, the inclusion of H_2O/CO_2 absorbers will further reduce their content below 1 ppm. Aside this, a system for regular recycling of the methoxide catalyst can be included in the process. Methoxide for example is produced from NaOH and MeOH reaction with either evaporation or drying of water [40, 47, 48]. Hence recycling of the catalyst system due to deactivation from NaOH and MeOH formation to restore methoxide activity is expected to be highly feasible. Ultimately, the air-blown ATR LTMS process presents a cheaper and promising alternative to current MeOH production.

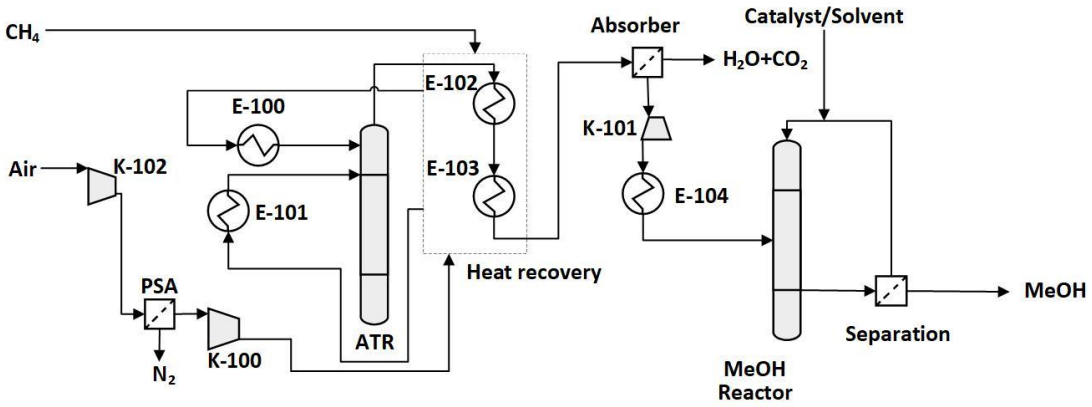

Figure 8.9: Simplified flow diagram of a complete air-blown LTMS process design

8.4 Summary

The Aspen HYSYS program has been used to simulate and optimize a complete air-blown LTMS process. Two components of the process, namely syngas production and MeOH synthesis were individually simulated to obtain optimized reaction conditions. The presence of N_2 was observed to influence overall MeOH production, such that both normal air-blown and O_2 enriched air-blown systems were simulated for the complete process. The N_2 composition was 39 and 7 % for the normal and enriched air-blown systems respectively, while the CH_4/O_2 ratio was kept at 2. In the ATR, 20 bar and 1200 ^oC were selected as optimal conditions for high conversion and low side reactions. Our calculations indicated that more than 99 % feed conversion per pass could be attained at 100 and 60 bar for the normal and enriched air-blown systems respectively at 100 ^oC MeOH synthesis reaction. In both air-blown systems, the total energy generated in the process was enough to cover the energy demand for heating with a surplus energy. However, when the surplus energy is not recovered, the heat lost in the normal air-blown system will be higher than the enriched air-blown system. The estimated energy required for compression per MeOH production was estimated to be 2270 and 983 MJ/ton MeOH product for the normal air and enriched air-blown systems respectively. Hence, the enriched air-blown system has considerable advantage over the normal air-

blown system. Finally, an overall process design was proposed based on optimized conditions for the enriched air-blown process.

9 Overall Summary and Suggested Further Work

9.1 Main Conclusions

- XRD and TEM characterization of a once-through slurry catalyst system has shown that spherical Cu_2O and Cu nanoparticles made during hydride reduction of copper (II) acetate coupled with methoxide, effectively catalyse the LTMS reaction at 100 ^oC temperature. Increase in active surface area due to decreasing Cu nanoparticle size, enhanced MeF hydrogenolysis and consequently increased MeOH production. Agglomeration due to the densification of softer Cu nanoparticles during the MeOH production over a period is one major Cu catalyst deactivation path in the LTMS process.
- Aside hydrogenolysis, the MeF intermediate undergoes either decarbonylation to form CO and MeOH or nucleophilic substitution to form DME and NaOOCH, dictated by solvent polarity in the presence of methoxide. While decreasing polarity enhanced decarbonylation, increasing polarity enhanced the nucleophilic substitution reaction. Hence, aside heat dissipation by the presence of solvents, the polarity of solvent plays a significant role in LTMS reaction, such that solvents with similar polarity as diglyme (ε= 7.2) enhanced MeOH production.
- Hydrogenolysis of MeF increases with decreasing Cu nanoparticles as well as methoxide loading to a certain maximum, after which additional methoxide leads to side reactions such as decarbonylation. This suggests that the presence of methoxide promotes hydrogenolysis process and subsequently a certain level of synergistic relationship exists between the two catalysts in the LTMS reaction. The hydrogenolysis of Cu nanoparticles catalyst can be extended to hydrogenate CO_2 at 100 ^oC, via dimethyl carbonate intermediate, with comparable conversions as MeF, without the need for methoxide promotor.

- The use of the SDR presents one fast approach for making targeted Cu nanoparticle sizes for MeOH synthesis by changing physical parameters such as disk rotation speed and flow rate, while maintaining the same chemical recipe and protocols. By varying physical conditions, the degree of micromixing time, mean residence time and relative residence time distribution can be tightened which subsequently lead to uniform nucleation and ultimately smaller Cu nanoparticle sizes formation with narrow particle size distribution.
- Finally, a process design for a complete LTMS process was proposed based on Aspen HYSYS simulation tool, using an O_2 enriched air-blown autothermal reformer, for a full conversion per pass at 60 bar syngas (0.31 CO: 0.62 H_2: 0.07 N_2) and 100 ^oC MeOH synthesis temperature.

9.2 Suggestions for Further Work

- One major challenge in the use of the SDR for Cu nanoparticle production was isolation of the produced nanoparticles, which was colloidal in starch. A different stabilization agent that can easily be isolated would ease the post-production handling difficulty. Alternatively, the replacement of the water solvent with a solvent that will be used for the MeOH synthesis would imply no isolation before MeOH synthesis.
- Other areas of the nanoparticles fabrication using the SDR, such as inclusion of different Cu (I) salts will help to deepen the understanding of the hydride reduction mechanism.
- The SDR precipitation process can be extended to a co-precipitation reaction to include other metallic oxides as support for the Cu nanoparticles' stability during MeOH synthesis reaction.
- Further investigation to identify a stronger oxide support of the Cu nanoparticles to reduce the relative decline in activity due to Cu agglomeration as well as help in separation during post MeOH synthesis handling.

- Further investigation to identify a replacement for the alkoxide catalyst, which is less prone to the formation of NaOOCH, will help to reduce possible side reactions during the LTMS reaction.
- Detailed surface spectroscopic study on the Cu-alkoxide interaction will help in deepening the understanding of the synergistic relationship studies.
- Improvement of the Cu-based catalyst as well as inclusion of a co-catalyst or promoters will help to optimize CO_2 utilization, directly or indirectly for MeOH production at low temperature conditions.

Reference

[1] EIA International Energy Outlook 2017, https://www.eia.gov/outlooks/ieo/pdf/0484(2017).pdf, (Date accessed: 20.02.2018).
[2] M.K. Hubbert, Energy from Fossil Fuels, Science, 109 (1949) 103-109.
[3] A.M.M. Masih, K. Albinali, L. DeMello, Price dynamics of natural gas and the regional methanol markets, Energy Policy, 38 (2010) 1372-1378.
[4] Z.J. Schiffer, K. Manthiram, Electrification and Decarbonization of the Chemical Industry, Joule, 1 (2017) 10-14.
[5] N. von der Assen, J. Jung, A. Bardow, Life-cycle assessment of carbon dioxide capture and utilization: avoiding the pitfalls, Energy & Environmental Science, 6 (2013) 2721-2734.
[6] A.J. Moulijn, M. Makkee, A.V. Diepen, Chemical Process Technologgy, John Wiley & Sond Ltd.2001.
[7] World Energy Outlook, Executive Summary 2014, https://www.iea.org/publications/freepublications/publication/WEO_2014_ES_English_WEB.pdf, (Date accessed: 28.10.2017).
[8] G.M. Salameh, Impact Of Us Shale Oil Revolution On The Global Oil Market, The Price Of Oil & Peak Oil, International Association for Energy Economics, 2013, pp. 27-31.
[9] M.P. Hekkert, F.H.J.F. Hendriks, A.P.C. Faaij, M.L. Neelis, Natural gas as an alternative to crude oil in automotive fuel chains well-to-wheel analysis and transition strategy development, Energy Policy, 33 (2005) 579-594.
[10] M. Alvarado, The changing face of the global methanol industry, Insights, IHS Chemical Bulletin, 2016, pp. 10-11.
[11] G.A. Olah, Beyond Oil and Gas: The Methanol Economy, Angewandte Chemie International Edition, 44 (2005) 2636-2639.
[12] http://www.methanol.org/the-methanol-industry/, The Methanol Industry, Methanol Institute, (Date accessed 08.02.2018).
[13] A. Goeppert, M. Czaun, J.-P. Jones, G.K. Surya Prakash, G.A. Olah, Recycling of carbon dioxide to methanol and derived products - closing the loop, Chemical Society Reviews, 43 (2014) 7995-8048.
[14] U. Olsbye, S. Svelle, M. Bjørgen, P. Beato, T.V.W. Janssens, F. Joensen, S. Bordiga, K.P. Lillerud, Conversion of Methanol to Hydrocarbons: How Zeolite Cavity and Pore Size Controls Product Selectivity, Angewandte Chemie International Edition, 51 (2012) 5810-5831.
[15] K.C. Waugh, Methanol Synthesis, Catalysis Today, 15 (1992) 51-75.
[16] K. Klier, Methanol Synthesis, in: D.D. Eley, H. Pines, P.B. Weisz (Eds.) Advances in Catalysis, Academic Press1982, pp. 243-313.
[17] M.S. Wainwright, Catalytic Processes for Methanol Synthesis – Established and Future, in: D.M. Bibby, C.D. Chang, R.F. Howe, S. Yurchak (Eds.) Studies in Surface Science and Catalysis, Elsevier1988, pp. 95-108.
[18] W.J. Thomas, S. Portalski, Thermodynamics in Methanol Synthesis, Industrial & Engineering Chemistry, 50 (1958) 967-970.

[19] J.-P. Lange, Methanol synthesis: a short review of technology improvements, Catalysis Today, 64 (2001) 3-8.
[20] M. Marchionna, M. Di Girolamo, L. Tagliabue, M.J. Spangler, T.H. Fleisch, A review of low temperature methanol synthesis, Studies in Surface Science and Catalysis, Volume 119 (1998) 539-544.
[21] D.J. Wilhelm, D.R. Simbeck, A.D. Karp, R.L. Dickenson, Syngas production for gas-to-liquids applications: technologies, issues and outlook, Fuel Processing Technology, 71 (2001) 139-148.
[22] J.B. Hansen, P.E. Højlund Nielsen, Methanol Synthesis, in: G. Ertl, H. Knozinger, F. Schuth, J. Weitkamp (Eds.) Handbook of Heterogeneous Catalysis, Wiley-VCH Verlag GmbH & Co. KGaA, Weinheim, Germany, 2008, pp. 2920-2949.
[23] J.A. Christiansen, Method of producing methyl alcohol, U.S. Patent 1,302,011, 1919.
[24] S.P. Tonner, D.L. Trimm, M.S. Wainwright, N.W. Cant, The base-catalysed carbonylation of higher alcohols, Journal of Molecular Catalysis, 18 (1983) 215-222.
[25] T. Turek, D.L. Trimm, N.W. Cant, The Catalytic Hydrogenolysis of Esters to Alcohols, Catalysis Reviews, 36 (1994) 645-683.
[26] S. Ohyama, Low-Temperature Methanol Synthesis in Catalytic Systems Composed of Copper-Based Oxides and Alkali Alkoxides in Liquid Media: Effects of Reaction Variables on Catalytic Performance, Top Catal, 22 (2003) 337-343.
[27] Z. Liu, J.W. Tierney, Y.T. Shah, I. Wender, Kinetics of two-step methanol synthesis in the slurry phase, Fuel Processing Technology, 18 (1988) 185-199.
[28] S. Ohyama, Low-temperature methanol synthesis in catalytic systems composed of nickel compounds and alkali alkoxides in liquid phases, Applied Catalysis A: General, 180 (1999) 217-225.
[29] S. Ohyama, In situ FTIR study on reaction pathways in Ni(CO)4/CH3OK catalytic system for low-temperature methanol synthesis in a liquid medium, Applied Catalysis A: General, 220 (2001) 235-242.
[30] C. Voegtlin, Toxicity of certain heavy metal carbonyls, in: U.S.A.E. Commission (Ed.)University of Rochester, 1947.
[31] B. Li, K. Jens, Liquid-Phase Low-Temperature and Low-Pressure Methanol Synthesis Catalyzed by a Raney Copper-Alkoxide System, Top Catal, 56 (2013) 725-729.
[32] S. Ohyama, H. Kishida, Physical mixture of CuO and Cr2O3 as an active catalyst component for low-temperature methanol synthesis via methyl formate, Applied Catalysis A: General, 172 (1998) 241-247.
[33] S. Ohyama, H. Kishida, XRD, HRTEM and XAFS studies on structural transformation by milling in a mixture of CuO and Cr2O3 as an active catalyst component for low-temperature methanol synthesis, Applied Catalysis A: General, 184 (1999) 239-248.
[34] R.W. Howarth, R. Santoro, A. Ingraffea, Methane and the greenhouse-gas footprint of natural gas from shale formations, Climatic Change, 106 (2011) 679.
[35] B. Li, K.-J. Jens, Low-Temperature and Low-Pressure Methanol Synthesis in the Liquid Phase Catalyzed by Copper Alkoxide Systems, Industrial & Engineering Chemistry Research, 53 (2013) 1735-1740.
[36] A.B. Stiles, Methanol, past, present, and speculation on the future, AIChE Journal, 23 (1977) 362-375.

[37] C. Lormand, Industrial Production of Synthetic Methanol, Industrial & Engineering Chemistry, 17 (1925) 430-432.
[38] K.A. Ali, A.Z. Abdullah, A.R. Mohamed, Recent development in catalytic technologies for methanol synthesis from renewable sources: A critical review, Renewable and Sustainable Energy Reviews, 44 (2015) 508-518.
[39] J.A. Christiansen, LIV.-The equilibrium between methyl formate and methyl alcohol, and some related equilibria, Journal of the Chemical Society (Resumed), 129 (1926) 413-421.
[40] Hendriyana, Subagjo, H. Susanto, Carbonylation of Methanol with CO in Presence Potassium Methoxide Catalyst, Procedia Chemistry, 16 (2015) 716-722.
[41] L. Chen, J. Zhang, P. Ning, Y. Chen, W. Wu, Kinetics of Methanol Carbonylation to Methyl Formate Catalyzed by Sodium Methoxide, Journal of Energy Chemistry, 13 (2004) 225-230.
[42] S.P. Tonner, M.S. Wainwright, D.L. Trimm, N.W. Cant, Solubility of carbon monoxide in alcohols, Journal of Chemical & Engineering Data, 28 (1983) 59-61.
[43] P. Caubere, Unimetal super bases, Chemical Reviews, 93 (1993) 2317-2334.
[44] P. Caubère, Complex Reducing Agents (CRA's)—Versatile, Novel Ways of Using Sodium Hydride in Organic Synthesis, Angewandte Chemie International Edition in English, 22 (1983) 599-613.
[45] J.J. Brunet, P. Gallois, P. Caubere, Activation of reducing agents. Sodium hydride containing complex reducing agents. 12. New convenient, highly active, and selective nickel hydrogenation catalysts, The Journal of Organic Chemistry, 45 (1980) 1937-1945.
[46] J.M. McCabe Dunn, A. Duran-Capece, B. Meehan, J. Ulis, T. Iwama, G. Gloor, G. Wong, E. Bekos, The Safe Use of Sodium Hydride on Scale: The Process Development of a Chloropyrimidine Displacement, Organic Process Research & Development, 15 (2011) 1442-1446.
[47] K. Komers, J. Machek, R. Stloukal, Biodiesel from rapeseed oil, methanol and KOH. 2. Composition of solution of KOH in methanol as reaction partner of oil, European Journal of Lipid Science and Technology, 103 (2001) 359-362.
[48] M. Xiong, C. Wang, D. Shao, Preparing Sodium Methoxide from Sodium Hydroxide by Reaction Coupling with Separation Processes Advanced Materials Research, 986-987 (2014) 101-105.
[49] A. Sakakibara, Hydrogenolysis, in: S.Y. Lin, C.W. Dence (Eds.) Methods in Lignin Chemistry, Springer Berlin Heidelberg, Berlin, Heidelberg, 1992, pp. 350-368.
[50] P.Å. Sørum, Hydrogenolysis of Esters, Conversion of Methyl Formate to Methanol, The Department of Industrial Chemistry, The Norwegian Institute of Technology, Trondheim, 1981.
[51] G. Braca, A.M.R. Galletti, G. Sbrana, M. Lami, M. Marchionna, Hydrogenolysis of formic esters with homogeneous and heterogeneous rhenium catalysts, Journal of Molecular Catalysis A: Chemical, 95 (1995) 19-26.
[52] R.S. Sapienza, W.A. Slegeir, O.H. T.E., D. Mahajan, Low Temperature Catalyst System for Methanol Production, U.S. Patent 4,623,634, 1986.
[53] R.S. Sapienza, W.A. Slegeir, O.H. T.E., D. Mahajan, Low temperature catalysts for methanol production, U.S. Patent 4,614,749, 1986.

[54] S. Ohyama, Transformation of the nickel precursor in catalytic systems for low-temperature methanol synthesis in liquid phase, Applied Catalysis A: General, 181 (1999) 87-93.
[55] S. Ohyama, Catalytically active species in Ni-based catalytic systems for low-temperature methanol synthesis probed by in situ ATR/FTIR in combination with reaction kinetics, Applied Catalysis A: General, 313 (2006) 58-62.
[56] D.L. Kurta, B.S. Dean, E.P. Krenzelok, Acute nickel carbonyl poisoning, The American journal of emergency medicine, 11 (1993) 64-66.
[57] S. Ohyama, Low-temperature methanol synthesis via methyl formate in liquid phase, Current Topics in Catalysis, 5 (2006) 1-5.
[58] S. Ohyama, Liquid-phase CO hydrogenation over silica-supported transition metal and Cu−Zn−Cr oxide catalysts, Reaction Kinetics and Catalysis Letters, 61 (1997) 331-336.
[59] H. Adkins, R. Connor, The catalytic hydrogenation of organic compounds over copper chromite, Journal of the American Chemical Society, 53 (1931) 1091-1095.
[60] H. Adkins, E.E. Burgoyne, H.J. Schneider, The Copper—Chromium Oxide Catalyst for Hydrogenation, Journal of the American Chemical Society, 72 (1950) 2626-2629.
[61] T.-W. Chiu, C.-H. Tu, Y.-T. Chen, Fabrication of electrospun CuCr2O4 fibers, Ceramics International, 41 (2015) S399-S406.
[62] S.G. Hosseini, R. Abazari, A. Gavi, Pure CuCr2O4 nanoparticles: Synthesis, characterization and their morphological and size effects on the catalytic thermal decomposition of ammonium perchlorate, Solid State Sciences, 37 (2014) 72-79.
[63] W. Yuan, X. Liu, L. Li, Synthesis, characterization and photocatalytic activity of cubic-like CuCr2O4 for dye degradation under visible light irradiation, Applied Surface Science, 319 (2014) 350-357.
[64] A.M. Kawamoto, L.C. Pardini, L.C. Rezende, Synthesis of copper chromite catalyst, Aerospace Science and Technology, 8 (2004) 591-598.
[65] T.M. Yur'eva, L. Plyasova, O.V. Makarova, T.A. Krieger, V.I. Zaikovskii, Nanometer size copper particles in copper chromite catalysts, in: G. Poncelet, J. Martens, B. Delmon, P.A. Jacobs, P. Grange (Eds.) Studies in Surface Science and Catalysis, Elsevier1995, pp. 533-537.
[66] K.L. Deutsch, B.H. Shanks, Active species of copper chromite catalyst in C–O hydrogenolysis of 5-methylfurfuryl alcohol, Journal of Catalysis, 285 (2012) 235-241.
[67] T.M. Yurieva, L.M. Plyasova, O.V. Makarova, T.A. Krieger, Mechanisms for hydrogenation of acetone to isopropanol and of carbon oxides to methanol over copper-containing oxide catalysts, Journal of Molecular Catalysis A: Chemical, 113 (1996) 455-468.
[68] H. Liu, T. Chen, G. Yang, G.-Y. Wang, Investigation of Active Center of Cu-Based Catalyst for Low Temperature Methanol Synthesis from Syngas in Liquid Phase: The Contribution of Cu+ and Cu0, ChemistrySelect, 2 (2017) 8000-8007.
[69] O.Y. Prudnikova, O.V. Makarova, T.M. Yurieva, Active state of copper in catalysts for low-temperature methanol synthesis, Reaction Kinetics and Catalysis Letters, 14 (1980) 413-416.

[70] H. Jahangiri, J. Bennett, P. Mahjoubi, K. Wilson, S. Gu, A review of advanced catalyst development for Fischer-Tropsch synthesis of hydrocarbons from biomass derived syn-gas, Catalysis Science & Technology, 4 (2014) 2210-2229.
[71] D.M. Monti, N.W. Cant, D.L. Trimm, M.S. Wainwright, Hydrogenolysis of methyl formate over copper on silica: I. Study of surface species by in situ infrared spectroscopy, Journal of Catalysis, 100 (1986) 17-27.
[72] D.M. Monti, N.W. Cant, D.L. Trimm, M.S. Wainwright, Hydrogenolysis of methyl formate over copper on silica: II. Study of the mechanism using labeled compounds, Journal of Catalysis, 100 (1986) 28-38.
[73] S.P. Tonner, D.L. Trimm, M.S. Wainwright, N.W. Cant, Dehydrogenation of methanol to methyl formate over copper catalysts, Industrial & Engineering Chemistry Product Research and Development, 23 (1984) 384-388.
[74] Z. Liu, J.W. Tierney, Y.T. Shah, I. Wender, Methanol synthesis via methylformate in a slurry reactor, Fuel Processing Technology, 23 (1989) 149-167.
[75] N.W. Cant, S.P. Tonner, D.L. Trimm, M.S. Wainwright, Isotopic labeling studies of the mechanism of dehydrogenation of methanol to methyl formate over copper-based catalysts, Journal of Catalysis, 91 (1985) 197-207.
[76] V.M. Palekar, H. Jung, J.W. Tiemey, I. Wender, Slurry phase synthesis of methanol with a potassium methoxide/copper chromite catalytic system, Applied Catalysis A: General, 102 (1993) 13-34.
[77] Y. Du, C. Wang, H. Jiang, C. Chen, R. Chen, Insights into deactivation mechanism of Cu–ZnO catalyst in hydrogenolysis of glycerol to 1,2-propanediol, Journal of Industrial and Engineering Chemistry, 35 (2016) 262-267.
[78] T. Salmi, R. Hakkarainen, Kinetic Study of the Low-Temperature Water-Gas Shift Reaction over a Cu—ZnO Catalyst, Applied Catalysis, 49 (1989) 285-306.
[79] Y. Choi, H.G. Stenger, Water gas shift reaction kinetics and reactor modeling for fuel cell grade hydrogen, Journal of Power Sources, 124 (2003) 432-439.
[80] N. Tsubaki, M. Ito, K. Fujimoto, A New Method of Low-Temperature Methanol Synthesis, Journal of Catalysis, 197 (2001) 224-227.
[81] N. Tsubaki, J. Zeng, Y. Yoneyama, K. Fujimoto, Continuous synthesis process of methanol at low temperature from syngas using alcohol promoters, Catalysis Communications, 2 (2001) 213-217.
[82] T.-S. Zhao, K. Zhang, X. Chen, Q. Ma, N. Tsubaki, A novel low-temperature methanol synthesis method from CO/H2/CO2 based on the synergistic effect between solid catalyst and homogeneous catalyst, Catalysis Today, 149 (2010) 98-104.
[83] Y. Zhang, R. Yang, N. Tsubaki, A new low-temperature methanol synthesis method: Mechanistic and kinetics study of catalytic process, Catalysis Today, 132 (2008) 93-100.
[84] P. Reubroycharoen, T. Yamagami, T. Vitidsant, Y. Yoneyama, M. Ito, N. Tsubaki, Continuous Low-Temperature Methanol Synthesis from Syngas Using Alcohol Promoters, Energy & Fuels, 17 (2003) 817-821.
[85] B. Xu, R. Yang, F. Meng, P. Reubroycharoen, T. Vitidsant, Y. Zhang, Y. Yoneyama, N. Tsubaki, A New Method of Low Temperature Methanol Synthesis, Catal Surv Asia, 13 (2009) 147-163.
[86] J. Zeng, K. Fujimoto, N. Tsubaki, A New Low-Temperature Synthesis Route of Methanol: Catalytic Effect of the Alcoholic Solvent, Energy & Fuels, 16 (2002) 83-86.

[87] R. Yang, Y. Zhang, Y. Iwama, N. Tsubaki, Mechanistic study of a new low-temperature methanol synthesis on Cu/MgO catalysts, Applied Catalysis A: General, 288 (2005) 126-133.
[88] L. Fan, Y. Sakaiya, K. Fujimoto, Low-temperature methanol synthesis from carbon dioxide and hydrogen via formic ester, Applied Catalysis A: General, 180 (1999) L11-L13.
[89] Y. Sakaiya, L. Fan, K. Fujimoto, Methanol Synthesis from Carbon Dioxide and Hydrogen via Formic Ester, Journal of The Japan Petroleum Institute, 41 (1998) 354-357.
[90] P. Reubroycharoen, T. Vitidsant, Y. Yoneyama, N. Tsubaki, Development of a new low-temperature methanol synthesis process, Catalysis Today, 89 (2004) 447-454.
[91] Y. Jeong, I. Kim, J.Y. Kang, H. Jeong, J.K. Park, J.H. Park, J.C. Jung, Alcohol-assisted low temperature methanol synthesis from syngas over Cu/ZnO catalysts: Effect of pH value in the co-precipitation step, Journal of Molecular Catalysis A: Chemical, 400 (2015) 132-138.
[92] T.-S. Zhao, Y. Yoneyama, K. Fujimoto, N. Yamane, K. Fujimoto, N. Tsubaki, Promotional Effect of Potassium Salt in Low-temperature Formate and Methanol Synthesis from CO/CO2/H2 on Copper Catalyst, Chemistry Letters, 36 (2007) 734-735.
[93] B. Hu, Y. Yamaguchi, K. Fujimoto, Low temperature methanol synthesis in alcohol solvent over copper-based catalyst, Catalysis Communications, 10 (2009) 1620-1624.
[94] B. Hu, K. Fujimoto, High-performance Cu/MgO–Na catalyst for methanol synthesis via ethyl formate, Applied Catalysis A: General, 346 (2008) 174-178.
[95] B. Hu, K. Fujimoto, Promoting behaviors of alkali compounds in low temperature methanol synthesis over copper-based catalyst, Applied Catalysis B: Environmental, 95 (2010) 208-216.
[96] B. Hu, K. Fujimoto, Low Temperature Methanol Synthesis in Slurry Phase With a Hybrid Copper-Formate System, Catalysis Letters, 129 (2009) 416-421.
[97] S. Vukojević, O. Trapp, J.-D. Grunwaldt, C. Kiener, F. Schüth, Quasi-Homogeneous Methanol Synthesis Over Highly Active Copper Nanoparticles, Angewandte Chemie International Edition, 44 (2005) 7978-7981.
[98] W.-J. Shen, Y. Ichihashi, Y. Matsumura, Low temperature methanol synthesis from carbon monoxide and hydrogen over ceria supported copper catalyst, Applied Catalysis A: General, 282 (2005) 221-226.
[99] M. Tamura, T. Kitanaka, Y. Nakagawa, K. Tomishige, Cu Sub-Nanoparticles on Cu/CeO2 as an Effective Catalyst for Methanol Synthesis from Organic Carbonate by Hydrogenation, ACS Catalysis, 6 (2016) 376-380.
[100] C. Lian, F. Ren, Y. Liu, G. Zhao, Y. Ji, H. Rong, W. Jia, L. Ma, H. Lu, D. Wang, Y. Li, Heterogeneous selective hydrogenation of ethylene carbonate to methanol and ethylene glycol over a copper chromite nanocatalyst, Chemical Communications, 51 (2015) 1252-1254.
[101] I. Chorkendorff, J.W. Niemantsverdriet, Concepts of Modern Catalysis and Kinetics, 2nd, Rev. & Enlarged ed., WILEY-VCH Verlag GmbH & Co. KGaA, Weinheim2007.
[102] G.A. Somorjai, Introduction to Surface Chemistry and Catalysis, John Wiley & Sons, Inc.1994.
[103] K. Philippot, P. Serp, Concepts in Nanocatalysis, Nanomaterials in Catalysis, Wiley-VCH Verlag GmbH & Co. KGaA2013, pp. 1-54.

[104] R.M. Richards, Introduction to Nanoscale Materials in Chemistry, Edition II, Nanoscale Materials in Chemistry, John Wiley & Sons, Inc.2009, pp. 1-14.
[105] K.P. McKenna, Unique Bonding in Nanoparticles and Powders, Nanoscale Materials in Chemistry, John Wiley & Sons, Inc.2009, pp. 15-36.
[106] S. Bordiga, E. Groppo, G. Agostini, J.A. van Bokhoven, C. Lamberti, Reactivity of Surface Species in Heterogeneous Catalysts Probed by In Situ X-ray Absorption Techniques, Chemical Reviews, 113 (2013) 1736-1850.
[107] N.C.f.B. Information, PubChem Compound Database; CID=23978, https://pubchem.ncbi.nlm.nih.gov/compound/23978, (Date accessed 12.02.2018).
[108] D.S. Jacob, J. Lellouche, E. Banin, A. Gedanken, Microwave Preparation of Metal Fluorides and their Biological Application, Nanoscale Materials in Chemistry, John Wiley & Sons, Inc.2009, pp. 71-110.
[109] S.G. Kwon, T. Hyeon, Kinetics of Colloidal Chemical Synthesis of Monodisperse Spherical Nanocrystals, Nanoscale Materials in Chemistry, John Wiley & Sons, Inc.2009, pp. 127-153.
[110] M.B. Gawande, A. Goswami, F.-X. Felpin, T. Asefa, X. Huang, R. Silva, X. Zou, R. Zboril, R.S. Varma, Cu and Cu-Based Nanoparticles: Synthesis and Applications in Catalysis, Chemical Reviews, 116 (2016) 3722-3811.
[111] D. Mott, J. Galkowski, L. Wang, J. Luo, C.-J. Zhong, Synthesis of Size-Controlled and Shaped Copper Nanoparticles, Langmuir, 23 (2007) 5740-5745.
[112] M.A. Malik, M.Y. Wani, M.A. Hashim, Microemulsion method: A novel route to synthesize organic and inorganic nanomaterials: 1st Nano Update, Arabian Journal of Chemistry, 5 (2012) 397-417.
[113] H.-t. Zhu, C.-y. Zhang, Y.-s. Yin, Rapid synthesis of copper nanoparticles by sodium hypophosphite reduction in ethylene glycol under microwave irradiation, Journal of Crystal Growth, 270 (2004) 722-728.
[114] A. Bhattacharjee, M. Ahmaruzzaman, Facile synthesis of 2-dimensional CuO nanoleaves and their degradation behavior for Eosin Y, Materials Letters, 161 (2015) 20-25.
[115] K. Lingaraju, H.R. Naika, K. Manjunath, G. Nagaraju, D. Suresh, H. Nagabhushana, Rauvolfia serpentina-Mediated Green Synthesis of CuO Nanoparticles and Its Multidisciplinary Studies, Acta Metallurgica Sinica (English Letters), 28 (2015) 1134-1140.
[116] J. Kim, S.W. Kang, S.H. Mun, Y.S. Kang, Facile Synthesis of Copper Nanoparticles by Ionic Liquids and Its Application to Facilitated Olefin Transport Membranes, Industrial & Engineering Chemistry Research, 48 (2009) 7437-7441.
[117] S. Mohammadi, A. Harvey, K.V.K. Boodhoo, Synthesis of TiO2 nanoparticles in a spinning disc reactor, Chemical Engineering Journal, 258 (2014) 171-184.
[118] K.V.K. Boodhoo, S.R. Al-Hengari, Micromixing Characteristics in a Small-Scale Spinning Disk Reactor, Chemical Engineering & Technology, 35 (2012) 1229-1237.
[119] D. Reay, C. Ramshaw, A. Harvey, Reactors, Process Intensification, Butterworth-Heinemann, Oxford, 2008, pp. 103-186.
[120] K. Boodhoo, Spinning Disc Reactor for Green Processing and Synthesis, Process Intensification for Green Chemistry, John Wiley & Sons, Ltd, Chichester, UK, 2013, pp. 59-90.

[121] Z. Huang, F. Cui, H. Kang, J. Chen, X. Zhang, C. Xia, Highly Dispersed Silica-Supported Copper Nanoparticles Prepared by Precipitation−Gel Method: A Simple but Efficient and Stable Catalyst for Glycerol Hydrogenolysis, Chemistry of Materials, 20 (2008) 5090-5099.
[122] J. Xiong, Y. Wang, Q. Xue, X. Wu, Synthesis of highly stable dispersions of nanosized copper particles using l-ascorbic acid, Green Chemistry, 13 (2011) 900-904.
[123] D. Harvey, Modern Analytical Chemistry, The McGraw-Hill Co.2000.
[124] E. Hoffman, V. Stroobant, Mass Spectrometry, Principles and Applications, 3rd Ed., John Wiley & Sons, Ltd., West Sussex, England, 2007.
[125] H. Züchner, J. W. Niemantsverdriet: Spectroscopy in catalysis — an introduction, VCH Verlagsgesellschaft, Weinheim, ISBN 3-527-28593-8, 1993, 289 Seiten, Preis DM 148,—, Berichte der Bunsengesellschaft für physikalische Chemie, 98 (1994) 1349-1350.
[126] https://www.bruker.com/products/x-ray-diffraction-and-elemental-analysis/x-ray-diffraction/xrd-software/topas/rietveld-analysis-software.html, (Date accessed: 28.10.2016).
[127] B. Fultz, J. Howe, The TEM and Its Optics, in: B. Fultz, J. Howe (Eds.) Transmission Electron Microscopy and Diffractometry of Materials, Springer Berlin Heidelberg, Berlin, Heidelberg, 2013, pp. 59-115.
[128] D.B. Williams, C.B. Carter, The Instrument, in: D.B. Williams, C.B. Carter (Eds.) Transmission Electron Microscopy: A Textbook for Materials Science, Springer US, Boston, MA, 1996, pp. 131-153.
[129] https://warwick.ac.uk/fac/cross_fac/sciencecity/programmes/internal/themes/am2/booking/particlesize/intro_to_dls.pdf, Malvern Instrument, Technical Note, (Date accessed: 21.02.2018).
[130] B.H. Stuart, Introduction, Infrared Spectroscopy: Fundamentals and Applications, John Wiley & Sons, Ltd2005, pp. 1-13.
[131] B.H. Stuart, Experimental Methods, Infrared Spectroscopy: Fundamentals and Applications, John Wiley & Sons, Ltd2005, pp. 15-44.
[132] N.P. Fitzsimons, W. Jones, P.J. Herley, Studies of copper hydride. Part 1.-Synthesis and solid-state stability, Journal of the Chemical Society, Faraday Transactions, 91 (1995) 713-718.
[133] G.N. Glavee, K.J. Klabunde, C.M. Sorensen, G.C. Hadjipanayis, Borohydride Reduction of Nickel and Copper Ions in Aqueous and Nonaqueous Media. Controllable Chemistry Leading to Nanoscale Metal and Metal Boride Particles, Langmuir, 10 (1994) 4726-4730.
[134] R. Battino, T.R. Rettich, T. Tominaga, The Solubility of Oxygen and Ozone in Liquids, Journal of Physical and Chemical Reference Data, 12 (1983) 163-178.
[135] T.H. Fleisch, R.L. Mieville, Studies on the chemical state of Cu during methanol synthesis, Journal of Catalysis, 90 (1984) 165-172.
[136] J.R. Jensen, T. Johannessen, H. Livbjerg, An improved N2O-method for measuring Cu-dispersion, Applied Catalysis A: General, 266 (2004) 117-122.
[137] J.T. Sun, I.S. Metcalfe, M. Sahibzada, Deactivation of Cu/ZnO/Al2O3 Methanol Synthesis Catalyst by Sintering, Industrial & Engineering Chemistry Research, 38 (1999) 3868-3872.

[138] K.K. Nanda, A. Maisels, F.E. Kruis, H. Fissan, S. Stappert, Higher Surface Energy of Free Nanoparticles, Physical Review Letters, 91 (2003) 106102.
[139] A.S. Myerson, R. Ginde, 2 - Crystals, crystal growth, and nucleation, Handbook of Industrial Crystallization (Second Edition), Butterworth-Heinemann, Woburn, 2002, pp. 33-65.
[140] K. Suttiponparnit, J. Jiang, M. Sahu, S. Suvachittanont, T. Charinpanitkul, P. Biswas, Role of Surface Area, Primary Particle Size, and Crystal Phase on Titanium Dioxide Nanoparticle Dispersion Properties, Nanoscale Res Lett, 6 (2010) 1-8.
[141] L. Xing-Quan, W. Yu-Tang, L. Shi-Zhong, Y. Zing-Chun, L. Zhao-Xia, L. Shun-Fen, C. Wen-Kai, Y. Zuo-Long, Concurrent Synthesis of Methanol and Methyl Formate Catalysed by Copper-based catalysts II. Influences of solvents and H2/CO mole ratios, Journal of Natural Gas Chemistry, 8 (1999) 203-210.
[142] A. Rabaron, G. Cavé, F. Puisieux, M. Seiller, Physical methods for measurement of the HLB of ether and ester non-ionic surface-active agents: H-NMR and dielectric constant, International Journal of Pharmaceutics, 99 (1993) 29-36.
[143] C. Wohlfarth, Static Dielectric Constants of Pure Liquids and Binary Liquid Mixtures, in: M.D. Lechner (Ed.) Supplement to IV/6, Springer Berlin Heidelberg, Berlin, Heidelberg, 2008.
[144] Physical Constants of Organic Compounds, in: D.R. Lide (Ed.) CRC Handbook of Chemistry and Physics2003.
[145] E.S. Domalski, E.D. Hearing, Condensed Phase Heat Capacity Data, NIST Chemistry WebBook, NIST Standard Reference Database Number 69, National Institute of Standards and Technology, Gaithersburg MD, (Date access: 08.03.2018).
[146] X. Wei, G. Xu, Z. Ren, G. Shen, G. Han, Room-Temperature Synthesis of BaTiO3 Nanoparticles in Large Batches, Journal of the American Ceramic Society, 91 (2008) 3774-3780.
[147] X.B. Zhao, X.H. Ji, Y.H. Zhang, B.H. Lu, Effect of solvent on the microstructures of nanostructured Bi2Te3 prepared by solvothermal synthesis, Journal of Alloys and Compounds, 368 (2004) 349-352.
[148] G. Tunell, E. Posnjak, C.J. Ksanda, Geometrical and optical properties, and crystal structure of tenorite, Zeitschrift fuer Kristallographie, Kristallgeometrie, Kristallphysik, Kristallchemie, 90 (1935) 120-142.
[149] B.T.F. Weybye, The cristobalite structure, American Journal of Science, 23 (1932) 350-356.
[150] C. Vogelpohl, C. Brandenbusch, G. Sadowski, High-pressure gas solubility in multicomponent solvent systems for hydroformylation. Part II: Syngas solubility, The Journal of Supercritical Fluids, 88 (2014) 74-84.
[151] O. Jogunola, T. Salmi, M. Kangas, J.P. Mikkola, Determination of the kinetics and mechanism of methyl formate synthesis in the presence of a homogeneous catalyst, Chemical Engineering Journal, 203 (2012) 469-479.
[152] S.E. Stein, Infrared Spectra by NIST Mass Spec Data Center, in: P.J. Linstrom, W.G. Mallard (Eds.) NIST Chemistry WebBook, NIST Standard Reference Database Number 69(date accessed: 29.11.2016).
[153] A.J. Parker, Protic-dipolar aprotic solvent effects on rates of bimolecular reactions, Chemical Reviews, 69 (1969) 1-32.

[154] Q. Cai, C. Jin, B. Lu, H. Tangbo, Y. Shan, Synthesis of Dimethyl Carbonate from Methanol and Carbon dioxide using Potassium Methoxide as Catalyst under Mild Conditions, Catalysis Letters, 103 (2005) 225-228.
[155] X. Yang, Metal Hydride and Ligand Proton Transfer Mechanism for the Hydrogenation of Dimethyl Carbonate to Methanol Catalyzed by a Pincer Ruthenium Complex, ACS Catalysis, 2 (2012) 964-970.
[156] F. Hasanayn, A. Baroudi, A.A. Bengali, A.S. Goldman, Hydrogenation of Dimethyl Carbonate to Methanol by trans-[Ru(H)2(PNN)(CO)] Catalysts: DFT Evidence for Ion-Pair-Mediated Metathesis Paths for C–OMe Bond Cleavage, Organometallics, 32 (2013) 6969-6985.
[157] J. Zhang, G. Leitus, Y. Ben-David, D. Milstein, Efficient Homogeneous Catalytic Hydrogenation of Esters to Alcohols, Angewandte Chemie International Edition, 45 (2006) 1113-1115.
[158] R. Zevenhoven, S. Eloneva, S. Teir, Chemical fixation of CO2 in carbonates: Routes to valuable products and long-term storage, Catalysis Today, 115 (2006) 73-79.
[159] T. Sugimoto, S. Chen, A. Muramatsu, Synthesis of uniform particles of CdS, ZnS, PbS and CuS from concentrated solutions of the metal chelates, Colloids and Surfaces A: Physicochemical and Engineering Aspects, 135 (1998) 207-226.
[160] C.Y. Tai, Y.-H. Wang, H.-S. Liu, A green process for preparing silver nanoparticles using spinning disk reactor, AIChE Journal, 54 (2008) 445-452.
[161] I.H. Leubner, Particle nucleation and growth models, Current Opinion in Colloid & Interface Science, 5 (2000) 151-159.
[162] J. Bałdyga, R. Pohorecki, Turbulent micromixing in chemical reactors — a review, The Chemical Engineering Journal and the Biochemical Engineering Journal, 58 (1995) 183-195.
[163] S. Mohammadi, K.V.K. Boodhoo, Online conductivity measurement of residence time distribution of thin film flow in the spinning disc reactor, Chemical Engineering Journal, 207-208 (2012) 885-894.
[164] D. Ghiasy, M.T. Tham, K.V.K. Boodhoo, Control of a Spinning Disc Reactor: An Experimental Study, Industrial & Engineering Chemistry Research, 52 (2013) 16832-16841.
[165] R.E. Mesmer, W.L. Jolly, The Hydrolysis of Aqueous Hydroborate, Inorganic Chemistry, 1 (1962) 608-612.
[166] J.C. Ingersoll, N. Mani, J.C. Thenmozhiyal, A. Muthaiah, Catalytic hydrolysis of sodium borohydride by a novel nickel–cobalt–boride catalyst, Journal of Power Sources, 173 (2007) 450-457.
[167] M.-H. Chang, H.-S. Liu, C.Y. Tai, Preparation of copper oxide nanoparticles and its application in nanofluid, Powder Technology, 207 (2011) 378-386.
[168] I. Dybkjaer, Tubular reforming and autothermal reforming of natural gas — an overview of available processes, Fuel Processing Technology, 42 (1995) 85-107.
[169] D.-Y. Peng, D.B. Robinson, A New Two-Constant Equation of State, Industrial & Engineering Chemistry Fundamentals, 15 (1976) 59-64.
[170] S. Sircar, Pressure Swing Adsorption, Industrial & Engineering Chemistry Research, 41 (2002) 1389-1392.

[171] P. Rao, M. Muller, Industrial Oxygen, Its Generation and Use, Energy Efficiency in Industry, ACEEE Summer Study, 2007, pp. 124-135.
[172] V. Ganapathy, L. Faulkner, Industrial Boilers and Heat Recovery Steam Generators, CRC Press, Boca Raton, 2002.

Appendices A

Table A.1: List of chemicals mostly supplied by Sigma-Aldrich (* from VWR)

Chemicals	*Formula*	*% Purity*	*State*
Toluene	C_7H_8	≥99.5	Liquid
Diethyl ether	$C_4H_{10}O$	≥99.9	Liquid
Diglyme	$C_6H_{14}O_3$	≥99.5	Liquid
THF	C_4H_8O	≥99.9	Liquid
Glyme	$C_4H_{10}O_2$	99.5	Liquid
Tetraglyme	$C_{10}H_{22}O_5$	>99	Liquid
Acetonitrile	C_2H_3N	99.8	Liquid
DMSO	C_2H_6OS	≥99	Liquid
Copper (II) acetate	$Cu(CH_3COO)_2$	98	Solid
Sodium hydride	NaH	95	Solid
Sodium hydride dispersed in minera	NaH	60	Solid
Sodium methoxide	$NaOCH_3$	95	Solid
Sodium methoxide in MeOH	$NaOCH_3$	25	Liquid
Methanol	CH_3OH	99.8	Liquid
Copper (II) nitrate	$Cu(NO_3)_2$	99	Solid
Copper (II) chloride	$CuCl_2$	97	Solid
Sodium hydroxide	NaOH	≥98	Solid
Sodium borohydride	$NaBH_4$	≥96	Solid
Silica in water	SiO_2	40	Colloidal
L-ascorbic acid	$C_6H_8O_6$	≥98	Solid
Sodium formate	$NaOOCH_3$	≥99	Solid
Dimethyl carbonate	$CH_3OCOOCH_3$	≥99	Liquid
Methyl formate	CH_3OOCH	99	Liquid
Heptane	C_7H_{16}	99	Liquid
Copper (II) methoxide*	$Cu(CH_3O)_2$	98	Solid

Table A.2: List of gases

Gas	*Composition*	*Supplier*
Syngas Mixture 1	1CO:2H_2	Yara Prexair
Syngas Mixture 2	1CO:2H_2:2N_2	Yara Prexair
Syngas Mixture 3	10CO:5CO_2:20H_2:65N_2	Yara Prexair
Carbon dioxide (5.3)	CO_2	AGA
Helium (5.0)	He	AGA
Hydrogen	H_2	AGA
Nitrogen (5.0)	N_2	AGA

GC-analysis

GC analysis was based on mathematical treatment of integrated peak areas from the GC response. For the liquid analysis, five standards were prepared at varying concentrations of the different components and analysed with the GC-MSD. The same amount of heptane was added to each of the standards as an internal standard. Peak area verses component concentration was plotted for the calibration curve and the equation of a straight line derived for each component, which was used to deduce their concentration from their area response, as expressed in Equation A.1.

$$Concentration = \frac{Peak\ area - Intercept}{Slope} \qquad (A.1)$$

A typical chromatograph from the GCMS is shown in **Figure A1**. The components were identified from the molecular fragments of each peak, assisted by the Enhanced Data Analysis Software's library of the MSD. Multiplication of the concentration by the total volume and number of carbon in the molecule gives the amount of each component

present in C mmol. Conversion, selectivity and productivity from the liquid phase analysis was determined as illustrated in Equations (A.2) (A.3) and (A.4) respectively.

$$Conversion\ (C\ \%) = \frac{total\ number\ of\ C\ products\ (mol)}{amount\ of\ starting\ CO\ (mol)} \times 100 \quad (A.2)$$

$$Selectivity\ (C\ \%) = \frac{number\ of\ C\ product\ (mol)}{total\ number\ of\ C\ products\ (mol)} \times 100 \quad (A.3)$$

$$Productivity\ (\frac{mol}{mol(Cu) \times h}) = \frac{amount\ of\ MeOH\ produced}{amount\ of\ Cu_{catalyst} \times reaction\ time} \quad (A.4)$$

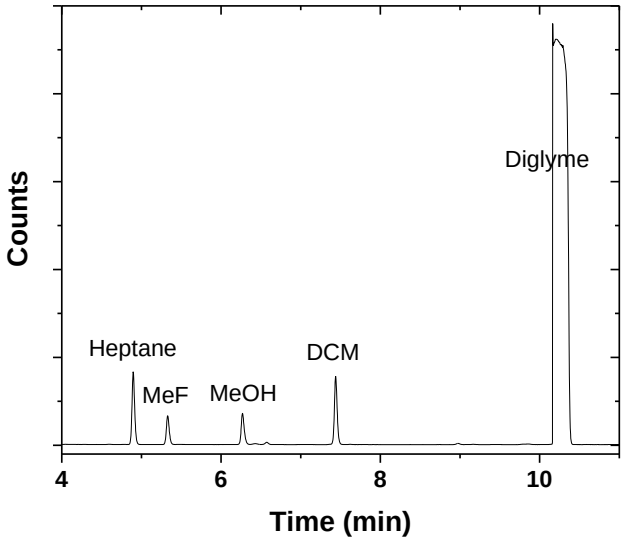

Figure A1: A chromatograph from the liquid phase analysis in the GCMS

The gas phase analysis was performed using the GC-TCD and a typical chromatograph shown in **Figure A2**. Here the calibrations were done by determining response factor, k_x from the peak area response of each molecule (x) with their concentrations in calibration mixture as expressed in Equation (A.5). Multiplication of the k_x by the peak area gave the concentration of the corresponding molecule. N_2 was included as an inert gas to help calculate conversion as illustrated in Equation (A.6). The calculations of the selectivity followed a similar approach as was done in the liquid phase (Equation (A.3) by combining the amount of products determined from both liquid and gas phase.

$$k_x = \frac{concentration\ of\ molecule\ x}{average\ peak\ area} \qquad (A.5)$$

$$Conversion = \frac{Conc_{reactant\ in} - Conc_{out} \times \frac{(Conc_{inert\ in})}{(Conc_{inert\ out})}}{Conc_{reactant\ in}} \times 100 \qquad (A.6)$$

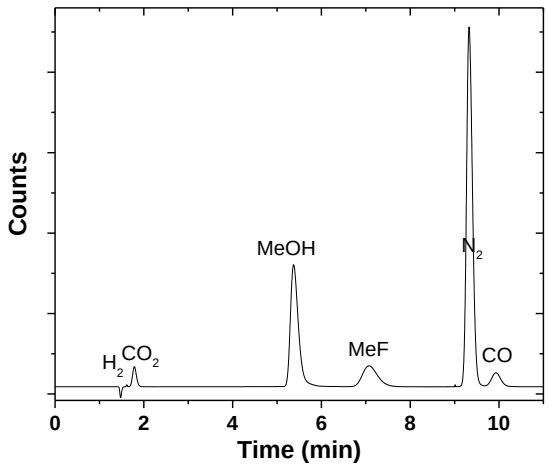

Figure A2: A chromatograph from the gas phase analysis in the GC-TCD.

Appendices B (Papers 1-4)

Paper 1

Low temperature methanol synthesis catalysed by copper nanoparticles

Ahoba-Sam C., Olsbye U., Jens K-J.

Catalysis Today, 2018, 299, 112-119, doi.org/10.1016/j.cattod.2017.06.038

Catalysis Today 299 (2018) 112–119

Contents lists available at ScienceDirect

Catalysis Today

journal homepage: www.elsevier.com/locate/cattod

Low temperature methanol synthesis catalyzed by copper nanoparticles

Christian Ahoba-Sam[a], Unni Olsbye[b], Klaus-Joachim Jens[a,*]

[a] Department of Process, Energy and Environmental Technology, University College of Southeast Norway, Kjølnes Ring 56, 3918 Porsgrunn, Norway
[b] Department of Chemistry, University of Oslo, P.O. Box 1033, Blindern, N-0315 Oslo, Norway

ARTICLE INFO

Keywords:
Methanol synthesis
Low temperature
Cu
Nanoparticle size
Deactivation

ABSTRACT

A one pot catalytic system which involves Cu and an alkoxide co-catalyst has been used for methanol (MeOH) synthesis at low temperature. Up to about 92% syngas conversion per pass and more than 90% selectivity to MeOH (the rest is methyl formate) was obtained depending on the amount of catalyst employed at 100 °C and 20 bar syngas pressure. Low temperature methanol synthesis presents a good alternative to current technology for methanol production since the former is thermodynamically favored and gives a high yield per pass. Cu particles sized around 10 ± 5 nm were found to be involved in the catalytic process. Cu nanoparticles of increasing size was synthesized by varying temperature. However, methanol production decreased with increasing Cu nanoparticle size. Moreover, the maximum conversion at the end of each successive batch declined as a function of the number of cycles performed. Decrease in catalyst activity corresponded to Cu nanoparticle densification, suggesting agglomeration to be a major catalyst deactivation pathway.

1. Introduction

Methanol (MeOH) has been identified as a potential multipurpose molecule for energy and CO_2 storage [1]. It stores both carbon and hydrogen in the liquid form, it is readily transportable and it serves as a base chemical for direct conversion into light olefins, gasoline and hydrocarbons over acidic zeolites [2], thereby providing an alternative to today's fossil energy sources and petrochemical feedstocks.

MeOH is currently synthesized from syngas (made up of $CO/CO_2/H_2$) over $Cu/ZnO/Al_2O_3$ catalysts, which operate at 250 °C and 70–100 bar of pressure [3,4]. Though this technology is highly optimized, it is capital intensive and syngas conversion per pass is thermodynamically limited. This is because conversion of syngas to methanol is an exothermic reaction (Eq. (1)) and lower temperature is required to achieve full conversion per pass. Furthermore, syngas production accounts for more than half of the total capital cost in current methanol processes [5]. Complete syngas conversion per pass will allow use of air instead of pure oxygen in the syngas section of the methanol process. This will significantly reduce the overall cost in methanol synthesis. Hence, there is a need for low temperature methanol synthesis catalysts.

$$CO + 2H_2 \leftrightarrow CH_3OH \quad \Delta H = -90.6 kJ/mol \tag{1}$$

A low temperature methanol synthesis (LTMS) reaction was identified by Christiansen in 1919 [6], which presented the possibility of almost full syngas conversion to MeOH per pass at low temperature (120 °C) conditions. This approach is known to involve firstly, carbonylation of methanol to form methyl formate (MF) and secondly, MF hydrogenolysis to form MeOH as indicated in Eqs. (2) and (3), leading to Eq. (1) as the overall reaction.

$$CO + CH_3OH \leftrightarrow HCOOCH_3 \tag{2}$$

$$HCOOCH_3 + 2H_2 \leftrightarrow 2CH_3OH \tag{3}$$

It is suggested that alkali metal promotes alcohol (methanol) carbonylation by forming metal alkoxide which has an increased electron density on their oxygen compared to the oxygen on alcohols [7]. The hydrogenolysis of the MF is suggested to occur via a formaldehyde intermediate [8] and subsequent reduction to form MeOH.

Catalyst systems reported in previous works for the carbonylation and hydrogenolysis steps of the LTMS reaction are a combination of an alkali-metal, an alcohol solvent and a transition-metal compound. Various Ni-based compounds such as $Ni(CO)_4$ and $Ni(OCOCH_3)_2$ in combination with alkali-metal alkoxide co-catalysts have been shown to be very active for syngas conversion between 80 to 120 °C and 10 to 50 bar [9,10]. However, the metal alkoxide component of the catalyst forms a stable hydroxide when in contact with water, and therefore brings the reaction to a halt. Furthermore, the tetracarbonyl nickel [10] complex is volatile and highly toxic [11], and therefore poses a potential handling risk on an industrial scale.

Copper-based materials have also been reported to be active methanol synthesis catalysts at 80–120 °C and 10–20 bar pressure. Raney

* Corresponding author.
E-mail addresses: christian.ahoba-sam@hit.no (C. Ahoba-Sam), unni.olsbye@kjemi.uio.no (U. Olsbye), Klaus.J.Jens@hit.no (K.-J. Jens).

http://dx.doi.org/10.1016/j.cattod.2017.06.038
Received 31 October 2016; Received in revised form 2 June 2017; Accepted 29 June 2017
Available online 01 July 2017

copper, copper on silica support, copper chromate as well as copper alkoxide are among the identified copper-based materials, though these are not as efficient as Ni [12–14]. The copper chromate catalyst seems to be most widely used. An enhanced catalytic activity is observed when physical mixture of CuO/Cr_2O_3 catalyst is milled by creating lattice defects leading to an increased surface area. [14,15].

We have focused on the copper alkoxide LTMS system. We could show that Raney copper works well as a LTMS hydrogenolysis catalyst [13]. Subsequently we reported the catalytic behavior of a $Cu(OCH_3)_2$/NaH/CH_3OH catalyst system. This catalyst system exhibited 75% syngas conversion at 120 °C and 20 bar, showing however linear catalyst deactivation when syngas was charged multiple times [16]. In order to optimize this catalyst system, there is a need to characterize it and gain insight into the gradual catalyst activity decline.

In this work, we report Cu nanoparticles to be involved in the LTMS reaction. We present a simple method of making Cu nanoparticles which catalyze methanol synthesis at 100 °C and investigate the effect of Cu particle size on this reaction. Finally we characterized the catalyst after repeated test cycles.

2. Experimental section

2.1. Materials and experimental setup

Copper (II) acetate ($Cu[OAc]_2$, 98%), dry sodium hydride (NaH = 95%), methanol (MeOH, anhydrous 99.8%) and diglyme (1-methoxy-2-[2-methoxyethoxy]ethane, ≥99.5%) were purchased from Sigma Aldrich. The syngas made up of $1CO:2H_2$ (± 2%) was purchased from Yara Praxair AS. All chemicals were used as received unless otherwise stated.

The synthesis of both catalyst and methanol were done in a 200 ml (60 mm diameter) stainless steel high pressure type hpm-020 autoclave batch reactor (Premex Reactor AG). The reactor was equipped with a dip tube for sampling, pressure sensors and a thermocouple inserted into the reactor to monitor internal pressure and temperature respectively. A Nupro security valve was set at 100 bar for safety and the magnetic stirrer head was attached to a stirrer with oblique impeller blades (approximately 30 angle) which extended near to the bottom of the reactor to ensure adequate mixing. The magnetic stirrer head was externally attached to an electric BCH Servo Motor that is paired with lexium 23 drive to give between 1000 to 3000 rpm, with a high degree of precision. The reactor was heated in oil block controlled by a Huber Ministat 230 thermostat. The internal temperature and pressure in the reactor was independently logged onto a PC.

2.2. Copper catalyst preparation

Typically, about 3.6 mmol of $Cu(OAc)_2$, 18.5 mmol of dry NaH and 50 ml diglyme were placed in the reactor. Under N_2 blanket set to about 1 bar, the mixture was stirred at 3000 rpm and heated to a predetermined temperature for 2 h. The set point temperatures for Cu catalyst preparation were 80, 100, 126 or 149 °C for the different catalyst systems. Thereafter the reaction in the reactor was cooled to ambient temperature (< 30 °C) followed by 52 mmol MeOH addition. This mixture was stirred at ambient temperature for 30 min to ensure that all NaH had reacted to give the sodium methoxide co-catalyst. An approximate 2 ml sample was taken for analysis using the dip tube in-between the reaction steps.

2.3. Catalytic testing

The reactor with the remaining slurry described in Section 2.2 was purged with syngas and charged to about 20 bar, then stirred at 3000 rmp and heated to 100 °C. After 2 h the reactor was cooled to about 25 °C. Syngas conversion was determined by the difference in pressure between the start and after reactor cooling to room temperature. Typically, the amount of carbon products in liquid reaction mixture after cooling compared to the syngas pressure drop represented about 85 ± 2% of syngas consumed, assuming $CO/2H_2$ were proportionally consumed.

The liquid portion of the resulting reaction was sampled after it had been allowed to settle and was analyzed by gas chromatography equipped with both liquid and gas injection valves (Agilent 7890A). The liquid injection port was connected to a CARBOWAX 007 series 20 M column with dimensions 60 m × 320 µm × 1.2 µm; and was programmed as follows; temperature was ramped by 15 °C/min from 40 °C initial temperature to 200 °C and held at 200 °C for 3 min, at 0.47 bar (6.8 psi) constant pressure. The liquid sample was injected via an Agilent 7683 B autosampler. The products were identified and quantified by an Agilent 5975 mass spectrometer detector. 0.54 mg Heptane was used as internal standard and added to each sample vial. The gas injection valve was connected to 2.7 m Porapak Q and 1.8 m Molecular Sieve 5 Å packed columns connected to a TCD for analysis of permanent gases and up to C_2 hydrocarbons. This set-up was connected to a 0.9 m Hayesep Q back flush column.

2.4. Cu catalyst characterization

The Cu catalysts were analyzed by XRD and TEM before and after the low temperature methanol synthesis (LTMS) reaction. A Bruker D8 A25 powder diffractometer using Mo Kα radiation with wavelength, λ = 0.71076 Å and Lynxeye detector with “hardened” chip for Mo radiation was used. Total Pattern Analysis Solution (TOPAS) software was employed for quantitative Rietveld analysis of the diffractogram. This software operates by fitting theoretical diffraction pattern to a measured diffraction pattern using non-linear least square algorithms [17]. The samples were analyzed as slurry which was pipetted into a capillary tube with 0.5 mm internal diameter. The tube was centrifuged at 2000 rmp for 10 min to settle the solid portion at the bottom and was thereafter mounted on capillary spinner. X-ray diffractograms were measured at 0.023° step/s for an interval of 15–35° 2 θ.

The TEM imaging was performed with a Joel 2100F instrument. Samples were diluted in methanol, and particles were separated in an ultrasound bath for 30 min. The solution was then dropped on a carbon film on a copper grid. Cu particles were ascertained to be present using EDS and electron diffraction. Generally, particle sizes were determined by using the average of 15 particles diameter ± mean deviation from the TEM images for each sample.

Cu particles agglomeration effect on activity was estimated by assuming spherical Cu particles and constant total volume of Cu before and after deactivation.

$$\frac{Numberoffreshcuparticles}{NumberofspentCuparticles} = \left(\frac{VolumeoffreshCu}{VolumeofspentCu}\right)^{-1} \quad (4)$$

$$\frac{SurfaceareaoffreshCuparticles}{SurfaceareaofspentCuparticles} = \left(\frac{AreaoffreshCuparticles}{AreaofspentCuparticles}\right) \times \left(\frac{VolumeoffreshCu}{VolumeofspentCu}\right)^{-1} = \frac{DiameterofspentCuparticles}{DiameteroffreshCuparticles} \quad (5)$$

3. Results and discussion

3.1. Typical LTMS reaction at 100 °C

Fig. 1 shows the experimental procedure for a typical LTMS reaction. In step A, NaH is expected to react with Cu^{2+} ions to give Cu in a reduced oxidation state, either Cu^+ or Cu^0 or a mixture of the two. In the former case CuH could be a possible reaction product as Cu^+ may react with H^- although this compound is expected to be highly unstable at the working conditions [18]. Step A resulted in about 0.35 bar pressure increase, and was determined with GC/TCD to be H_2 (illustrated by Eq. (6)). Addition of excess MeOH in step B was to ensure

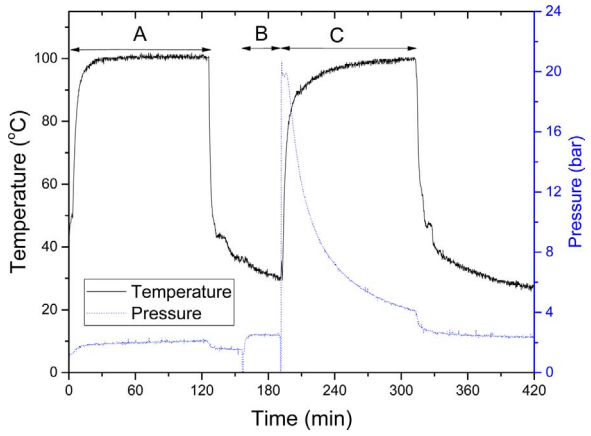

Fig. 1. Typical LTMS procedure employed in this work, A = 3.6 mmol Cu(OAc) 2 + 18 mmol NaH in 50 ml diglyme, B = addition of 49 mmol MeOH, C = 20 bar $2H_2$:1CO charged.

that all the NaH was consumed to produce $NaOCH_3$ which is the co-catalyst for the LTMS. After 30 mins of stirring, pressure increased by 1.38 bar as a result of H_2 evolution (according to Eq. (7)). Syngas was added at step C for the methanol synthesis at 100 °C. Syngas conversion was estimated based on pressure drop, and in this case, 89% syngas conversion was achieved.

$$Cu^{2+}_{(diglyme)} + 2H^{-} \rightarrow Cu + H_2 \quad (6)$$

$$NaH_{(s)} + CH_3OH_{(l)} \rightarrow CH_3ONa_{(diglyme)} + H_{2(g)} \quad (7)$$

To determine the oxidation state, composition and crystallite size of Cu in the slurry, XRD of the slurry was measured. Fig. 2a shows the X-ray diffractogram of the catalyst system after the steps A, B and C. Diffractogram A indicated Cu, Cu_2O and NaH crystals present. Diffractogram B indicated a mixture of Cu_2O and Cu whilst that of C showed predominantly Cu^0. The XRD diffractogram showed that, surplus NaH was undissolved after step A before addition of methanol but it was consumed for the formation of the co-catalyst, $NaOCH_3$ upon addition of methanol, as illustrated in Eq. (7), hence the pressure rise of the mixture during the step B in Fig. 1.

The X-ray diffractogram for C (Fig. 2a) showed mainly Cu^0 reflections with an average crystallite size of 10 ± 1 nm. This indicates a slight increase in the average Cu particle size during the LTMS reaction. The metallic Cu^0 phase observed after methanol synthesis was not surprising considering the presence of a highly reducing environment made up of 20 bar of H_2 and CO mixture at 100 °C for 2 h. An XPS study of the chemical state of Cu catalyst has shown that 2 bar of syngas reduces Cu^{2+} to Cu^0 at 250 °C in 1 h while at 100 °C, Cu^{2+} reduces to Cu^+ [19]. Therefore, considering the presence of Cu^+ and Cu^0 after step B, further reduction of the remaining Cu^+ to Cu^0 at 100 °C observed in this work is in order.

The average crystallite size of Cu_2O was estimated to be 7.6 ± 0.8 nm from XRD line broadening using the Rietveld analysis for B (Fig. 2b). The observed Cu_2O rather than expected Cu^0 could be due to presence of some amount of oxygen in the reaction system. Glavee et al. [20] observed that borohydride reduction of Cu^{2+} in water or diglyme yielded Cu^0 with stoichiometric release of H_2, when done under vacuum, however isolation of the Cu under ambient condition resulted in some amount of Cu_2O. Oxygen is also known to be soluble in organic solvents such as ethers with the solubility following the hydrocarbon chain length [21]. Therefore, the oxygen source could be dissolved oxygen in the solvent since the reaction was not done under vacuum.

Fig. 3a and b show the TEM images of the Cu catalyst after steps A and B respectively. Since the sample preparation for TEM imaging involved addition of MeOH to all samples, both A and B were expected to give similar Cu particles sizes. The particle sizes were around 10 ± 5 nm with some agglomerates. The observed particle sizes fall within the range of the crystallite size estimated for B from the XRD which was around 7.6 ± 0.8 nm.

Fig. 3c shows TEM imaging and the electron diffraction after the LTMS reaction. Here the particles were about 10 ± 3 nm. The image appeared to give a narrower particle size distribution as compared to that of the initial steps A and B. Again, the average crystallite size estimated by XRD was similar to the observed particle sizes by TEM. Electron diffraction showed the particles to be polycrystalline and indexing confirmed a metallic Cu phase to be present.

3.2. Deactivation test of the catalyst system

Multiple charging of the catalyst system was performed to investigate the recycle stability of the Cu catalyst system. The test sequence was similar to the first sequence (Fig. 1) except that the catalyst concentration was slightly higher. Syngas was charged to about 20 bar, heated to 100 °C and stirred to react for 2 h after which the reactor was cooled to about 25 °C and then degassed. This was repeated for 6 times as shown in Fig. 4a. Fig. 4b shows syngas conversion and selectivity for 7 consecutive charges. Syngas conversion decreased after each consecutive batch from 92% (1st charge) to 61% (6th charge). Selectivity to methanol and methyl formate were 94 and 6% respectively after the sixth charge. Liquid sampling for analysis was done just before and after the sixth charge so as not to reduce the amount of catalyst.

Syngas conversion decreased by 31% from the first to sixth charge. Since there are two components of catalysts involved, approximately 31% addition of one of the component should restore activity if that is responsible for the deactivation. As a consequence of that, 8 mmol NaH in 49 mmol MeOH was injected into the reactor. This represents a 31% increase of the initial methoxide content in the reactor. The syngas conversion increased slightly to 70% with 95 and 5% selectivity to methanol and methyl formate respectively. This indicated that even with 31% increase in the amount of co-catalyst, conversion increased by 9% with no significant change in selectivity. The 99.8% anhydrous MeOH purity used in the methoxide co-catalyst contain some ppm of water (≤0.002% according to the product specification sheet). However the total contribution of this to the conversion if methoxide reacted with water should by < 0.02% which is insignificant in our conversion range. This suggested that methoxide may not be the main or the only source of deactivation.

The Cu catalyst was characterized by XRD and TEM after the sixth charge which is shown in Fig. 5. A sharper and more intense Cu diffraction peak was observed for the sample of the 6th charged (spent catalyst) as compared to the fresh sample (i.e. sample slurry before the 1st charge), which showed predominantly Cu_2O phase. The crystallite size was 16 ± 1 nm for the spent catalyst sample while that of the fresh sample was 8 ± 1 nm. The TEM image of the spent catalyst after the 6th charge showed a wide particle size distribution ranging from 6 to about 25 nm though the larger sizes dominated. Estimation of surface area ratio between the fresh Cu catalyst and spent catalyst after the 6th charge based on the Cu crystallite sizes from the XRD and Eq. (5) is 2.

Figs. 4b and 5 can be compared to Figs. 2a and 3c to make some inferences. First of all, the oxidation state of Cu after the 1st and 6th charge was Cu^0. Despite the fact that Cu_2O was the starting component, the high activity of the Cu catalyst already after the first charge suggests that the probable active Cu phase of the Cu for LTMS reaction is Cu^0. An earlier, in-situ XPS study has shown Cu to be reduced during syngas conversion to MeOH at 100 °C [19]. Since our reaction conditions exposes the Cu catalyst system to 20 bar syngas which is expected to be a highly reducing atmosphere for Cu, metallic Cu surface is suspected to be active in the LTMS reaction.

Secondly, Cu crystallite and particle size after the 6th charge had increased significantly. Clearly there is an approximate doubling of crystal size between the 1st and the 6th charge. An estimation based on

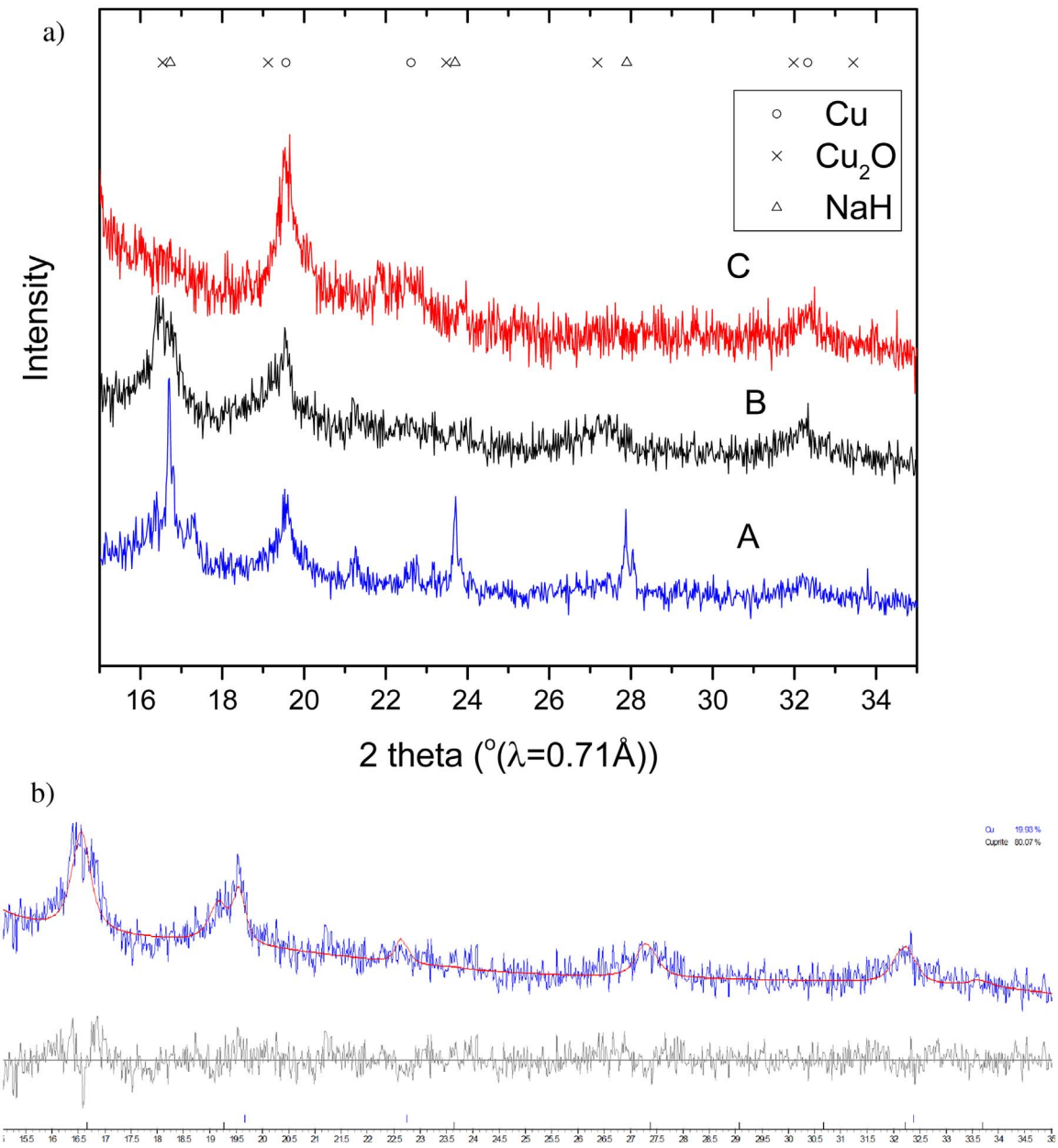

Fig. 2. X-ray diffractogram of the slurry at the different stages in Fig. 1. a: X-ray diffractogram of the slurry after the steps A, B and C. b: Rietveld analysis of diffffractogram B in Fig. 2.

Eq. (5) for the effect of agglomeration gives a surface area ratio between the 1st and 6th charge to be 1.6. This is comparable to the decline in syngas conversion of about 1.5 (=92/61). That is, there is a strong correlation between the reduction of active Cu surface available and the catalyst deactivation. On the other hand, it has also been suggested elsewhere [9] that the slight catalyst deactivation in LTMS reaction is due to the high sensitivity of alkoxide to CO_2 and H_2O which may be formed in trace amounts during methanol synthesis as a byproduct. Although there is a possibility of some ppm of water in the anhydrous MeOH used as the source of the methoxide, this will not be adequate to cause the repetitive decline of catalytic activity. This notwithstanding, our observations point towards gradual decline of activity not only due to the alkoxide deactivation but rather due to a contribution from less available active site of the Cu nanoparticles.

The observed decline of activity after the successive batches can be attributed to loss of available active Cu surface. Although the reactants, CO and H_2 can compete for available Cu active sites, the degassing of the gas after successive batches ensures less effect from CO poisoning from previous batches. Moreover, our observed reduction of surface area after the successive batches suggests that the number of Cu active sites for the reactions reduced. Considering that the methyl formate hydrogenolysis is an exothermic reaction [22], increase in temperature of the reaction at the Cu surface during hydrogenation occurs, which can lead to the agglomeration of the Cu nanoparticles with time. Cu crystallite sintering is known to be a common deactivating factor to Cu catalysts [23]. Cu surface energy is expected to be high with around 10 nm Cu particles without any support, such that reacting with each other to form bigger crystals is highly possible[24]. We suggest therefore that the starting 'Cu' catalyst is soft or porous but agglomerates over time which led to decrease in the number of Cu active site for MeOH synthesis.

3.3. Varying Cu catalyst particle sizes with temperature

The Cu catalyst preparation was varied to study the influence of temperature on crystallite size and subsequently on LTMS reactivity. Fig. 6a shows the X-ray diffractogram of the effect of temperature on Cu catalyst preparation (same as steps A and B in Fig. 1). Preparation

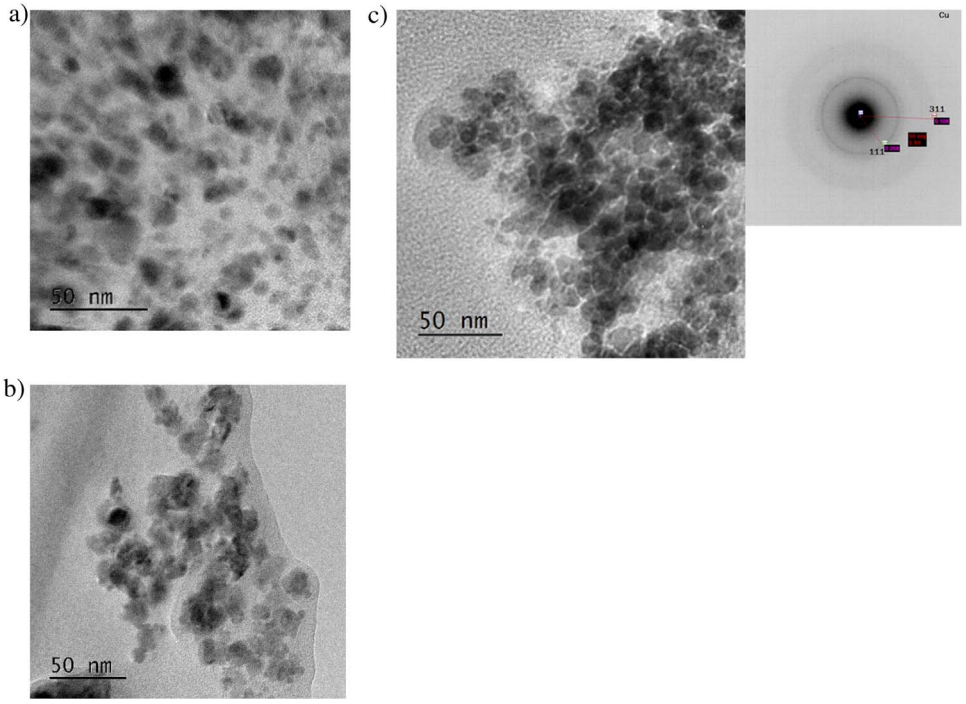

Fig. 3. Catalyst slurry TEM images of Cu nanoparticles for a typical 100 °C LTMS reaction shown in Fig. 1. a: TEM image after step A showing 10 ± 5 nm particle sizes. b: TEM image after step B showing 10 ± 5 nm particle sizes. c: TEM image after step C showing 10 ± 3 nm particle sizes.

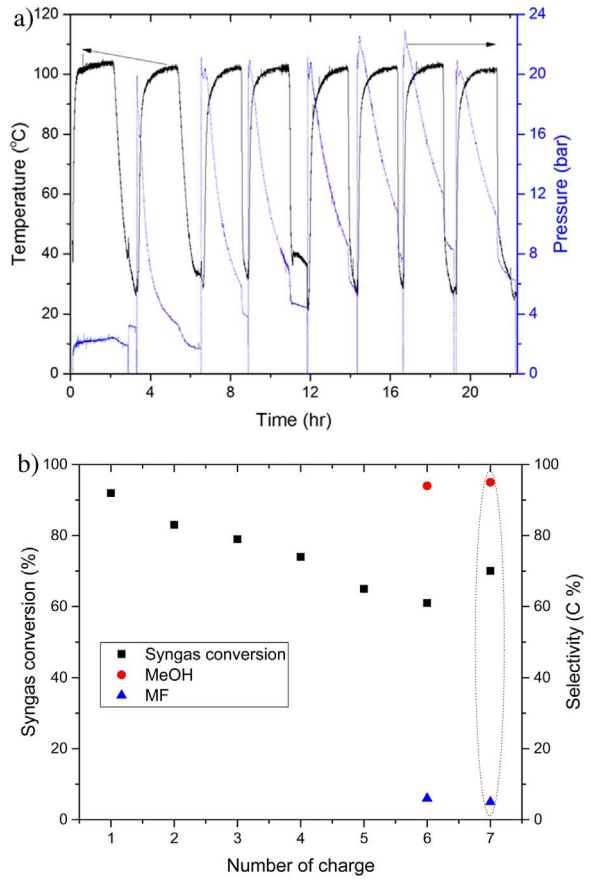

Fig. 4. Multiple charging of syngas, $Cu(OAc)_2$ = 5.0 mmol, NaH = 25 mmol, in 50 ml diglyme, MeOH = 73.0 mmol and $2H_2$:CO = 20 bar, at 100 °C. a: Temperature and pressure procedure of the multiple charging, cooling and degassing of syngas showing repeated charging over time. b: Syngas conversion and selectivity of the multiple charging of syngas reaction.

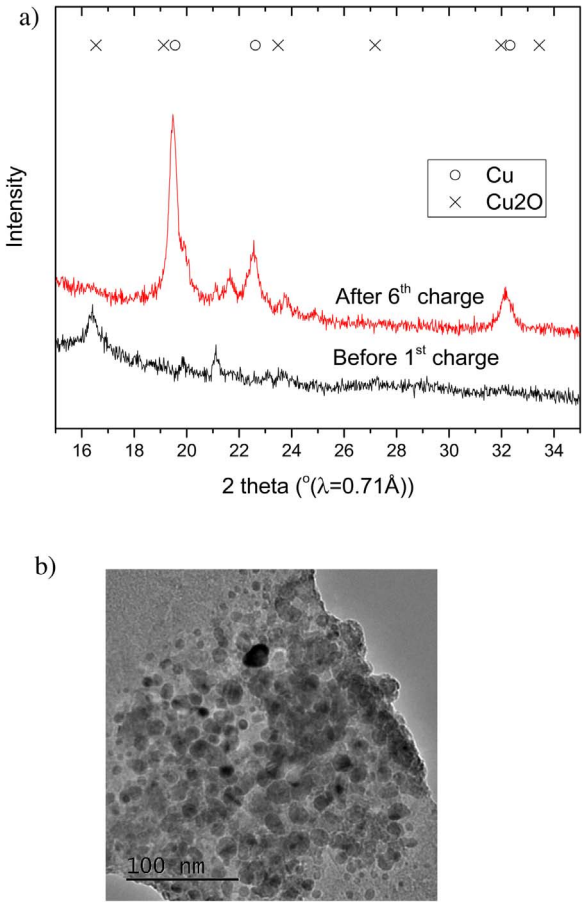

Fig. 5. X-ray diffraction and TEM image of spent Cu catalyst slurry (+ XRD of fresh). a: X-ray diffractogram of fresh (before 1st charge) and spent (after 6th charge) slurry of the LTMS reaction. b: TEM image after the 6th charge showing wide particle size distribution from 6 to 25 nm.

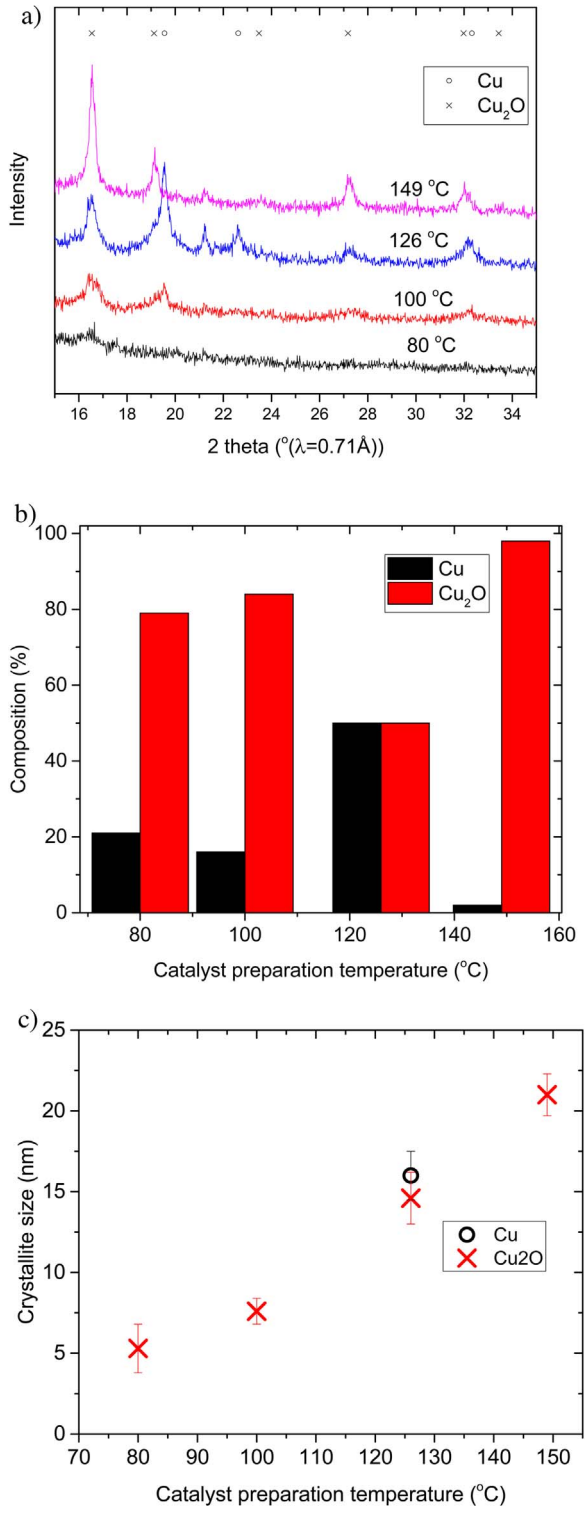

Fig. 6. X-ray diffractogram analysis of Cu crystallites before LTMS reaction. a: X-ray diffractogram of the slurry of the catalyst system. b: Rietveld analysis of the composition of Cu crystallites. c: Rietveld analysis of Cu crystallite sizes before LTMS reaction.

temperature was varied from 80 to 149 °C. Generally, the diffraction pattern showed that the intensity and sharpness of the peaks followed an increase in the temperature. The X ray shows densification of the Cu as temperature increased. This suggested that crystallization is enhanced by temperature.

The results of a Rietveld analysis of the diffraction patterns is shown in Fig. 6b and c for% composition of the Cu phases and their respective crystallite sizes. Increased fraction of Cu_2O and less of Cu^0 was

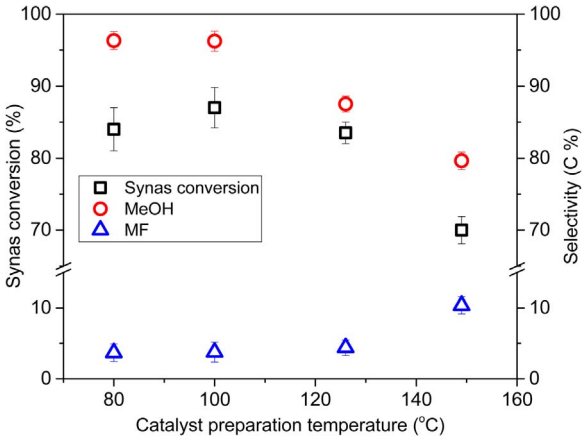

Fig. 7. Syngas conversion and selectivity verses catalyst preparation temperature; Cu $(OAc)_2$ = 3.6 mmol, NaH = 18 mmol in 50 ml diglyme, MeOH = 49 mmol, $2H_2$:1CO = 20 bar, at 100 °C.

observed, similar to the 100 °C catalyst system, except at 126 °C, which showed a composition of about 50/50 Cu_2O/Cu^0. This result indicated that reduction of the Cu takes place during catalyst preparation just as was discussed for catalyst preparation at 100 °C. The crystallite sizes were observed to exponentially increase with temperature, with the average size increasing from 5 ± 2 nm at 80 °C to 21 ± 1 nm at 149 °C. This is in agreement with theory [25] since particle nucleation exponentially depends on temperature.

The different nanoparticles were tested in the LTMS reaction at 100 °C similar to step C in Fig. 1. Fig. 7 shows conversion and selectivity versus catalyst system prepared at different temperatures. The syngas conversion was about 84, 89, 83, and 65% at 80, 100, 126, and 149 °C Cu catalyst systems respectively. Each test was done thrice and the average and standard deviations plotted. The selectivity to methanol was 96, 96, 88, and 80% at 80, 100, 126, and 149 °C catalyst systems respectively.

Syngas conversion and selectivity to MeOH were highest for the 80 and 100 °C catalyst systems. The Cu particles prepared under these temperatures resulted in producing Cu crystallites below 10 nm which the smallest compared to those which were prepared at higher temperatures. The syngas conversion for the 80 °C catalyst system was slightly lower than that of the 100 °C system. This could be due to less amount of Cu actually crystalizing out of solution at 80 °C within the reaction time considering the fact that temperature enhanced crystal growth, coupled with the observed very low intensity of the diffraction peaks in Fig. 6a. Though the 126 °C system produced about 83% syngas conversion, the 88% selectivity to MeOH was lower compared to that of 80 and 100 °C systems. Hence, the yield of MeOH generally decreased with increasing Cu crystallite size.

The reaction slurry was characterized by XRD and TEM at the end of the LTMS reaction. Fig. 8a shows the XRD diagrams of the spent slurry after the LTMS. The diffraction pattern shows predominantly the Cu^0 phase. Fig. 8b shows the results of the Rietveld analysis of the diffraction patterns shown in Fig. 8a as compared to the fresh crystallite sizes before the LTMS reaction. Generally, the average Cu crystallite sizes increased by about 2 nm for each catalyst system after the methanol synthesis.

The spent Cu catalyst was also studied by TEM imaging in order to compare Cu particle size distributions at the different preparation temperatures. Fig. 9 the TEM images of the Cu catalyst system prepared at varied temperatures. The Cu particle sizes were about 7 ± 4 nm for the 80 °C system. At 126 °C preparation, Cu particles sizes were about 18 ± 6 with some agglomerates up to 40 nm. The particles sizes were about 25 ± 6 and up to 50 nm agglomerates for the 149 °C system. The particles prepared at 100 °C were shown earlier to be about 10 ± 5 nm (Fig. 3c). Generally, the catalyst system prepared at 100 °C showed a

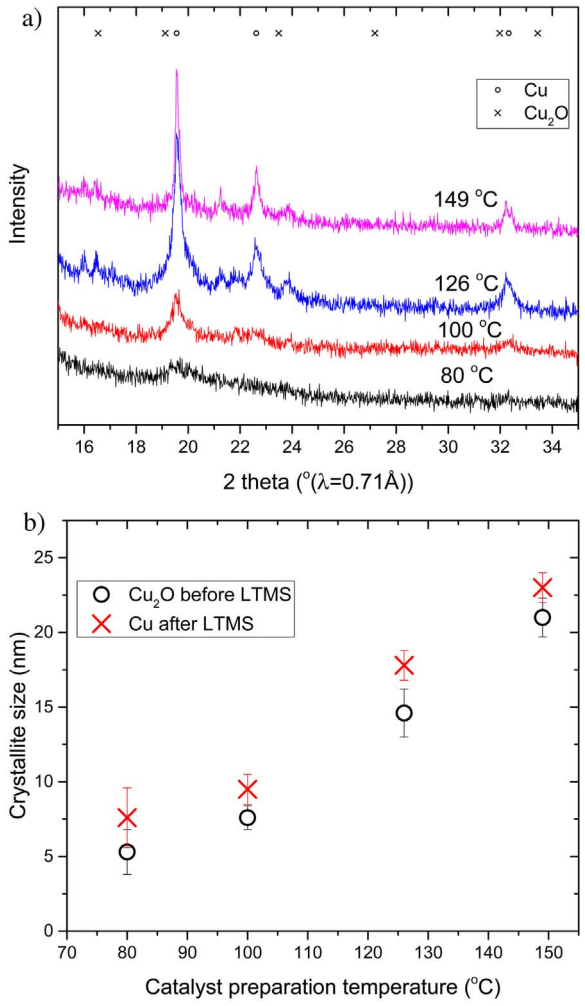

Fig. 8. X-ray diffractogram analysis of Cu crystallites after LTMS reaction. a: X-aray diffractogram of the slurry of the catalyst system. b: Rietveld analysis of Cu crystallite sizes.

much narrower particle distribution than the other systems. This could be due to the fact that both catalyst preparation and the LTMS reaction were done at the same temperature and therefore maintained a stable particle size as smaller particles often fuse together.

All in all, the particle sizes increased exponentially from about 3–50 nm agglomerates with increasing catalyst preparation temperature. This follows a similar pattern as was observed from the X-ray diffraction crystallite size estimations. In general, there are reports of strong correlation between particle size and the surface area [14,26]. Ohyama and Kishida [14] for example, reported an increase in surface area of CuO/CrO_3 due to milling, which enhanced activity of methanol production. The smaller the particle size, the more the available surface area is exposed per gram catalyst. Therefore if Cu is an active component, then methanol production increased with decreasing particle size. In our case, using traditional methods [27] to estimate Cu surface area would be challenging and not representative of the actual surface area as higher temperature than we operated is required. Nevertheless, the decrease in activity correlated well with densification of Cu nanoparticles.

4. Conclusion

We have used a once-through system for methanol synthesis at 100 °C. Hydride reduction of Cu^{2+} in diglyme at varied temperatures led to Cu^0 nanocrystals varying from 5 to 23 nm in size. Increasing temperature from 80 to 149 °C increased the crystallite sizes of the

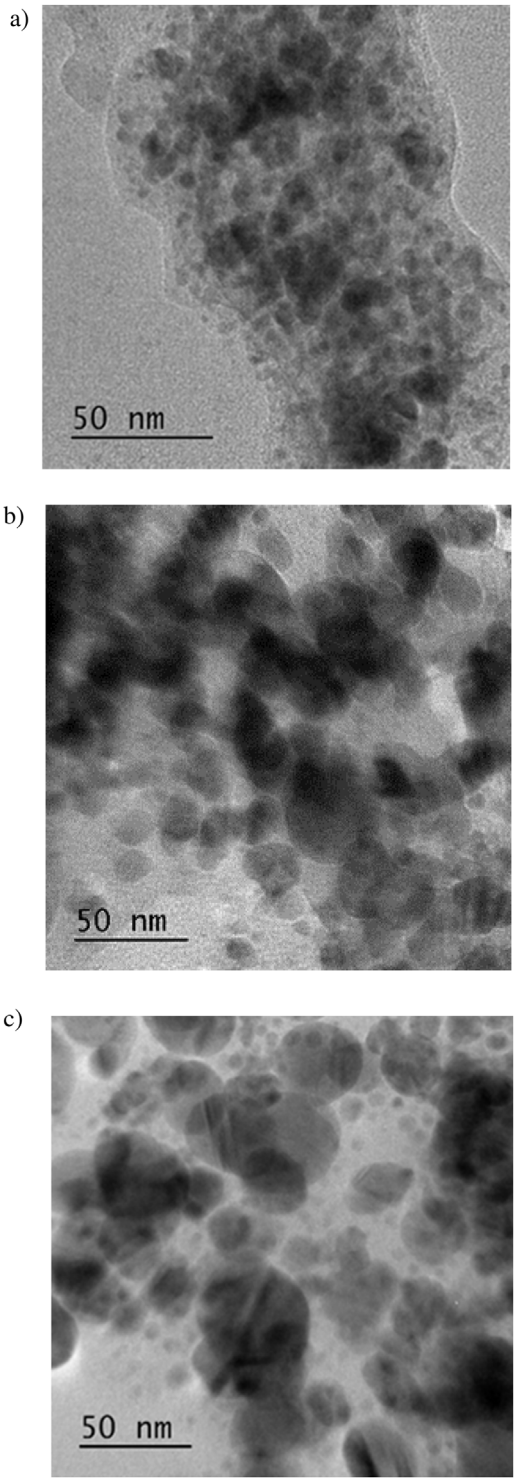

Fig. 9. Catalyst slurry TEM image of Cu catalyst prepared at varied temperatures after LTMS reaction. a: Catalyst system prepared at 80 °C showing 7 ± 4 nm particle sizes. b: Catalyst system prepared at 126 °C showing 18 ± 6 nm particle sizes. c: Catalyst system prepared at 149 °C showing 25 ± 6 nm particle sizes.

nanoparticles exponentially. Up to 92% conversion and 94% selectivity to methanol could be achieved at 100 °C and 20 bar syngas in liquid medium depending on Cu catalyst size. Generally, increasing particle size led to lower MeOH yield, and hence the smaller the nanoparticles the higher the methyl formate hydrogenolysis activity. The Cu nanoparticles densify over time during the catalytic process, which is proposed to be the major catalyst deactivation route.

Acknowledgements

This work is funded by the Research Council of Norway, NFR project number 228157/O70.

We acknowledge the use of RECX (the Norwegian national resource center for X-ray diffraction and scattering) and NorTEM (the Norwegian Center for Transmission Electron Microscopy) both in Oslo.

References

[1] G.A. Olah, Beyond oil and gas: the methanol economy, Angew. Chem. Int. Ed. 44 (2005) 2636–2639.
[2] U. Olsbye, S. Svelle, M. Bjørgen, P. Beato, T.V.W. Janssens, F. Joensen, S. Bordiga, K.P. Lillerud, Conversion of methanol to hydrocarbons: how zeolite cavity and pore size controls product selectivity, Angew. Chem. Int. Ed. 51 (2012) 5810–5831.
[3] K.A. Ali, A.Z. Abdullah, A.R. Mohamed, Recent development in catalytic technologies for methanol synthesis from renewable sources: a critical review, Renew. Sustain. Energy Rev. 44 (2015) 508–518.
[4] J.B. Hansen, P.E. Højlund Nielsen, Methanol synthesis, in: G. Ertl, H. Knozinger, F. Schuth, J. Weitkamp (Eds.), Handbook of Heterogeneous Catalysis, Wiley-VCH Verlag GmbH & Co KGaA, 2008, pp. 2920–2949.
[5] M. Marchionna, M. Di Girolamo, L. Tagliabue, M.J. Spangler, T.H. Fleisch, A review of low temperature methanol synthesis, in: D.S.F.F.A.V.A. Parmaliana, F. Arena (Eds.), Studies in Surface Science and Catalysis, Elsevier, 1998, pp. 539–544.
[6] J.A. Christiansen, Method of producing methyl alcohol, U.S. Patent 1,302,011, 1919.
[7] S.P. Tonner, D.L. Trimm, M.S. Wainwright, N.W. Cant, The base-catalysed carbonylation of higher alcohols, J. Mol. Catal. 18 (1983) 215–222.
[8] T. Turek, D.L. Trimm, N.W. Cant, The catalytic hydrogenolysis of esters to alcohols, Catal. Rev. 36 (1994) 645–683.
[9] S. Ohyama, Low-temperature methanol synthesis in catalytic systems composed of nickel compounds and alkali alkoxides in liquid phases, Appl. Catal. A: Gen. 180 (1999) 217–225.
[10] S. Ohyama, In situ FTIR study on reaction pathways in Ni(CO)4/CH3OK catalytic system for low-temperature methanol synthesis in a liquid medium, Appl. Catal. A: Gen. 220 (2001) 235–242.
[11] C. Voegtlin, Toxicity of Certain Heavy Metal Carbonyls, in: U.S.A.E. Commission (Ed.), University of Rochester, 1947.
[12] Z. Liu, J.W. Tierney, Y.T. Shah, I. Wender, Kinetics of two-step methanol synthesis in the slurry phase, Fuel Process. Technol. 18 (1988) 185–199.
[13] B. Li, K. Jens, Liquid-phase low-temperature and low-pressure methanol synthesis catalyzed by a raney copper-alkoxide system, Top. Catal. 56 (2013) 725–729.
[14] S. Ohyama, H. Kishida, Physical mixture of CuO and Cr2O3 as an active catalyst component for low-temperature methanol synthesis via methyl formate, Appl. Catal. A: Gen. 172 (1998) 241–247.
[15] S. Ohyama, H. Kishida, XRD, HRTEM and XAFS studies on structural transformation by milling in a mixture of CuO and Cr2O3 as an active catalyst component for low-temperature methanol synthesis, Appl. Catal. A: Gen. 184 (1999) 239–248.
[16] B. Li, K.-J. Jens, Low-temperature and low-pressure methanol synthesis in the liquid phase catalyzed by copper alkoxide systems, Ind. Eng. Chem. Res. 53 (2013) 1735–1740.
[17] https://www.bruker.com/products/x-ray-diffraction-and-elemental-analysis/x-ray-diffraction/xrd-software/topas/rietveld-analysis-software.html. (Date accessed: 28.10.2016).
[18] N.P. Fitzsimons, W. Jones, P.J. Herley, Studies of copper hydride. Part 1.-Synthesis and solid-state stability, J. Chem. Soc. Faraday Trans. 91 (1995) 713–718.
[19] T.H. Fleisch, R.L. Mieville, Studies on the chemical state of Cu during methanol synthesis, J. Catal. 90 (1984) 165–172.
[20] G.N. Glavee, K.J. Klabunde, C.M. Sorensen, G.C. Hadjipanayis, Borohydride reduction of nickel and copper ions in aqueous and nonaqueous media. controllable chemistry leading to nanoscale metal and metal boride particles, Langmuir 10 (1994) 4726–4730.
[21] R. Battino, T.R. Rettich, T. Tominaga, The solubility of oxygen and ozone in liquids, J. Phys. Chem. Ref. Data 12 (1983) 163–178.
[22] J.A. Christiansen, LIV.-The equilibrium between methyl formate and methyl alcohol, and some related equilibria, J. Chem. Soc. (Resumed) 129 (1926) 413–421.
[23] J.T. Sun, I.S. Metcalfe, M. Sahibzada, Deactivation of Cu/ZnO/Al2O3 methanol synthesis catalyst by sintering, Ind. Eng. Chem. Res. 38 (1999) 3868–3872.
[24] K.K. Nanda, A. Maisels, F.E. Kruis, H. Fissan, S. Stappert, Higher surface energy of free nanoparticles, Phys. Rev. Lett. 91 (2003) 106102.
[25] A.S. Myerson, R. Ginde, 2 − Crystals, Crystal Growth, and Nucleation, Handbook of Industrial Crystallization, Second edition, Butterworth-Heinemann, Woburn, 2002, pp. 33–65.
[26] K. Suttiponparnit, J. Jiang, M. Sahu, S. Suvachittanont, T. Charinpanitkul, P. Biswas, Role of surface area, primary particle size, and crystal phase on titanium dioxide nanoparticle dispersion properties, Nanoscale Res. Lett. 6 (2010) 1–8.
[27] J.R. Jensen, T. Johannessen, H. Livbjerg, An improved N2O-method for measuring Cu-dispersion, Appl. Catal. A: Gen. 266 (2004) 117–122.

Paper 2

The role of solvent Polarity on Low-Temperature Methanol Synthesis Catalyzed by Cu Nanoparticles

Ahoba-Sam C., Olsbye U., Jens K-J.

Frontiers in Energy Research, 2017, 5, 15(1-11),
doi.org/10.3389/fenrg.2017.00015

frontiers in Energy Research

ORIGINAL RESEARCH
published: 14 July 2017
doi: 10.3389/fenrg.2017.00015

The Role of Solvent Polarity on Low-Temperature Methanol Synthesis Catalyzed by Cu Nanoparticles

*Christian Ahoba-Sam[1], Unni Olsbye[2] and Klaus-Joachim Jens[1]**

[1] Department of Process, Energy and Environmental Technology, University College of Southeast Norway, Porsgrunn, Norway, [2] Department of Chemistry, University of Oslo, Oslo, Norway

Methanol syntheses at low temperature in a liquid medium present an opportunity for full syngas conversion per pass. The aim of this work was to study the role of solvents polarity on low-temperature methanol synthesis reaction using eight different aprotic polar solvents. A "once through" catalytic system, which is composed of Cu nanoparticles and sodium methoxide, was used for methanol synthesis at 100°C and 20 bar syngas pressure. Solvent polarity rather than the 7–10 nm Cu (and 30 nm Cu on SiO_2) catalyst used dictated trend of syngas conversion. Diglyme with a dielectric constant (ε) = 7.2 gave the highest syngas conversion among the eight different solvents used. Methanol formation decreased with either increasing or decreasing solvent ε value of diglyme (ε = 7.2). To probe the observed trend, possible side reactions of methyl formate (MF), the main intermediate in the process, were studied. MF was observed to undergo two main reactions; (i) decarbonylation to form CO and MeOH and (ii) a nucleophilic substitution to form dimethyl ether and sodium formate. Decreasing polarity favored the decarbonylation side reaction while increasing polarity favored the nucleophilic substitution reaction. In conclusion, our results show that moderate polarity solvents, e.g., diglyme, favor MF hydrogenolysis and, hence, methanol formation, by retarding the other two possible side reactions.

Keywords: methanol synthesis, low temperature, solvent polarity, "once through" reaction, Cu, nanoparticle size, syngas conversion

OPEN ACCESS

Edited by:
Peter Styring, University of Sheffield, United Kingdom

Reviewed by:
Antoine Buchard, University of Bath, United Kingdom
Peter P. Edwards, University of Oxford, United Kingdom
Joan Ramón Morante, Institut de Recerca de l'Energia de Catalunya, Spain

***Correspondence:**
Klaus-Joachim Jens
Klaus.J.Jens@usn.no

Specialty section:
This article was submitted to Carbon Capture, Storage, and Utilization, a section of the journal Frontiers in Energy Research

Received: *31 January 2017*
Accepted: *19 June 2017*
Published: *14 July 2017*

Citation:
Ahoba-Sam C, Olsbye U and Jens K-J (2017) The Role of Solvent Polarity on Low-Temperature Methanol Synthesis Catalyzed by Cu Nanoparticles. Front. Energy Res. 5:15. doi: 10.3389/fenrg.2017.00015

INTRODUCTION

Methanol (MeOH) is a multipurpose molecule, which has a high potential as a C_1 building block for both energy and CO_2 storage (Olah, 2005). It stores both carbon and hydrogen in liquid form at ambient temperature and is readily transportable as it is liquid at ambient temperature. Methanol can be directly converted to valuable hydrocarbons, such as light olefins and gasoline, over acidic microporous materials (Olsbye et al., 2012), thereby providing an alternative to the main fossil energy sources and petrochemical feedstocks used today.

The current technology for MeOH synthesis is based on conversion of syngas (made up of $CO/CO_2/H_2$) over a $Cu/ZnO/Al_2O_3$ catalyst, operating around 250°C and 100 bar (Hansen and Højlund Nielsen, 2008; Ali et al., 2015). Although this technology is highly optimized including recycling of unreacted syngas, its thermodynamic restriction limits syngas conversion per pass coupled with

operating conditions, such as temperature and pressure, to make the process capital intensive. Since syngas conversion to methanol is an exothermic reaction (Eq. 1), lower temperature is required to achieve full conversion per pass. Moreover, syngas production accounts for more than half of the total capital cost in current methanol processes (Marchionna et al., 1998). The lowest cost of syngas production is by the use of air rather than pure O_2-blown autothermal reformer (Hansen and Højlund Nielsen, 2008). Full conversion per pass will allow the use of N_2 diluted syngas for methanol production since recycling will not be necessary. Hence, there is a need for the development of a low-temperature approach to MeOH synthesis.

$$CO + 2H_2 \rightleftharpoons CH_3OH\ \Delta H = -90.6\,kJ/mol \quad (1)$$

A low-temperature methanol synthesis (LTMS) reaction presents the possibility for full syngas conversion per pass around 100–120°C at relatively low pressure, for example below 50 bar (Christiansen, 1919). The LTMS reaction is known to occur in two major steps shown in Eqs 2 and 3. CO carbonylation of MeOH to methyl formate (MF) is catalyzed by alkali metal alkoxide (Eq. 2) (Christiansen, 1919; Tonner et al., 1983); hydrogenolysis of MF to MeOH, which is usually the rate-limiting step, is catalyzed by transition metal-based compounds (Turek et al., 1994; Ohyama, 1999).

$$CO + CH_3OH \rightleftharpoons HCOOCH_3 \quad (2)$$

$$HCOOCH_3 + 2H_2 \rightleftharpoons 2CH_3OH \quad (3)$$

Several different Cu-based catalysts have been reported to be active for LTMS reaction between 80 and 120°C. Examples of Cu-based materials reported for the hydrogenolysis reaction include CuO/Cr_2O_3, Raney Cu, Cu on SiO_2, $CuCl_2$, and Cu alkoxide (Ohyama and Kishida, 1998; Xing-Quan et al., 1999a; Li and Jens, 2013a,b). Prolonged milling of a physical mixture of CuO and Cr_2O_3, for example, correlated well with the surface area of Cu, which enhanced methanol synthesis activity (Ohyama and Kishida, 1998, 1999). Hence, the particle size of Cu plays an important role in the LTMS reaction, such that syngas conversion increases with decreasing Cu particle sizes.

The LTMS reaction is normally conducted in a "once through" approach, where the two steps are performed simultaneously. A kinetic study by Liu et al. (1988) has shown that when the two steps are performed together, the rate of MeOH formation is higher than when the two steps are separated. The reaction rates of MeOH carbonylation and its reverse rates were observed to occur at about five orders of magnitude faster than the rate of MF hydrogenolysis. A synergistic relationship between the two steps has been proposed (Li and Jens, 2013b) but the actual relationship involved is yet to be understood.

Traditionally, the LTMS reaction is performed in liquid phase in a solvent. The liquid solvent plays an important role as MeOH synthesis is exothermic and the solvent can help to dissipate excess heat generated during the process. However, aside energy dissipation, could there be other roles for the solvent to play? While most attention has been on finding the right LTMS catalyst system, little attention has been placed on the influence of solvent on the LTMS process. Quan et al. (Xing-Quan et al., 1999b) reported on the influence of solvent polarity in a Cu–Cl and Cu–Cr catalyzed LTMS reaction. They observed that as solvent polarity increased MeOH formation decreased; however, an adequate explanation was not given.

We focus on a Cu nanoparticle/alkoxide catalyst system for the LTMS reaction (Li and Jens, 2013a,b). We have recently reported that Cu nanoparticles are responsible for MeOH synthesis, including that particle aggregation led to decrease in activity. Furthermore, when Cu nanoparticles size were varied from 7 ± 2 to 21 ± 1 nm, MeOH yield were observed to decrease linearly with Cu nanoparticles sizes (Ahoba-Sam et al., 2017). In this work, we will revisit the effect of solvent on the reaction. Particularly, we have studied the influence of solvent polarity in a "once through" MeOH reaction as well as the effect on MF intermediate side reactions. Furthermore, the influence of the solvent on Cu nanoparticle synthesis will be discussed. To the best of our knowledge, this influence of solvents with different hydrocarbon chain length and polarity on Cu nanoparticles size has not been reported. In order to eliminate any influence of the different Cu particles sizes on the effect of solvent polarity, a heterogeneous Cu/SiO_2 catalyst containing 30 nm Cu nanoparticles was used as a reference.

MATERIALS AND METHODS

Materials and Experimental Setup

Copper (II) acetate ($Cu[OAc]_2$, 98%), dry sodium hydride (NaH = 95%), methanol (MeOH, anhydrous 99.8%), MF (99%), sodium methoxide ($NaOCH_3$, 95%), $Cu(NO_3)_2{\cdot}3H_2O$, Ludox HS-40 colloidal silica (40 wt% SiO_2 dispersed in water), L-ascorbic acid, and the various solvents used in this work, listed in **Table 1**, were all purchased from Sigma Aldrich. The syngas contained 1CO: $2H_2$ (± 2%) and was purchased from Yara Praxair AS. All chemicals were used as received unless otherwise stated.

Methanol synthesis and some of the catalyst components were prepared in a 200 ml (60 mm diameter) stainless steel high pressure type hpm-020 autoclave batch reactor (Premex Reactor AG). The reactor was equipped with a dip tube for sampling, a pressure sensor, and a thermocouple inserted into the reactor to measure internal pressure and temperature, respectively. A Nupro security valve attached to the reactor was set at 100 bar for safety. A magnetic stirrer head was attached to a stirrer equipped with oblique impeller blades (approximately 30° angle) and reaching near to the bottom of the reactor for adequate mixing. The magnetic stirrer head was externally attached to an electric BCH Servo Motor paired with a lexium 23 drive to give up to 3,000 rpm, with a high degree of precision. The reactor was heated in an oil block controlled by a Huber Ministat 230 thermostat. The internal temperature and pressure in the reactor was independently logged by a PC.

"Once Through" System

Generally, about 3.6 mmol of $Cu(OAc)_2$,18 mmol of dry NaH, and 50 ml solvent were placed in the reactor. This was set under 1 bar N_2 blanket and the mixture stirred at 3,000 rpm and heated to 100°C for 2 h. The resulting reaction mixture was cooled to ambient temperature (<30°C). After degassing the gaseous phase,

TABLE 1 | List of Solvents used and their properties, adopted from CRC (2003–2004) and Wohlfarth (2008) (ε = dielectric constant).

Solvent	Short form	Formula	ε	Boiling point/°C	% Purity
Methylbenzene	Toluene	C_7H_8	2.33	110.6	≥99.5
Diethyl ether	DEE	$C_4H_{10}O$	4.19	35	≥99.9
1-Methoxy-2-(2-methoxyethoxy)ethane	Diglyme	$C_6H_{14}O_3$	7.23	162	≥99.5
Tetrahydrofuran	THF	C_4H_8O	7.36	66	≥99.9
1,2-Dimethoxyethane	Glyme	$C_4H_{10}O_2$	7.55	84.5	99.5
2,5,8,11,14-Pentaoxapentadecane	Tetraglyme	$C_{10}H_{22}O_5$	7.79	275	>99
Acetonitrile	MeCN	C_2H_3N	35.87	82	99.8
Dimethyl sulfoxide	DMSO	C_2H_6OS	47.13	189	≥99

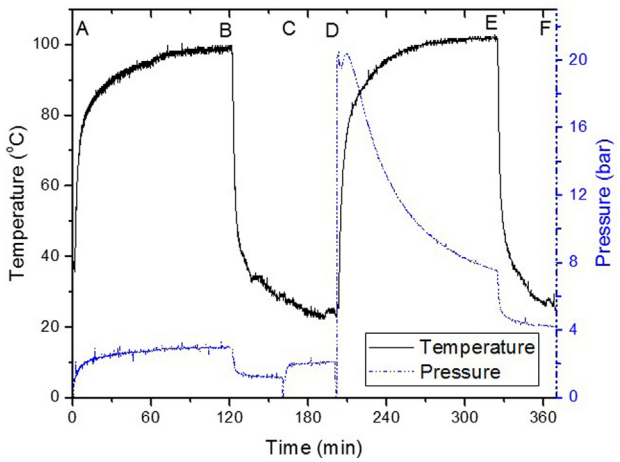

FIGURE 1 | Typical "once through" low-temperature methanol synthesis reaction, (A) 3.6 mmol $Cu(OAc)_2$ + 18 mmol NaH in solvent, (B) rapid cooling in 50 ml solvent, (C) addition of 52 mmol MeOH, (D) 20 bar $CO/2H_2$ charging, (E) rapid cooling, (F) sampled for further analysis.

52 mmol MeOH was added and stirred at ambient temperature for 30 min to ensure that all NaH had reacted to sodium methoxide co-catalyst.

The reactor was purged with syngas and charged to about 20 bar, then stirred at 3,000 rmp and heated to 100°C. After 2 h, the reactor was cooled to about 25°C. Syngas conversion was determined by the difference in pressure between the start of reaction and after reactor cooling to room temperature (~25°C) at the end of reaction (**Figure 1**). The reactor was then degassed, and the liquid portion analyzed. Typically, the amount of carbon products in liquid reaction mixture after cooling as compared to the syngas pressure drop represented about 85% of the syngas consumed, assuming $CO/2H_2$ were proportionally consumed.

The liquid portion of the sample as well as the gas phase were analyzed by a gas chromatograph equipped with both liquid and gas injection valves (Agilent 7890 A). The liquid injection port was connected to a CARBOWAX 007 series 20 M column with dimensions 60 m × 320 μm × 1.2 μm and was programmed as follows; the temperature was ramped at 15°C/min from 40°C initial temperature to 250°C and held at 250°C for 3 min, at 0.47 bar (6.8 psi) constant pressure. The liquid sample was injected *via* an Agilent 7683B autosampler. The products were identified and quantified by an Agilent 5975 mass spectrometer detector (MSD). 0.54 mg heptane was added to each sample vial as internal standard. The gas injection valve was connected to 2.7 m Porapak Q and 1.8 m Molecular Sieve 5 Å packed columns connected to a thermal conductivity detector for analysis of permanent gases including up to C_2 hydrocarbons. This set-up was connected to a 0.9 m Hayesep Q back flush column.

CuO/SiO_2 Catalyst Preparation

CuO/SiO_2 catalyst was prepared by similar steps as reported in Huang et al. (2008) and Xiong et al. (2011) albeit with some modifications. 100 ml of 0.5 M $Cu(NO_3)_2{\cdot}3H_2O$ was prepared in a three-necked round bottomed flask. 100 ml of 1 M L-ascorbic acid was added dropwise while stirring. 49 g of 40 wt% SiO_2 dispersed in water was added to the mixture. This was stirred at 100°C for 3 h. The cooled resulting mixture was then centrifuged and washed three times with distilled water and dried at 70°C in an oven. The dried particles were then calcined at 550°C for 3 h. The calcined CuO/SiO_2 catalyst was used for LTMS reaction in a similar way as was done for the "once through" experiment.

MF Side Reaction Study

11 mmol sodium methoxide dissolved in 97 mmol methanol and 33 mmol MF were added to 20 ml of each solvent. The mixture was stirred under 1 bar N_2 and heated to 100°C for 1 h. The cooled resulting liquid mixture was analyzed using Perkin-Elmer Spectrum One FT-IR spectrometer and Agilent GC.

Catalyst Characterization

The Cu and CuO/SiO_2 catalysts were analyzed by XRD and TEM. A Bruker D8 A25 powder diffractometer using Mo Kα radiation with a wavelength, λ = 0.71076 Å and a Lynxeye detector with "hardened" chip for Mo radiation was used. Total Pattern Analysis Solution (TOPAS) software was employed for quantitative Rietveld analysis of the diffractogram. This software operates by fitting theoretical diffraction pattern to a measured diffraction pattern using non-linear least square algorithms. The samples were analyzed as slurry which was pipetted into a capillary tube with 0.5 mm internal diameter. The tube was centrifuged at 2,000 rmp for 10 min to settle the solid portion at the bottom. The capillary was mounted on the capillary spinner such that the X-ray beam measured around the capillary bottom where the particles were concentrated. The X-ray diffractogram was determined at 0.023° step/s for an interval of 15–35° 2 theta.

The TEM imaging was performed with a Joel 2100F instrument. Samples were diluted in methanol, and particles were dispersed in an ultrasound bath for 30 min. The solution was then deposited onto a carbon film on a copper grid. Cu particles were ascertained to be present using EDS and electron diffraction. Generally, particle size distributions were determined by measuring the diameters of the TEM images as the particles sizes using MATLAB assuming that the Cu particles were circular droplets. Typically, an average of 30-particle diameters ± SD from the TEM images for each sample was used for particle size determination.

RESULTS AND DISCUSSION

Typical "Once Through" LTMS

Figure 1 shows the steps involved in the LTMS reaction using diglyme as solvent. Typically, Cu nanoparticles were made by hydride reduction of Cu^{2+} ($Cu(AOc)_2$) in steps A and B with NaH at 100°C (Glavee et al., 1994). Addition of MeOH at step C led to the formation of $NaOCH_3$ (sodium methoxide) and $H_{2\,(g)}$ which resulted in an increase in pressure. Syngas was added at step D, where after an induction period due to increase in temperature, pressure declined rapidly with time. After 2 h (E), the reaction was stopped by cooling to about 25°C at F. We deliberately stopped the reaction after 2 h and so the activity of the catalyst was not optimized for determining TOF or TON. Moreover, our batch reactor system did not allow for time on steam analysis of individual products except the changes in pressure and temperature, which were continuously monitored during the reaction. The pressure drop represented 89% syngas conversion. The liquid products composition after 2 h showed 96 and 4% C selectivity to MeOH and MF, respectively.

The slurry was further analyzed by XRD to determine oxidation state and crystallite size of the Cu catalyst involved in the LTMS reaction. **Figure 2** shows the X-ray diffractogram of the slurry at steps B, C and E as illustrated in **Figure 1**. The XRD samples were taken right after steps B, C, and D were completed, respectively. The diffractogram after step B showed mainly Cu_2O and NaH phases, while that after step C showed Cu_2O and Cu^0 phases [X-ray powder diffraction files referenced from Neuburger (1930), Wyckoff (1963), Smura et al. (2011)]. The diffractogram after E showed predominantly Cu^0 oxidation state.

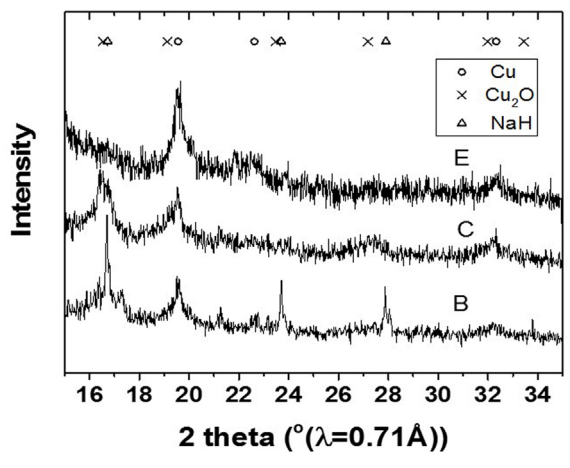

FIGURE 2 | X-ray diffractogram of the slurry after the steps B, C, and D in **Figure 1.**

This indicated that reduction of the Cu^{2+} precursor took place during the process by hydride reduction during step B. Moreover, all NaH was reacted upon the addition of methanol since no NaH pattern was observed in the diffraction at step C. The steps C to D resulted in the pressure rise illustrated in **Figure 1**, as H_2 was released in the process. Furthermore, the LTMS reaction under highly reducing environment of CO and H_2 led to Cu^0 oxidation state at E. The average Cu crystallite sizes were estimated by Reitveldt analysis. The slurry at step C was composed of about 50/50% Cu^0/Cu_2O with average crystallite sizes of about 7.5 ± 0.7 nm. After the LTMS reaction, the Cu^0 crystallite sizes at step E was 9.5 ± 0.9 nm. This showed about 2 nm increase in the average crystallite size of the Cu after methanol synthesis occurred. **Figure 3** shows TEM image of the Cu particles. The Cu particle size was about 10 ± 3 nm. Electron diffraction also confirmed [111] and [311] Cu^0 planes present.

Solvent Variation in "Once Through" Synthesis

As indicated in **Table 1**, different aprotic solvents were employed to study the influence of solvent polarity on the LTMS reaction. Aprotic solvents were used because of the presence of NaH, which can react easily with protons. Moreover, the $NaOCH_3$ co-catalyst may be consumed in the presence of protic solvent. Five out of the chosen solvents were ethers with different chain lengths and polarity.

Figure 4 shows the activity of the catalyst system in the "once through" reaction plotted versus dielectric constant (ε) of the solvents. 51% syngas conversion was observed when diethyl ether (DEE) was used as solvent with the least ε = 4.19. In diglyme with ε = 7.23, 89% syngas conversion was observed. Then after, syngas conversion decreased to 85, 80, and 74% in tetrahydrofuran (THF), glyme, and tetraglyme, respectively, following the order of slight decreasing in ε. Thereafter, syngas conversion sharply declined to 30 and 14% in acetonitrile (MeCN) (ε = 36) and dimethyl sulfoxide (DMSO) (ε = 47), respectively. Despite the more noticeable changes in the syngas conversion in the various solvents, selectivity to MeOH was always >90% indicating that selectivity was barely affected by the solvents' dielectric constant or polarity.

The chosen ether solvents differ in polarity (represented by their ε), boiling point, and chain length (or molar mass) which is shown in **Table 1** [from CRC (2003–2004), Wohlfarth (2008)]. The dielectric constant is known to be proportional to the solvents polarity (Rabaron et al., 1993). Among these properties, the observed syngas conversion pattern followed the ε of the solvents with the optimum around ε = 7.2 for diglyme. Notably, slight differences in the ε with regards to diglyme, THF, glyme, and tetraglyme depicting the slight differences in their polarity, such that syngas conversion followed the order

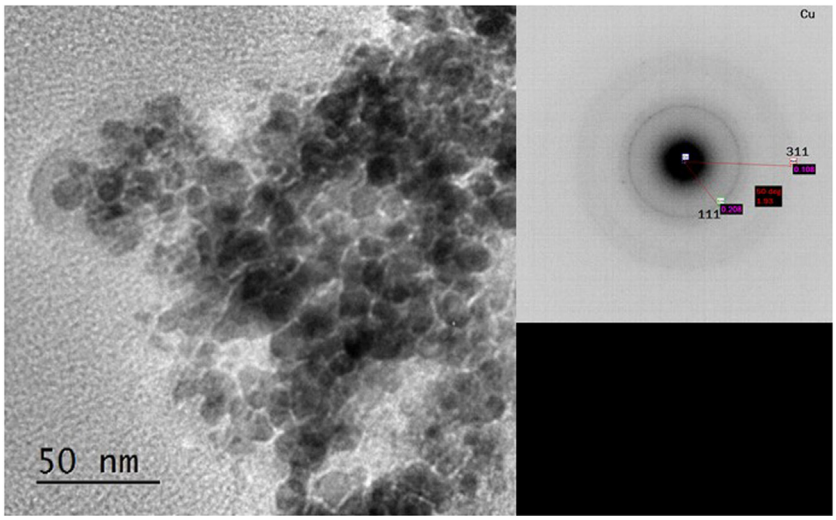

FIGURE 3 | TEM image and electron diffraction of Cu from step F with 10 ± 2 nm particles sizes and [111] and [311] Cu^0 planes.

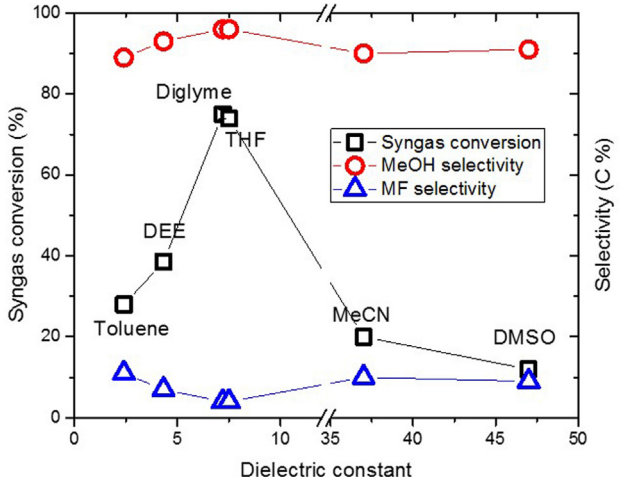

FIGURE 4 | Syngas conversion and selectivity versus dielectric constant of solvent in the "once through" Cu nanoparticles catalyzed reaction.

diglyme > THF > glyme > tetraglyme. On the other hand, the order of increasing solvent chain length as well as boiling point is THF < glyme < dilgyme < tetraglyme. Clearly, the syngas conversion did neither follow solvent's chain length nor their boiling point, but preferred less polar solvents among these ether solvents.

The solvent polarity range was extended beyond the ethers, such as MeCN and DMSO with $\varepsilon = 36$ and 47, respectively. These two, which are more polar than diglyme showed a very sharp decline in syngas conversion. Solvents with higher polarity than that of diglyme led to even lower MeOH formation. On the contrary, DEE with lower ε ($\varepsilon = 4.2$) than diglyme also showed lower syngas conversion, suggesting that lower polar solvents than diglyme may also lead to lower amount MeOH formation in LTMS reactions. This, therefore, suggest that solvent polarity plays an important role in the "once through" LTMS reaction such that solvents with similar polarity with diglyme showed higher MeOH formation.

Solvent Effect on Cu Nanoparticles in the "Once Through" Reaction

Copper nanoparticles were synthesized as described in Section "Typical "Once Through" Low Temperature Methanol Synthesis" for the "once through" catalyst. However, since different solvents were involved, there is a possibility that nucleation and crystallite growth of Cu nanoparticles will differ in the different reaction media. It is also important to note that Cu nanoparticles size plays an important role in MF hydrogenolysis (Ohyama and Kishida, 1998). This section, therefore, focuses on the effect of the different chosen solvents on Cu nanoparticles size.

Figure 5 shows the slurry X-ray diffractogram of the different solvents after LTMS reaction. Generally, a Cu^0 phase was predominately observed but with varying reflex intensity. The broadness of the reflexes confirm formation of nanoparticles in all employed solvents. **Figure 6** shows the Cu nanoparticle TEM images of the different solvents. **Figure 7** shows a summary of **Figures 5** and **6** in relation to the ε value of the solvents. Generally, the Cu crystallites and particles sizes in each particular solvent were about the same, considering the fact that the XRD measures the bulk average while the TEM images only show a few particles. On average, Cu particles in all ether solvents were within 9–10 nm, while in MeCN and DMSO solvents approximately 7 nm particle size was observed.

Cu particles sizes do not seem to have been influenced by the different ether solvents. Considering that, the ethers have different chain lengths as well as different amounts of oxygen per mole capable of forming chelates around a Cu atom, one could expect the particle size to vary with chain length. However, this was not observed which could be due to the fact that, the excess amount

of solvents used might have provided enough oxygen for dative bonding if chelate formation was necessary in tuning the particles sizes.

Cu nanoparticles sizes prepared in the non-ether solvents were smaller as compared to those made in ether solvents. DMSO with higher polarity ($\varepsilon = 47$) showed smaller Cu particles sizes than was observed for MeCN ($\varepsilon = 36$). The difference of the ether solvents ε values were relatively small ($\varepsilon = 4.2–7.8$) as compared to DMSO and MeCN. There is a possibility that the polarity difference in the solvents played a subtle role in the formation of Cu nanoparticles size, particularly when the polarity difference is larger. It has been reported that nucleation slows down with solvents polarity (Zhao et al., 2004; Wei et al., 2008). The consequence of slower rate of nucleation is that, larger crystals may be formed if longer growth time (>24 h) is allowed. However, we observed the opposite, which might be due to an inadequate aging time of 2 h in our system.

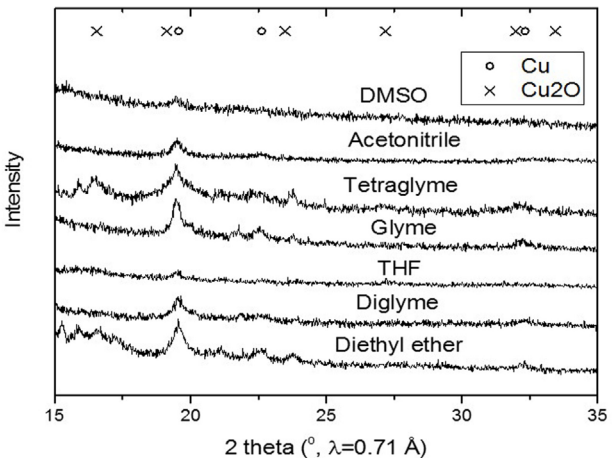

FIGURE 5 | X-ray diffractogram of the slurry after low-temperature methanol synthesis reaction for the different polar solvents.

The use of solvents with higher polarity in the LTMS reaction, despite generating smaller Cu nanoparticles, led to the least amount of MeOH formation. However, it is expected that the smaller the Cu nanoparticles the faster the hydrogenolysis of MF which is usually the limiting step in the LTMS reaction. Smaller Cu nanoparticles should, therefore, lead to higher MeOH formation. This on the contrary was not the case when solvents polarity was varied, suggesting that the solvent polarity was the bottleneck in our case rather than just the Cu particles sizes.

Solvent Variation using CuO/SiO_2 Catalyst

In Sections "Solvent Variation in "Once Through" Synthesis" and "Solvent Effect on Cu Nanoparticles in the "Once Through" Reaction," the lowest methanol formation was observed in the more polar solvents despite the fact that the smallest Cu nanoparticles were made in these solvents. The two main components that varied before LTMS reaction were the type of solvent used and slight changes in Cu NP sizes. A dry CuO/SiO_2 catalyst with larger particle size as compared to the 7–10 nm Cu NP slurry used above was prepared and used for the LTMS reaction as a control. This will help to differentiate between the influence of Cu nanoparticles size as against that of the solvents, as solvent polarity will be varied but with the same CuO/SiO_2 catalyst size.

Figure 8 shows the XRD diffractogram of the calcined CuO/SiO_2 catalyst. Crystalline CuO and amorphous SiO_2 were

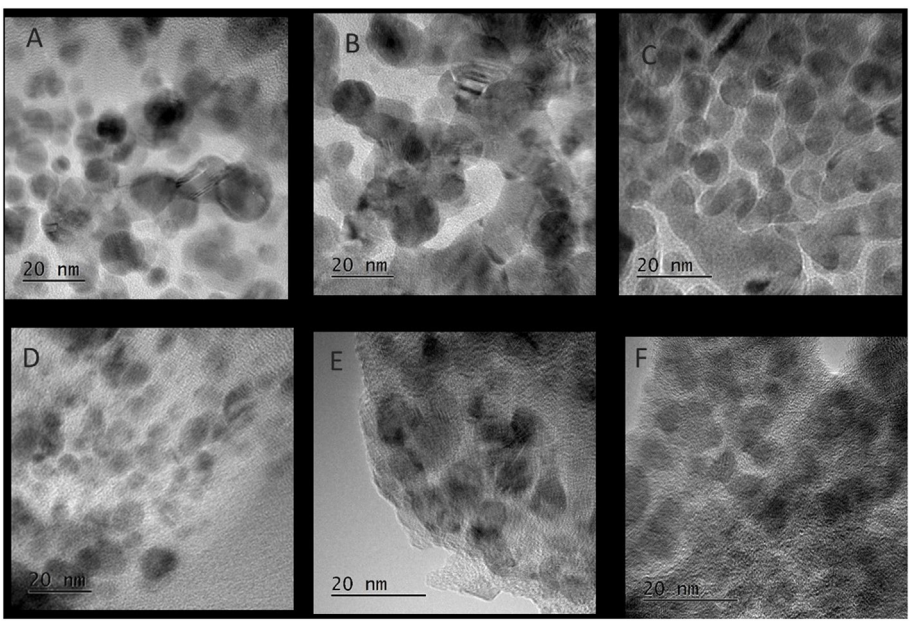

FIGURE 6 | TEM images of Cu nanoparticles after low-temperature methanol synthesis reaction in the different solvents, **(A)** diethyl ether, **(B)** glyme, **(C)** tetraglyme, **(D)** tetrahydrofuran, **(E)** acetonitrile, **(F)** dimethyl sulfoxide.

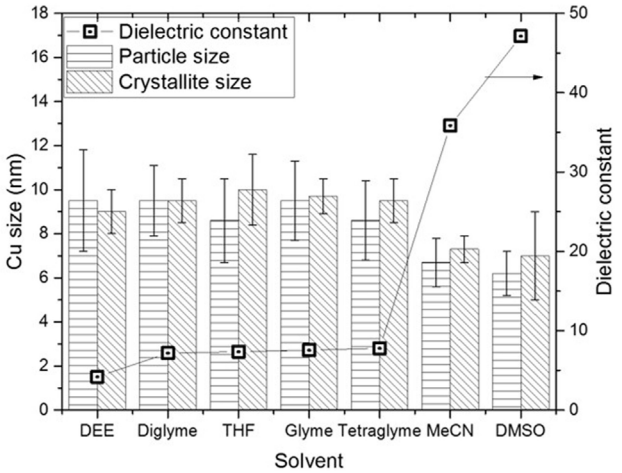

FIGURE 7 | Comparison of the Cu particles sizes and dielectric constants in the different solvents after low-temperature methanol synthesis reaction.

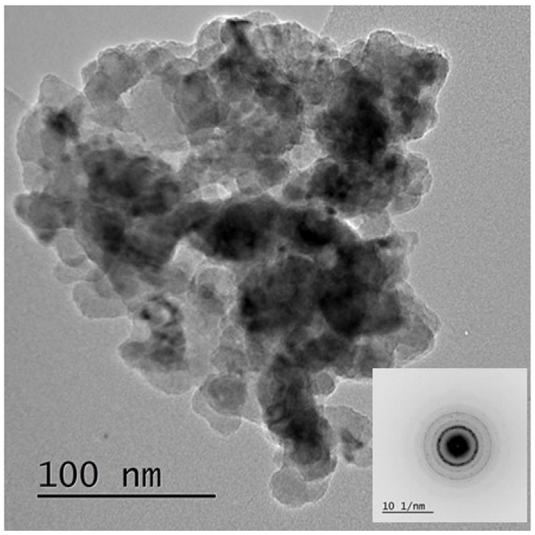

FIGURE 9 | TEM image and an inserted electron diffraction of the calcined CuO/SiO_2 catalyst.

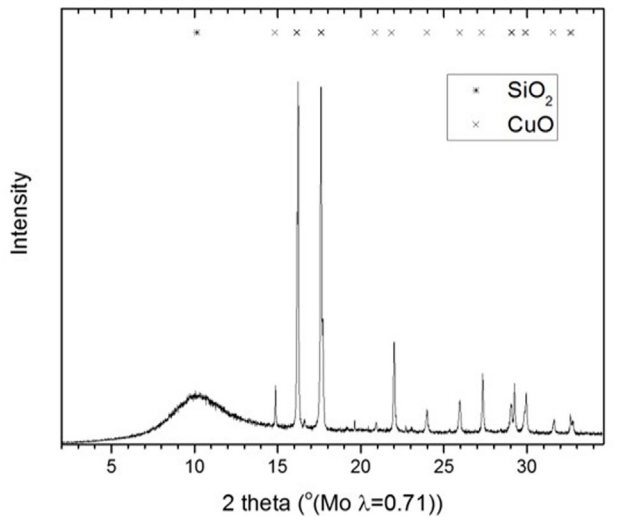

FIGURE 8 | X-ray diffractogram of calcined CuO/SiO_2 catalyst.

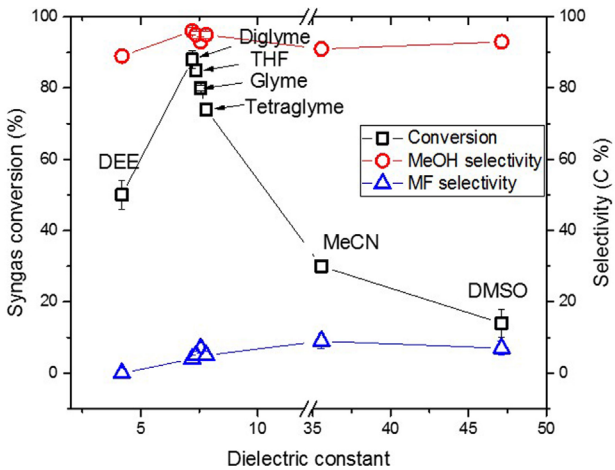

FIGURE 10 | Syngas conversion and selectivity versus dielectric constant of solvent in the CuO/SiO_2 catalyzed reaction.

observed [powder diffraction files referenced from Barth (1932), Tunell et al. (1935)]. The line broadening analysis indicated that, the CuO crystallite size was 30 ± 5 nm. **Figure 9** shows the TEM image and an inserted electron diffraction diagram of the CuO/SiO_2 catalyst. The TEM showed a good dispersion of the crystalline CuO on the SiO_2 support. The electron diffraction showed mainly [110], [002], [11-2], and [112] planes of CuO.

The CuO/SiO_2 catalyst was used for methanol synthesis, in a similar way to Section "Typical "Once Through" Low Temperature Methanol Synthesis," except that, the very first step for making Cu nanoparticles (**Figures 1A,B**) was omitted since the synthesized CuO/SiO_2 catalyst was used. **Figure 10** shows catalyst activity versus ε value for solvents of various polarity. Syngas conversion increased from 28 and 39%, respectively, in toluene and DEE, to 76% in diglyme but slightly decreased to 74% in THF and then sharply to 20 and 12% in MeCN and DMSO, respectively. Despite the large differences in syngas conversion, selectivity to methanol remained ≥90% and MF ≤10% in the different solvent.

Generally, syngas conversions were higher in the "once through" system for the Cu nanoparticles slurry as compared to the CuO/SiO_2 catalyst system. This is not surprising since the Cu catalysts involved in the two scenarios were different in support material and particles sizes. The CuO in the CuO/SiO_2 catalyst was about 30 nm compared with the ≤10 nm Cu particles made in the "once through" system. Moreover, our earlier report showed that within 7–21 nm sizes, methanol formation decreased with Cu particle size (Ahoba-Sam et al., 2017). Therefore, the observed

lower syngas conversion can be related to the larger Cu particle size. Despite this, selectivity to MeOH and MF as well as the trend in syngas conversion followed the same path as was observed in the **Figure 4** for the "once through" system. A similar trend has been reported for a CuO/Cr_2O_3 system with varying solvent polarity (Xing-Quan et al., 1999b). Therefore, solvent polarity plays an important role in LTMS reaction, such that solvents with ε values around 7.2 appear to give improved MeOH synthesis results.

The observed effect of solvent polarity on the LTMS reaction needs an explanation. What is the exact role of polarity in the LTMS reaction? Syngas is known to be less soluble in polar solvent compared to apolar solvents (Vogelpohl et al., 2014). This is so because strong interaction exists between polar molecules, which makes it difficult for relatively non-polar H_2 and CO to enter. However, while solubility cannot be totally ruled out in gas–liquid systems, the solubility explanation may only hold for solvents with ε values >7. Syngas conversion decreased with decreasing solvents' polarity in ε = 4.2 and 2.3 in DEE and toluene systems, respectively. Our recent results showed that increasing Cu nanoparticles sizes from 7 to 21 nm led to decrease in both conversion and selectivity to MeOH in diglyme. This coupled with similar trends observed for the different Cu sources suggests that hydrogenation was not the main step responsible for the above observation. The Section "Influence of Solvent Polarity on Side Reactions of the LTMS Reaction,"therefore, seeks to address the possible side reactions, which could limit the LTMS reaction in the different solvents.

Influence of Solvent Polarity on Side Reactions of the LTMS Reaction

The LTMS reaction involves two major steps, carbonylation and hydrogenolysis of MF (illustrated in Eqs 2 and 3, respectively). However, the main intermediate product, MF can also undergo possible side reactions as shown in Eqs 4 and 5. It has been reported that the formation of MF from MeOH and CO (Eq. 2) is highly reversible (Christiansen, 1926; Liu et al., 1988). Moreover, it has also been observed that MF can react with $NaOCH_3$, to form dimethyl ether (DME) and NaOOCH (sodium formate) (Christiansen, 1926; Jogunola et al., 2012). Therefore, during the LTMS reaction, if MF hydrogenolysis is not fast enough, MF can either decarboxylate back to CO and MeOH and/or react with $NaOCH_3$ to give DME and NaOOCH.

$$CH_3OOCH \rightleftharpoons CO + CH_3OH \quad (4)$$

$$CH_3OOCH + NaOCH_3 \rightleftharpoons CH_3OCH_3 + NaOOCH \quad (5)$$

The influence of solvents' polarity on the possible side reactions involved in the LTMS reaction was then studied. This was done by heating MF in the presence of $NaOCH_3$ in a predetermined solvent under 1 bar N_2 gas. The IR spectrum of the resulting liquid mixture is shown in **Figure 11**. The gray lines in **Figure 11** (B–G) represent the pure solvent while the black lines represent the reaction mixture. These were compared with MeOH, MF, and NaOOCH shown in **Figure 11**A. Typically, bands observed at 2,830, 2,770, 1,650, 1,570, 1,360, and 770 cm^{-1} were not observed in pure solvent or in methanol and MF. These bands were typical NaOOCH bands when compared with standard spectra from NIST data base (Stein, 2016). The NaOOCH bands appeared in all the spectra of the different solvents, which indicated that formate was formed in all the different solvents.

Table 2 shows the rise in pressure and relative amount of CO released for the different solvents tested. Although DME and methanol were present in the gas phase, it was difficult to separate them on the Porapak Q column as their peaks superimposed on each other leading to a shoulder peak. Therefore, only N_2 and CO, which were well separated on the mol sieve column, were quantified for this analysis. The CO equivalence in these chromatograms should be regarded as a relative measure to N_2 and not as an absolute measure. The amount of CO released generally decreased with increasing solvent polarity.

The amount of MF drastically decreased from 33 mmol initial amount to less than 4 mmol in the side reaction test for all solvents. Trace amounts of DME were observed in the liquid sample analysis (using the MSD) of all solvents. MF was, therefore, involved for all solvents in the two reactions; (i) decarbonylation into CO and MeOH and (ii) nucleophilic substitution to form DME and NaOOCH, as illustrated in Eqs 4 and 5. Although DME and NaOOCH were observed, we were not able to quantify them. However, assuming that decarbonylation and nucleophilic substitution are the main MF side reactions occurring and considering the high MF reactivity in the solvent tests, the relative amount of CO released in these reactions can be used to determine which of the two pathways is predominant for the different solvents.

The released CO amount decreased with increasing polarity of the solvent. This suggested that decarboxylation was enhanced in less polar solvents. The decreasing amount of CO released with increased solvent polarity suggested that the nucleophilic substitution pathway is enhanced with increased solvent polarity which appears logical since this reaction pathway involves ionic salt formation which is expected to be stabilized by polar rather than non-polar solvents (Parker, 1969).

Maximum syngas conversion was observed for a solvent ε value around 7.2 (see Solvent Variation in "Once Through" Synthesis and Solvent Variation using CuO/SiO_2 Catalyst). Considering the nucleophilic substitution pathway to be favored by polar solvents and the decarbonylation pathway to be favored by low polarity solvents, a relatively moderate polar solvent is a good compromise to supress unwanted side reactions, maximizing the MF hydrogenolysis pathway. The above results indicate that the different MF reaction pathways in the LTMS reaction, i.e., hydrogenolysis, decarboxylation, and nucleophilic substitution, may have comparable activation barriers. Changing the polarity might influence the path which intermediates are better favored by the polarity of the solvent. Hence, MF is a transient intermediate, which will always be present at relatively low concentration in the reaction mixture.

NaOOCH formation is detrimental to the overall catalytic cycle because $NaOCH_3$, the co-catalyst, is consumed by this reaction. Previously, we observed Cu catalyst agglomeration to be a major source of LTMS reaction deactivation as Cu particles growth corresponded to a lower activity. Our current study indicates that the nucleophilic substitution side reaction is also

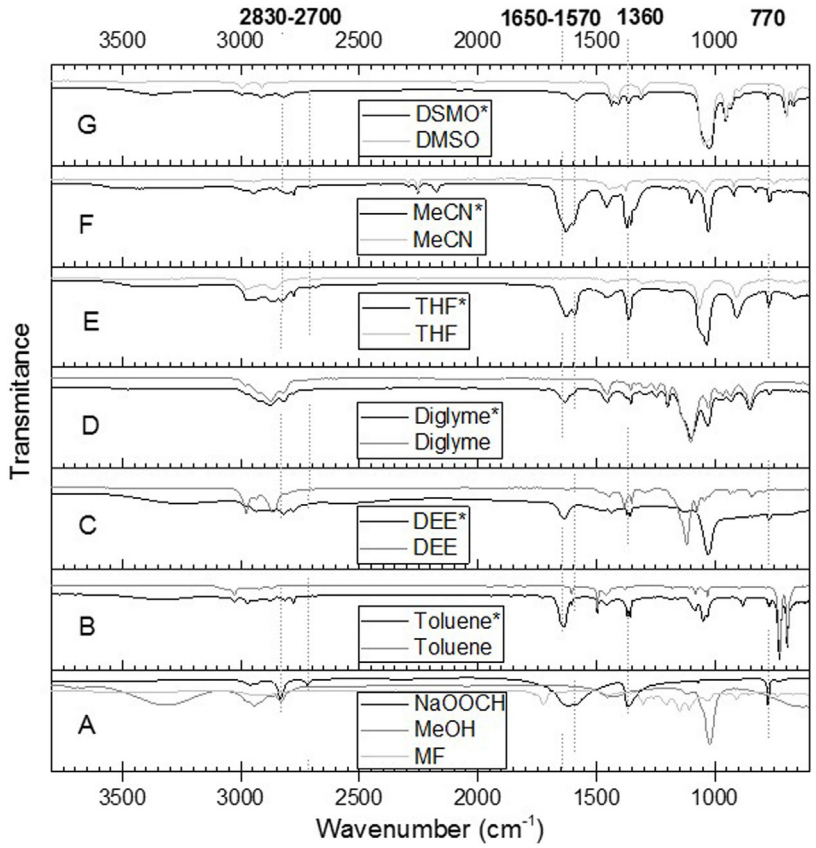

FIGURE 11 | ATR-IR spectra of solvent (B–G in gray), and reaction mixture (B–G, black with *). The spectra A is for MeOH, methyl formate, and NaOOCH. The NaOOCH (in black) was adopted from NIST data base (Stein, 2016).

TABLE 2 | Solvent effect on side reaction, CO equivalent = CO/(CO + N_2) × Pressure rise, CO and N_2 was determined from gas analysis while the MF was determined from liquid analysis.

Solvent	Pressure rise/ bar	CO equivalent/ bar	MF remaining/ mmol
Toluene	3.00	1.91	3.43
Diethyl ether	2.94	1.66	2.12
Diglyme	2.46	1.23	1.77
Tetrahydrofuran	1.95	0.90	2.33
Acetonitrile	1.23	0.59	1.00
Dimethyl sulfoxide	0.82	0.32	0.41

a potential source of LTMS reaction deactivation which will increase in importance especially in more polar solvents.

CONCLUSION

The liquid-phase LTMS reaction is influenced by solvent polarity. Solvents with moderate polarity similar to diglyme with $\varepsilon = 7.2$ give highest syngas conversion among eight different selected solvents covering a wide range of polarity. MeOH formation increased with increasing ε value until that of diglyme (7.2) and decreased thereafter with further increase of the ε value. This trend was independent of Cu catalyst nanoparticle size. Our results indicated that MF, the main intermediate LTMS reaction product undergoes two side reactions (i) decarbonylation to form CO and MeOH and (ii) a nucleophilic substitution reaction to form DME and sodium formate. Solvent polarity distinguishes between these side reactions such that decarbonylation is favored as solvent polarity decreases while nucleophilic substitution is favored as solvent polarity increases. Our results show that moderate polarity solvents, e.g., diglyme favor MF hydrogenolysis by retarding the other two possible side reactions.

Safety Warning

Large amount of compressed CO and H_2 gas were used, with potential poisoning and flammable hazards, respectively, and hence, the appropriate equipment and detectors must be used to avoid unwanted releases. The solvents used especially diglyme and glyme are toxic and must be handled with care.

AUTHOR CONTRIBUTIONS

CA-S was involved in conception and design of experiment, acquisition of data, and analysis and interpretation of data for this work. He drafted the work, approved the final version of the work to be submitted and agreed to be accountable for all aspects of the work in ensuring that questions related to accuracy or integrity of

any part of the work are appropriately investigated and solved. UO was involved in conception of experiment and interpretation of data for this work. She approved the final version of the work to be submitted and agreed to be accountable for all aspects of the work in ensuring that questions related to accuracy or integrity of any part of the work are appropriately investigated and solved. K-JJ was involved in conception and design of experiment and analysis and interpretation of data for this work. He was involved in revising the draft of the work and approved the final version of the work to be submitted and agreed to be accountable for all aspects of the work in ensuring that questions related to accuracy or integrity of any part of the work are appropriately investigated and solved.

ACKNOWLEDGMENTS

This work is funded by the Research Council of Norway, NFR project number 228157/O70. The authors acknowledge the use of RECX (the Norwegian national resource center for X-ray diffraction and scattering) and NorTEM (the Norwegian Center for Transmission Electron Microscopy) both in Oslo.

REFERENCES

Ahoba-Sam, C., Olsbye, U., and Jens, K.-J. (2017). Low temperature methanol synthesis catalyzed by copper nanoparticles. *Catal. Today.* doi:10.1016/j.cattod.2017.06.038

Ali, K. A., Abdullah, A. Z., and Mohamed, A. R. (2015). Recent development in catalytic technologies for methanol synthesis from renewable sources: a critical review. *Renew. Sustain. Energ. Rev.* 44, 508–518. doi:10.1016/j.rser.2015.01.010

Barth, T. F. W. (1932). The cristobalite structures. I. High-cristobalite. *Am. J. Sci.* 23, 350–356. doi:10.2475/ajs.s5-23.136.350

Christiansen, J. A. (1919). *Method of Producing Methyl Alcohol*. U.S. Patent 1,302,011.

Christiansen, J. A. (1926). LIV.-The equilibrium between methyl formate and methyl alcohol, and some related equilibria. *J. Chem. Soc.* 129, 413–421. doi:10.1039/JR9262900413

CRC. (2003–2004). "Physical constants of organic compounds," in *CRC Handbook of Chemistry and Physics*, 84th edn, ed. D. R. Lide (Boca Raton, FL: CRC Press), 3p, 4–547. Available at: http://www.znu.ac.ir/data/members/rasoulifard_mohammad/crc.pdf

Glavee, G. N., Klabunde, K. J., Sorensen, C. M., and Hadjipanayis, G. C. (1994). Borohydride reduction of nickel and copper ions in aqueous and nonaqueous media. Controllable chemistry leading to nanoscale metal and metal boride particles. *Langmuir* 10, 4726–4730. doi:10.1021/la00024a055

Hansen, J. B., and Højlund Nielsen, P. E. (2008). "Methanol synthesis," in *Handbook of Heterogeneous Catalysis*, eds G. Ertl, H. Knozinger, F. Schuth, and J. Weitkamp (Wiley-VCH Verlag GmbH & Co. KGaA, Haldor Topsoe: Kgs. Lyngby), 2920–2949.

Huang, Z., Cui, F., Kang, H., Chen, J., Zhang, X., and Xia, C. (2008). Highly dispersed silica-supported copper nanoparticles prepared by precipitation−gel method: a simple but efficient and stable catalyst for glycerol hydrogenolysis. *Chem. Mater.* 20, 5090–5099. doi:10.1021/cm8006233

Jogunola, O., Salmi, T., Kangas, M., and Mikkola, J. P. (2012). Determination of the kinetics and mechanism of methyl formate synthesis in the presence of a homogeneous catalyst. *Chem. Eng. J.* 203, 469–479. doi:10.1016/j.cej.2012.06.085

Li, B., and Jens, K.-J. (2013a). Liquid-phase low-temperature and low-pressure methanol synthesis catalyzed by a Raney copper-alkoxide system. *Top. Catal.* 56, 725–729. doi:10.1007/s11244-013-0031-4

Li, B., and Jens, K.-J. (2013b). Low-temperature and low-pressure methanol synthesis in the liquid phase catalyzed by copper alkoxide systems. *Ind. Eng. Chem. Res.* 53, 1735–1740. doi:10.1021/ie401966w

Liu, Z., Tierney, J. W., Shah, Y. T., and Wender, I. (1988). Kinetics of two-step methanol synthesis in the slurry phase. *Fuel Process. Technol.* 18, 185–199. doi:10.1016/0378-3820(88)90095-1

Marchionna, M., Di Girolamo, M., Tagliabue, L., Spangler, M. J., and Fleisch, T. H. (1998). "A review of low temperature methanol synthesis," in *Studies in Surface Science and Catalysis*, eds A. Parmaliana and F. Arena (Amsterdam: Elsevier), 539–544.

Neuburger, M. C. (1930). Praezisionsmessung der Gitterkonstante von Cuprooxyd Cu2O. *Zeitschrift fuer Physik* 67, 845–850. doi:10.1007/BF01390765

Ohyama, S. (1999). Low-temperature methanol synthesis in catalytic systems composed of nickel compounds and alkali alkoxides in liquid phases. *Appl. Catal. A Gen.* 180, 217–225. doi:10.1016/S0926-860X(98)00338-X

Ohyama, S., and Kishida, H. (1998). Physical mixture of CuO and Cr2O3 as an active catalyst component for low-temperature methanol synthesis via methyl formate. *Appl. Catal. A Gen.* 172, 241–247. doi:10.1016/S0926-860X(98)00135-5

Ohyama, S., and Kishida, H. (1999). XRD, HRTEM and XAFS studies on structural transformation by milling in a mixture of CuO and Cr2O3 as an active catalyst component for low-temperature methanol synthesis. *Appl. Catal. A Gen.* 184, 239–248. doi:10.1016/S0926-860X(99)00111-8

Olah, G. A. (2005). Beyond oil and gas: the methanol economy. *Angew. Chem. Int. Ed.* 44, 2636–2639. doi:10.1002/anie.200462121

Olsbye, U., Svelle, S., Bjørgen, M., Beato, P., Janssens, T. V. W., Joensen, F., et al. (2012). Conversion of methanol to hydrocarbons: how zeolite cavity and pore size controls product selectivity. *Angew. Chem. Int. Ed.* 51, 5810–5831. doi:10.1002/anie.201103657

Parker, A. J. (1969). Protic-dipolar aprotic solvent effects on rates of bimolecular reactions. *Chem. Rev.* 69, 1–32. doi:10.1021/cr60257a001

Rabaron, A., Cavé, G., Puisieux, F., and Seiller, M. (1993). Physical methods for measurement of the HLB of ether and ester non-ionic surface-active agents: H-NMR and dielectric constant. *Int. J. Pharm.* 99, 29–36. doi:10.1016/0378-5173(93)90319-B

Smura, C. F., Parker, D. R., Zbiri, M., Johnson, M. R., Gál, Z. A., and Clarke, S. J. (2011). High-spin cobalt(II) ions in square planar coordination: structures and magnetism of the oxysulfides Sr2CoO2Cu2S2 and Ba2CoO2Cu2S2 and their solid solution. *J. Am. Chem. Soc.* 133, 2691–2705. doi:10.1021/ja109553u

Stein, S. E. (2016). "Infrared spectra by NIST mass spec data center," in *NIST Chemistry WebBook, NIST Standard Reference Database Number 69*, eds P. J. Linstrom and W. G. Mallard (Gaithersburg, MD: National Institute of Standards and Technology), 20899. Available at: http://webbook.nist.gov

Tonner, S. P., Trimm, D. L., Wainwright, M. S., and Cant, N. W. (1983). The base-catalysed carbonylation of higher alcohols. *J. Mol. Catal.* 18, 215–222. doi:10.1016/0304-5102(83)80122-9

Tunell, G., Posnjak, E., and Ksanda, C. J. (1935). Geometrical and optical properties, and crystal structure of tenorite. *Zeitschrift fuer Kristallographie, Kristallgeometrie, Kristallphysik, Kristallchemie* 90, 120–142.

Turek, T., Trimm, D. L., and Cant, N. W. (1994). The catalytic hydrogenolysis of esters to alcohols. *Catal. Rev.* 36, 645–683. doi:10.1080/01614949408013931

Vogelpohl, C., Brandenbusch, C., and Sadowski, G. (2014). High-pressure gas solubility in multicomponent solvent systems for hydroformylation. Part II: syngas solubility. *J. Supercrit. Fluids* 88, 74–84. doi:10.1016/j.supflu.2014.01.017

Wei, X., Xu, G., Ren, Z., Shen, G., and Han, G. (2008). Room-temperature synthesis of BaTiO3 nanoparticles in large batches. *J. Am. Ceram. Soc.* 91, 3774–3780. doi:10.1111/j.1551-2916.2008.02695.x

Wohlfarth, C. (2008). "Static dielectric constants of pure liquids and binary liquid mixtures," in *Supplement to IV/6*, ed. M. D. Lechner (Berlin, Heidelberg: Springer).

Wyckoff, R. W. G. (1963). *New York Rocksalt Structure*. New York: Interscience Publishers.

Xing-Quan, L., Yu-Tang, W., Shi-Zhong, L., Zing-Chun, Y., Zhao-Xia, L., Shun-Fen, L., et al. (1999a). Concurrent synthesis of methanol and methyl formate catalysed by copper-based catalysts I. Influences of temperature and pressure. *J. Nat. Gas Chem.* 8, 115–200.

Xing-Quan, L., Yu-Tang, W., Shi-Zhong, L., Zing-Chun, Y., Zhao-Xia, L., Shun-Fen, L., et al. (1999b). Concurrent synthesis of methanol and methyl formate catalysed by copper-based catalysts II. Influences of solvents and H2/CO mole ratios. *J. Nat. Gas Chem.* 8, 203–210.

Xiong, J., Wang, Y., Xue, Q., and Wu, X. (2011). Synthesis of highly stable dispersions of nanosized copper particles using L-ascorbic acid. *Green Chem.* 13, 900–904. doi:10.1039/c0gc00772b

Zhao, X. B., Ji, X. H., Zhang, Y. H., and Lu, B. H. (2004). Effect of solvent on the microstructures of nanostructured Bi2Te3 prepared by solvothermal synthesis. *J. Alloys Comp.* 368, 349–352. doi:10.1016/j.jallcom.2003.08.070

Conflict of Interest Statement: The authors declare that the research was conducted in the absence of any commercial or financial relationships that could be construed as a potential conflict of interest.

frontiers in Energy Research

CORRECTION
published: 09 April 2018
doi: 10.3389/fenrg.2018.00024

Corrigendum: The Role of Solvent Polarity on Low-Temperature Methanol Synthesis Catalyzed by Cu Nanoparticles

Christian Ahoba-Sam[1], *Unni Olsbye*[2] *and Klaus-Joachim Jens*[1]*

[1] Department of Process, Energy and Environmental Technology, University College of Southeast Norway, Porsgrunn, Norway, [2] Department of Chemistry, University of Oslo, Oslo, Norway

Keywords: methanol synthesis, low temperature, solvent polarity, "once through" reaction, Cu, nanoparticle size, syngas conversion

OPEN ACCESS

Edited and reviewed by:
Peter Styring,
University of Sheffield,
United Kingdom

***Correspondence:**
Klaus-Joachim Jens
klaus.j.jens@usn.no

Specialty section:
This article was submitted to Carbon Capture, Storage, and Utilization, a section of the journal Frontiers in Energy Research

Received: *22 January 2018*
Accepted: *20 March 2018*
Published: *09 April 2018*

Citation:
Ahoba-Sam C, Olsbye U and Jens K-J (2018) Corrigendum: The Role of Solvent Polarity on Low-Temperature Methanol Synthesis Catalyzed by Cu Nanoparticles. Front. Energy Res. 6:24. doi: 10.3389/fenrg.2018.00024

A corrigendum on

The Role of Solvent Polarity on Low-Temperature Methanol Synthesis Catalyzed by Cu Nanoparticles

by Ahoba-Sam, C., Olsbye, U., and Jens, K.-J. (2017). Front. Energy Res. 5:15. doi: 10.3389/fenrg.2017.00015

In the original article, there was an interchange of the dataset in the graphs of **Figures 4**, **10** as published. The correct graph for the dataset appears below. The authors apologize for this error and state that this does not change the scientific conclusions of the article in any way.

The original article has been updated.

Conflict of Interest Statement: The authors declare that the research was conducted in the absence of any commercial or financial relationships that could be construed as a potential conflict of interest.

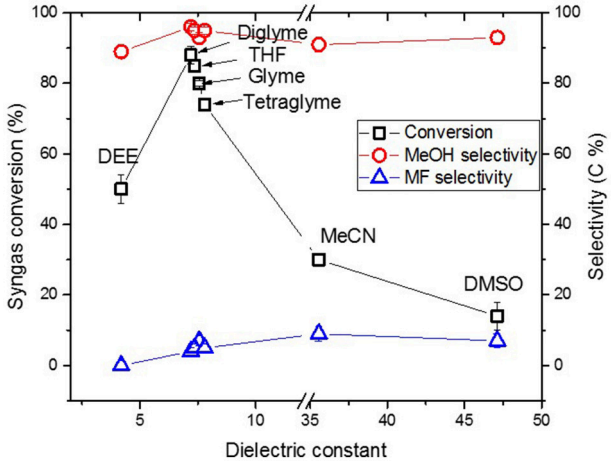

FIGURE 4 | Syngas conversion and selectivity versus dielectric constant of solvent in the "once through" Cu nanoparticles catalyzed reaction.

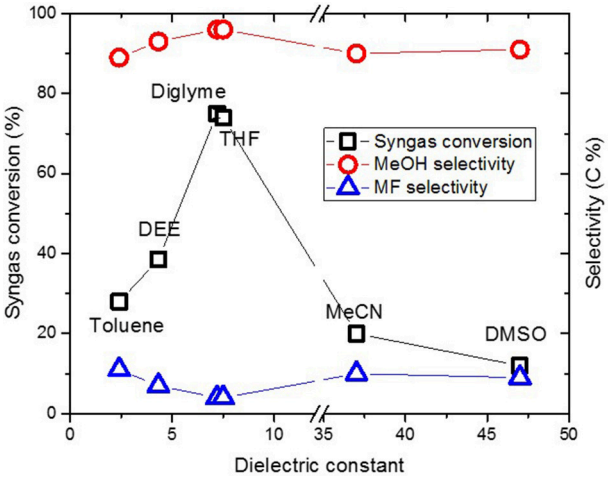

FIGURE 10 | Syngas conversion and selectivity versus dielectric constant of solvent in the CuO/SiO_2 catalyzed reaction.

Paper 3

Tailoring Cu nanoparticles catalyst for methanol synthesis using the spinning disk reactor

Ahoba-Sam C., Boodhoo K.V.K, Olsbye U., Jens K-J.

Materials, 2018, 11, 154 (1-12), DOI: 10.3390/ma11010154

materials

MDPI

Article

Tailoring Cu Nanoparticle Catalyst for Methanol Synthesis Using the Spinning Disk Reactor

Christian Ahoba-Sam [1], Kamelia V. K. Boodhoo [2], Unni Olsbye [3] and Klaus-Joachim Jens [1,*]

[1] Department of Process, Energy and Environmental Technology, University College of Southeast Norway, Kjølnes Ring 56, 3918 Porsgrunn, Norway; christian.ahoba-sam@usn.no

[2] School of Engineering, Merz Court, Newcastle University, Newcastle Upon Tyne NE1 7RU, UK; kamelia.boodhoo@newcastle.ac.uk

[3] Department of Chemistry, University of Oslo, P.O. Box 1033, Blindern, N-0315 Oslo, Norway; unni.olsbye@kjemi.uio.no

* Correspondence: Klaus.J.Jens@usn.no; Tel.: +47-3557-5193

Received: 22 December 2017; Accepted: 15 January 2018; Published: 17 January 2018

Abstract: Cu nanoparticles are known to be very active for methanol (MeOH) synthesis at relatively low temperatures, such that smaller particle sizes yield better MeOH productivity. We aimed to control Cu nanoparticle (NP) size and size distribution for catalysing MeOH synthesis, by using the spinning disk reactor. The spinning disk reactor (SDR), which operates based on shear effect and plug flow in thin films, can be used to rapidly micro-mix reactants in order to control nucleation and particle growth for uniform particle size distribution. This could be achieved by varying both physical and chemical operation conditions in a precipitation reaction on the SDR. We have used the SDR for a Cu borohydride reduction to vary Cu NP size from 3 nm to about 55 nm. XRD and TEM characterization confirmed the presence of Cu_2O and Cu crystallites when the samples were dried. This technique is readily scalable for Cu NP production by processing continuously over a longer duration than the small-scale tests. However, separation of the nanoparticles from solution posed a challenge as the suspension hardly settled. The Cu NPs produced were tested to be active catalyst for MeOH synthesis at low temperature and MeOH productivity increased with decreasing particle size.

Keywords: Cu nanoparticles; spinning disc reactor; methanol synthesis; low temperature

1. Introduction

Methanol (MeOH) is a multi-purpose molecule widely used as a base chemical, for energy, and CO_2 storage [1]. It is used as a solvent or as an intermediate for the production of formaldehyde, methyl tert-butyl ether, acetic acid, methyl methacrylate, and other fine chemicals. MeOH can also be used as fuel blend or directly converted to valuable hydrocarbons such as gasoline over acidic microporous materials [2], thereby providing alternative sources of petrochemical feedstock used today.

Currently, the technology for MeOH synthesis is based on conversion of synthesis gas (composed largely of $2H_2/CO$ with about 5% CO_2) over $CuO/ZnO/Al_2O_3$ catalyst operating at around 250–300 °C and 50–100 bar [3]. Even though this process is highly optimized, the thermodynamics of the reaction limit syngas conversion per pass, which, coupled with other operational costs, make the process capital intensive. For example, more than 60% of the total capital cost in current MeOH processes is associated with the syngas plant [4].The lowest cost of syngas production is by the use of air rather than a pure cryogenic O_2-blown autothermic reformer [3]. Syngas conversion to MeOH is highly exothermic (shown in Equation (1)) and lower temperatures are required to achieve full conversion per pass. A full conversion per pass process allows the use of N_2 diluted syngas for MeOH

production, which implies no need for recycling of unconverted reactants. Consequently, the carbon footprint is reduced [5] as a result of the full conversion.

$$CO + 2H_2 \rightleftharpoons CH_3OH\ \Delta H = -90.6\,\text{kJ/mol} \quad (1)$$

Alternatively, low temperature MeOH synthesis (LTMS), which proceeds rapidly in liquid medium at about 100 °C presents the possibility for full syngas conversion per pass [6]. This technology is known to occur in two steps as shown in Equations (2) and (3). The carbonylation of MeOH to methyl formate (Equation (2)) is catalysed by an alkali alkoxide, while a transition metal based compound catalyses the hydrogenolysis of methyl formate (Equation (3)).

$$CO + CH_3OH \rightleftharpoons HCOOCH_3 \quad (2)$$

$$HCOOCH_3 + 2H_2 \rightleftharpoons 2CH_3OH \quad (3)$$

The Cu-based catalyst is one catalyst which has received a lot of attention for LTMS [7–11]. Examples of Cu-based materials reported for the hydrogenolysis reaction include CuO/Cr_2O_3, Raney Cu, Cu on SiO_2, $CuCl_2$, and Cu alkoxide. Prolonged milling of a physical mixture of CuO and Cr_2O_3, for example, enhanced MeOH synthesis activity [7]. We have also observed that Cu nanoparticle (NP) sizes influenced MeOH production, such that MeOH productivity increased with decreasing the particle size [10]. In both instances, MeOH productivity correlated well with increasing total surface area. This implies that producing the right-sized Cu particles as a catalyst for MeOH synthesis is important. In general, different Cu NPs sizes can be synthesized by following different experimental protocols and recipes [12]. Based on MeOH yield dependence on the Cu NP sizes, an on-purpose physical method for making Cu NP catalyst of different sizes using a specific chemical recipe will be a valuable contribution. In this work, we will focus on the use of spinning disk reactor (SDR), a technique that can fine-tune the Cu NP catalyst size for MeOH synthesis.

The SDR is a continuous-flow process intensification reactor with enhanced production efficiency, safety, minimal cost, and minimal waste technology [13,14]. A thin film liquid is formed in the SDR due to centrifugal acceleration created by rotation of the disk. The key characteristics of the thin film flow include rapid mixing, heat and mass transfer, plug flow, and short residence times in the order of seconds [15]. For example, the residence time, t_{res} of liquid reagents traveling with Q flow rate, from r_i to r_o on the disk based on the Nusselt theory can be expressed by Equation (4), where μ is dynamic viscosity and ω is angular velocity. Hence, increasing the flow rate and rotation speed for example will lead to a shorter residence time and consequently affect crystallization process.

$$t_{res} = \frac{3}{4}\left(\frac{12\pi^2\mu}{Q^2\omega^2}\right)^{\frac{1}{3}}\left(r_o^{\frac{4}{3}} - r_i^{\frac{4}{3}}\right) \quad (4)$$

The SDR can therefore be employed in sol-gel precipitation processes where homogenous mixing of the reactants at the molecular level is essential for controlling crystallite and particle size. Recently, the SDR has been used in several precipitation reactions for nanoparticles production [13,16–18]. Tai et al. [17], for example, used the SDR to produce 40–50 nm CuO nanoparticles using $Cu(SO_4)$ and $Na(CO_3)_2$ as reactants for nanofluid application.

In this work, we have used the SDR to produce different Cu NP sizes and size distributions, in a more environmentally friendly condition, using aqueous borohydride and $Cu(NO_3)_2$ as reactants. Our aim was to find out if the SDR could be used to purposefully produce Cu NP catalysts for MeOH synthesis. We found out that varying physical parameters of the SDR could fine-tune Cu NP catalyst sizes using specific chemical recipe. Furthermore, we scaled-up the Cu NP production for catalytic application in low temperature MeOH synthesis.

2. Results and Discussion

The SDR technique involves continuous flow of reactant and product stream with short residence time (in seconds) and therefore the process of producing fine nanoparticles must be a fast reaction. In view of this, our Cu particles were made using borohydride reduction (Equation (5)) [19] which occurs instantaneously when Cu^{2+} react with $NaBH_4$. Our preliminary test in a flask stirred at 700 rpm showed that when 0.011 M Cu^{2+} solution was added dropwise to 0.021 M BH_4^- solution, a black precipitation occurred instantaneously. Figure 1 shows the X-ray diffraction (XRD) and SEM images of 70 °C oven dried samples. Although Cu^0 was the expected product, the oven drying in air easily leads to Cu^0 surface oxidation. The XRD and SEM confirmed the formation of Cu_2O with 9 ± 1 and 25 ± 1 nm crystallite sizes.

$$Cu(NO_3)_2 + 2NaBH_4 + 6H_2O \rightarrow Cu \downarrow + 7H_2 + 2NaNO_3 + 2B(OH)_3 \quad (5)$$

The following sections will however focus on the use of the SDR to control Cu particle size. Here, the Cu salt and borohydride solution comes into contact at a shorter and easily controllable residence time compared with the stirred tank approach described above. The resulting slurry from the SDR was collected in starch to avoid settling and agglomeration of the particles after collection [16,20]. The starch serves as a capping agent to stabilize the Cu NPs made as well as to prevent further growth of particles.

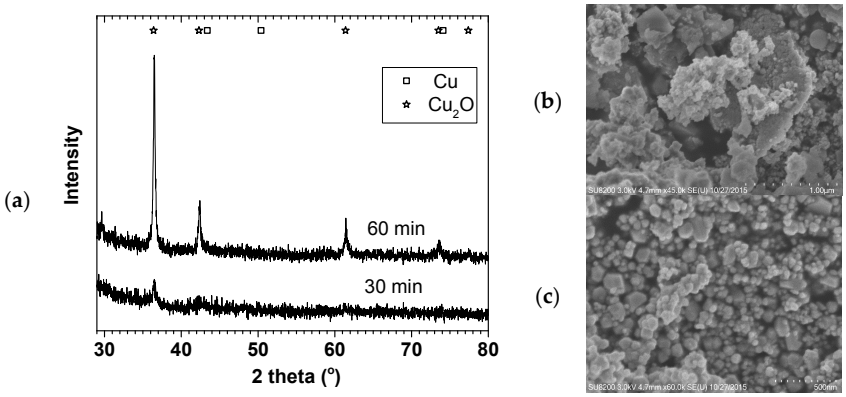

Figure 1. XRD (**a**) and SEM ((**b**) = 30 min & (**c**) = 60 min) of Cu NP made in a stirred tank; 0.011 M $Cu(CH_3COO)_2$ and 0.021 M $NaBH_4$.

2.1. Effect of Rotation of Disk Speed and Flow Rate

Figure 2 shows the effect of the disk rotation speed on particle size distribution (PSD) for a 0.01 M $Cu(NO_3)_2$ and 0.02 M $NaBH_4$ solution at 5 mL/s total flow rate. The faster the rotation, the narrower the PSD, while the mean particle sizes decreased from 35 ± 2 to 7.6 ± 0.5 nm for the 0.01 M $Cu(NO_3)_2$, with increasing disk speed from 400 to 2400 rpm, respectively. This trend was the same at both 0.01 and 0.05 M $Cu(NO_3)_2$ starting concentrations. Figure 3 shows the effect of the total flow rate on PSD, at constant 0.02 M $NaBH_4$ flow to 0.01 M $Cu(NO_3)_2$ flow ratio of 2 and 2400 rpm disk rotation speed. Similarly, mean particle sizes decreased from 14 ± 1 to 3.2 ± 0.2 nm with narrowing PSD as the flow rate was increased from 3 to 9 mL/s, respectively.

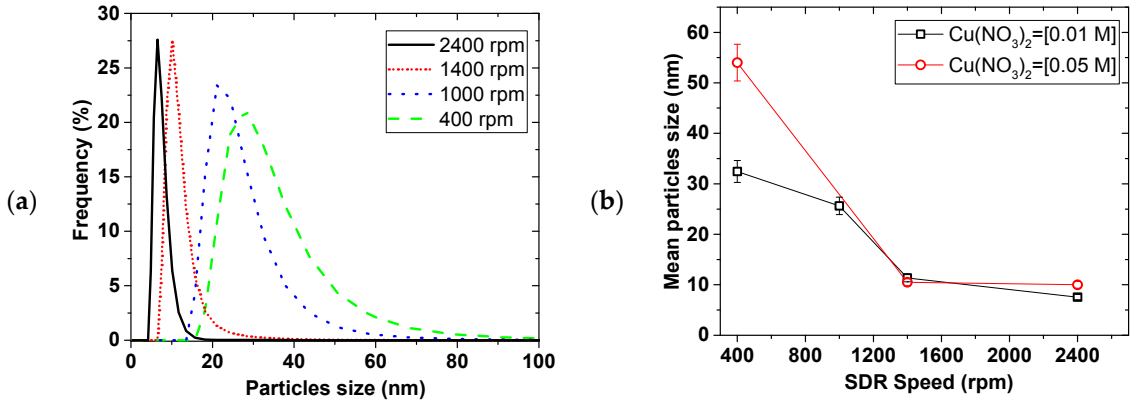

Figure 2. Effect of SDR spinning on (**a**) PSD for 0.01 M $Cu(NO_3)_2$ and (**b**) mean particle size, at 1.7 mL/s of 0.01 M and 0.05M $Cu(NO_3)_2$; 3.3 mL/s of 0.02 M and 0.10 M $NaBH_4$ (in 0.004 M NaOH).

The narrowing of particle size distribution with disk rotation speed and flow rate can be explained by the degree of micromixing achieved under the tested conditions. It is expected that shear effect of thin film formed on the disk and surface wave intensity both increase with increasing disk rotation speed and flow rate [13,14]. Mohammadi et al. [13] for example, showed that higher rotation speed and faster flow rate led to shorter micromixing time in the precipitation of titanium hydroxide. This results in more rapid homogeneous mixing at the molecular level coupled with more uniform supersaturation being attained. Short micromixing time favours nucleation over growth [21] leading to small particle formation. Uniformly sized nuclei lead to narrow particle size distribution as observed at high disk rotation speeds and faster flow rates.

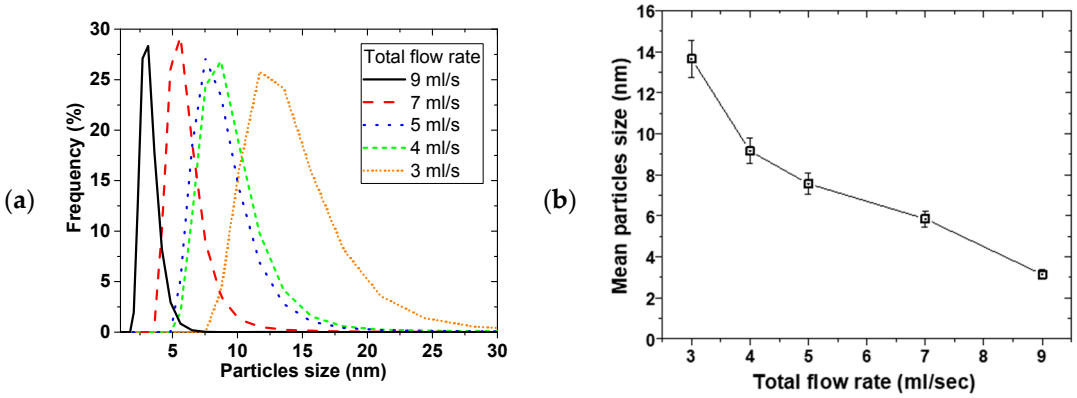

Figure 3. Effect of flow rate on (**a**) PSD and (**b**) mean particle size, 0.02 M $NaBH_4$ (in 0.004 M NaOH)/0.01 M $Cu(NO_3)_2$ flow ratio = 2, disk speed = 2400 rpm.

The SDR mean residence time and its residence time distribution (RTD) also have a significant influence on the final particle size and PSD respectively [13,22–24]. Increasing the rotation speed and flow rate leads to shorter residence time of the nuclei formed on initial contact of the reactants on the disk, thereby limiting the extent of particle growth and agglomeration in the SDR. It is also well-established that under conditions of high disk speeds and high flowrate, the RTD of the film approaches a near plug flow profile [23]. Under a plug flow regime, practically all particles will be subjected to the same mean residence time and processing conditions due to minimal radial dispersion and will exit the disk with a uniform particle size, resulting in tight PSDs. Clearly, the beneficial effects of high disk speeds and reagent flowrates on the film hydrodynamics are wide ranging and have a considerable impact on the formation of Cu NPs in this work. The best operating conditions are found to be 2400 rpm and 9 mL/s total flow rate.

Figure 4a shows X-ray diffraction of the NPs made at the 0.05 M $Cu(NO_3)_2$ starting concentration (in Figure 2) oven dried at 70 °C. The XRD showed predominantly Cu_2O phase with some Cu phase (plus some $NaNO_3$ reflections). The crystallite sizes estimated using the TOPAS software for the Cu_2O phase were 10 ± 1, 9.5 ± 0.7, and 9.5 ± 0.5 nm for 400, 1400, and 2400 rpm respectively. The crystallite sizes were similar for the three rotations despite their particle sizes and distribution differences. Figure 4b shows the XRD and TEM image of the NP made at 9 mL/s flow rate and 2400 rpm disk speed (in Figure 3). Similarly, Cu_2O phase was predominant with 4 ± 1 nm crystallite size. Furthermore, TEM image of the sample showed about 3–5 nm spherical shaped crystals surrounded by large amorphous materials likely to be the starch used to keep the particles from agglomerating. The XRD and TEM confirmed that Cu_2O NPs were made in the process with representative PSD as reported using the dynamic light scattering method.

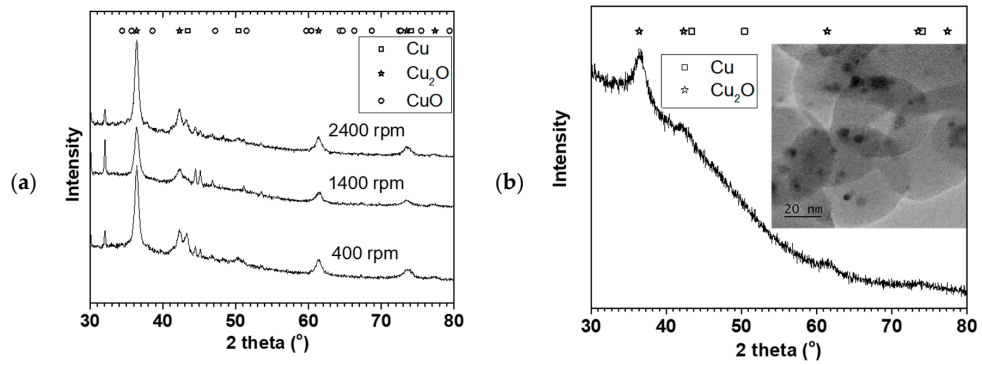

Figure 4. (**a**) XRD of the 0.05 M Cu precursor samples in Figure 2b, and (**b**) XRD with TEM image of the 9 mL/s sample in Figure 3.

2.2. Effect of Rotation Speed on Particles Using Different Cu Precurors

Figure 5 shows the effect of the rotation speed on the particles size and PSD of different Cu precursors. Considering the error margin, the three precursors appear to show similar mean particles sizes with a slight distinction at 1400 rpm, where $Cu(CH_3COO)_2$ gave the smallest particle of 8.1 nm. Nevertheless, the mean particle size decreased and PSD narrowed with the increasing SDR rotation speed. Overall, the mean particle size ranged between 24 ± 2 to 6.8 ± 0.7 nm with increasing rotation speed. The trend was similar to what was observed and discussed earlier with the $Cu(NO_3)_2$ precursor. This suggested that the micromixing, residence time, and RTD of the SDR dictated the mean particles and PSD size as discussed earlier rather than the source of the Cu precursor.

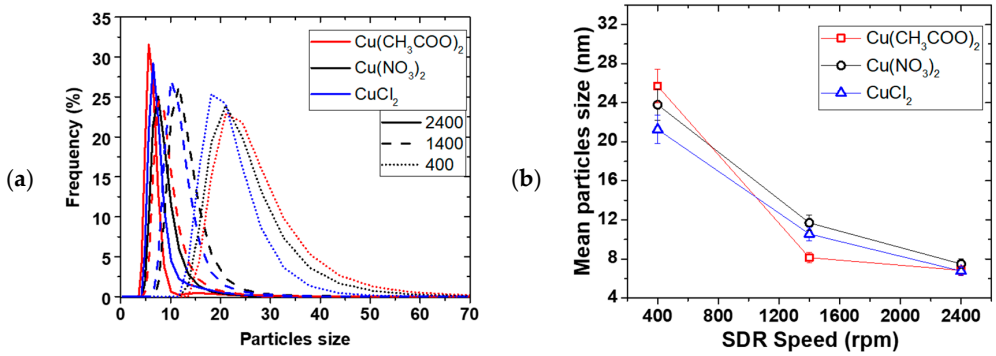

Figure 5. Effect of SDR disk speed on (**a**) PSD and (**b**) mean particle size of different Cu precursors, 3 mL/s of 0.01 M Cu^{2+} and 3 mL/s of 0.04 M $NaBH_4$ (in 0.004 M NaOH).

2.3. Effect of Reducing Agent and pH of the Reducing Agent

Figure 6 shows the effect of the reducing agent on the particle size and PSD. As illustrated in Figure 6a, the mean particle size decreased with reducing flow ratio of $Cu(NO_3)_2/NaBH_4$ (i.e., increasing $NaBH_4$ flow at the expense of $Cu(NO_3)_2$ flow), from 17 ± 1 to 7.6 ± 0.5 nm then the sizes levelled off after ratio of 0.5. Figure 6b illustrates that increasing the concentration of $NaBH_4$ at a constant $Cu(NO_3)_2$ concentration led to an initial decrease in mean particle sizes, and then levelled off after 0.04 M $NaBH_4$ concentration. However, when $Cu(NO_3)_2$ and $NaBH_4$ concentration and flow rates were kept constant and the amount of NaOH was varied, PSD widened and mean particle sizes increased linearly with pH (Figure 6c).

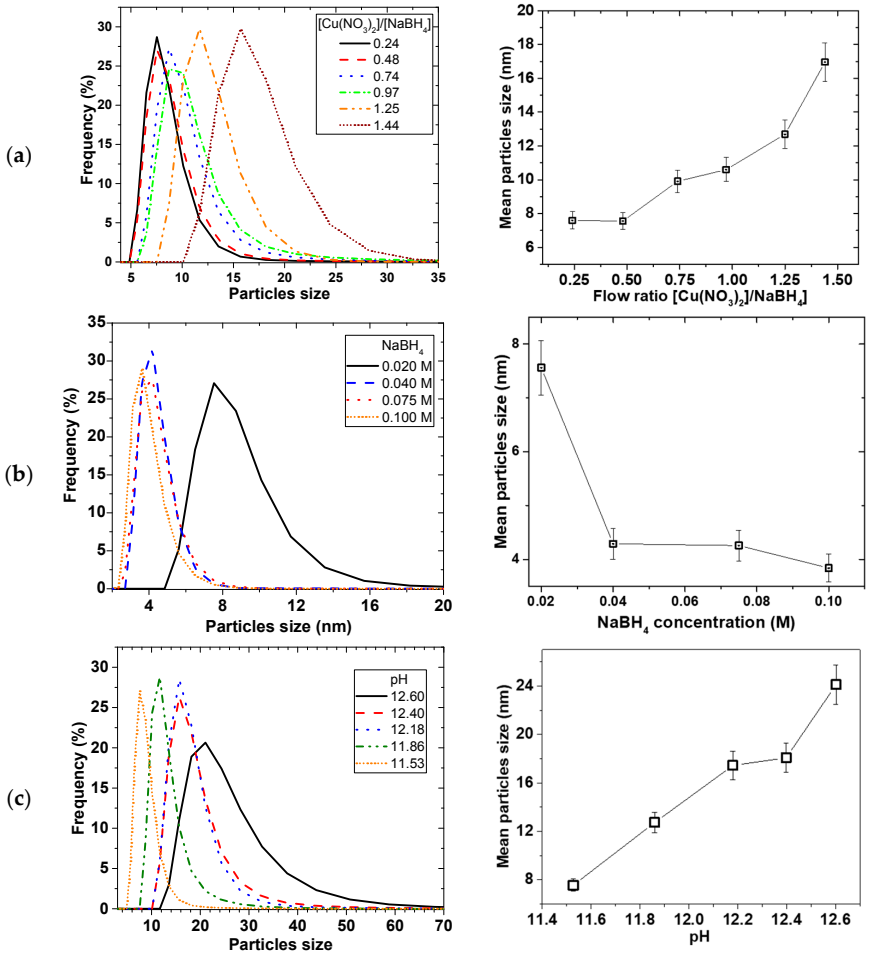

Figure 6. Effect of reducing agent on PSD (**left**) and mean particle size (**right**), (**a**) Effect of flow ratio, (**b**) Effect of $NaBH_4$ concentration, (**c**) Effect of pH, (by varying only NaOH concentrations); 0.01 M $Cu(NO_3)_2$, 0.02 M $NaBH_4$ (in 0.004 M NaOH), at 2400 rpm disk speed, 5 mL/s total flow rate.

Equation (5) showed that the Cu^{2+} reduction involves $NaBH_4$ hydrolysis. Since $NaBH_4$ is both soluble and reactive in water, NaOH was added to keep the $NaBH_4$ in solution for the reduction process. It has been reported that the rate of $NaBH_4$ hydrolysis increases with decreasing pH [25]. Ingersoll et al. [26] also reported that the amount of hydrolysis of $NaBH_4$ can be enhanced catalytically, such that in the presence of $NiCl_2$ and $CoCl_2$ salts, the rate of hydrolysis decreased with increasing NaOH concentration. Considering the relatively short residence time for the reagents on the SDR, any factor that affects the reactivity and accessibility of the BH_4^- can have consequence on the precipitation reaction to affect the particle size and PSD. This was evident when particle size linearly increased with pH (Figure 6c) as the amount of OH^- increased supressing the reactivity of the $NaBH_4$.

Furthermore, the stoichiometry of the reaction (Equation (5)) requires that the amount of $NaBH_4$ should be more than the $Cu(NO_3)_2$ to reduce all the Cu precursor towards precipitation. When $NaBH_4$ becomes the limiting reagent, the amount of reactive $NaBH_4$ readily available for the Cu^{2+} reduction is decreased, thereby increasing the time to attain homogeneity of the mixture. Subsequently, this leads to less uniform nuclei formation and there is delay in adequate micromixing, leading to patchy growth. Considering the short retention time involved in the process, wider PSD with bigger particles occurs as the amount of $NaBH_4$ decreased. On the other hand, when the amount of $NaBH_4$ increases to a certain maximum (for e.g., 0.04 M BH_4^-:0.01 M Cu^{2+}), the relative increase in reactive $NaBH_4$ reaches a saturation point and all the Cu reacts with $NaBH_4$ in a shorter time such that excess $NaBH_4$ will have no further effect.

2.4. Scaling up Cu NP Production and Methanol Synthesis

To apply the Cu NP as catalyst for MeOH synthesis, a larger amount of NP production was required over a longer continuous processing time. Firstly, 1 L of different starting $Cu(NO_3)_2$ concentrations were used at a 2400 rpm rotation speed and 1$Cu(NO_3)_2$:2$NaBH_4$ flow rate. Figure 7a,b shows the PSD and X-ray diffraction for 0.01, 0.025, and 0.050 M starting $Cu(NO_3)_2$ concentrations. The mean particle sizes increased from 7.6 ± 0.5 to 22 ± 2 nm and the PSD widened when the $Cu(NO_3)_2$ concentration was increased. Separation of the NP from solution was challenging and we resorted to oven drying at 90 °C. Mainly Cu_2O and Cu crystallite (+ some $NaNO_3$ phase) were observed and the crystallite sizes slightly increased from 8.6 ± 0.2 to 10.8 ± 0.3 nm with increasing concentration even though the mean particle sizes were generally larger. A similar observation was made by Chang et al. [17] where mean particle size increased from 48.3 to 93.0 nm when $Cu(SO_4)_2$ concentration was increased from 0.01 to 0.40 M. As concentration increased, the probability of nuclei colliding with each other increased leading to agglomeration and larger particles size as well as wider PSD.

Figure 7c shows the TEM image and electron diffraction of the Cu NP made at 0.01 M $Cu(NO_3)_2$ starting concentration. The spherical shaped polycrystalline Cu_2O observed in the TEM image, which showed particle sizes around 10 nm, confirmed that the method can be scaled-up. The challenge however, is the separation of the particles from the starch, as the starch gelatine used was no more soluble in water. Given that the resulting slurry was colloidal in nature, it was difficult to use a centrifuge to isolate the NPs. As a result, the slurry was dried at 90 °C, which could lead to possible increase in agglomeration of particles. If the reaction were carried out in solvent of interest for further processes or the catalysis in our case, then there would not be any need for separation or drying. However, our equipment at the time of this study was not materially compatible with ether solvents and we resorted to the use of water as a solvent.

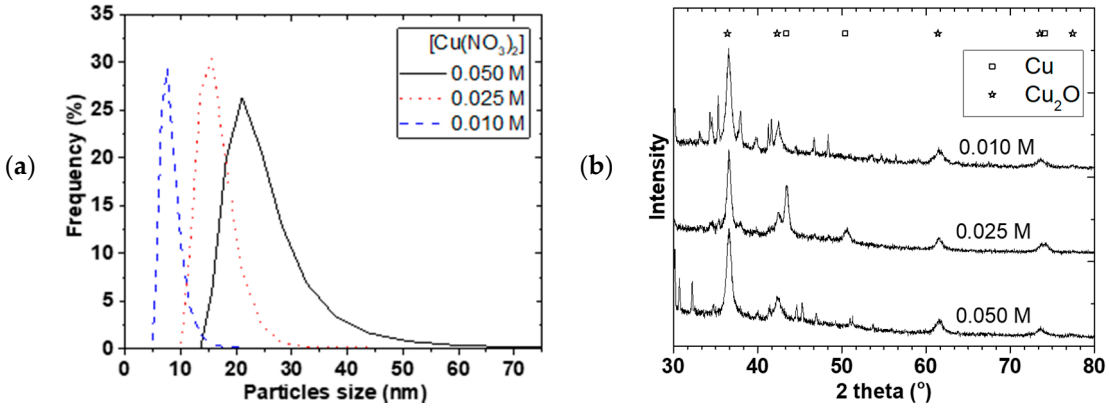

Figure 7. *Cont.*

(**c**)

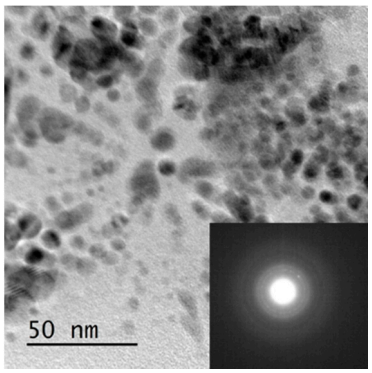

Figure 7. Effect of $Cu(NO_3)_2$ concentration on NP, (**a**) Effect of concentration on PDS, (**b**) XRD of the dried samples, (**c**) TEM image and diffraction of the dried 0.01 M sample; at 2400 rpm, $1Cu^{2+}$:$4BH_4^-$ concentration, 9 mL/s flow.

Furthermore, based on our knowledge of controlling Cu NP from the above, three tailored Cu NP with different mean particle sizes collected in starch were used for MeOH synthesis. Figure 8 shows XRD and TEM characterization for some 90 °C oven dried samples. These particles were spherical and polycrystalline, with mainly Cu_2O and Cu^0 phases. The crystallite sizes were 8.6 ± 0.5, 9.0 ± 0.6, and 9.5 ± 0.7 nm with 21 ± 1, 26 ± 2 and 29 ± 2 nm particles sizes for B1 S, B 4 S, and B 5 S respectively (S = with starch, see Figure 9). In addition, for comparison, B1 was repeated without starch (NS), where CuO was the predominant phase with 9.4 ± 0.7 nm crystallite and 38 ± 2 nm mean particle sizes. This suggested that aside from reducing agglomeration of the particles, the starch also reduced the amount of surface oxidation of the resulting NPs.

Syngas conversion over the selected samples ranged from about 50% to 70% conversion per batch, which is around the same range achieved in other Cu-alkoxide systems [8,27]. However, for comparison reasons, the amount of MeOH produced per amount of Cu (in mol/(mol·h)) is presented. Figure 9 shows the MeOH productivity compared with particle sizes. The MeOH productivity generally increased with decreasing particles sizes. This has already been attributed to the increase in total surface area as particle sizes decreased [7,10].

(**a**)

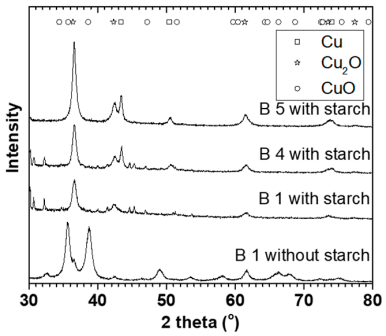

(**b**)

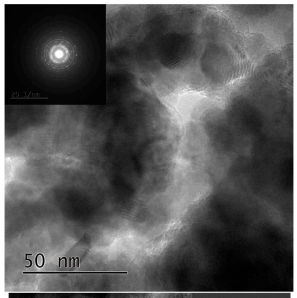

(**c**)

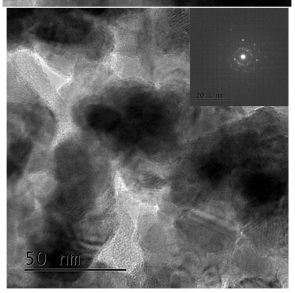

Figure 8. Scale-up Cu NP for MeOH synthesis, S = in starch, NS = No starch, (**a**) XRD, (**b**) TEM image of B 4S, (**c**) TEM image of B 5S.

The B1 NS sample showed a higher MeOH productivity than all the smaller particles collected in the starch. This sample differed from the other starch containing specimens by particle size and Cu phases present. Previous results have shown that in the presence of 20 bar $CO/2H_2$ at 100 °C, reduction of Cu^{2+} is rapid [10,28], and that the active Cu phase for the MeOH synthesis is assumed to be in the Cu^{+}/Cu° oxidation state [29]. This implies that it is not likely that the Cu phase in the B 1 NS catalyst contributed to the difference in the activity but rather the absence of starch. Hence, the lower activity of the catalyst samples containing starch could be due to mass transfer limitations of the substrate in accessing the surface of the Cu NP. This is in contrast to the B 1 NS catalyst where no starch is present on the surface. Nevertheless, the scaled-up Cu materials made with the SDR were active for MeOH synthesis either with or without starch present and can be further explored for optimization.

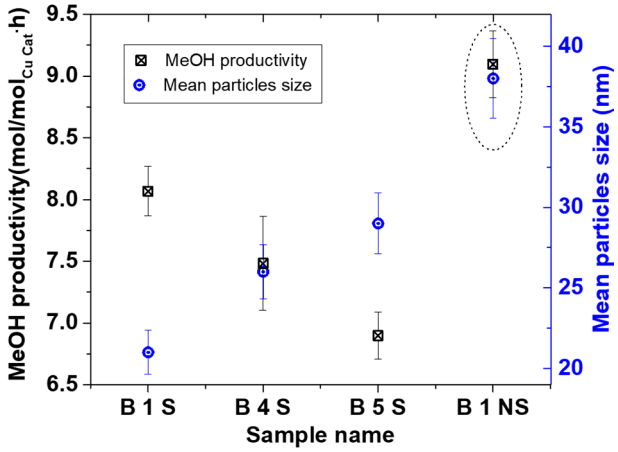

Figure 9. Low temperature MeOH synthesis of scale-up Cu NP; $2H_2/CO$ = 20 bar, THF solvent = 30 mL, for MeOH synthesis.

3. Materials and Methods

3.1. Spinning Disk Reactor

The set-up used in this work is shown in the schematic diagram in Figure 10 similar to the one described elsewhere [13,14]. The 10 cm diameter smooth surfaced stainless steel disk was driven by a 125 W electric motor, coupled with a digitally controlled rotating disk. A temperature controlled water-bath was circulated beneath the disk to ensure constant disk temperature (at 25 °C). $Cu(NO_3)_2$ solution in one line and $NaBH_4$ dissolved in NaOH solution in another line were fed onto the centre of the spinning disk. A Watson Marlow 323 peristaltic pump coupled with a dampener at the discharge end was used to control smooth flow of the two reagents. Each feed tube made of Viton, with 3.2 mm hole ends was set at a distance 6 mm perpendicular to the centre of the spinning disk. The reaction was carried out in a N_2 blanket to minimize direct contact of the reaction with air.

As shown in the Equation (5), Cu particles were precipitated by borohydride reduction. Typically, 0.01–0.05 M standard solutions of $Cu(NO_3)_2$ was reacted with 0.02–0.20 M $NaBH_4$ dissolved in about 17 *w*/*w* % NaOH. Since $NaBH_4$ is both soluble and reactive in water, adding the NaOH was necessary to keep $NaBH_4$ in solution. To avoid agglomeration and settling of the particles after collection from the SDR, samples were collected in starch as has been used elsewhere [16]. Thus, the resulting product was collected in 1 wt % starch gelatine solution. The starch gelatine was prepared by dissolving 10 g starch in 1000 mL water heated to 90 °C. The influence of starch on the particle size distribution for a period is shown in the supplementary material Figure S1.

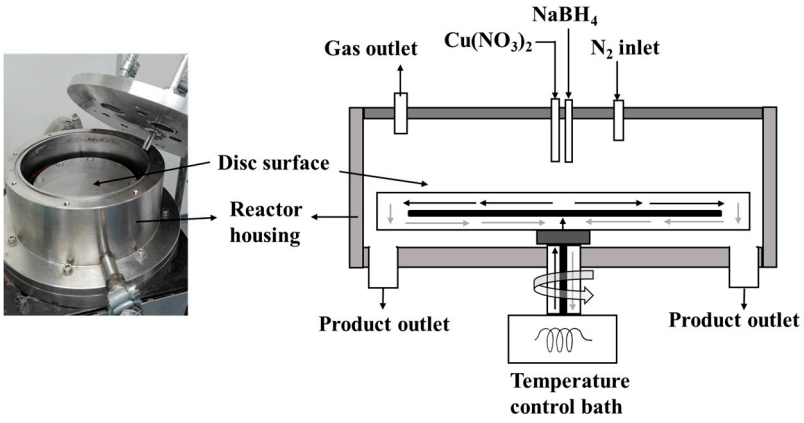

Figure 10. Scheme of SDR set-up used in making Cu NP.

3.2. Characterization of Cu Nanoparticles and Methanol Synthesis

Mean particle sizes and particles size distributions were analysed using dynamic light scattering (Malvern instrument, Model HPPS) with a He-Ne laser as light source (λ = 633 nm) and measured at 25 °C. Samples to be used for MeOH synthesis were dried at 90 °C for further characterization. A Bruker D8 discover powder diffractometer using Cu K-α-1 radiation (λ = 1.5 Å) selected by a Ge (111) Johansen monochromator and a Lynxeye detector were used. The diffractogram was measured at 0.025° steps per second. Total Pattern Analysis Solution (TOPAS) software was employed for quantitative Rietveld analysis of the diffractogram. This software operates by fitting a theoretical diffraction pattern to a measured diffraction pattern using non-linear least square algorithms [30]. The SEM imaging was performed using SU8230 ultra-high resolution cold-field emission SEM from Hitachi. The TEM imaging was performed with a Joel 2100F instrument. Diluted samples were dispersed in an ultrasound bath for 30 min and then deposited onto a carbon film on a copper grid.

MeOH synthesis was done similar to the process described in [10,31] in a 200 mL stainless high pressure hpm-020 autoclave batch reactor (Premex Reactor AG), equipped with a pressure sensor and thermocouple inserted. Weighed Cu NP and sodium methoxide ($NaCHO_3$) were added to 50 mL diglyme placed in the reactor. The reactor was charged to about 20 bar syngas ($1CO{:}2H_2$), then stirred at 3000 rpm and heated to 100 °C. The cooled liquid products were analysed using Agilent 7890 A GC with Agilent 7683B autosampler coupled with Agilent 5975 mass spectrometer detector (MSD). A CARBOWAX 007 series 20 M column with dimensions 60 m × 320 µm × 1.2 µm was used and programmed at 15 °C/min temperature ramp from 40 °C to 200 °C and held at 200 °C for 3 min, at 0.47 bar (6.8 psi) constant pressure. 0.54 mg heptane was as an internal standard.

Dry powdery sample was used for most of the characterization (XRD and TEM) and MeOH synthesis. Given that the collected sample from the SDR was colloidal in nature when collected in starch, it was difficult to use centrifuge for isolating the Cu NP. Slurry samples in smaller proportions were oven dried at 90 °C overnight. The dry samples were used for the MeOH synthesis without purification. MeOH productivity was calculated as shown in Equation (6).

$$Productivity = \frac{amount\ of\ MeOH\ (\mathrm{mol})}{amount\ of\ Cu_{catalyst}\ (\mathrm{mol}) \times reaction\ time\ (\mathrm{h})} \quad (6)$$

4. Conclusions

The SDR was used for making varying copper NP sizes based on copper borohydride reduction reaction. The Cu NP sizes and distributions were varied by changing physical and chemical parameters involved in the precipitation reaction. Particle size distribution narrowed with a corresponding decrease in particle size when micro-mixing time was shortened by, for example, increasing SDR rotation speed and total flow rates. Particle sizes in the range of 3 to 55 nm were obtained, which upon

oven drying at 70 or 90 °C showed predominantly polycrystalline Cu_2O and Cu phases. The advantage of the current technique is that it provides a faster approach to fine tuning Cu NP sizes for MeOH synthesis by varying physical parameters but using the same chemical recipe. The NPs were tested to be active for MeOH synthesis at low temperature (100 °C) and MeOH productivity increased with decreasing particle sizes.

Supplementary Materials: The following are available online at www.mdpi.com/1996-1944/11/1/154/s1, Figure S1: Effect of starch concentration on PSD.

Acknowledgments: This work was funded by the Research Council of Norway, NFR project number 228157/O70. We acknowledge that part of the work was carried out at RECX (the Norwegian national resource centre for X-ray diffraction and scattering) and NorTEM (the Norwegian Centre for Transmission Electron Microscopy) both in Oslo.

Author Contributions: Christian Ahoba-Samv, Unni Olsbye, and Klaus-Joachim Jens conceived the idea, Christian Ahoba-Samv and Kamelia V. K. Boodhoo designed the experiment; Christian Ahoba-Samv performed the experiments and drafted the work; Christian Ahoba-Samv, Unni Olsbye, Klaus-Joachim Jens, and Kamelia V. K. Boodhoo analysed and interpreted the data, revised the final version, and gave their approval for submission.

Conflicts of Interest: The authors declare no conflict of interest.

References

1. Olah, G.A. Beyond Oil and Gas: The Methanol Economy. *Angew. Chem. Int. Ed.* **2005**, *44*, 2636–2639. [CrossRef] [PubMed]
2. Olsbye, U.; Svelle, S.; Bjørgen, M.; Beato, P.; Janssens, T.V.; Joensen, F.; Bordiga, A.; Lillerud, K.P. Conversion of Methanol to Hydrocarbons: How Zeolite Cavity and Pore Size Controls Product Selectivity. *Angew. Chem. Int. Ed.* **2012**, *51*, 5810–5831. [CrossRef] [PubMed]
3. Hansen, J.B.; Højlund Nielsen, P.E. Methanol Synthesis. In *Handbook of Heterogeneous Catalysis*; Ertl, G., Knözinger, H., Weikamp, J., Eds.; Wiley-VCH Verlag GmbH & Co. KGaA: Weinheim, Germany, 2008; pp. 2920–2949.
4. Marchionna, M.; Di Girolamo, M.; Tagliabue, L.; Spangler, M.J.; Fleisch, T.H. A review of low temperature methanol synthesis. *Stud. Surf. Sci. Catal.* **1998**, *119*, 539–544.
5. Schiffer, Z.J.; Manthiram, K. Electrification and Decarbonization of the Chemical Industry. *Joule* **2017**, *1*, 10–14. [CrossRef]
6. Christiansen, J.A. Method of Producing Methyl Alcohol. U.S. Patent 1,302,011, 29 April 1919.
7. Ohyama, S.; Kishida, H. Physical mixture of CuO and Cr_2O_3 as an active catalyst component for low-temperature methanol synthesis via methyl formate. *Appl. Catal. A Gen.* **1998**, *172*, 241–247. [CrossRef]
8. Li, B.; Jens, K.-J. Low-Temperature and Low-Pressure Methanol Synthesis in the Liquid Phase Catalyzed by Copper Alkoxide Systems. *Ind. Eng. Chem. Res.* **2013**, *53*, 1735–1740. [CrossRef]
9. Xing-Quan, L.; Wu, Y.; Luo, S.; Yang, Y.; Jia, Z.; Li, S.; Chen, W.; Yu, Z. Concurrent Synthesis of Methanol and Methyl Formate Catalysed by Copper-based catalysts II. Influences of solvents and H_2/CO mole ratios. *J. Nat. Gas Chem.* **1999**, *8*, 203–210.
10. Ahoba-Sam, C.; Olsbye, U.; Jens, K.-J. Low temperature methanol synthesis catalyzed by copper nanoparticles. *Catal. Today* **2018**, *299*, 112–119. [CrossRef]
11. Ohyama, S.; Kishida, H. XRD, HRTEM and XAFS studies on structural transformation by milling in a mixture of CuO and Cr_2O_3 as an active catalyst component for low-temperature methanol synthesis. *Appl. Catal. A Gen.* **1999**, *184*, 239–248. [CrossRef]
12. Gawande, M.B.; Goswami, A.; Felpin, F.X.; Asefa, T.; Huang, X.; Silva, R.; Zou, X.; Zboril, R.; Varma, R.S. Cu and Cu-Based Nanoparticles: Synthesis and Applications in Catalysis. *Chem. Rev.* **2016**, *116*, 3722–3811. [CrossRef] [PubMed]
13. Mohammadi, S.; Harvey, A.; Boodhoo, K.V.K. Synthesis of TiO_2 nanoparticles in a spinning disc reactor. *Chem. Eng. J.* **2014**, *258*, 171–184. [CrossRef]
14. Boodhoo, K.V.K.; Al-Hengari, S.R. Micromixing Characteristics in a Small-Scale Spinning Disk Reactor. *Chem. Eng. Technol.* **2012**, *35*, 1229–1237. [CrossRef]
15. Boodhoo, K. Spinning Disc Reactor for Green Processing and Synthesis. In *Process Intensification for Green Chemistry*; John Wiley & Sons, Ltd.: Chichester, UK, 2013; pp. 59–90.

16. Tai, C.Y.; Wang, Y.-H.; Liu, H.-S. A green process for preparing silver nanoparticles using spinning disk reactor. *AIChE J.* **2008**, *54*, 445–452. [CrossRef]
17. Chang, M.-H.; Liu, H.-S.; Tai, C.Y. Preparation of copper oxide nanoparticles and its application in nanofluid. *Powder Technol.* **2011**, *207*, 378–386. [CrossRef]
18. He, F.; Zhao, D. Preparation and Characterization of a New Class of Starch-Stabilized Bimetallic Nanoparticles for Degradation of Chlorinated Hydrocarbons in Water. *Environ. Sci. Technol.* **2005**, *39*, 3314–3320. [CrossRef] [PubMed]
19. Glavee, G.N.; Klabunde, K.J.; Sorensen, C.M.; Hadjipanayis, G.C. Borohydride Reduction of Nickel and Copper Ions in Aqueous and Nonaqueous Media. Controllable Chemistry Leading to Nanoscale Metal and Metal Boride Particles. *Langmuir* **1994**, *10*, 4726–4730. [CrossRef]
20. Bashir, O.; Hussain, S.; AL-Thabaiti, S.A.; Khan, Z. Synthesis, optical properties, stability, and encapsulation of Cu-nanoparticles. *Spectrochim. Acta Part A Mol. Biomol. Spectrosc.* **2015**, *140* (Suppl. C), 265–273. [CrossRef] [PubMed]
21. Leubner, I.H. Particle nucleation and growth models. *Curr. Opin. Colloid Interface Sci.* **2000**, *5*, 151–159. [CrossRef]
22. Bałdyga, J.; Pohorecki, R. Turbulent micromixing in chemical reactors—A review. *Chem. Eng. J. Biochem. Eng. J.* **1995**, *58*, 183–195. [CrossRef]
23. Mohammadi, S.; Boodhoo, K.V.K. Online conductivity measurement of residence time distribution of thin film flow in the spinning disc reactor. *Chem. Eng. J.* **2012**, *207–208* (Suppl. C), 885–894. [CrossRef]
24. Ghiasy, D.; Tham, M.T.; Boodhoo, K.V.K. Control of a Spinning Disc Reactor: An Experimental Study. *Ind. Eng. Chem. Res.* **2013**, *52*, 16832–16841. [CrossRef]
25. Mesmer, R.E.; Jolly, W.L. The Hydrolysis of Aqueous Hydroborate. *Inorg. Chem.* **1962**, *1*, 608–612. [CrossRef]
26. Ingersoll, J.C.; Mani, N.; Thenmozhiyal, J.C.; Muthaiah, A. Catalytic hydrolysis of sodium borohydride by a novel nickel-cobalt-boride catalyst. *J. Power Sources* **2007**, *173*, 450–457. [CrossRef]
27. Li, B.; Jens, K. Liquid-Phase Low-Temperature and Low-Pressure Methanol Synthesis Catalyzed by a Raney Copper-Alkoxide System. *Top. Catal.* **2013**, *56*, 725–729. [CrossRef]
28. Fleisch, T.H.; Mieville, R.L. Studies on the chemical state of Cu during methanol synthesis. *J. Catal.* **1984**, *90*, 165–172. [CrossRef]
29. Liu, H.; Chen, T.; Yang, G.; Wang, G.Y. Investigation of Active Center of Cu-Based Catalyst for Low Temperature Methanol Synthesis from Syngas in Liquid Phase: The Contribution of Cu^{+} and Cu^{0}. *ChemistrySelect* **2017**, *2*, 8000–8007. [CrossRef]
30. TOPAS. Available online: https://www.bruker.com/products/x-ray-diffraction-and-elemental-analysis/x-ray-diffraction/xrd-software/topas/rietveld-analysis-software.html (accessed on 28 October 2016).
31. Ahoba-Sam, C.; Olsbye, U.; Jens, K.-J. The Role of Solvent Polarity on Low-Temperature Methanol Synthesis Catalyzed by Cu Nanoparticles. *Front. Energy Res.* **2017**, *5*. [CrossRef]

Tailoring Cu nanoparticles catalyst for methanol synthesis using the spinning disk reactor

Christian Ahoba-Sam[1], Kamelia V.K. Boodhoo[2], Unni Olsbye[3] and Klaus-Joachim Jens[1,*]

[1] Department of Process, Energy and Environmental Technology, University College of Southeast Norway, Kjølnes Ring 56, 3918 Porsgrunn, Norway; christian.ahoba-sam@usn.no
[2] School of Engineering, Merz Court, Newcastle University, Newcastle Upon Tyne NE1 7RU, UK; kamelia.boodhoo@newcastle.ac.uk
[3] Department of Chemistry, University of Oslo, P.O. Box 1033, Blindern, N-0315, Oslo, Norway; unni.olsbye@kjemi.uio.no
[1*] Correspondence: Klaus.J.Jens@usn.no; Tel.: +47 35575193

Supplementary data

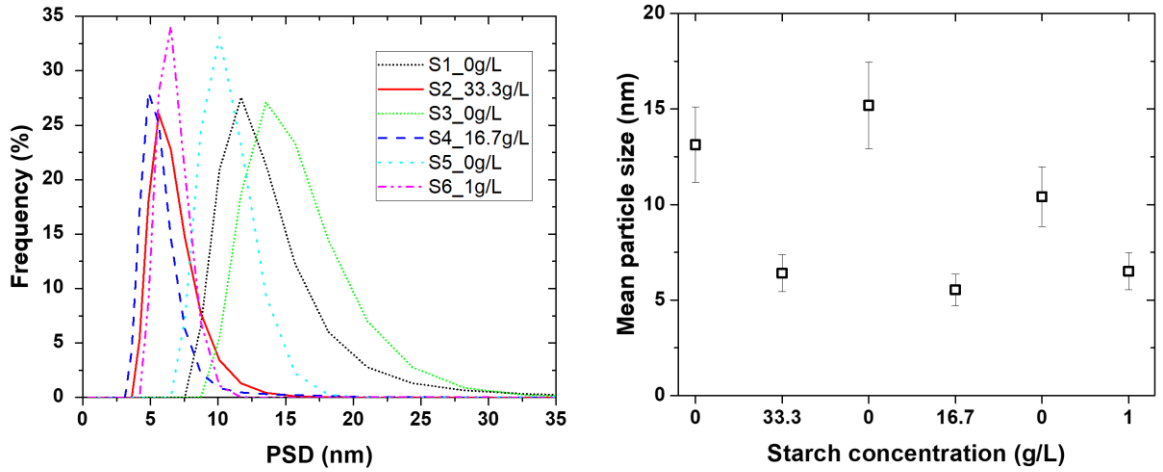

Figure S1. Effect of starch concentration on PSD (a) and mean particles size (b), 0.01 M $Cu(NO_3)_2$/0.02 M $NaBH_4$, flow ratio=2, flow rate=5.5 ml/s disk speed= 2400 rpm

In order to keep the Cu nanoparticles from agglomerating, corn-starch was dissolved in 90 ^oC hot water to form starch gelatine. Fig S1 shows the effect of varying starch concentration on the particles size after 1 day. When no starch was added, wider particles size distribution (PSD) was observed, with varying mean particles sizes, ranging from 10 to 15 nm. However when the particles were collected in starch gelatine, narrow PSD was observed and the mean particles size was about 6±1 nm. Moreover, no significant difference in both the PSD and the mean particle sizes were observed from the 1 to 33.3 1 g/L starch. As a result, the Cu nanoparticles made with the SDR were collected directly into 10 ml of 1 wt % (10g/L) starch gelatine.

Paper 4

Process Design of a Novel Low Temperature Methanol Synthesis Process Using an Air-blown Autothermal Reformer

Ahoba-Sam C., Øi L.E., Jens K-J.

Submitted manuscript to Linköping Electronic Conference Proceedings

Process Design of a Novel Low Temperature Methanol Synthesis Process Using an Air-blown Autothermal Reformer

Christian Ahoba-Sam, Lars Erik Øi, Klaus-Joachim Jens

Department of and Process, Energy and Environmental Technology, University College of Southeast Norway, Norway

lars.oi@usn.no

Abstract

Methanol (MeOH) synthesis at low temperature (100 ^{o}C) presents an opportunity for full syngas conversion per pass. This presents a cheaper alternative for MeOH synthesis using an air-blown autothermal reformer (ATR) rather than the conventional high temperature (>250 ^{o}C) MeOH synthesis approach which requires an expensive cryogenic O_2-blown ATR. The aim of this work was to use the process simulation program Aspen HYSYS to simulate and optimize the reactor conditions for a complete MeOH process design using an air-blown ATR. Our results revealed that, while syngas produced from 'normal' air-blown ATR (syngas composition 0.20CO:0.40H_2:0.39N_2) required 100 bar to obtain full conversion per pass, syngas produced from enriched air-blown ATR (syngas composition 0.31CO:0.62H_2:0.07 N_2) required 60 bar total syngas pressure to achieve the same. Even though the energy generated in both processes was enough to cover the heating demand in the total process with surplus, the enriched air-blown system provides a better energy recovery if the surplus energy is not used for extra power generation. The total process energy demand due to compression was estimated to be 2270 and 983 MJ/ton MeOH product for the normal air-blown and enriched air-blown systems respectively. A process design was proposed based on the optimized conditions for the enriched air-blown process.

Keywords: Air-blown reformer, syngas, methanol, low temperature, simulation, Aspen HYSYS

1 Introduction

Methanol (MeOH) is a multi-purpose molecule widely used as a base chemical, and for storage of energy and CO_2 (Olah, 2005). MeOH can be used as a fuel blend or directly converted to valuable hydrocarbons such as gasoline over acidic microporous materials (Olsbye et al., 2012), thereby providing an alternative source of petrochemical feedstock used today.

The current technology for MeOH synthesis is based on conversion of syngas and operate around 250-300 ^{o}C and 50-100 bar (Hansen & Højlund Nielsen, 2008). While this technology is highly optimized, the relatively high operating temperature limits conversion to barely 20 % per pass due to thermodynamics of the exothermic MeOH synthesis reaction (Equation (1)). As a result, the current process requires several recycling steps to optimize production (Lange, 2001).

Furthermore, the low conversion per pass of this process requires the use of a rather 'pure' syngas other than a N_2-diluted syngas for the MeOH synthesis. Such pure syngas production alone accounts for more than half of the total operation and capital cost in current methanol processes (Marchionna, Di Girolamo, Tagliabue, Spangler, & Fleisch, 1998). This is due to the use of expensive cryogenic O_2 for partial oxidation of hydrocarbons. The lowest cost of syngas production is by the use of either an ordinary air or an O_2 enriched air rather than cryogenic O_2-blown autothermic reformer (ATR) (Hansen & Højlund Nielsen, 2008). The highly exothermic syngas conversion to MeOH requires a relatively low temperature to achieve a full conversion per pass. Hence, such low temperature process will allow for the use of N_2 diluted syngas for MeOH production, with reduced capital and operation cost as there will be no need for recycling.

$$CO + 2H_2 \rightleftharpoons CH_3OH \quad \Delta H = -90.6\,\frac{kJ}{mol} \qquad (1)$$

Alternatively, a low temperature MeOH synthesis (LTMS) process which proceeds rapidly in a liquid medium at about 100 ^{o}C presents the possibility for full syngas conversion per pass (Christiansen, 1919). The LTMS process is known to occur in two steps (Equations (2) and (3)), via a methyl formate intermediate (Ohyama & Kishida, 1998). Typically alkali alkoxide is known to catalyse the carbonylation step (Equation 1) and Cu based materials catalyse the hydrogenolysis step (Equation 2). Cu nanoparticles due to largely exposed surface area accelerates the hydrogenolysis step in the LTMS process (Ahoba-Sam, Boodhoo, Olsbye, & Jens, 2018). For example, in diglyme solvent, Cu nanoparticles in combination with sodium methoxide led to up to 92 % conversion per batch with 20 bar syngas composed of 0.33CO:0.67H_2, at 100 ^{o}C (Ahoba-Sam, Olsbye, & Jens, 2018).

$$CO + CH_3OH \rightleftharpoons HCOOCH_3 \qquad (2)$$
$$HCOOCH_3 + 2H_2 \rightleftharpoons 2CH_3OH \qquad (3)$$

In this paper, our focus was to design a complete process for the LTMS reaction using Aspen HYSYS simulation

program. Considering that the LTMS process can tolerate N_2 diluent, the use of ordinary air and other O_2 enriched air can be simulated for the syngas production, and subsequently be used to design a complete MeOH plant. Even though the concept has been described as a 'dream reaction' (Hansen & Højlund Nielsen, 2008), the current work demonstrates that the suggested concept is feasible. The specific aim of this work was to simulate and optimize the reactor conditions in order to propose a complete design of the LTMS process using an air-blown ATR. Different parameters such as chemical compositions, temperature and pressure in the reactors were varied to optimize the process parameters.

2 Process Description

2.1 Principles of the Syngas Production

The syngas production process involved partial oxidation of methane (CH_4) using air, illustrated in Equation (4). The Figure 1 shows a syngas production process using air as the source of O_2. The process consists of a reactor (ATR), compressor and heat exchangers. Compressed air was used to make-up for the stoichiometry between CH_4 to O_2. The CH_4 feed used was assumed to be pure, without any sulphur or heavier hydrocarbon present, while the air feed consisted of only O_2 and N_2 to simplify the simulation. The compressed air together with the CH_4 feed were pre-heated and fed directly into the reactor.

$$CH_4 + \frac{1}{2}O_2 \rightleftharpoons CO + 2H_2 \quad \Delta H = -36\,\frac{kJ}{mol} \quad (4)$$

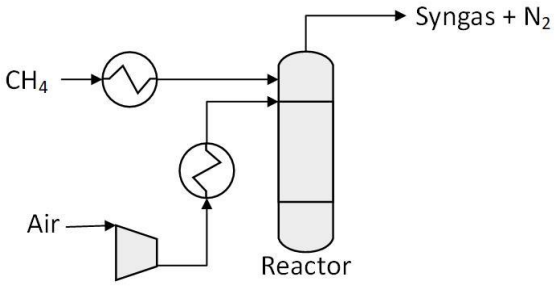

Figure 1. Principle for the syngas production process

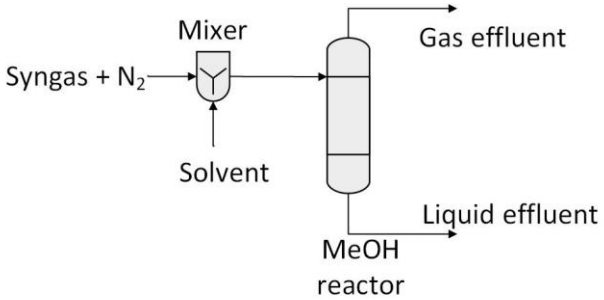

Figure 2. Principle for the low temperature MeOH synthesis process

2.2 Principles of the MeOH Synthesis Process

Figure 2 shows the MeOH synthesis process using N_2 containing syngas as feed. The LTMS process involved a MeOH reactor and a mixing unit. Since this step is highly exothermic (see Equation (1)) and requires lower operating temperature, the process is often carried out in liquid medium to absorb excess heat to minimize adiabatic rise in temperature beside other solvent's polarity role for the catalysis (Ahoba-Sam, Olsbye, & Jens, 2017). The syngas feed is mixed with a liquid solvent and fed into the MeOH reactor. For simplicity of the model, we have taken MeOH as a solvent and due to the 100 % thermodynamic syngas conversion, we have neglected the effect of MeOH solvent in the equilibrium calculations.

3 Models

All the simulations were performed using the Aspen HYSYS (version 8.6) program. Gibbs reactors were employed for both the syngas production and LTMS processes. A Gibbs reactor calculates the composition with the theoretical free energy minimum, which is the theoretical equilibrium composition. The Peng-Robinson equation of state (Peng & Robinson, 1976) fluid package was used in all the simulations. The equilibrium for the partial oxidation of CH_4 was calculated for the process in the ATR reactor, while CH_4 was assumed to be inert in the MeOH reactor. After the individual reactors were optimized, an overall system was designed.

Separating units were added in the overall system to represent, (i) a pressure swing adsorber (PSA) and (ii) H_2O/CO_2 absorber. The PSA was included to help regulate the O_2/N_2 composition that is fed into the ATR. The H_2O/CO_2 absorber was used to separate the H_2O and CO_2 from the syngas effluent before the MeOH reactor. After establishing reasonable pressure and temperature conditions in the individual reactors, the total compression, and heating requirements were simulated, to find out whether additional heating was necessary for the total process.

4 Process Simulations

4.1 Simulation and Optimization of the ATR for Syngas Production

To optimize the feed composition, different mole fractions of the CH_4: air (containing O_2 and N_2) were fed into the ATR reactor. The O_2/N_2 ratio was kept constant at air composition of 21/79. The Figure 3 shows the effect of the ratio of CH_4/O_2 on the syngas produced at 600 °C. The highest amount of CO + H_2 coupled with the least H_2O and CO_2 side product (3 and 1 % respectively) was observed at CH_4/O_2=2. While H_2O and CO_2 side products increased below the CH_4/O_2=2

ratio due to increase in oxidation, lower CH_4 conversion was observed at higher CH_4/O_2 ratio as the amount of O_2 became limiting. When the ratio of CH_4/O_2 was kept constant and O_2/N_2 ratios were varied (not shown), no variation was observed in the composition of the products. Overall CH_4/O_2=2 was chosen as a reasonable composition as this gave the highest amount of syngas ($CO+H_2$) with H_2/CO=2.

The temperature was varied to determine a reasonable temperature required for the feed inlet. Figure 4 shows the effect of temperature on the syngas produced between 600 to 1600 ^oC. This was done at $0.30CH_4$:$0.15O_2$:$0.55N_2$ feed composition set to 20 bar. Generally, the overall CH_4 conversion increased while side products decreased with increasing temperature. After 1200 ^oC, subtle changes were observed in the main products such that both the amount of syngas and H_2/CO=2 were similar. The amount of H_2O and CO_2 side product at 1200 ^oC decreased from 0.36 and 0.06 % to 0.06 and 0.01 % respectively at 1600 ^oC. Nevertheless, considering the exothermic nature of the process and its significance on the reactor material, 1200 ^oC was the temperature of choice for the syngas production.

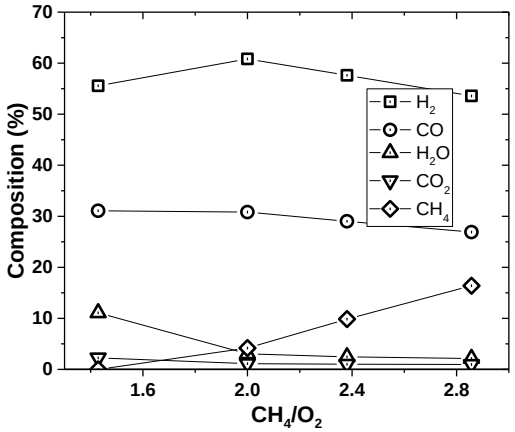

Figure 3. Effect of feed composition on the syngas production, at 600 ^oC and 10 bar**.**

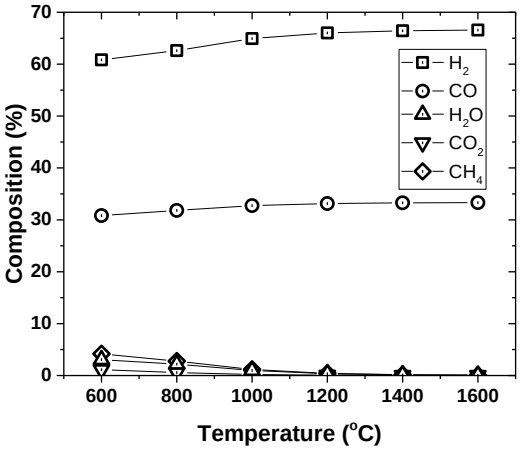

Figure 4. Effect of temperature on the syngas production, 20 bar

Furthermore, the total inlet pressure was varied to determine a reasonable pressure required for the optimal feed inlet. Figure 5 shows the effect of pressure on the syngas produced between 10 to 100 bar. This was done using similar syngas composition as was done for the temperature ($0.30CH_4$:$0.15O_2$:$0.55N_2$) at 1200 ^oC. The overall CH_4 conversion increased while side products decreased with decreasing pressure. After 30 bar, no significant changes were observed as both the amount of syngas produced and H_2/CO=2 remained the same. Therefore 20 bar was a reasonable pressure of choice for the syngas production.

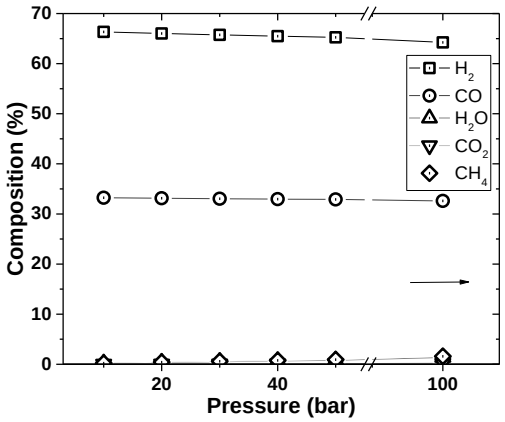

Figure 5. Effect of pressure on the syngas production

4.2 Simulation and Optimization of the MeOH Synthesis Process

The operating conditions for MeOH production was simulated to optimize the LTMS process. Figure 6 shows the effect of temperature on conversion at 20 and 100 bar syngas pressure. This was calculated using syngas ratio of 0.21 H_2 : 0.41 CO : 0.39 N_2. The syngas conversion rose exponentially from 300 ^oC to 120 ^oC and then increased slightly with decreasing temperature. The optimum temperature however depends on the operating pressure as the 20 and 100 bar syngas pressures showed similar trend but different conversions.

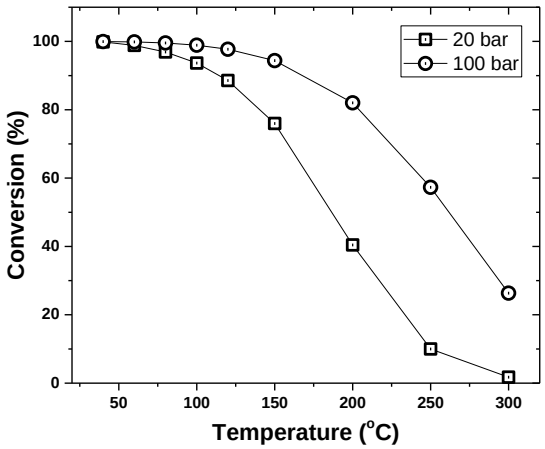

Figure 6. Effect of temperature on the LTMS process

Figure 7 shows the effect of pressure with and without N_2 at 100 ^oC. The conversion with N_2 was calculated using $0.21H_2$:0.41CO:0.39 N_2 syngas ratio while the conversion without N_2 was calculated based on $0.67H_2$:0.33CO composition. The syngas without N_2 showed more than 99 % conversion from 5 to 100 bar total syngas pressure. The syngas with N_2 however exponentially increased with pressure such that about 99 % conversion was achieved at 100 bars. This indicated the importance of N_2 diluent on the partial pressures of the syngas composition required for optimal conversion. Nevertheless, a reasonable pressure chosen for achieving optimal conversion in the presence of 39 % N_2 syngas diluent was 100 bar.

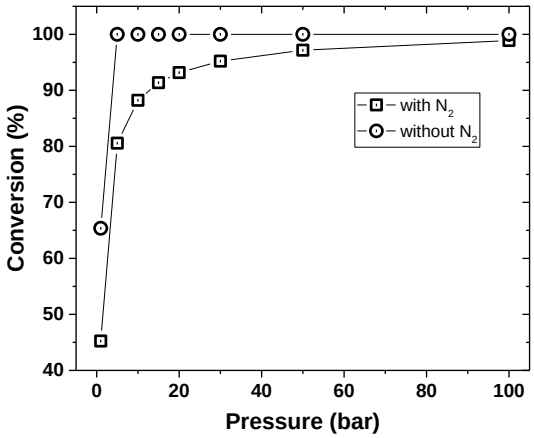

Figure 7. Effect of pressure on the LTMS process

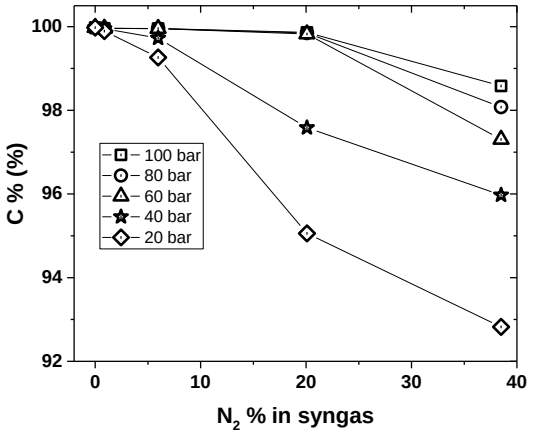

Figure 8. Effect of N_2 diluent concentration on LTMS process at different pressures

Furthermore, the importance of N_2 diluent was determined by varying its composition in the syngas. Figure 8 shows the effect of N_2 composition in the MeOH synthesis at 100 ^oC at different syngas total pressures. Syngas conversion increased with decreasing the amount of N_2 diluent in the syngas. Interestingly, a slight decrease of the amount of N_2 in the syngas from 39 % (from normal air composition) to 20 %, leads to full conversion even at 60 to 100 bar. Further N_2 reduction below 7 % in syngas will thermodynamically allow more than 99 % conversion at 100 ^oC and 20-100 bar. PSA for example can easily be used to enrich air up to 90 % O_2 content in air (Rao & Muller, 2007). Hence for the enriched air, 7 % N_2 in syngas, which can achieve full conversion per pass at 60 bar was chosen for the LTMS process.

4.3 Simulation of the Overall LTMS Process

The optimized operation conditions for the two reactors were put together as an overall LTMS process. Two scenarios were considered; one involving 'normal' air-blown ATR (0.21 O_2:0.79 N_2) and the other involving an O_2 enriched air-blown-blown (0.70 O_2:0.30 N_2) system. Figure 9 shows the Aspen HYSYS flow-sheet for the overall standard LTMS process for an enriched air-blown ATR. The set-up in the Figure 9 differs from the normal air-blown system by the inclusion of a PSA unit for enriching the air.

The details of the selected operating conditions used for the calculation is tabulated in Table 1. The partial oxidation was carried out at 1200 ^oC and effluent from the ATR cooled down to 30 °C in both systems. The 20 bar N_2 containing syngas produced was compressed to either 60 or 100 bar in the compressor where adiabatic efficiencies were specified to 75 %. Starting with 3990 kmol/h CH_4 flow, the normal air-blown system yielded 3842 kmol/h MeOH at 100 bar syngas pressure while that with the enriched air-blown yielded 3919 kmol/h MeOH at 60 bar.

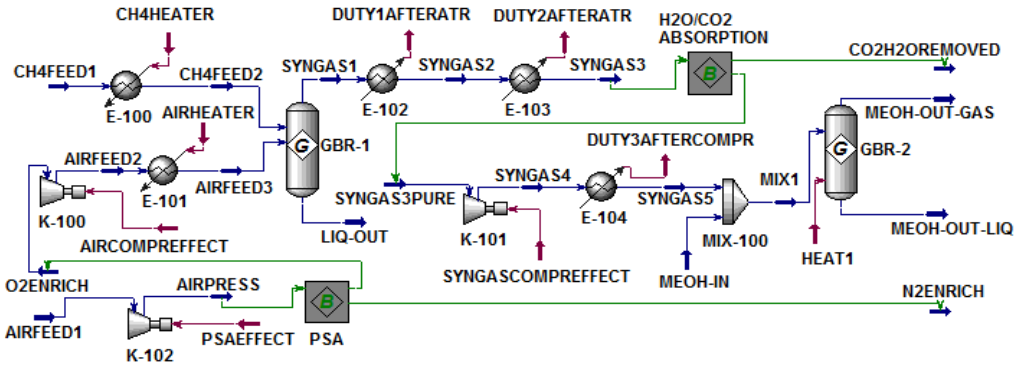

Figure 9. Aspen HYSYS flow-sheet for the overall standard LTMS process

Table 1. Specifications of Operation Conditions for the Overall LTMS Process as used in Figure 9

	Air-blown ATR system				*Enriched air-blown ATR system*			
Parameter	**Molar flow (kmol/h)**	**Pressure (bar)**	**Temperature (ºC)**	**Main composition**	**Molar flow (kmol/h)**	**Pressure (bar)**	**Temperature (ºC)**	**Main Composition**
CH_4Feed	3990	20	20	1 CH_4	3990	20	20	1 CH_4
CH_4Feed2	‘’	‘’	1200	‘’	‘’	‘’	1200	‘’
AirFeed	9500	1.01	20	0.21 O_2 : 0.79 N_2	14250	1.01	20	0.21 O_2:0.79 N_2
AirPress	-	-	-	-	‘’	1.50	66.5	‘’
O_2Enrich	-	-	-	-	2850	1.10	67	0.70 O_2:0.30 N_2
AirFeed2	9500	20	515	0.21 O_2 : 0.79 N_2	‘’	20	595	‘’
AirFeed3	‘’	‘’	1200	‘’	‘’	‘’	1200	‘’
Syngas1	19375	‘’	1356	0.20 CO : 0.40 H_2 : 0.39 N_2	12727	‘’	1439	0.31 CO:0.62 H_2:0.07 N_2
Syngas2	‘’	‘’	652	‘’	‘’	‘’	687	‘’
Syngas3	‘’	‘’	30	‘’	‘’	‘’	30	‘’
Syngas3pure	-	-	-	-	12678	20	33.5	‘’
Syngas4	19375	100	265	0.20CO:0.40H_2:0.39N_2	‘’	60	186	‘’
Syngas5	‘’	‘’	30	‘’	‘’	60	100	‘’
Mix1	‘’	‘’	‘’	‘’	‘’	‘’	‘’	‘’
MeOH out (Liquid+Gas)	11642	‘’	100	0.33CH_3OH: 0.64N_2	4839	‘’	‘’	0.81CH_3OH: 0.18 N_2

Table 2. Heat/Energy flow for the overall LTMS process in reference to Figure 9

Heating	***Air-blown (10^6kJ/h)***	***Enriched-air (10^6kJ/h)***
CH4HEATER (-)	306	306
AIRHEATER (-)	219	60.2
DUTY1AFTERATR (+)	451	315
DUTY2AFTERATR (+)	366	252
DUTY3AFTERCOMPR (+)	141	32.2
HEAT1 (+)	335	377
Compression		
PSAEFFECT	-	19.4
AIRCOMPREFFECT	144	47.6
SYNGASCOMPREFFECT	135	56.4

The heat/energy flow for the two systems is shown in Table 2. The negative signs in the table represent heating demands, while the positive represented heat release. For the normal air-blown system, a surplus (after recovery) of $7.68x10^8$ kJ/h heat was released as calculated from the heating and cooling. The total energy demand for the compressors was estimated to be $2.80x10^8$ kJ/h or 2270 MJ/ton MeOH product for the air-blown system. For the enriched air-blown system, a surplus (after recovery) of $6.10x10^8$ kJ/h heat was released when the heating and cooling streams were considered. The energy demand due to compression was estimated to be $1.23x10^8$ kJ/h or 983 MJ/ton MeOH product required for the enriched air-blown system. Overall the heat demand is covered by the surplus heat in both air-blown ATR systems.

5 Discussion of the Process

The air-blown ATR process for LTMS technology differ from conventional MeOH synthesis technology by the inclusion of N_2 diluent. The use of normal air for syngas production presents a cheaper alternative rather than a cryogenic O_2 which is more capital intensive. Alternatively, cheaper O_2 enrich air can be produced either by PSA or membrane separation technologies. PSA was preferred for the model since membrane separation is usually economical only at small scale (e.i < 20 ton/day). When an enriched air is used, the cost of production using a PSA will be cheaper than the use of a cryogenic air separation (Rao & Muller, 2007) considering the 70 % O_2 (in air) purity estimated for the partial oxidation in this work.

The exothermic partial oxidation reaction for the syngas production generates excess energy. The reaction specified at 1200 °C indicates outlet temperatures between 1350-1440 °C. This can raise concerns about the choice of the reactor material. Nevertheless, a typical ATR reactor has a burner operating above 2000 °C (Dybkjaer, 1995), and hence a 1440 °C stream outlet with a good heat transfer does not pose extra danger compared to the existing reactors. It also important to note that the partial oxidation process is already a commercial process in ammonia plants (York, Xiao, & Green, 2003) and considering the high operating temperature, the conversions obtain are practically close to equilibrium.

Furthermore, the difference in energy input and output due to heating indicated surplus of 7.68×10^8 and 6.10×10^8 kJ/h released in the normal air-blown and the enriched air-blown processes respectively. This indicated that heat generated in the process was enough to cover the heating demand in the total process. If the surplus energy is not recovered, the heat lost will be higher in the normal air-blown system. The surplus energy can however be used for power production for example in steam turbines (Ganapathy & Faulkner, 2002). The energy demand will therefore be due to feed compression, which can be reduced by the power generated from the surplus energy.

Thermodynamically, a full conversion per pass can be attained at lower temperatures below 120 °C. This however, depended on the partial pressure of the syngas components. When 39 % N_2 (from normal air-blown) in syngas was used as feed, full syngas conversion was possible at 100 bar. One disadvantage is the need for larger reactor volumes due to the space occupied by the N_2 diluent. However, with the enrichment of the air, same conversion could be attained with 7 % N_2 in syngas at 60 bar. The energy demand from compression relative to MeOH production was therefore estimated to 2270 and 983 MJ/ton MeOH product for the normal air-blown and the enriched air-blown systems respectively.

The optimized LTMS process was put together and a complete process design proposed. The Figure 10 shows a simplified diagram of the proposed air-blown LTMS process. Even though full syngas conversion can be achieved at 100 °C and 60 bar, there are a few experimental drawbacks. H_2O and CO_2 for example are catalyst poisons, and are required to be less than 10 ppm (Liu, Tierney, Shah, & Wender, 1988; Ohyama, 2003). The amount of methoxide diminishes by reacting with H_2O and CO_2 to produce hydroxide and carbonate respectively. As a results, there is a need to have an absorbing unit to remove H_2O and CO_2 from the syngas. Moreover, as MeOH is separated from the product stream some of the catalyst system which has undergone recycling can be reintroduced into the reactor. Overall, the air-blown ATR for a complete LTMS process design is a promising process for cheaper MeOH production.

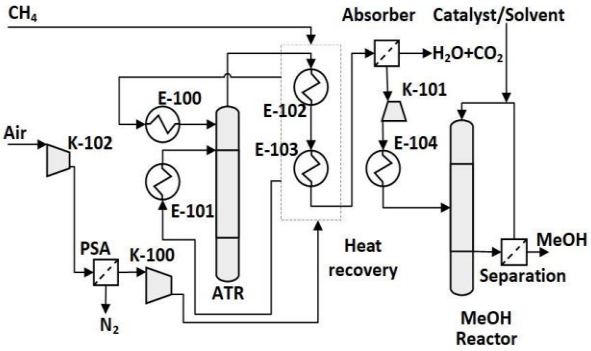

Figure 10. Simplified flow diagram of a complete LTMS process design

6 Conclusion

Simulations and optimizations of air-blown ATR and MeOH synthesis were performed to design a complete LTMS process. A normal air and an O_2 enriched air-blown ATR were optimized for syngas production in the low temperature MeOH synthesis process. Overall, the air-blown system containing 39 % N_2 (from air) in the syngas required about 100 bar to achieve full conversion, while the enriched air-blown system which contained 7 % N_2 in syngas could achieve same conversion at 60 bar. In both cases, the energy generated in the process was enough to cover the heating demand in the total process. When the surplus energy is not recovered, the heat lost will be higher in the normal air-blown system than the enriched air-blown system. The energy required for compression was therefore estimated to be 2270 and 983 MJ/ton MeOH product for the normal air and enriched air-blown systems respectively. An overall design was proposed based on the optimized conditions for the air-blown process.

References

Ahoba-Sam, C., Boodhoo, K., Olsbye, U., & Jens, K.-J. (2018). Tailoring Cu Nanoparticle Catalyst for Methanol Synthesis Using the Spinning Disk Reactor. *Materials, 11*(1), 154.

Ahoba-Sam, C., Olsbye, U., & Jens, K.-J. (2017). The Role of Solvent Polarity on Low-Temperature Methanol Synthesis Catalyzed by Cu Nanoparticles. *Frontiers in Energy Research, 5*(15). doi:10.3389/fenrg.2017.00015

Ahoba-Sam, C., Olsbye, U., & Jens, K.-J. (2018). Low temperature methanol synthesis catalyzed by copper nanoparticles. *Catalysis Today, 299*, 112-119. doi:https://doi.org/10.1016/j.cattod.2017.06.038

Christiansen, J. A. (1919). U.S. Patent 1,302,011.

Dybkjaer, I. (1995). Tubular reforming and autothermal reforming of natural gas — an overview of available processes. *Fuel Processing Technology, 42*(2), 85-107. doi:https://doi.org/10.1016/0378-3820(94)00099-F

Ganapathy, V., & Faulkner, L. (2002). *Industrial Boilers and Heat Recovery Steam Generators*. Boca Raton: CRC Press.

Hansen, J. B., & Højlund Nielsen, P. E. (2008). Methanol Synthesis. In G. Ertl, H. Knozinger, F. Schuth, & J.

Weitkamp (Eds.), *Handbook of Heterogeneous Catalysis* (Vol. 6, pp. 2920-2949). Weinheim, Germany: Wiley-VCH Verlag GmbH & Co. KGaA.

Lange, J.-P. (2001). Methanol synthesis: a short review of technology improvements. *Catalysis Today, 64*(1), 3-8. doi:https://doi.org/10.1016/S0920-5861(00)00503-4

Liu, Z., Tierney, J. W., Shah, Y. T., & Wender, I. (1988). Kinetics of two-step methanol synthesis in the slurry phase. *Fuel Processing Technology, 18*(2), 185-199. doi:http://dx.doi.org/10.1016/0378-3820(88)90095-1

Marchionna, M., Di Girolamo, M., Tagliabue, L., Spangler, M. J., & Fleisch, T. H. (1998). A review of low temperature methanol synthesis. *Studies in Surface Science and Catalysis, Volume 119*, 539-544. doi:http://dx.doi.org/10.1016/S0167-2991(98)80487-4

Ohyama, S. (2003). Low-Temperature Methanol Synthesis in Catalytic Systems Composed of Copper-Based Oxides and Alkali Alkoxides in Liquid Media: Effects of Reaction Variables on Catalytic Performance. *Topics in Catalysis, 22*(3), 337-343. doi:10.1023/A:1023500725571

Ohyama, S., & Kishida, H. (1998). Physical mixture of CuO and Cr2O3 as an active catalyst component for low-temperature methanol synthesis via methyl formate. *Applied Catalysis A: General, 172*(2), 241-247. doi:http://dx.doi.org/10.1016/S0926-860X(98)00135-5

Olah, G. A. (2005). Beyond Oil and Gas: The Methanol Economy. *Angewandte Chemie International Edition, 44*(18), 2636-2639. doi:10.1002/anie.200462121

Olsbye, U., Svelle, S., Bjørgen, M., Beato, P., Janssens, T. V. W., Joensen, F., . . . Lillerud, K. P. (2012). Conversion of Methanol to Hydrocarbons: How Zeolite Cavity and Pore Size Controls Product Selectivity. *Angewandte Chemie International Edition, 51*(24), 5810-5831. doi:10.1002/anie.201103657

Peng, D.-Y., & Robinson, D. B. (1976). A New Two-Constant Equation of State. *Industrial & Engineering Chemistry Fundamentals, 15*(1), 59-64. doi:10.1021/i160057a011

Rao, P., & Muller, M. (2007). *Industrial Oxygen, Its Generation and Use.* Paper presented at the Energy Efficiency in Industry.

York, A. P. E., Xiao, T., & Green, M. L. H. (2003). Brief Overview of the Partial Oxidation of Methane to Synthesis Gas. *Topics in Catalysis, 22*(3), 345-358. doi:10.1023/A:1023552709642

Doctoral dissertation no. 6
2018

—

Low temperature methanol synthesis catalysed by a copper nanoparticle-alkoxide system

Dissertation for the degree of Ph.D

—

Christian Ahoba-Sam

—

ISBN: 978-82-7206-479-1 (print)
ISBN: 978-82-7206-480-7 (online)

usn.no